14th International Conference on Physics of
5th Autumn School of Advanced Materials

Abstract Book ICPAM-14

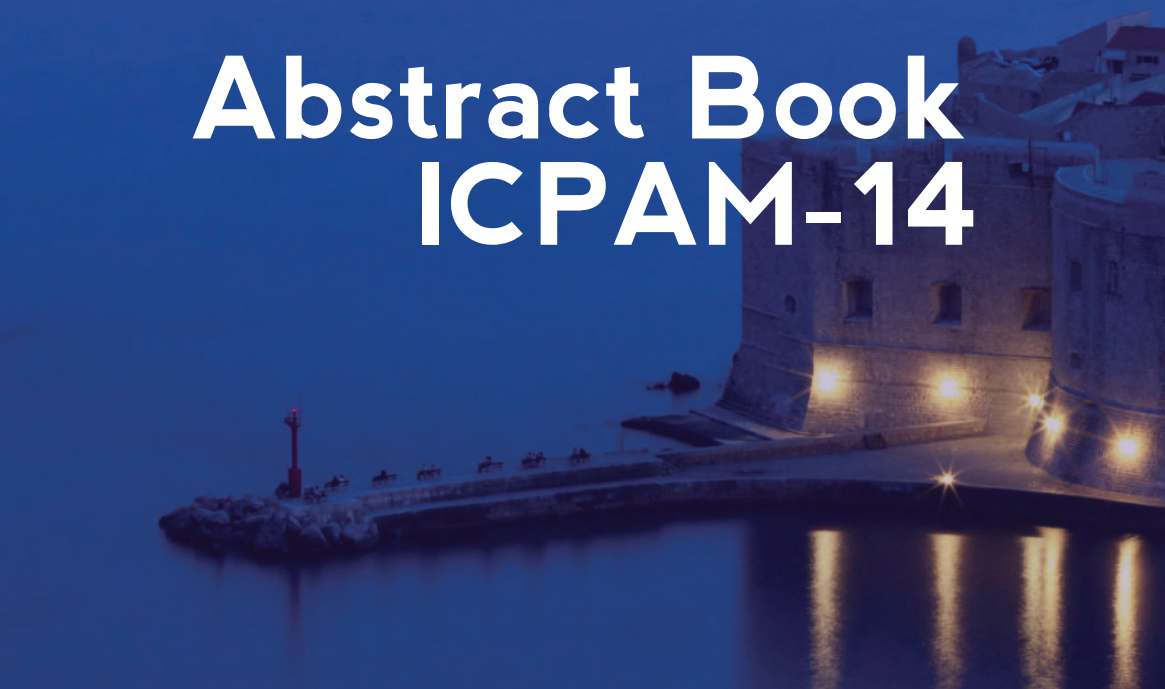

September 8-15, 2022
Dubrovnik, Croatia
www.icpam.ro

ICPAM-14

14th International Conference on Physics of Advanced Materials

September 08-15, 2022, Dubrovnik, Croatia
www.icpam.ro

Daily Program

&

Abstracts

Aurelian Rotaru
Daniel Moraru
Sebastian Popescu

Cover: Dragos Dutu

Foreword

The 14th International Conference on Physics of Advanced Materials (ICPAM-1) continues the tradition of the previous conferences organized by the Faculty of Physics of Alexandru Ioan Cuza University of Iasi at every four years, since 1980, and at every two years since 2012.

Beginning with 2012, the conference has as co-organizers prestigious institutions. Due to their contribution, the scientific quality of the conference increased, the conference papers being published in special issues in *Materials Science and Engineering*: B; *Applied Surfce Science, Thin Solid Films* and *Material Today: Proceedings*.

In 2014 the first autumn school on Physics of Advanced Materials, PAMS-1 was held in parallel with ICPAM-10. This event is focused on providing interdisciplinary expert training, involving both fundamental knowledge and current research topics. The fact that the school is organized in parallel with the conference assures a better interaction between the conference participants involved in different fields of physics of advanced materials and the participants attending the school. In the same year we beggan the collaboration with the 4th International Festival of NanoArt, promoting the art and science interaction.

Since 2016, beginning with ICPAM-11, the conference and the events hosted by the conference became itinerant.

For the first time, the 13th edition, the 4th Autumn School on Physics of Advanced Materials (PAMS-4), and the 5th International Festival of NanoArt were organized in a hybrid form.

Over 180 participants contributed with around 200 abstracts (ICPAM-13 and PAMS-4) for plenary, invited, oral and poster presentations.
Beginning with 2021 these events will be organized every year.
We invite participants to publishe their results, presented in the conference, in the special issues of Coatings, Materials and Nanomaterials journals. These journals are partners and sponsors at the same time, sustaining the conference and the autumn school.
The special Issues are:

New trends in Functional Materials and Devices, published by Coatings

New developments in physics of advanced materials, published by Materials

New Achievements in Nanostructured and Low Dimensional Materials and Systems, published by Nanomaterials.

Novel Materials with Target Functionalities published in the open access journal Nanomaterials.

Manuscripts should follow the instructions and the deadlines given on https://icpam.ro/papers-publication/ .

We would like to thank all participants for their important scientific contribution and the sponsors and partners for their support.

ICPAM-14, PAMS-5 General Chairs

Felicia IACOMI, Alexandru Ioan Cuza University of Iasi, Romania
Valentin CRACIUN, National Institute for Laser, Plasma and Radiation Physics, Magurele, Romania
Romulus TETEAN, Babes Bolyai University, Cluj-Napoca, Romania
Isabelle BERBEZIER, Institute for Materials, Microelectronic and Nanosciences of Provence, France
Marijana PECAREVIC, University of Dubrovnik, Croatia

Co-organizers:

ICPAM-14, PAMS-4 Committees

Secretariate & IT & Communication

Laura LACKO, Secretariate Manager
Dragos DUTU, Event planner
Madalin IONEL, Production Manager, Streambox
Marijana LUJO, University of Dubrovnik, Croatia
Marijana MILATIC, University of Dubrovnik, Croatia
Tihi BILAS, University of Dubrovnik, Croatia
Davorka TURCINOVIC, University of Dubrovnik, Croatia
Mislav CIMIC, University of Dubrovnik, Croatia
Cristina PACHIU, National Institute for R&D in Microtechnologies, Bucharest, Romania
Razvan HIRIAN, Babes-Bolyai University, Cluj-Napoca
Radu UDREA, Apel Laser, Bucharest
Stefan IRIMICIUC, National Institute for Laser, Plasma & Radiation Physics, Magurele, Romania
Roman ATANASOV, Faculty of Physics Babes-Bolyai University, Cluj-Napoca, Romania
Izabela BALASZ, Faculty of Physics Babes-Bolyai University, Cluj-Napoca, Romania

Organizing Committee

Sanja TOMSIC, University of Dubrovnik, Croatia
Josip MIKUS, University of Dubrovnik, Croatia
Daniel TIMPU, Petru Poni Institute of Macromolecular Chemistry, Iași, Romania
Ioan DUMITRU, Alexandru Ioan Cuza University of Iasi, Romania
Liviu LEONTIE, Alexandru Ioan Cuza University of Iași, Romania

Mirela SUCHEA, National Institute of R&D for Microelectronics, Bucharest, Romania; Hellenic Mediterranean University, Heraklion, Greece
Shizutoshi ANDO, Tokyo University of Science, Tokio, Japan
Luc FAVRE, Institute for Materials, Microelectronic and Nanosciences of Provence Marseille, France
Violeta DEDIU, National Institute of R&D for Microelectronics, Bucharest, Romania
Aurelian ROTARU, Stefan cel Mare University of Suceava, Romania
Emmanuel KOUDOUMAS, Hellenic Mediterranean University, Heraklion, Greece

Advisory Committee

Kruno BONACIC, University of Dubrovnik, Croatia
Cristian SILVESTRU, Babes-Bolyai University, Cluj-Napoca, member of Romanian Academy
Bogdan C. SIMIONESCU, Petru Poni Institute of Macromolecular Chemistry, Iasi, member of Romanian Academy
Raluca MULLER, National Institute for R&D in Microtechnologies, Bucharest, Romania
Munizer PURICA, National Institute for R&D in Microtechnologies, Bucharest, Romania
Emil BURZO, Babes-Bolyai University, Cluj-Napoca, member of Romanian Academy
Nikolaos KATSARAKIS, Hellenic Mediterranean University, Heraklion, Greece
Jean-Noel AQUA, Institut des NanoSciences de Paris, France
Yoshimasa KAWATA, Shizuoka University, Hamamatsu, Japan

Norbert KUCERKA, Joint Institute for Nuclear Research, Russian Federation
Cristian FOCSA, University of Lille, France

Conference topics and topics chairpersons

T1: Thin Films and Nanostructures for Modern Electronics
Daniel MORARU, Research Institute of Electronics, Shizuoka University
T2: Fundamentals of Plasma and Laser-Material Interactions and Processing
Ionut TOPALA, Alexandru Ioan Cuza University of Iasi, Romania
T3: Materials for Energy and Environment
Silviu COLIS, University of Strasbourg, France
T4**:** Magnetic Materials, Spintronics and Related Devices
Coriolan TIUSAN, Babes-Bolyai, Cluj-Napoca, Romania
Aurelian ROTARU, Stefan cel Mare University, Suceava, Romania
T5: Nanostructures and Low Dimensional Systems
Mathieu Abel, Institute for Materials, Microelectronic and Nanosciences of Provence, Marseille, France
T6: Emerging Electronic Memory Materials and Devices
Shashi PAUL, De Montfort University, Leicester, United Kingdom
T7: Polymer Materials and Composites
Valeria HARABAGIU, Petru Poni Institute of Macromolecular Chemistry, Romania
T8: Biomaterials and Healthcare Applications
Daniela UHRIKOVA, Comenius University, Bratislava
T9: Functional Materials. Processing and Characterization
Abdullah YILDIZ, Ankara Yıldırım Beyazıt University, Turkey

T10**:** New Developments in Sensing M Thursdayaterials and Sensor Devices
Jan LANCOK, Institute of Physics of the Czech Academy of Sciences, Czech Republic
T11: Trends in Condensed Matter Theory
Liviu CHIONCEL, Augsburg University, Germany
T12: Self-assembly and Patterning
Joerg K. N. LINDNER, Paderborn University, Germany
T13**:** Advanced photonic materials and devices
Dana CRISTEA, National Institute for Research and Development in Microtechnologies, Bucharest
T14: Waste materials and bioeconomy
Branko GLAMUZINA, University of Dubrovnik, Croatia
Simona PINZARU, Babes-Bolyai University Cluj-Napoca
T15: Materials in conservation-restauration of cultural heritage monuments and objects
Josko BOGDANOVIC, University of Dubrovnik, Croatia

Sponsors

Partners

Thursday, September 08, 2022

Akademis Academia

Foyer

16:00 Venue & Registration

18:00 Welcome Cocktail & “Microscopic Art in Science”

19:30 Dinner

Friday, September 9, 2022

08:00	**Registration**
08:20	**Opening** HALL 1-University of Dubrovnik
09:00	**Plenary Session** HALL 1
10:10	**Coffee break**
11:40	**Plenary Session** HALL 1
12:45	**Lunch**
15:00	**Invited and Oral Sessions** HALL 1, HALL 2
17:20	**Coffee break**
17:50	**Invited and Oral Sessions** HALL 1, HALL 2
19:30	**Dinner**

PL-online: Doping and interface effects on polarization of ferroelectric HfO_2

F. Sanchez

Institut de Ciència de Materials de Barcelona (ICMAB-CSIC), Campus UAB, 08193 Bellaterra, Spain

Ferroelectric HfO_2 is a promising material for new memory devices, but the microstructure of the films needs to be better controlled and some properties such as endurance need to be improved. Research of ferroelectric HfO_2 has been focused mainly on polycrystalline films. Epitaxial films, of great interest to understand properties and prototyping devices, are now being investigated. I this talk I will show the impact of i) the epitaxial interface [1-3] and ii) doping (oxygen vacancies and cations) on the stabilization of the ferroelectric phase [3-5].

[1] T. Song, H. Tan, S. Estandia, J. Gazquez, M. Gich, N. Dix, I. Fina, F. Sanchez, **2022**, 4, 2337
[2] T. Song, S. Estandia, N. Dix, J. Gazquez, M. Gich, I. Fina, F. Sanchez, J. Mater. Chem. C **2022**, 10, 8407
[3] I. Fina and F. Sanchez, ACS Appl. Electron. Mater. **2021**, 3, 1530
[4] T. Song, H. Tan, R. Bachelet, G. Saint-Girons, I. Fina, F. Sanchez, ACS Appl. Electron. Mater. **2021**, 3, 4809
[5] T. Song, R. Solanas, M. Qian, I. Fina, F. Sanchez, J. Mater. Chem. C **2022**, 10, 1084

PL: High-resolution (S)TEM studies on self-organized nanostructures and materials

J. K. N. Lindner

Dept. of Physics and Center for Optoelectronics and Photonics Paderborn (CeOPP), Paderborn University, 33098 Paderborn, Germany

Bottom-up techniques in nanopatterning of solid surfaces bare the inherent advantage in comparison to top-down methods such as light optical or electron beam lithography that they allow to fabricate myriads of periodically arranged nanoobjects in a highly parallel way and therefore allow to fabricate nanopatterns on large areas in short times and with little effort. Out of the different bottom-up techniques that have emerged in the last two decades, nanosphere lithography and block-copolymer lithography will be considered in detail in this presentation. The aim is to show what the state-of-the-art is with these techniques, which applications are possible and how these techniques can be combined to fabricate hierarchical nanostructures. Since the minimum feature size of nanostructures that can be obtained has reached the sub-ten nanometer range, it also has become ever more important to be able to characterize nanoobjects at ultimate spatial resolution, morphologically and chemically. For this, low-voltage analytical (scanning) transmission electron microscopy (S)TEM is employed, and examples will be given where in polymeric materials almost molecular resolution, in inorganic materials even sub-atomic resolution is achieved.

PL: Scanning electron microscopy for nano-scale fabrication

A. Dinescu[1], M. Dragoman[1], A. Mueller[1], D. Dragoman[2]

[1]IMT Bucharest, Romania
[2]Faculty of Physics, University of Bucharest, Romania

Many advances in fabrication precesses at micro and nanoscale in the past two decades were possible due to scanning electron microscopy, which is now an indispensable tool for analizing and fabricating new nanostructures and nanomaterials.
The development of very efficient in-lens detectors for SEM and the capability to use low energy electron probes are the gateway to the revelation of new features and new properties of nanomaterials that have been hidden by the use of high accelerating voltages and large interaction of volume, in the high-resolution SEM.

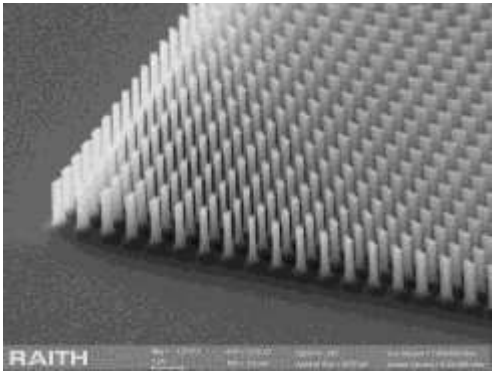

Fig. 1. DOE fabricated on silicon by electron beam lithography and cryogenic DRIE.

Electron beams have been used for lithography for decades and pattern generators can be fitted to all modern SEMs, converting them in very powerful nanolithographic tools, whitout degrading or limiting their imaging capabilities. The SEM became a very versatile tool for micro and nanofabrication, the same equipment used for fabrication being used to view the resulting nanostructures.
To illustrate the patterning capabilities of electron microscopy, the second part of the talk will be focused on fabrication of a few nanoelectronic devices, like field effect transistors on graphene [1,2] and on SOI wafers for quantum computing or diffractive optical elements (Fig.1).

[1] M. Dragoman, A. Dinescu, D. Dragoman, Nanotechnology, **2014**, 25(41), 415201.
[2] M. Dragoman, A. Dinescu, D. Dragoman, IEEE Trans. Nanotechnol., **2018**, 17(2), 362-367.

PL: Versatile Plasmonic and Fluorescence-Based Nanoprobes for Optical Bioimaging and Light-Activated Therapy

S. Astilean[1,2]

[1]*Department of Bimolecular Physics, Faculty of Physics, Babes-Bolyai University, M Kogalniceanu Str 1, 40084, Cluj-Napoca, Romania*
[2]*Nanobiophotonics and Laser Microspectroscopy Center, Interdisciplinary Research Institute in Bio-Nano-Sciences, T. Laurian Str. 42, 400271, Babes-Bolyai University, Cluj-Napoca, Romania*

Optical nanoprobes are designed for monitoring biological events at the cellular levels via optical and spectroscopic signals in order to perform early detection, accurate diagnosis,

and image-guided treatment of diseases. Due to several advantages such as unique optical signature, easy surface functionalization and favorable pharmacokinetic feature, plasmonic and fluorescent nanoplatforms have been extensively investigated in recent years as new versatile optical nanoprobes. In this presentation, we give an overview on our current approaches in fabrication plasmonic-based nanoplatforms and their implementation in a large variety of applications from cell imaging, drug delivery and light-activated nanotherapeutics. Since several years, our group has successfully synthetized a large variety of gold or silver nanoparticles with well-defined optical properties, providing the right size (2-100 nm), shape (sphere, rod, prism, star-like shape…), required biocompatibility and specific functionality to be translated into in vitro and in vivo studies. For instance, several classes of biocompatible “optically hot” biopolymer (chitosan, poly(ethylene) glycol, pluronic, gelatin…)-coated plasmonic nanoparticles were implemented as versatile nanoprobes for spectroscopic investigation of cells by intracellular imaging via surface-enhanced Raman scattering (SERS), localized surface plasmon resonant scattering (LSPR-S) and steady-state and fluorescent lifetime imaging (FLIM). Scanning confocal Raman microscopy combined with dark-field and confocal fluorescence microscopy were used to record relevant intracellular information as nanoparticle localization, chemical interaction and pH mapping. In recent years, our research group has developed several “proofs of concept” for light-activated nanotherapies against cancer by integration into a single plasmonic nanoplatform of plasmon-induced photothermal therapy (PTT), plasmon-enhanced photodynamic therapy (PE-PDT) and delivery of

chemotherapeutic drugs (doxorubicin, cisplatin) [1,2]. Currently, we focus on the development of new organic and hybrid fluorescent nanoprobes with potential to serve as near-infrared (NIR) contrast agents for real-time image-guided surgery of ovarian cancer [3].

Aknowledjments. This work was supported by a grant of Ministry of Research and Innovation, CNCS-UEFISCDI, project number PN-III-P4-ID-PCCF-2016-0142, within PNCDI III.

[1]. M. Potara, T. Nagy Simon, A. M. Craciun, S. Suarasan, E. Licarete, F. I. Lucaci, S. Astilean, ACS Appl. Mater. Interfaces **2017**, 9, 32565–32576.
[2]. S. Suarasan, A-M Craciun, E. Licarete, M. Focsan, K. Magyari, S. Astilean, ACS Appl. Mater. Interfaces, **2019**, 11, 7812−7822.
[3]. R. Borlan, M. Focsan, et al. Biomater. Sci. **2021**, 9, 6183-6202

PL: Sustainable bio-based materials for non-conventional energy production and environment protection

V. Harabagiu[1], P. Samoila[1], C. Cojocaru[1], A.C. Enache[1], S.F. Cosmulescu[2], G. Predeanu[3]

[1]Laboratory of Inorganic Polymers, "Petru Poni" Institute of Macromolecular Chemistry, Romanian Academy, 700487 Iasi, Romania
[2]S.C. COSFEL ACTUAL S.R.L., 010705 Bucharest, Romania
[3]Research Center for Environmental Protection and Ecotehnologies, University Politehnica of Bucharest, 011061 Bucharest, Romania

Energy and environment related issues are, between others, acute challenges in the complex context of actual socio-economic development and of capital importance for the future of the human society. The vanishing fossil energy resources should be replaced, while friendly/sustainable

technologies and materials for environment protection have to be imagined and developed.

In this respect, our research team revisited the properties of some regenerable polymeric materials of vegetal and animal origin and proposed simple approaches to yield polyelectrolyte membranes for fuel cells and sorbents for oil spills or for heavy metal cations from contaminated waters [1-4]. Details on the preparation methods and the properties of the resulted materials will be given.

Further, the project "Innovative and integrated recovery of biopolymer waste through intelligent microwave-assisted synthesis processes to obtain carbon materials for niche applications" (acronym, 4WASTEUPGRADE) aims:

- to build an innovative and integrated pilot line for preparation of activated carbons (ACs) through a microwave-assisted process;
- capitalizing some biopolymer/lignocellulosic wastes that are not currently exploited, such as: fruit seeds and shells;
- to demonstrate the feasibility of ACs on the designed pilot line and the performances of the as obtained ACs in wastewater treatment by adsorption and catalytic processes.

Acknowledgements. The support of European Regional Development Fund, Competitiveness Operational Programme 2014–2020; POC/163/1/3 – Project 4WASTEUPGRADE (Contract no. 386/390062/04.10.2021, MySMIS code: 120696) is gratefully acknowledged.

[1] A.C. Humelnicu, P. Samoila, M. Asandulesa, C. Cojocaru, A. Bele, A.T. Marinoiu, A. Sacca, V. Harabagiu, Polymers **2020**, 12(5) Art. no. 1125.

[2] P. Samoila, I. Grecu, M. Asandulesa, C. Cojocaru, V. Harabagiu,

React. Funct. Polym. **2021,** 165, 104967.
[3] B.-C. Condurache, C. Cojocaru, P. Samoila, M. Ignat, V. Harabagiu, Int J. Env. Sci.Technol. **2022**, 19(1), 367-378.
[4] R. Rotaru, M.E. Fortună, C. Cojocaru, P. Samoilă, L. Pricop, V. Harabagiu, Env. Eng. Manag. J. **2019**, 18(6), 1193-1200.

Invited and Oral Session (HALL1)

T10-I: Pulsed Laser Deposited active films for chemical sensors

J. Lancok[1], M. Novotny[1], L. Volfova[1], P. Fitl[2], M. Vrnata[2], M. Vorokhta[a]

[1] Institute of Physics of the Czech Academy of Sciences, Na Slovance 2, 182 21 Prague 8, Czechia
[2]Department of Physics and Measurements, University of Chemistry and Technology Prague, Technicka 5, 166 28 Prague 6, Czechia
3Department of Surface and Plasma Science, Faculty of Mathematics and Physics, Charles University, V Holesovckach 2, 180 00 Prague 8, Czechia

Although the first functional chemiresistors with semiconductor metal oxide sensitive layers were constructed in 1960's [1] and since1990's they are commercially produced in large series, their research and development is far from being completed. Chemiresistor is a sensing element which converts chemical input quantity (concentration of detected gaseous analyte) into electrical output quantity. The functionality of chemiresistor consists of changing electric resistance/impedance of semiconducting sensitive layer when gases with either oxidizing or reducing properties appear in surrounding atmosphere. When measuring sensor resistance, current flows through its sensitive layer; for this reason transducer function is partially influenced by "volume"

phenomena in morphological constituents of active layer (larger grains, nanocrystallic grains, one-dimensional nanowires, ribbons etc.) and partially by "surface phenomena" - i.e. nature of contacts between these constituents. It is apparent that morphology of sensitive layer has a serious impact to both receptor and transducer function. When given oxidic material is nanostructured, its electrophysical properties and chemical properties are modified. Due to this fact nowadays, while chemical composition of sensitive layers (metallic oxide, dopant, and catalyst) has been usually optimized, the boom of nanotechnologies in recent years brings new challenges how to improve chemiresistors by tuning morphology of their sensitive layers. There are many recent reports in literature signalizing that this topic is still actual [2]. Pulsed Laser Deposition is well established and suitable and flexible techniques for fabrication of metal oxide thin films with various structural and morphological properties.

In presentation the extensively overview of the metal oxide thin films fabricated by PLD for chemical sensors focused on n-type SnO_2, ZnO, WO_3 and p-type Cu_2O will be given. Among other features of the films attention will be paid to near-ambient pressure photoelectron spectroscopy (NAP-XPS) as a powerful tool that enables in-situ studies of chemisorption of wide range of gaseous such as ethanol, hydrogen, NO_2 and acetaldehyde [3,4]. The idea was to observe the reaction of species on the surfaces in the atmosphere in case when pressure in measuring cell total will correspond to their partial pressure at common atmosphere, when they are contained at concentrations of units of ppm. The following chemical

responses of the sensors were measured at the same condition as NAP-XPS.

[1] Seiyama, T., et al., A new detector for gaseous components using semiconductive thin films Analytical Chemistry, **1962** 34(11) 1502-1503.
[2] Malik R. et al., Appl. Phys. Rev. **2020,** 7, 021301
[3] Vorokhta M. et.al. Surf. Sci. **2018**, 677, 284
[4] Hozak P. et. Al., J. of Phys. Chem. C **2019**, 123, 29739.

T9-I: Ge-Sb-Te thin films: fabrication and characterization

P. Nemec

Department of Graphic Arts and Photophysics, University of Pardubice, Pardubice, Czech Republic

More than 50 years ago, reversible electrical swiching phenomenon in amorphous chalcogenides was first time reported by Ovshinsky [1]. In the end of 1980s and beginning of 1990s, phase change materials based on Ge-Sb-Te and/or Ag-In-Sb-Te systems have been discovered. The main scientific as well as technological interest of these inorganic materials is their ability to transform quickly and reversibly between amorphous and crystalline phases. Fast phase transformation can be induced reversibly through varying the electric field or temperature by heating via a laser pulse in optical recording applications. The extraordinary properties of phase change materials based on Ge-Sb-Te ternary system are connected with changes of optical reflectivity (up to 30%) and/or electrical resistivity (several orders of magnitude) taking place upon phase transition [2].
This contribution covers the investigations performed regarding fabrication (via magnetron sputtering and pulsed laser deposition) and characterization of Ge-Sb-Te thin films. The characterization of thin films in as-deposited state (amorphous

phase) as well as in crystalline state (induced by thermal annealing) was performed exploiting atomic force microscopy, scanning electron microscopy with energy-dispersive X-ray analysis, X-ray diffraction, electrical resistivity, and variable angle spectroscopic ellipsometry data. The results are discussed in relation with the chemical composition of the fabricated thin films.

Acknowledgements. The financial support of the Czech Science Foundation under the project No. 22-07635S is greatly acknowledged.

[1] S. R. Ovshinsky, Phys. Rev. Lett. **1968,** 21, 1450-1453.
[2] M. Bouska, S. Pechev, Q. Simon, R. Boidin, V. Nazabal, J. Gutwirth, E. Baudet, P. Nemec, Scientific Reports **2016**, 6, 26552.

T9-I: Optical properties and phonon behaviour in $BiFeO_3$, $BiCrO_3$, and $BiFe_xCr_{1-x}O_3$, a material system different from its parents

C. Himcinschi[1], F. Drechsler[1], J.L. Proschwitz[1], A. Ozden[1], D.S. Walch[2,3], A. Bhatnagar[2,3], A. A. Belik[4], J. Kortus[1]

[1]Institute of Theoretical Physics, TU Bergakademie Freiberg, D-09596 Freiberg, Germany
[2]Zentrum für Innovationskompetenz SiLi-nano, Martin-Luther-Universität Halle-Wittenberg, D-06120 Halle (Saale), Germany
[3]Institut für Physik, Martin-Luther-Universität Halle-Wittenberg, D-06120 Halle (Saale), Germany
[4]International Center for Materials Nanoarchitectonics (WPI-MANA), National Institute for Materials Science (NIMS), Namiki 1-1, Ibaraki, Tsukuba 305-0044, Japan

Raman spectroscopy became a well-established method for studying the lattice dynamics in the class of oxides with perovskite structures and can be used to follow the

temperature induced phase transitions in these material systems. In this presentation the temperature dependence of the Raman spectra of $BiFe_xCr_{1-x}O_3$ is shown and compared with the spectra of the parents compounds $BiCrO_3$ [1] and $BiFeO_3$ [2]. Except for the different temperature behaviour, in the $BiFe_xCr_{1-x}O_3$ system a new Raman mode at ~670 cm^{-1} with a strong intensity dependence on the excitation line was detected [3]. For this Raman mode, a resonant activation of the higher order scattering was found and explained in the frame of Franck–Condon mechanism. The Raman spectra measured with different excitation lines for a sample with a stoichiometry of x=0.7 is presented in Fig.1 in comparison to the spectra of $BiCrO_3$ and $BiFeO_3$.

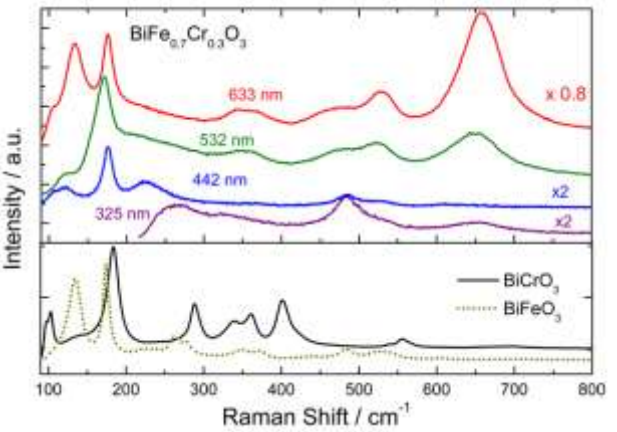

Fig. 1. Raman spectra of a $BiFe_{0.7}Cr_{0.3}O_3$ sample measured for different excitations lines, in comparison to the spectra of the parent $BiFeO_3$ and $BiCrO_3$ compounds measured with 633 nm excitation.

The mode can be attributed to an oxygen (octahedral) breathing vibration being mediated by the charge transfer between the Fe and Cr ions. In the case of $BiFe_{0.5}Cr_{0.5}O_3$ an optical absorption peak at ~2.27 eV, was measured by

ellipsometry. This absorption peak, which is absent in the parent compounds, lowers the bandgap of $BiFe_{0.5}Cr_{0.5}O_3$ to 2.07 eV, in comparison to the bandgap values of 2.95 eV for $BiCrO_3$ or 2.8 eV for $BiFeO_3$. Due to the lower bandgap and its extended absorption of the solar spectrum, $BiFe_xCr_{1-x}O_3$ is promising material in the field of photovoltaic applications.

[1] C. Himcinschi, I Vrejoiu, T Weißbach, K Vijayanandhini, A Talkenberger, C. Röder, S. Bahmann, D.R.T. Zahn, A.A. Belik, D. Rafaja, J. Kortus, J. Applied Physics **2011**, 110 (7), 073501
[2] C. Himcinschi, J. Rix, C. Röder, M. Rudolph, M.M. Yang, D Rafaja, J. Kortus, M. Alexe, Scientific Reports **2019**, 9, 379.
[3] C. Himcinschi, F. Drechsler, D.S. Walch, A. Bhatnagar, A.A. Belik, J. Kortus, Nanomaterials **2022**, 12 (9), 1607.

T9-I: Advanced materials based on electrodeposited iron group metals and alloys

N. Tsyntsaru[1,2]

[1] *Faculty of Chemistry and Geosciences, Vilnius University, Naugarduko str. 24, 03225 Vilnius, Lithuania*
[2] *Institute of Applied Physics, 5 Academiei str., 2028, Chisinau, Moldova*

Applying electrochemically deposited coatings is a convenient way to improve surface properties of a metal substrate. Electrodepositions possess the merits of low energy consumption, flexibility, convenience, and scalability, which have been considered as potential methods to acquire diverse micro-/nanostructured materials, which can provide selected functional properties. Theoretical and practical studies of the electrodeposition of iron group metals and alloys are conducted worldwide. This research is encouraged by the pronounced electrochemical, sensing, mechanical, tribological,

and magnetic properties as well as the corrosion resistance of these materials.

However, electrodeposition typically operates far from equilibrium conditions [1]. Consequently, the material obtained can show a non-equilibrium structure, which can manifest as small grain sizes and the associated large volume fraction of grain boundaries and triple junctions, as well as non-equilibrium phases. In addition, alloys produced by this method can show considerable extensions of the solid solubility range similar to what is observed in materials produced by other non-equilibrium processing routes, such as e.g. rapid solidification. The given overview will present versatile possibilities of iron group metals and alloys as multiscale materials obtained by electrodeposition, which are suitable candidates to meet many technological demands at macro-, micro- and nano-scale as coating films, composites and nanowires.

Acknowledgements: This project has received funding from the EU H2020 MSCA SMARTELECTRODES project, Nº 778357.

[1] L. A. Ricelli, B. Bozzini, C. Mele, L. D'Uzo, L. Int. J. Electrochem. Sci., **2008,** 3(4), 356-408.

T9-I-online: Elementary Reactions and Crystallographic Transformations in Shape Memory Alloys

O. Adiguzel

Firat University, Department of Physics, Elazig, Turkey

Shape memory effect is a peculiar property exhibited by a series of alloy systems, which is initiated with cooling and deformation processed, and performed thermally on heating

and cooling, with which crystal structure of materials cycle between detwinned martesnsite structure and ordered parent phase structure. Therefore, this behavior is called thermoelasticity. This phenomenon is governed by successive dual thermal induced, and stress induced martensitic transformations. Thermal induced transformation occurs along with lattice twinning on cooling and ordered parent phase structures turn into twinned martensite structure. Twinned martensite structures turn into detwinned martensite structure by means of stress induced transformation by stressing material in martensitic condition. Lattice twinning occurs with cooperative movements of atoms in two opposite directions, <110 > -type directions on the {110}-type close packed plane of austenite matrix. The twinning occurs with internal stresses, while detwinning occurs with the external stresses, and they play important role at the transformations. These alloys exhibit another property called superelasticity performed by stressing and releasing in elasticity limit at a constant temperature in parent phase region, and shape recovery is performed instantly and simultaneously upon releasing the applied stress. Although, superelasticity exhibits elastic material behavior, stress-stran profile is nonlinear at stress-strain diagram. Also, stressing and releasing paths are different, and hysteresis loops refers to the energy dissipation. These allys are used in building industry with these properties, against seismic events. Superelasticity is also a result of stress induced martensitic transformation and ordered parent phase structures turn into the detwinned structures with stressing. Also, crystal structure of materials cycle between detwinned martesnsite structure and ordered parent phase structure on stressing and

releasing. Copper based alloys exhibit this property in metastable β-phase region. Lattice twinning is not uniform in these alloys, and the ordered parent phase structures martensitically undergo the the non-conventional complex layered structures. In the present contribution, x-ray diffraction and transmission electron microscope studies were carried out on copper based CuZnAl and CuAlMn alloys. These alloy samples have been heat treated for homogenization in the β-phase fields and quenched in iced brine and aged at room temperature. X-ray diffraction profiles and electron diffraction patterns exhibit super lattice reflections inherited from parent phase. X-ray diffractograms taken in a long-time interval show that diffraction angles and intensities of diffraction peaks change with the aging time at room temperature, and this result refers to rearrangement of atoms in diffusive manner.

T2-O: On the impossibility of ionic oscillations in laser produced plasmas

S. A. Irimiciuc[1], R. Udrea[2], P. Garoi[1], D. Craciun[1], V. Craciun[1,3]

[1]*INFLPR, 409 Atomistilor street, Magurele, RO-077125, ROMANIA*
[2] *Physics Faculty, University of Bucharest, Bucharest-Magurele, Romania*
[3]*Extreme Light Infrastructure for Nuclear Physics, Romania*

Recent developments in the newly developed high-power system from ELI-NP have been closely related to the intense research on providing the adequate characterization/diagnostic tools to ensure the correct performance of all adjacent systems. One of the core drawbacks which was identified while using these high-power laser systems is the relatively short life-time of optical

components due to damage and stress induced by the laser beam-mirror interaction. the ability to have a real time feedback loop from the beam line becomes mandatory as structural and functional changes should be signaled before permanent damage is induced. Permanent damage on the optical components is defined as observable post-ablation at surface level, and thus the ablation threshold is a clear, quantifiable limit of these component.

The aim of this work is centered on developing based on an electrical diagnostic system a flexible, in situ monitoring tool for sub threshold measurements during laser matter interaction that can span fs up to ns irradiation regimes. For sub threshold ablation conditions, the pre-plasma vapor cloud which consists mostly of electrons and ions has a wide energy distribution with a wide cumulative peak defining this state. With the increase of laser fluence, fast narrow distributions are induced on the LP signal accompanied by a luminous structure, which signals the plasma ignition fluence. Analyzing the charge particle distribution as a function of the laser fluence we were able to predict the ablation threshold fluence. Further investigations provided information on the ablation mechanism involved in this fluence regime and on the properties of the ejected cloud, the so called pre-plasma state of the ablated vapor.

Our results reflect well the existing data from literature and provides an extra layer of understanding as we are able to prove the existence of an energetic plateau around the ablation threshold. The plateau strongly depends on the nature of the target and defines the fluence range where structural changes are occurring at the surface. SEM and XPS investigations of the irradiated area provided information

about the morphological and surface chemistry process induced during irradiation in the threshold range.

Acknowledgments. This work was supported by Romanian Ministry of Education and Research, under Romanian Nat. Nucleu Program LAPLAS VI –n. 16N/2019 and ELI-RO_2020_12.

Invited and Oral Session (HALL2)

T3-I: Time-dependent 3D simulation of heat and oxygen transport in Czochralski growth of silicon for PV applications

D. Vizman[1], A. Popescu[2]

[1]*Faculty of Physics, West University of Timisoara, Timisoara, Romania*
[2]*Faculty of Physics, West University of Timisoara, Timisoara, Romania*

The best conversion efficiencies of sun-light into electricity at industrial level can be obtained by mono crystalline based silicon solar cells grown by the Czochralski (CZ) method. The Cz-Si market for PV applications is expected to increase in the next years as fabrication techniques are optimized and the cost is reduced . Although, Si produced with Cz method is considered of high purity and homogeneity, there are always defects introduced during the process. In Czochralski (Cz) single-crystal growth the dissolution of the quartz crucible at high temperatures contaminates the melt with oxygen, which is then reflected in the growing ingot. The ultimate efficiency potential of each material is limited by the presence of defects and impurities, which reduce the minority carrier lifetime. Oxygen contributes to the resistivity in the form of thermal donors [1]. Therefore, the striations pattern in the crystal is a picture of how impurities (mainly phosphorous, boron and

oxygen) are incorporated through segregation in the crystals. One should also notice that the segregation process is strongly dependent by the local growth velocity (different by the pulling rate) which is strongly dependent by the temperature fluctuations in the melt. Using STHAMAS 3D software we performed extensive simulations in order to predict the temperature and impurities concentration fluctuation in the melt, induced by natural convection and forced convection due to crucible and crystal rotation in a 200mm Cz-Si process [2].

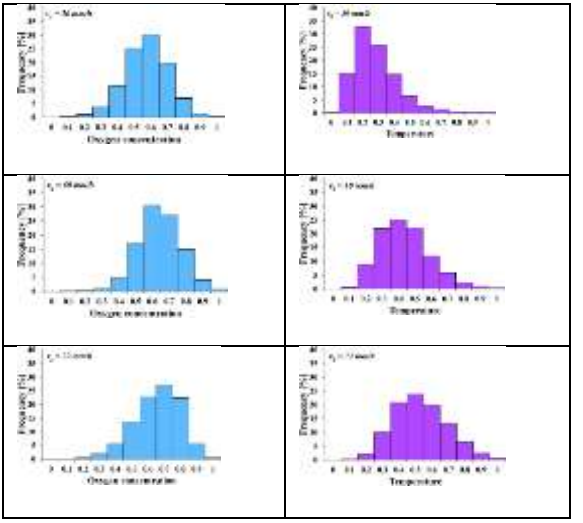

Fig. 1. Histograms of temperature and oxygen fluctuations in a monitor point under the S-L interface

In order to study the influence of crucible rotation on the temperature and oxygen concentration distribution, four crucible rotation rates were considered, 2, 4, 6 and 8 rpm. We found that melt flow behavior at the crystal axis under the S-L interface is dominated by buoyancy and is less influenced by

the increase of crucible rotation. Regarding the O-concentration distribution, it was found that the concentration has a homogeneously radial distribution under the solid-liquid interface. Also, it was concluded that by increasing the crucible rotation rate, first the level of oxygen concentration under the S-L interface decreases and, from a critical crucible rotation rate, the O-concentration increases. Looking in a monitor point under the S-L interface (figure 1), for the smallest value of the growth velocity v_g, we obtained a right skewed distribution: higher frequencies of smaller temperature values which suggest that the temperature has mostly values above the average value. Increasing the growth velocity leads to a decrease of the skewness such that for v_g = 72 mm/h we have and almost symmetric distribution.

[1] K. Wada - Physical Review B **1984**, 30, 5884
[2] A. Popescu, M. Bellmann, D. Vizman, Crystengcomm, **2021**, 23/2, 308-316.

T3-I: New trends in triphenylamine-based polymers for less-energy intensive electrochromic devices

M.D. Damaceanu, C.P. Constantin

"Petru Poni" Institute of Macromolecular Chemistry, Electroactive Polymers and Plasmochemistry Laboratory, Aleea Gr. Ghica Voda 41A, Iasi 700487, Romania

Electrochromic (EC) devices based on electroactive polymers can be regarded as viable alternatives to the conventional electrochromic devices based on inorganic materials, facing challenges like durability and versatility in electrochromic characteristics [1]. Along the years, various polymers showed appealing characteristics in electrochromism due to their

facile processability, high flexibility, reduced cost, and ability to modulate the color at potential sweep by chemical modifications. In terms of EC performance, conjugated polymers have been noticed for the high coloration efficiency, color versatility, large color contrasts, rapid response times, and low power consumption during the device operation. More importantly, many polymers can exhibit more than two redox states and generate multiple colours [2].

Polycarbazoles, polythiophenes, polypyrroles, poly(3,4-ethylenedioxythiophene)s, polyanilines and polytriphenylamines are the most commonly used conjugated polymeric materials in EC devices. Among these, polymers containing triphenylamine have been extensively applied for various electronic and optical devices due to their superior hole transporting ability and good photo- and electroactive performances [3]. For the particular case of EC polymers, triphenylamine is an attractive building block since it can endow the neutral state of polymers with absorptions in the UV region, thus allowing the development of completely colorless EC polymer films able to switch to colored films under an applied potential. In addition, triphenylamine based polymers can display tunable colors in oxidized states when structural alteration of the polymer chains is considered. The triphenylamine unit can be easily oxidized to form stable radical cations as long as the *para*-position of the phenyl rings is protected, and the oxidation process is always associated with a strong change of coloration. However, polytriphenylamines are easily oxidized under air, and it is difficult to control the EC reaction under ambient conditions. Thus, triphenylamine was mostly used in copolymers in

combination with an electron acceptor such as imide, pyridinium, anhydride, or nitrothiophene.
During the past decade, a library of high-performance polymers, typically aromatic polyamides and polyimides containing triphenylamine have been prepared and investigated in regard to their electrochromic applications [4]. Polyimides are attractive EC polymers due to their excellent mechanical properties, thermal stability, and morphological features. They belong to the class of the most heat-resistant polymers and are widely used as adhesives, photoresistors, dielectrics, nonlinear optical materials, membranes for separation, liquid crystal alignment layers, composites, electroluminescent materials, polymer electrolyte fuel cells, polymer memories, etc [5]. Along these lines, this work provides new strategies for the development of high performance EC materials based on triphenylamine-containing polyimides. Some particular investigations with regard to their opto-electronic properties are discussed along with their efficiency in EC devices.

Acknowledgements. This work was supported by a grant of the Ministry of Research, Innovation and Digitization, CNCS/CCCDI – UEFISCDI Romania, project PN-III-P2-2.1-PED-2019-3520, contract no. 438PED/01.11.2020, within PNCDI III.

[1] V. Rai, R. S. Singh, D. J. Blackwood, D. Zhili, Adv. Eng. Mater. **2020,** 22, 2000082.
[2] T. Abidin, Q. Zhang, K. L. Wang, D.J Liaw, Polymer **2014,** 55, 5293-5304.
[3] H. Wang, M. Barrett, B. Duane, J. Gu, F. Zenhausern, Mater. Sci. Eng. B **2018**, 228, 167-174.
[4] H.J. Yen, G. S. Liou, Polym. Chem. **2018**, 9, 3001-3018.

[5] A. S. Hicyilmaz, A. C. Bedeloglu, SN Applied Sciences **2021,** 3, 363

T7-O: Flexible films based on semiaromatic copolyimides for energy storage applications

I. Butnaru, A. P. Chiriac, M. D. Damaceanu

"Petru Poni" Institute of Macromolecular Chemistry, Electroactive Polymers and Plasmochemistry Laboratory, 41A Grigore Ghica Voda Alley, Iasi, Romania

The field of non-rigid electronics represents an attractive research topic that registered an accelerated development due to the stringent demands of the industry [1]. Energy devices must follow the same trend by replacing its bulk and rigid support into a portable, flexible/stretchable shape. Although new types of electronic devices on non-rigid substrates were introduced on the market, their benefits are somewhat limited because they are still manufactured on rigid supports having few non-rigid components [2,3]. In order to be used as reliable power sources, energy-storage devices need to provide stable and persistent electricity output, to maintain adequate performances under various deformations such as bending, twisting and stretching.

On the other hand, the successful development of materials simultaneously endowed with high dielectric constant, low dissipation factor, strong mechanical properties, high breakdown strength, as well as high temperature resistance is still a demanding task [4,5]. The struggle to obtain polymer film capacitors for higher temperature applications is a continuous challenge due to a series of requirements which include good processability and self-clearing capability along

with high dielectric permittivity, thermal conductivity and dielectric breakdown strength. When an additional criteria of high power performance is imposed, the materials used in capacitor dielectrics may lack in achieving the overall properties.

Polyimide is known as one of the most successful dielectric material for such applications due to the advantageous combination of thermal, chemical and mechanical stabilities. Although there are some polyimide structures that can fulfil some of the above requests, it is challenging to attain all at the same time and always a trade-off should be considered.

Here we report on the synthesis of a series of copolyimides incorporating both soft and hard segments by using nitrile-containing aromatic diamines in combination with an aliphatic diamine and a carbonyl-containing aromatic dianhydride. This strategy enabled the formation of thermostable copolyimides with unprecedented high-k values and excellent stretchability and toughness that may open new perspectives in using polyimides as dielectrics in stretchable electronics.

Acknowledgements. This work was supported by a grant of the Ministry of Research, Innovation and Digitization, CNCS/CCCDI – UEFISCDI Romania, project no. PN-III-P1-1.1-TE-2021-1110, contract no. TE 83/2022, within PNCDI III.

[1] S.A. Bozorgavari, J. Aghaei, S. Pirouzi, A. Nikoobakht, H. Farahmand, M. Korpas, Renew. Sust. Energ. Rev. **2020**, 123, 109739.

[2] J. A. Rogers, T. Someya, Y. Huang, Science **2010**, 327, 1603–1607.

[3] C. Tuloup, W. Harizi, Z. Aboura, Y. Meyer, K. Khellil, R. Lachat, Compos. Struct. **2019**, 215, 127–149.

[4] S. Ho, S. G. Greenbaum, ACS Appl. Mater. Interfaces **2018**, 10, 29189-29218.
[5] J. Ho, M. Schroeder, in Polyimide for Electronic and Electrical Engineering Applications, ed. S. Diaham, IntechOpen, **2020**, DOI: 10.5772/intechopen.92643.

T7-O-online: An efficient, eco-friendly and sustainable one-pot synthesis of a new fluorinated aromatic polyester

A. Nan, T. Radu, X. Filip, M. Dan

National Institute for Research and Development of Isotopic and Molecular Technologies, 67-103 Donat Str., 400293 Cluj-Napoca, Romania

Fluorinated polymers are a niche of polymers that play an integral role in modern life. Mainly due to the properties of fluorine (including, among others, large electronegativity, low polarizability, and small van der Waals radius (1.32 Å)) and the strong C−F bonds (485 $kJ \cdot mol^{-1}$), they exhibit unique and outstanding attributes. Their applications span engineering thermoplastics and high-performance elastomers, weatherproof coatings, automotive and aeronautics industries, biomedical materials, membranes for use in Li-ion batteries, fuel cells, and many more [1-7]. The synthesis of fluorinated polyesters is difficult for a variety of reasons. For example, as a result of their instability, fluorinated polyesters that were prepared from perfluorinated acids have not been used as polyurethane prepolymers. In this work, we illustrate the synthesis, characterization and few properties of a new fluorinated aromatic polyester.
Poly(fluoromandelic acid) (PFMA) is a new polymer with multiple fluorine atoms on the polymer chain. Simple heating of 4-fluoromandelic acid without using a solvent or a catalyst

under controlled conditions leads to poly(fluoromandelic acid). The reaction runs in the solid state by the elimination of water. The resulting poly(fluoromandelic acid) configuration consists mainly of polyester moieties decorated with fluorine atoms and carboxyl and hydroxyl groups at the end of the polymer chain. The structure of the polymer chain was elucidated by mass spectrometry, solid-state ^{13}C nuclear magnetic resonance (^{13}C CP-MAS-NMR) and Fourier-transform infrared spectroscopy (FTIR). The thermal properties of the polymer were also evaluated using a thermal conductivity test and thermogravimetric analysis. In the case of poly(fluoromandelic acid), the thermal conductivities were measured by the transient plane source (TPS) technique, also referred to as the Hot Disk method. The thermal conductivity measured at different temperatures will also be discussed in relation to the structure of the analyzed polymer as correlated with the crystallinity degree of the polymer structure determined by powder XRD diffraction. The new fluorinated polyester exhibited also remarkable hydrophobicity.

Acknowledgements. This work was supported by a grant from the Ministry of Research, Innovation and Digitization, CNCS/CCCDI – UEFISCDI, project number PN-III-P4-ID-PCE-2020-1595, within PNCDI III.

[1] S. Ebnesajjad, Expanded PTFE Applications Handbook: Technology, Manufacturing and Applications; Elsevier Science: Norwich, NY, **2016**.
[2] J. Gardiner, Aust. J. Chem., **2015**, 68, 13−22.
[3] B. Ameduri, Chem. Rev. **2009**, 109, 6632−6686.
[4] F. Boschet, B. Ameduri, Chem. Rev. **2014**, 114, 927−980.
[5] J. Zhao, X. Wang, L. Liu, J. Yu, B. Ding, ACS Appl. Mater. Interfaces **2018**, 10, 30887-30894.

[6] Y. Zhang, T.T. Li, B.C. Shiu, F. Sun, H.T. Ren, X. Zhang, C.W. Lou, J.H. J. Lin, Clean. Prod. **2021**, 282, 124455.
[7] H. Holmquist, S. Schellenberger, I.V.D. Veen, G.M. Peters, I.T. Cousins, Environ. Int. **2016**, 91, 251–264.

T7-O-online: Characteristics of dielectric elastomers containing metal complexes as fillers

A. Soroceanu

Inorganic Polymers Department, "Petru Poni" Institute of Macromolecular Chemistry Iasi, Romania

High energy density, rapid response times, a low Young's modulus, and a high breaking strain value are all characteristics of silicone-based dielectric elastomer materials, which are sensitive polymeric materials used in actuation and energy harvesting. Further, advantages of silicone-based materials include chemical and structural stability under a variety of technical and environmental circumstances, such as temperature, humidity, and the electrical frequency of the applied energy.
The above discussion focuses on changes in the mechanical and dielectric properties of dielectric elastomers formed from reactions between polymers of different molecular weights of polydimethylsiloxane and Schiff-base metal complexes produced from condensation reactions of 1,3-bis(aminopropyl)tetramethyldisiloxane and 3,5-di-bromo-2-hydroxybenzaldehyde. All the results demonstrate how the molecular weight of a silicone polymer affects its mechanical and electrical characteristics, and they can be used to select silicones with the best molecular weight for particular applications based on the desired ratio of mechanical strain,

dielectric constant, strength and conductivity, and water vapor sorption. Because they have an organosiloxane chain in a metal complex structure that enables silicone matrix empathy, the fillers used are clearly recognizable.

Acknowledgements**.** This work was supported by a grant of the Ministry of National Education, CNCS – UEFISCDI, project number PN-III-P1-1.1-PD-2021-0687 (Contract 33/2022).

Invited and Oral Session (HALL 1)

T4-I: Soft magnetic composite powders and compacts obtained by mechanosynthesis and spark plasma sintering

I. Chicinas[1], T.F. Marinca[1], F. Popa[1], B.V. Neamtu[1], L. Cotojman[1], O. Isnard[2]

[1]Department of Materials Science and Engineering, Technical University of Cluj-Napoca, Cluj-Napoca, Romania
[2] Institut Néel, CNRS / Université Grenoble-Alpes, BP166, 38042 Grenoble, Cédex 9, France

High magnetic properties (magnetic flux density and magnetic permeability) and high electrical resistivity are required in many AC applications for magnetic cores, in order to reduce core losses. Usually, magnetic alloys based on Fe powder are coated with a thin dielectric, organic or inorganic layer [1]. To avoid the decrease in the magnetic properties of the material by the dielectric layer, we use a magnetic dielectric layer which consists of a layer of soft magnetic ferrite particles with the nanometric size, in order to electrically isolate the metal particles from each other [2].

The nanocrystalline Permalloy/Supermalloy powders were obtained by mechanical alloying in high planetary ball mill Fritsch Pulverisette 6. The milling time was up to 12 h and the mean crystallite size was 18-20 nm. In Fe-Ni@$Me_1Me_2Fe_2O_4$ composite powders, the core is a large metal particle (Fe or nickel-iron alloy) and the shell is a pseudo-continuous layer of nanometric soft magnetic ferrite particles ($NiFe_2O_4$, $Ni_{0.5}Zn_{0,5}Fe_2O_4$, $Mn_{0.5}Zn_{0.5}Fe_2O_4$, $Ni_{0.5}Cu_{0.5}Fe_2O_4$). Composite particles with a pseudo-core-shell structure were prepared using acetone as the surfactant by mixing metal particles with very small particles of ferrite and subsequent annealing to argon.

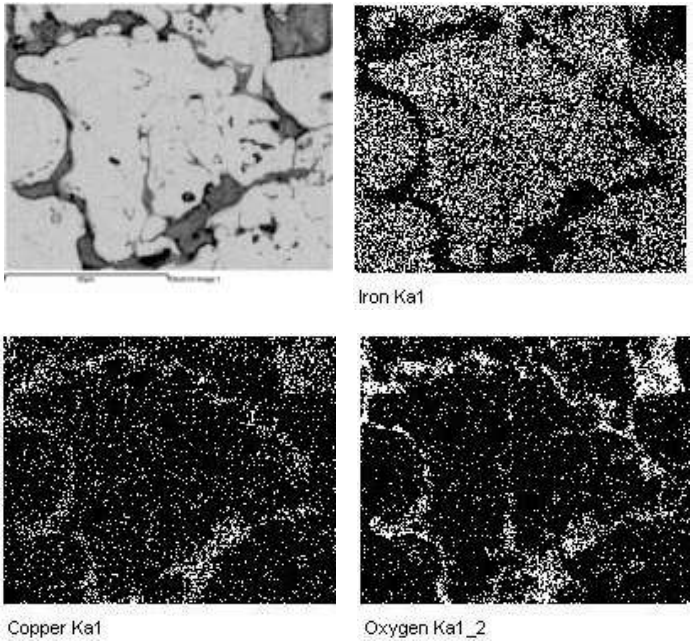

Figure 1 : SEM image on a section of SMC core and maps of distribution of Fe, Cu and O (EDX analysis)

The pseudo core-shell powders thus obtained were compacted by spark plasma sintering (400 ° C - 900 ° C, 30 MPa, 0 - 10 minutes).
The powders and sintered compacts were studied by: X-ray diffraction, in-situ high-temperature X-ray diffraction, scanning electron microscopy, energy dispersive X-ray spectrometry, magnetic hysteresis measurements (M (H) and B (H)) and electrical resistivity. In Fig. 1 can be observed that the alloy particles are surrounded by a pseudo-continuous layer of ferrite. A relative permeability of 75 at B = 0.7 T and 10 kHz was obtained for $Fe/CuFe_2O_4$ core. The electrical resistivity of SPS-ed composite cores is 3 to 4 orders of magnitude higher than the electrical resistivity of Fe-Si alloys.

[1] Robert W. Ward, David E. Gay, Composite iron material, US Patent No. 5,211,896/May 18, **1993**
[2] T.F. Marinca, B.V. Neamţu, F. Popa, V.F. Tarţa, P. Pascuta, A.F. Takacs, I. Chicinaş, , Appl. Surf. Sci. **2013,** 285P, 2– 9.

T4-I: The influence of Ni^{2+} and Co^{2+} ions doping on the magnetic properties of the $MnFe_2O_4/SiO_2$ nanocompozites

T. Dippong[1], R. Tetean[2], I. G. Deac[2]

[1] *Department of Chemistry and Biology, Technical University of Cluj-Napoca, North University Center of Baia-Mare, Romania*
[2] *Facultatea de Fizica, Universitatea Babes-Bolyai, Cluj-Napoca, Romania*

We report on the influence of Ni^{2+} and Co^{2+} ions doping on the magnetic properties of the $MnFe_2O_4/SiO_2$ nanocompozites, obtained by various inovative routes. Saturation magnetization (M_S), remanent magnetization (M_R), squareness (S), coercivity (H_C), magnetic moment per formula unit (n_B) and anisotropy constant (K) were determined since they are key

parameters for a magnetic material to be used in various applications. X-ray diffraction (XRD) indicated the presence of nanocrystalline mixed cubic spinel ferrites in the presence of several secondary phases. The crystallite sizes varie with the increase of the annealing temperature and with Ni and Co content. The shape of the hysteresis loops revealed the dependence of magnetic behavior on the structural properties. The saturation magnetization and coercivity increase with the degree of crystallinity, crystallite size and annealing temperature for the both Ni and Co containing systems. The coercive field behaves differently for different heat treatment temperatures, increasing for 800 C and decreasing for 1200 C with increasing Mn content.

The Ni-rich nanocomposites show superparamagnetic-like behavior, while the Mn-rich nanocomposites have paramagnetic behavior. For the Ni containing samples, the main magnetic parameters M_S, M_R, n_B and K increase, while H_c decreases with increasing Ni content. NCs annealed at 1200 ^oC have increased Ms (16.0-45.8 emu/g), M_R (4.5-16.8 emu/g), and K (2.876-5.430 erg/dm^3). The H_c (265-175 Oe), decreases with increasing Ni content at 1200 ^oC [1]. The different behavior of these samples from the un-coated Mn(Ni;Co)Fe_2O_4 particles came from the SiO_2 matrix and from the preparation routes [2].

For the Co doping samples, for 800 ^oC heat treatment temperature, M_S increase from 19.4 emu/g to 38.2 emu/g and K from 0.365 to $1.32 \cdot 10^{-3}$ erg/cm^{-1} while for 1200 ^oC M_S decreases from 32.6 emu/g at 18.3 emu/g. When Mn is replaced by Co the behavior is ferromagnetic-like for both low and high Co ions concentration. The magnetic properties were discussed in the frame of the collinear two-sublattices Néel's

theory and of the non-collinear Yafet-Kittel model considering the presence of hematite and some other parasitic phases [1,2].

[1] T. Dippong**,** I.G. Deac, O. Cadar, E.A. Levei, Nanomaterials **2021**, 11, 3455.
[2] T. Dippong**,** M.D. Lazar, I.G. Deac, P. Palade, I. Petean, G. Borodi, O. Cadar, J. Alloys Compd. **2022,** 895, 162715.

T4-I: Smart electronic devices based on molecular spin crossover compounds

A. Diaconu[1], R. Cimpan[1], G.-V. Ciobanu[1], L. Salmon[2], G. Molnar[2], A. Bousseksou[2], I. Seguy[3], A. Rotaru[1]

[1]FIESC & Research Center MANSiD, USV, Suceava, Romania
[2] LCC, CNRS & Université de Toulouse (UPS, INP), Toulouse 31013, France
[3]LAAS, CNRS & Université de Toulouse INSA, UPS F-31077 Toulouse, France

Bistable molecular complexes that can exist in two interchangeable states can act as switches under external stimuli. In this context, molecular spin crossover (SCO) compounds present a special interest due to their response to various external stimuli that might lead to a wide range of potential applications [1].
This research highlights the spin transition properties of spin crossover complexes in various forms such as powder, thin films and polymeric composites. We focused on the spin crossover complex with the chemical formula $[Fe(Htrz)_2(Trz)]BF_4$. This complex shows a spin transition above room temperature, with a large hysteresis, wich can be monitored by various detection techniques such as: magnetometry, dielectric spectroscopy, optical reflectivity etc. [2]. One important particularity of this system entails the spin

state dependence of the electrical conductivity which opens new opportunities tu use these materials in electronic and spintronic devices.

Thin films showing spin transition properties have been obtained by thermal evaporation. The SCO thin films have been integrated into both magnetic and non-magnetic metallic electrodes. The structures obtained with magnetic electrodes shows a magnetoresistive effect.

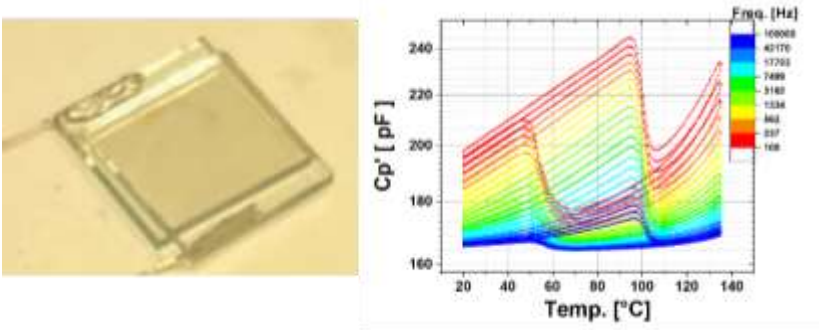

Fig. 1. (Left) SCO-PVP composite between two ITO electrodes and (Right) Temperature dependence of the capacitance.

The composites containing $[Fe(Htrz)_2(Trz)]BF_4$ nanoparticles incorporated in PVP (Polyvinylpyrrolidone) matrix have been synthesized and studied by various techniques such as FE-SEM, EDX, AFM, dielectric spectroscopy, magnetometry, Raman, FTIR. The obtained composites are optically transparents preserving the spin transition properties.

Acknowledgments. This work was funded by UEFISCDI, project number PN-III-P1-1.1-TE-2019-2194 (Contract No: TE 123/2020).

[1] A. Enriquez-Cabrera, et al., Coord. Chem. Rev., **2020,** 419, 213396

[2] A. Diaconu, et al., J. Phys. Chem. Lett., **2017**, 8, 3147-3151.

[3] C. Lefter, et al., Adv. Mater., **2016,** 28, 7508-7514.

T4-I: A revision of Kittel's theory for ferromagnetic domains

C. M. Teodorescu

National Institute of Materials Physics, Atomiștilor 405A, Măgurele – Ilfov, Romania

Kittel's model for ferromagnetic domains [1,2] starts with a infinite sample extent over two directions and with and a finite thickness d, though much larger than the typical domain size l, the domains being also infinite over the other in-plane direction. The surface magnetostatic energy density scales with ${M_0}^2 l$ ($\pm M_0$ being the magnetization of the domains) and the energy corresponding to 180° domain walls scales with $w_{wall} d/l$, where w_{wall} is the wall energy per unit area of the wall and it comprizes the uniaxial magnetic anisotropy constant K_v, the exchange interaction between neighboring atoms J and the interatomic distance a, $w_{wall} \propto (JK_v/a)^{1/2}$. By minimizing the total energy, one derives Kittel's scaling law of the domain size vs. the sample thickness $l \propto d^{1/2}$. Here we re-visit Kittel's theory of ferromagnetic domains, because in particular in Ref. [1], Kittel computes the average value of the square of the intensity of the magnetic field, $\langle \int H^2 dz \rangle$, while in Ref. [2] the scalar product between the magnetization and the intensity of the magnetic field $\langle - \int \boldsymbol{H} \cdot \boldsymbol{M} dz \rangle$ is computed. One needs to take into account the dipolar interaction energy, responsible for the shape anisotropy.

Some values derived by Kittel must be corrected, but the most important fact is that the magnetostatic volume density energy has to be written as [3]: $w = (\boldsymbol{B} \cdot \boldsymbol{H})/2 = (\mu_0 H^2)/2 +$

$(\mu_0 \boldsymbol{M} \cdot \boldsymbol{H})/2$. This means that one has to consider the energy from Ref. [1] with the energy from Ref. [2] with minus sign, thus in the approximation $l \ll d$ the total magnetostatic energy yields zero value! This finding requires a more detailed derivation of the magnetostatic energy. This can be easily achieved if one considers all solutions for the intensity of the magnetic field inside and outside the sample. An important parameter with dimensions of distance comprises the magnetic anisotropy energy, the exchange integral, the spin of one atom S and the interatomic distance a $d_0 = \pi^3(2JK_v a^{11})^{1/2}/(32S\mu_0{\mu_B}^2)$, where it was supposed that $M_0 \approx 2S\mu_B a^{-3}$, i. e. one spin S carries a magnetic moment $2S\mu_B$ (μ_B is the Bohr magneton), the gyromagnetic factor is 2 and this magnetic moment corresponds to a volume a^3 of the sample. This parameter has the value of about 0.8 nm for $a \approx 2.5$ Å, $J \approx 10$ meV , $K_v \approx 2$ μeV/atom , $S \approx 1$. For $d \lesssim d_0$, the minimization of the energy yields the validity of Kittel's scaling law, whereas for $d \gtrsim d_0$ the dependence $l(d)$ is almost linear. The same is obtained when the dipole-dipole interactions are included. On the other hand, experimental data on samples with perpendicular magnetocrystalline anisotropy [4] reported the validity of Kittel's scaling law up to sample thicknesses of hundreds of nanometers or even some micrometers. This means that the d_0 parameter is in the same range, which implies that the magnetic anisotropy energy is of some meV/atom. This is in line with theoretical previsions, where the magnetic anisotropy energy is in the range of the spin-orbit interaction [5].

In this case, the Stoner-Wohlfarth model fails to describe the hysteresis cycle of most solids. The coercive field should be in the range of $2K_v/M_0$, yielding tens of Tesla. The Curie-Weiss

mean field theory also fails to explain the coercive field in ferromagnets, its order of magnitude being of $J\eta S/\mu_B$, hundreds of Tesla for usual systems.

Kittel's model was adapted in the case of successive ferromagnetic domains with alternating sizes. Hysteresis cycles are derived in several hypotheses, by considering or not the dipolar interaction, or assuming or not the domain average size dependence on the applied field. Some models are able to predict non-rectangular hysteresis cycles with shapes quite similar to experimental ones [4,6], but the smallest coercive field is in the range of $\mu_0 M_0/4$ (μ_0 is the vacuum permeability) which is still too elevated with respect to experimental values (it yields some Tesla). Therefore none of the three basic models (Curie-Weiss mean field theory, Stoner-Wohlfarth theory of magnetization rotation in small magnetic nanoparticles, domain wall migration theory) is able to predict the small values observed in the coercive fields of most ferromagnetic materials. Band ferromagnetism could offer an explanation for the smallness of coercive fields [7].

The actual theory is discussed also for the case of ferroelectrics.

[1] C. Kittel, Phys. Rev. **1946**, 70, 965–971.

[2] C. Kittel, Rev. Mod. Phys.**1949**, 21, 541–583.

[3] J.D. Jackson, Classical Electrodynamics, Third Edition, Wiley, Hoboken, **1999**.

[4] O. de Abril, M. del Carmen Sáchez, C. Aroca, J. Appl. Phys. **2006**, 100, 063904.

[5] G. van der Laan, J. Phys. Cond. Matt. **1998**, 10, 3239–3253.

[6] L.-C. Garnier, M. Marangolo, M. Eddrief, D. Bisero, S. Fin, F. Casoli, M.G. Pini, A. Rettori, S. Tacchi, J. Phys.: Materials **2020**, 3, 024001.

[7] C.M. Teodorescu, Res. Phys. **2021**, 25, 104241.

T4-O-online: Spin current transport in multifunctional Pt/FeV_2O_4 heterostructures

A. Pena Corredor[1], A. Anadon[2], S. Petit-Watelot[2], J. C. Rojas-Sanchez[2], N. Viart[1], D. Preziosi[1], C. Lefevre[1]

[1]Institute of Physics and Chemistry of Materials of Strasbourg (University of Strasbourg). Strasbourg, France
[2]Jean-Lamour Institute (University of Lorraine). Nancy, France.

Iron vanadate, FeV_2O_4 (FVO), is a strongly correlated oxide which displays low-temperature ferrimagnetism [1], ferroelectricity [2] and multiferroism [3]. The material presents a strong spin-orbit coupling and both Fe^{2+} and V^{3+} cations are Jahn-Teller active. As a result, FVO adopts different crystal structures with varying temperatures, which are associated to different orbital orderings [4]. We have shown the possibility to grow epitaxial FVO films using a low Ar pressure [5], [6]. FVO films onto $SrTiO_3$ (STO) single crystals present a perpendicular magnetic anisotropy, providing a promising platform for spintronics studies.

In the present work, we have grown Pt/FVO//STO heterostructures via pulsed laser deposition and engineered Hall bar geometries (Fig. 1a) via optical lithography. Angle-dependent magnetotransport measurements in both Spin Magnetoresistance (SMR) and Anisotropy Magnetoresistance (AMR) configurations have been carried out at several magnetic field and temperature values. The amplitude of the magnetotransport signals within temperature varies as FVO changes its structure and orbital ordering, showing thus a strong interaction between Pt and the FVO underneath. SMR

was detected at all temperatures, even above the magnetic transition, and was found significantly larger (>1%) than that of better-known Pt/YIG heterostructures (≈0.1%) [7], other spinel-based systems (Pt/Fe_3O_4, ≈0.2%) [8] or other multifunctional oxides ($Pt/Ga_{0.6}Fe_{1.4}O_3$, ≈0.04) [9]. Additionally, our SMR and AMR measurements show an unusual unidirectional-like (Fig. 1b) behaviour – difference between 0º and 180º – whose underneath microscopic mechanism might be linked to the presence of a non-zero spin-orbit coupling in FVO. The observed giant SMR signal in high-quality Pt/FVO heterostructures opens the door to spinel iron vanadates as promising material platform for the next generation of oxide-based spintronics.

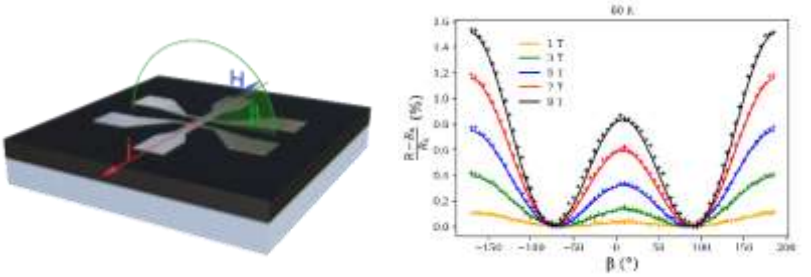

Fig. 1. (1a - left) Hall Bar lithographed on Pt/FVO/STO. (1b - right) angle scan for the caracterisation of the Spin Magnetoresistance.

[1] G. J. MacDougall, et al. Phys. Rev. B, **2012**, 86, 6, 060414.
[2]K.-H. Zhao, et al. Chinese Phys. Lett., **2015**, 32, 8, 087503.
[3]M. V. Eremin et al. Phys. Rev. B, **2019**, 100, 14, 140404.
[4]W. Xie et al. J of Appl. Phys., **2019**, 26, 24, 244904.
[5]F. Roulland et al. Materials Chemistry and Physics, **2022**, 276, 125360.
[6]A. Pena Corredor et al. J Appl Crystallogr, 2022, 55, 3, 526-532.
[7]M. Althammer et al., Phys. Rev. B, **2013**, 87, 22, 224401.

[8]Z. Ding et al. Phys. Rev. B, 2014, 90, 13, 134424.
[9]S. Homkar et al. ACS Appl. Electron. Mater., 2021, 3, 10, 4433-4440.

Invited and Oral Session (HALL 2)

T8-I: New biocomposites from waste materials

S. Cinta Pinzaru[1,2], G. Lazar[1,2], F. Nekvapil[1,2], R. Hirian[1], T. Tamas[3], L. Barbu-Tudoran[4,5] M. Suciu[4,5], M. Aluas[1], I. Bajama[1,2], D. A. Dumitru[1,2], S. Tomsic[6], B. Glamuzina[6]

[1]*Ioan Ursu Institute, Babes Bolyai University, Kogalniceanu 1, RO-400084 Cluj-Napoca, Romania*
[2]*RDI Institute in Applied Natural Science, Babes-Bolyai University, Fântânele 30, 400327, Cluj-Napoca, Romania*
[3]*Department of Geology, Babeş-Bolyai University, 1 Kogălniceanu, 400084 Cluj-Napoca, Romania*
[4] *Electron Microscopy Centre, Babeș-Bolyai University, Clinicilor 5-7, 400006 Cluj-Napoca, Romania*
[5]*Advanced Research and Technology Center for Alternative Energy, National Institute for Research and Development of Isotopic and Molecular Technologies, Donat 67-103, 400293 Cluj-Napoca, Romania*
[6]*Applied Ecology Department, University of Dubrovnik, Cira CariCa 4, 20 000, Dubrovnik, Croatia*

Our latest research results and outlook will be summarized to reveal amazing facets and properties of several biomaterials of aquatic, biogenic, origin. Their processing and reuse as added-value products such as new composites, new biostimulans, innovative drug carriers [1,2] will be highlighted (Fig. 1). The potential of such abundant materials for blue bioeconomy will be discussed. Formulations with improved biocompatibility and antioxidant character relying on organic-inorganic composite will be illustrated for new drug carriers or

innovative biostimulants for slow release. Along the processing steps to obtain, refine, load porous materials with certain solutions and tableting or pelleting, the composite materials are investigated using non-destructive Raman spectroscopy-based methods in conjunction with imaging and complemenary techniques, such as XRD, SEM-EDX and others.

Fig. 1. Graphical sketch of knowledge-based transforming waste biogenic materials into added-value products following the blue bioeconomy principle.

We further show how the translational research could turn biogenic wasted materials in added-value by-products such as smart materials for solutions loading and slow delivery, selective absorbents, smart bio-fertilizers or photonic materials. The crucial role of the high-quality scientific data generation and their management, from handling to results dissemination, education and communication following the FAIR data principle and general pillars of open science could

contribute in building synergies across sectors as an innovation speeder of Blue Growth.

Acknowledgements**.** This work was supported by a grant of the Romanian Ministry of Education and Research, CCCDI-UEFISCDI, project nr. PN-III-P2-2.1-PED-2019-4777, acronym *BluBioSustain*.

[1] F. Nekvapil, S. C. Pinzaru, .et al. Sci. Rep., **2020**, 10, 3019.
[2] G. Lazar, S C. Pinzaru et al., *ACS Omega,* **2021**, 6, 42, 27781–27790.

T8-I: Silicone microstructuring strategy for studying microorganisms and cells-topography interaction: attachment and growth

S. Stroescu (Nistorescu)[1, 2], A. M. Negrescu[3], L. Rusen[1], A. Bonciu[1], G. Gradisteanu[4], N. Dumitrescu[1], A. Cimpean[3], V. Dinca[1]

[1]INFLPR, 409 Atomistilor street, Magurele, RO-077125, Romania
[2]University of Bucharest, Faculty of Biology, Splaiul Independentei 91-95, Bucharest, R-050095, Romania
[3]Department of Biochemistry and Molecular Biology, Faculty of Biology, University of Bucharest, 91-95 Splaiul Independenței, 050095 Bucharest, Romania.
[4]ICUB, Bucharest, Romania

Nowadays, it is known that macrophages and bacterial adhesion have been implicated with both breast implant acceptance and complications, from capsular contracture to breast implant-associated anaplastic large cell lymphoma. Therefore, understanding the relationship between implant surface texture and cellular and microbial adhesion respresent still a challenge. In the present work, we obtained and characterized 7 types of PDMS microreplicated surfaces and the macrophages and microbial attachment onto the

different types of microtopographies of silicone were examinated.

The surfaces were tested in contact with *Staphylococcus aureus* ATCC 25923 bacterial strain by visualizing the biofilm formation up to 25 days using electron microscopy. The growth of bacteria was compared using various surface textures, from smooth to linear topographies. The results of bacterial attachment on the surfaces showed that the microbial adhesion to the texturated substrates is deficient and decreased in time, also numerous cellular remains are found on parallel continuous and interrupted linear patterns, which confirms the anti-biofilm effect of the PDMS microreplicated. Furthermore, RAW 264.7 cells were exposed for 24 and 72 h to PDMS microtopographies to investigate the cell viability, morphology, proliferation and cell adhesion that provide mechanical support, determine cell shape, and allow movement of the cell surface, thereby enabling cells to migrate. Morphological observations revealed good biocompatibility with the PDMS samples. Our preliminary results show that the *in vitro* assays revealed different macrophages adherence, from cells alignment to stretching depending on the patern disposal onto the substrates. As perspective, further molecular analysis are necessary to assess their adherence nature related to the patern disposal onto the surface.

T8-O: Synthesis of magnetic nanoparticles coated with three methacrylate-type polymers obtained by SI-ATRP functionalized with methotrexate for antineoplastic activity on HeLa cells

R. Ghiarasim, S-A. Ibanescu, C.-D. Varganici, N. Simionescu, M. Pinteala

Centre of Advanced Research in Bionanoconjugates and Biopolymers, "Petru Poni" Institute of Macromolecular Chemistry, 41 A Grigore Ghica Voda Alley, 700487 Iasi, Romania

In recent decades, nanomedicine has seen a rapid evolution in terms of the development of new biofunctionalized nanostructures for applications in cancer therapy. Knowing that the majority of tumor cells overexpress folic acid receptors on their cell surface and its antagonists such as methotrexate[1-3], in this work three nanocarriers involving methotrexate were synthesized. Thus, three methacrylate type polymers (biocompatible) were grown through surface-initiated atom transfer radical polymerization (SI-ATRP) such as poly(2-hydroxyethyl methacrylate) (PHEMA) which contains a single unit of ethylene glycol per polymeric repetitive structural unit, poly(poly(ethylene glycol)methacrylate (PPEGMA6) with 6 units of ethylene glycol and poly(poly(ethylene glycol)methacrylate) (PPEGMA10) with 10 units of ethylene glycol, from the surface of the nanoparticles magnetic (biocompatible), and than methotrexate was covalently bound to the hydroxyl groups on the side chains of the three polymers. The methotrexate drug has been used due to its double action, one to target folate receptor β, which leads to the internalization of the nanoparticles and their subsequent subjection to an acidic pH leads to the release of

methotrexate inside the cell, and the second due to the fact that this compound locks dihydrofolate reductase which contributes to cell division and thus cell division is stopped. The biocompatibility of these nanocarriers was determined by testing them on the human gingival fibroblast (HGF) cell line, and the antineoplastic activity of free methotrexate compared to that bound to polymers was highlighted by tests on the HeLa cell line.

Acknowledgments. This work was supported by a grant of the Romanian Ministry of Research and Innovation, CNCS – UEFISCDI, project number PN-III-P1-1.1-TE-2019-0922, within PNCDI III.

[1] N. Nakashima-Matsushita, et al., Arthritis Rheum, 1999 42(8), 1609-1616.
[2] P. T. Wong, S. K. Choi. Int J Mol Sci. **2015**, 16(1), 1772–1790.
[3] A. Cheung, et al., Oncotarget, 2016, 7 (32), 52553.

T8-O: Multi-shell gold nanoparticles functionalized with methotrexate for targeted therapy of breast cancer

D-I. Bostiog, N. Simionescu, M. Pinteala

Centre of Advanced Research in Bionanoconjugates and Biopolymers, "Petru Poni" Institute of Macromolecular Chemistry, 700487, Iasi, Romania

Breast cancer is one of the most common types of cancer worldwide and it's psycho-social and clinical impacts are extremely high. Methotrexate (MTX) is a folic acid antagonist routinely used in cancer treatment, including breast cancer. However, when taken for a longer period, side effects of MTX such as stomatitis, mucosal ulcers, bone marrow suppression, loss of appetite, and drug-induced hepatic fibrosis and cirrhosis are observed [1]. Moreover, MTX has poor water

solubility and low permeability, suggesting the administration of higher doses, which in turn decreases its bioavailability [2].

In order to overcome these problems, new strategies should be used, combating the side effects and effectively using MTX drug for a longer period of time. In this context, targeted therapies have been on the rise in recent years and functionalized gold nanoparticles could provide new tools for personalized medicine.

The aim of this study was to develop multi-shell gold nanoparticles functionalized with MTX with potential applications in breast cancer treatment. In the first step of the synthesis, the ability of small concentrated and stable phosphine-coated gold nanoparticles to be functionalized was investigated by using tailored oligomers of poly(ethylene glycol) for covalent attachment to the surfaces of the gold nanoparticles. Subsequently, short-branched poly(ethylene-imine) moieties were coupled as the second shell, followed by methotrexate covalent binding.

The functionalized gold nanoparticles were characterized from physico-chemical point of view in order to establish the degree of functionalization at each step of the preparation. The physico-chemical characterization showed the development of stable gold nanoparticles by the emergence of surface plasmon bands at 524 nm. Dynamic light scattering measurements revealed that the hydrodynamic diameter of nanoparticles started from 50 nm for phosphine coated gold nanoparticles up to 400 nm for nanoparticles containing methotrexate.

Lastly, the cytotoxicity of the nanosystem was determined *in vitro* on normal fibroblasts and MCF-7 breast cancer cell line using the Alamar Blue assay. The functionalized nanosystems

with very low MTX concentration (1,7 μg/mL) showed a cytotoxic trend in MCF-7 breast cancer cell line, but not in normal fibroblasts, compared to free MTX.
In conclusion, multi-shell gold nanoparticles functionalized with MTX developed in this study represent potential therapeutic tools for breast cancer.

Acknowledgements. This work was supported by a grant of the Romanian Ministry of Education and Research, CNCS - UEFISCDI, project number PN-III-P4-ID-PCE-2020-1523, within PNCDI III.

[1] N. K. Garg et al., Colloids Surf. B **2016**, 146.
[2] V. Yang et al., RSC Med. Chem. **2020**, 11.

T8-O: Triangular gold nanoparticles as efficient NIR photothermal agents in biological phantoms and melanoma cells

S. Suarasan[1], A. Campu[1], A. Vulpoi[2], M. Banciu[3], S. Astilean[1,4]

[1]Nanobiophotonics and Laser Microspectroscopy Center, Interdisciplinary Research Institute in Bio-Nano-Sciences, Babes-Bolyai University, Cluj-Napoca, Romania
[2]Nanostructured Materials and Bio-Nano-Interfaces Center, Interdisciplinary Research Institute in Bio-Nano-Sciences, Babes-Bolyai University, Cluj-Napoca, Romania
[3]Department of Molecular Biology and Biotechnology, Center of Systems Biology, Biodiversity and Bioresources, Faculty of Biology and Geology, Babes-Bolyai University, Cluj-Napoca, Romania
[4]Department of Biomolecular Physics, Faculty of Physics, Babes-Bolyai University, M Kogalniceanu Str. 1, 400084 Cluj-Napoca, Romania

Efficient photothermal agents are extremely important for photothermal therapy (PTT). Gold nanoparticles (AuNPs) based PTT agents under laser irradiation absorb photon energy and convert it into heat to induce hyperthermia, which

induces cellular death. Their properties influence the photothermal conversion efficiency [1].

Here, we evaluate the light-to-heat conversion features of gold nanotriangular nanoparticles (AuNTs) with three different localized surface plasmon resonances (LSPR) in- and out- of irradiating laser resonance of 785 nm. After identical NIR irradiation conditions, the AuNTs with LSPR response in resonance with the 785 nm laser exhibit the highest photothermal conversion efficacy of 80% correlated with a temperature increase of 22 °C. The PTT performance of irradiated AuNTs was further assessed inside skin-like biological phantoms that mimic the melanoma AuNTs treated tissue and surrounding healthy tissue (Figure 1).

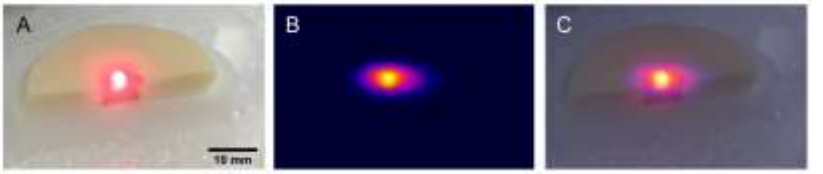

Fig. 1. A. Cross-section picture of a skin phantom with two different regions that mimic the normal and tumoral tissue treated with AuNTs, under NIR laser irradiation B. Thermal contrast image of the skin phantom after 5 min laser irradiation C. merged A and B images

Finally, the efficiency of these photothermal agents on melanoma cells PTT was validated by fluorescence staining and MTT assay performed on B16.F10 cells.

Therefore, in terms of PTT therapy, this study brings us a step forward to the understanding of the PTT effect on skin-like biological phantoms and melanoma cells, which could facilitate the AuNTs translation into clinical studies.

T8-O-online: Computational and experimental study of cysteamine capped magnetite nanoparticles (MNP@cys) stability in aqueous suspension

A. Les[1], D-E. Creanga[1], I. Motrescu[2]

[1]*Alexandru Ioan Cuza University, Iasi, Romania*
[2]*University of Life Sciences, Iasi, Romania*

Magnetite nanoparticles (MNP) functionalization represents a major challenge when designing nanomaterials for medical purposes.

We focused on the interaction of magnetite nanoparticles synthesized by chemical co-precipitation (MNP) with cysteamine based on this molecule's usefulness in biomedicine.

Cysteamine is an amino thiol compound known as radioprotector and recognized in treating cystinosis being also recommended for the treatment of Huntington's disease, Parkinson's disease, nonalcoholic fatty liver disease, malaria and cancer [1]. In the presence of transition metals – e.g. iron in our study, two phenomena occur: cysteamine oxidation and hydrogen peroxide generation [2] while magnetite could be involved in further degrading the hydrogen peroxide to hydroxyl radicals which recommend MNP@cys as an efficient and heterogeneous catalyst [3].

Computational calculations (Spartan '18 software) with DFT algorithms revealed the good kinetic stability for the chosen MNP capping agent, sustained by the similar HOMO-LUMO gap of the cysteamine molecule in gas and water, respectively. The promising reactivity of cysteamine molecule was emphasized by the increased value of the dipole moment when surrounded by water molecules.

The studies carried out by XRD (Shimadzu LabX XRD-6000 Diffractometer with a Cu Kα radiation, λ = 1.54059 Å) and SEM

(Quanta 450, FEI, ThermoScientific) showed good crystallinity and granularity of the cysteamine coated MNPs in water suspension. Raman spectroscopy (Renishaw, inVia device) was applied to analyze the binding of cysteamine to the synthesized MNP, the Raman peaks of MNP@cys being shifted (Fig. 1) in comparison to MNP and cysteamine spectrum [4].

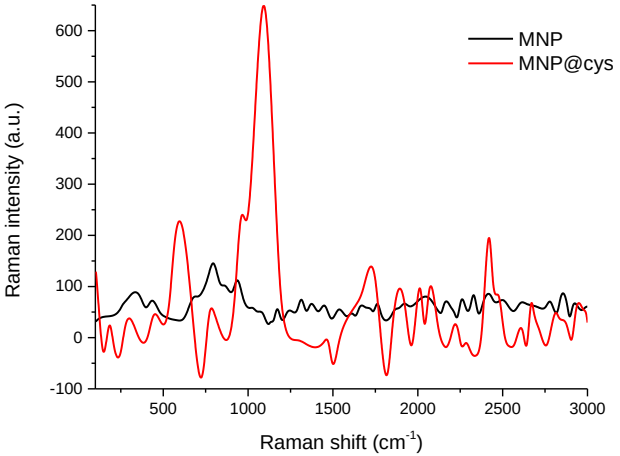

Fig. 1. Smoothed Raman spectra (processed in Origin) for MNP and MNP@cys; vibration bands for MNP@cys are shifted in comparison with the bands of pure cysteamine, available in literature.

Also, UV-vis absorption spectroscopy (Shimadzu, PharmaSpec device) analysis was done to reveal the formation of hydrogen peroxide in solution. Energy-dispersive X-ray spectroscopy (EDS) images of the MNP@cys showed they are better dispersed than pristine, uncoated MNP, that confirm the cysteamine binding and balancing the interparticle attraction forces. Further studies are planned to test the bio-toxicity of MNP@cys nanostructures in the environment where they are released finally following the use in drug delivery purpose.

[1] M. Besouw et al., Drug Discov Today, **2013**, 18(15-16), 785-92.
[2] C. Atallah et al., J. Pharm. Anal., **2020**, 10, 499-516.
[3] R. Maleki et al., 2017, Appl. Organomet. Chem., **2017**, 31(11) e3795
[4] X. Jiang et al., ACS Appl. Mater. Interfaces 2013. 5 (15) 6902–6908.

Saturday, September 10, 2022

08:00	**Plenary Session** HALL 1-University of Dubrovnik
10:20	**Coffee break**
11:50	**Plenary Session** HALL 1
12:25	**Lunch**
15:00	**Plenary Session** HALL 1
17:20	**Coffee break**
17:50	**Invited and Oral Sessions** HALL 1, HALL 2
19:30	**Dinner**

Plenary Session (HALL 1)

PL-online: A new look at metal oxides

T. Yamamoto

Materials Design Center, Kochi University of Technology, Kochi, Japan

Metal oxides are a group of materials that fulfill a wide variety of application properties or encourage evolution or development of near-future application. The applications, for example, include as follows: (1) power electronics such as high Ga_2O_3-based high-electron-mobility transistors (HEMTs) [1] and Field-effect transistors (FETs) [2] and optoelectronics such as vacuum ultraviolet (VUV) light emitter [3] and deep ultraviolet (DUV) light emitting diodes (LEDs) [4]; (2) transparent conductive electrodes for use in touch screen, LCD-TV, organic LED [5] and photovoltaic solar cells [6]; (3) Radiation resistant materials for space industry [7,8]; (4) biological and medical applications such as antibacterial agents [9,10].

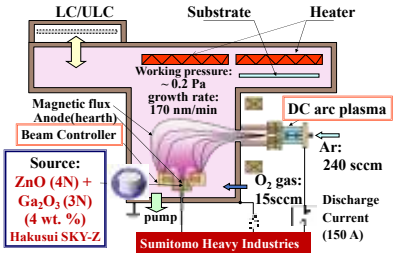

a)

b)

Fig. 1. a) A schematic diagram of reactive plasma deposition with dc arc discharge (RPD) for use of research. b) A photograph of RPD for the mass production line.

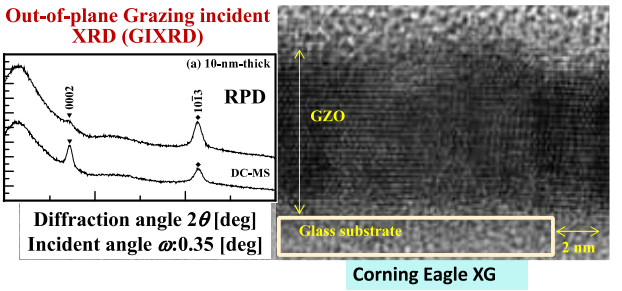

Fig. 2 (left): Out-of-plane grazing incident XRD profile of 10-nm-thick GZO films deposited by RPD and DC-magnetron sputtering as a reference. (right): cross-sectional TEM image of the above films.

I will discuss the features of metal oxides to give answers to the question below: Why metal oxides suitable for the applications?

In our group, we have been developing reactive plasma deposition with dc-arc discharge (see Fig. 1) which enables with the deposition of ZnO- and In_2O_3-based highly transparent conductive films causing the low damage to glass or polymer substrates [6,8,10]. I will make key points of materials design to meet the requirements of the applications. In addition, I will introduce the characteristics of Ga-doped ZnO (GZO) films (Fig. 2) showing the radiation resistant [8] and exhibit the specific antibacterial function [10].

[1] R. Singh et al., Mater. Sci. Semicond. **2020,** 119, 105216-1– 16.
[2] M. Higashiwaki et al., Appl. Phys. Lett. **2013,** 103, 123511-1 – 4.
[3] T. Onuma et al., Appl. Phys. Lett. **2021**, 119, 132105-1 – 5.
[4] Y-J Lu Z-F Shi, C-X Shan, D-Z. Shen, Chin. Phys. B, **2017**, 26, 047703.

[5] H. Linxiang, C. T. Sie, Mater. Sci. Eng. R Rep. **2016**, 109, 1–101.
[6] E. Kobayashi, Y. Watabe, T. Yamamoto, Y. Yamada, Sol. Energy Mater. Sol. Cells, **2016**, 149, 75–80.
[7] K. E. Sickafus et al., Sci. **2000**, 289, 748–751.
[8] C. Barone, V. Craciun, T. Yamamoto et al., Phys. Status Solid B **2021**, 2100469-1 – 5.
[9] S. V. Gudkov, et al., Front. Phys. **2021**, 9, 641481-1 –12
[10] T. Yamamoto, H. Makino, K. Shinomori, J. Jpn. Coat. Tech. Assoc. in Japanese, **2022**, 57, 44–53.

PL-online: Silicon Nano-Electro-Mechanical Resonators for Sensing and Information Processing

Y. Tsuchiya

Smart Electronic Materials and Systems (SEMS) Group, School of Electronics and Computer Science, University of Southampton, Southampton, UK

Silicon Nano-Electro-Mechanical Systems (NEMS) have been attracting considerable attention in development of modern electronics due to their exceptional features with mechanically movable objects and their friendliness with the stat-of-the-art Si nanofabrication technology [1].

Among various NEMS devices developed in recent decades, Nano-Electro-Mechanical (NEM) resonators have been investigated for ultra-sensitive mass detection [2] down to the single atom level [3]. Figure 1 (a) shows a schematic of a doubly-clamped NEM resonator and an SEM image of a suspended nanobeam, fabricated on Silicon-on-Insulator (SOI) in a CMOS-compatible manner [4,5]. A fundamental-mode resonance at 332 MHz, the highest of its kind has been shown in Fig. 1 (b) for an 800-nm-long beam [5]. Zeptogram (zg = 10^{-21}g) level mass responsivity estimated numerically for those

nanobeams [6] suggests their suitability for weighing nanoparticles.

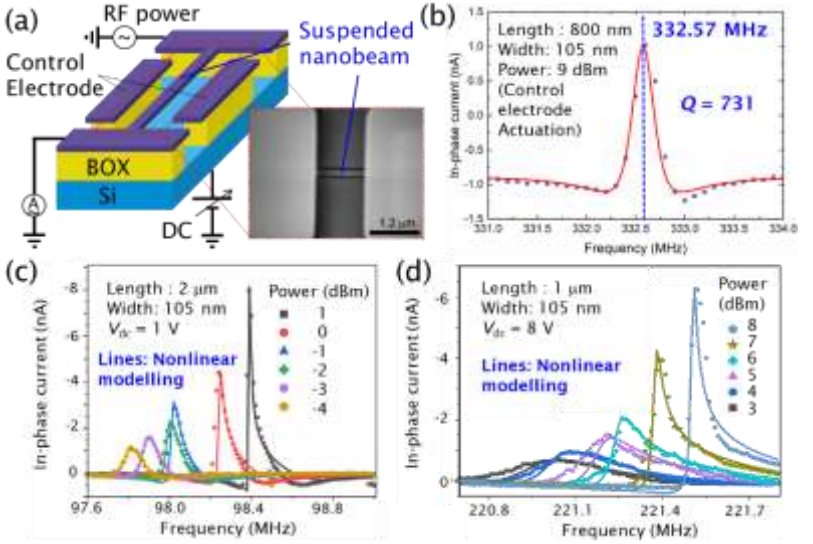

Fig. 1. (a) A schematic diagram of a Si NEM resonator with an SEM image of a suspended Si nanobeam [5]. (b) NEM resonance at 332 MHz observed for an 800-nm-long beam [5]. Nonlinear resonance characteristics of Si NEM resonators with the beam length of (c) 2 microns and (d) 1 micron are shown, respectively. The lines in (c) and (d) are drawn based on numerical solutions of a nonlinear Duffing oscillator model [8].

Integratable Si NEM resonators can be applied for coupled-oscillator-based information processing systems [7], where nonlinear characteristics of individual resonators play a key role in their neuromorphic operation. Figure 1 (c) and (d) show that the line shapes of the NEM resonances are changed from symmetric to asymmetric, and that the resonance peak positions are shifted higher with increasing the RF power for 2- and 1-micron-long beams, respectively. A series of

resonance data taken for the devices with varied beam lengths have been analysed with the Duffing equation and found well consistent between each other [8]. The analysis provides a solid basis of nonlinear NEM resonator modelling, which will be pivotal in developing large-scale integrated coupled NEM oscillator arrays in future.

[1] Y. Tsuchiya, H. Mizuta "NEMS Devices," in Nanoscale Silicon Devices, S. Oda & D. K. Ferry (Eds.), **2016**, CRC Press.
[2] K. L. Ekinci, M. L. Roukes, Rev. Sci Inst. **2005**, 76, 061101.
[3] J. Chaste et al., Nature Nanotech. **2012**, 7, 301.
[4] F. Arab Hassani, Tsuchiya et al., Sensors **2013**, 13, 9364.
[5] Y. Tsuchiya et al., IEEE MEMS **2018,** p515
[6] F. Arab Hassani, Tsuchiya et al., Microelec. Eng. **2011**, 88, 2879.
[7] G. Csaba, W. Porod, Appl. Phys. Rev. **2020**, 7, 011302.
[8] F. Ben, Y. Tsuchiya et al., IEEE MEMS **2021**, p515.

PL-online: Ultra-short laser pulses as material synthesis and lithography tool

S. Juodkazis, J. Maksimovic, D. Smith, S-H. Ng

Optical Sciences Centre, Swinburne University of Technology, Melbourne, Australia

High average power > 10W and high repetition rate ~1 MHz of ultra-short sub-1 ps lasers have become a widely available, affordable and reliable tool for material processing. We showed that average power of ultra-short lasers is increasing exponentially andfollows the Moore's law from 2000 [1]. Review of current developments in industrial applications of ultra-short lasers will be presented with focus on laser ablation, patterning, nanoscale alloying, and nano-texturing over large areas with cross sections in tens-of-centimeters.

Current strength of fs-laser processing is in the fields of micro-machining: cutting, drilling, inscribing refractive index patterns and waveguides. Flexibility of material processing for the additive and subtractive modes of micro-fabrication are demonstrated in variety of applications where different materials have to be modified, welded, joined, and alloyed. Complexity of approaches where fs-laser microfabrication is combined with other material processing steps including electron and ion beam modifications, plasma etching and stuttering, thermal post-processing further strengthens versatility of fs-laser micro-fabrication. We review recent trends in this field.

[1] M. Han, D. Smith, S.H. Ng, V. Anand, T. Katkus, S. Juodkazis, Ultra-Short-Pulse Lasers—Materials—Applications, **2021**, Eng. Proc., 11, 44.

PL-online: Single-charge tunneling functionalities in co-doped silicon nanostructures for dopant-based electronics

D. Moraru

Research Institute of Electronics, Shizuoka University, Japan

Silicon nano-electronics is rapidly advancing towards the end of the Moore's Law, as gate lengths of just a few nanometers have been already reported as feasible for transistors. In the nanostructures that act as channels in transistors or depletion layers in pn diodes, the role of dopants (impurities) becomes critical, since the transport properties will now depend only on a limited number of such dopants and/or on the random distribution of dopants.

Here, we will focus on systems of co-doped nano-structures, in which both phosphorus (P) donors and boron (B) acceptors

are introduced intentionally, in order to enhance the functionalities by the specific interplay between donors and acceptors. We will report the possibility of single-charge band-to-band tunneling (BTBT) in highly-doped pn diodes, resulting from the likely formation of quantum dots due to the random dopant distribution in nanoscale depletion layers of so-called tunnel (Esaki) diodes [1-3]. We will also report signatures of single-electron tunneling (SET) in nanoscale silicon-on-insulator field-effect transistors (SOI-FETs) doped heavily with P-donors [4], but also counter-doped with B-acceptors.
These reports build up on the established field of dopant-based electronics [5-10], in which SET or BTBT via individual dopant-states and/or few-donor clusters reveals basic transport mechanisms for future electronics.

Acknowledgments. This work was partially supported by Grant-in-Aid for Scientific Research (19K04529, 22K04216) from MEXT, Japan, and a Cooperative Research Project of the Research Institute of Electronics, Shizuoka University.

[1] G. Prabhudesai, et al., D. Moraru, Appl. Phys. Lett. **2019**, 114, 243502.
[2] A. Udhiarto et al., D. Moraru, Jpn. J. Appl. Phys. **2021**, 60, 024011.
[3] M. Tabe et al., D. Moraru, Appl. Phys. Lett. **2016**, 108, 093502.
[4] T. T. Jupalli et al., D. Moraru, Appl. Phys. Express 15, 065003 (2022).
[5] D. Moraru et al., Nanoscale Res. Lett. **2011**, 6, 479-1-9.
[6] A. Samanta, D. Moraru, T. Mizuno, M. Tabe, Sci. Rep. 2015, 5, 17377.
[7] D. Moraru, et al., Nanoscale Res. Lett., **2015**, 10, 377.
[8] D. Moraru, A. Samanta, L. T. Anh, T. Mizuno, H. Mizuta, M. Tabe, Sci. Rep., **2014**, 4, 6219.

[9] A. Samanta, D. Moraru et al., Appl. Phys. Lett. 2017, 110, 093107.
[10] A. Afiff et al., D. Moraru, Appl. Phys. Express, 2019, 12, 085004.

Plenary Session (Hall 1)

PL: Electric Transport and Photoresponse in 2D Materials-based Field-Effect Transistors

A. Di Bartolomeo[1,2], E. Faella[1,2], F. Giubileo[2], A. Kumar[1], K. Intonti[1], A. Pelella[1,2], L. Viscardi[1]

[1]*Department of Physics, University of Salerno, Fisciano, Italy*
[2]*CNR-SPIN, uo Salerno, Fisciano, Italy*

Two-dimensional materials hold great promise for electronics and optoelectronics applications. Their atomic thickness enables highly scaled field-effect transistors with reduced short-channel effects and relatively high carrier mobility. The intrinsic electrical transport properties of 2D materials are commonly investigated using back-gated field-effect transistors, due to the low density of process-induced defects and the easy fabrication.
In this presentation, the electrical and optical properties of several 2D materials are discussed. The focus is on the wide family of transition-metal dichalcogenides (TMDs), such as MoS_2, WSe_2, $ReSe_2$, $PtSe_2$, $PdSe_2$ (Fig.1) [1-3], as well as on black phosphorus (BP) and GeAs [4]. Electrical transport, modulation of the conductivity by a back-gate, effect of electron irradiation, role of surface adsorbates and photoresponse are investigated in nanosheets obtained by

either mechanical exfoliation or chemical vapor deposition on SiO_2/Si substrates.

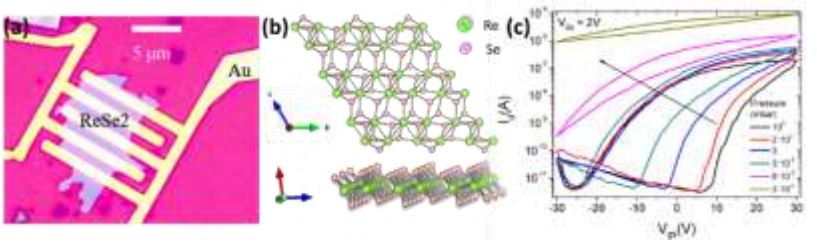

Fig. 1. (a) Optical image of a few-layer $ReSe_2$ field-effect transistor. (b) $ReSe_2$ atomic structure (the green and pink dots represent Re and Se atoms, respectively). (c) Transfer characteristics of $ReSe_2$ transistor for decreasing air pressure (room to 10^{-4} mbar).

The formation of low-resistance contacts and the control of process-induced defects or interface states are issues to consider in the electrical characterization of 2D materials. It is shown that the contact resistance can be tuned by electron irradiation that reduces the Schottky barrier and improves the 2D material/metal contacts [5-7]. It is demonstrated that adsorbates can change the polarity of the majority charge-carriers and enhance the hysteresis in the transfer characteristics of TMD-based field-effect transistors [8]. It shown that excitation from intrinsic or extrinsic trap states enables slow optical response and persistent photoconductivity [2]. It is highlighted how positive and negative photoconductivity can coexist in the same device, the dominance of one type over the other being controlled by the adsorbed oxygen.

The strong dependence of the channel conductance on the environmental gas, air pressure, light and electrical stress

make 2D materials-based devices suitable for memory, gas and light sensing applications.

Finally, the tunable conductivity and the sharp-edge geometry facilitate the extraction of electrons (field emission) from 2D materials upon application of an electric field [9-10]. It is shown that several 2D materials are effective field emitters and that their emission current can be modulated by a back-gate.

[1] E. Faella, K. Intonti, L. Viscardi, F. Giubileo, A. Kumar, H. T. Lam, K. Anastasiou, M. F. Craciun, S. Russo, A. Di Bartolomeo, Nanomaterials **2022**, 12, 1886.

[2] A. Grillo, E. Faella, A. Pelella, F. Giubileo, L. Ansari, F. Gity, P.K. Hurley, N. McEvoy, A. Di Bartolomeo, Adv. Funct. Mater. **2021**, 31, 2105722.

[3] A. Pelella, A. Grillo, F. Urban, F. Giubileo, M. Passacantando, E. Pollmann, S. Sleziona, M. Schleberger, A. Di Bartolomeo, Adv. Electron. Mater. **2021**, 7, 2000838.

[4] A. Grillo, A. Pelella, E. Faella, F. Giubileo, S. Sleziona, O. Kharsah, M. Schleberger, A. Di Bartolomeo 2D Materials **2022**, 9, 015028.

[5] A. Di Bartolomeo, F. Urban, A. Pelella, A. Grillo, M. Passacantando, X. Liu, F. Giubileo, Nanotechnology **2020**, 31, 375204.

[6] A. Pelella, O. Kharsah, A. Grillo, F. Urban, M. Passacantando, F. Giubileo, L. Lemmo, S. Sleziona, E. Pollmann, L. Madauß, M. Schleberger, A. Di Bartolomeo, ACS App. Mater. Interfaces, **2020**, 12, 40532.

[7] A. Grillo, A. Di Bartolomeo, Adv. Electron. Mater. **2021**, 7, 2000979.

[8] F. Urban et al., A. Di Bartolomeo, 2D Materials **2019**, 6, 045049.

[9] A. Grillo, M. Passacantando, Z. Alla, A. Pelella, A. Di Bartolomeo Small, **2020**, 16, 202002880.

[10] A. Di Bartolomeo, A. Pelella, F. Urban, A. Grillo, L. Iemmo, M. Passacantando, X. Liu, F. Giubileo Adv. Electron. Mater., **2020**, 6, 2000094.

PL: Emergence of transition metal oxynitrides as next-generation (photo)electrocatalysts

D. Kumar

Department of Mechanical Engineering, North Carolina A & T State University

The importance of research in the field of non-conventional energy generation and storage cannot be overemphasized in order to be less dependent on limited resources in nature. Our research has established the effectiveness of pulsed laser deposition method for the synthesis of an emerging class of transition metal oxynitride (TMON) material systems in epitaxial 2D, 1D, and 0D (e.g., quantum dot) geometries. The material systems cover a wide range of composition and exhibits the physicochemical properties needed in electrocatalysis, photocatalytic activity in visible light, extended-life electrochemical energy storage, and photodetector responsivity. The attraction of TMONs over more widely studied transition metal oxides (TMOs) is rooted in the polarizability, electronegativity, and anion charge of nitrogen versus that of oxygen, which induces an enormous change in the physical and chemical properties of the resulting compounds. The computational approach combining molecular dynamics (MD) simulation and Density Functional Theory (DFT) calculation has resulted in an expedited materials design with optimized chemical and electronic structures. A controlled modification in the electronic band structure of the TMON systems by aptly changing the oxygen

content and/or by manipulating its size has been used to produce semiconducting TMONs films with tunable conductivity and bandgaps. These features of the TMONs can be used in the fabrication of multijunction solar cells, electrocatalysts, photoelectrocatalysts, photodetectors, plasmonic, and metamaterial devices.

PL: New Insights into Visible Light Active Photocatalysts

S. C. Pillai

Nanotechnology and Bio-Engineering Research Group, Atlantic Technological University, ATU Sligo, Ash Lane, Sligo, Ireland

Nanomaterials exhibit photocatalytic/ hydrophilic activities under the ordinary light (typically >400 nm) is favored for various functional applications. As part of a research program to develop functional surface coatings, our investigations were aimed at developing various photocatalysts for anti-microbial applications. Titanium dioxide in its anatase form thermally stable up to the sintering temperature of the building material substrates (e.g., bathroom tiles) is ideal for various manufacturing applications. High temperatures anatase phase stability is one of the necessities for making such coatings on industrial scale. The preparation of novel photo-catalytic materials by modifying the bandgap using various dopants such as F, S, N and C will be discussed.

[1] P. Ganguly, S. Kumar, M. Muscetta, N. T. Padmanabhan, L. Clarizia, A. Akande, S. Hinder, S. Mathew, H. John, A. Breen, S. C. Pillai. Appl. Catal. B: Environ., **2021**, l 282, 119612.

[3] C. Byrne, G. Subramanian, S. C. Pillai. J. Environ. Chem. Eng. **2018**, 6, 3531-3555.

PL: Reorganization of Lipid Membranes Triggered by Amyloid-beta peptide

O. Ivankov[1], T. Murugova[1], S. Kurakin[1,2], E. Ermakova[1], E. Dushanov[1,3], D. Badreeva[1], Kh. Kholmurodov[1,3], A. Kuklin[1,4], N. Kucerca[1,5]

[1]*Joint Institute for Nuclear Research, Dubna, Russia*
[2]*Kazan Federal University, Kazan, Russia*
[3]*Dubna State University, Dubna, Russia*
[4]*Moscow Institute of Physics and Technology, Dolgoprudny, Russia*
[5]*Comenius University in Bratislava, Bratislava, Slovakia*

Alzheimer's disease (AD) is a conformational disease caused by the formation of senile plaques, consisting primarily of amyloid-beta (Aβ) peptides. The Aβ peptide is considered a key factor in AD ever since the discovery of the disease. The understanding of its damaging influence has however shifted recently from large fibrils observed in the inter-cellular environment to the small oligomers interacting with a cell membrane. By means of small angle neutron scattering (SANS), we have observed for the first time a spontaneous reformation of extruded unilamellar vesicles (EULVs) to discoidal bicelle-like structures (BLSs) and small unilamellar vesicles (SULVs). These changes in the membrane self-organization happen during the thermodynamic phase transitions of lipids and only in the presence of the peptide. We interpret the dramatic changes in the membrane's overall shape with parallel changes in its thickness as the Aβ triggered membrane damage and a consequent reorganization of its structure. The suggested process is consistent with an action

of separate peptides or small size peptide oligomers rather than the result of large Aβ fibrils.

Acknowledgements. This work has been supported by the Russian Science Foundation under grant 19-72-20186.

PL: Exogenous pulmonary surfactant as a drug delivery vehicle

D. Uhrikova[1], L. Hubcik, N. Kralovic[1], N. Kucerka[1], A. Calkovska[2]

[1]Department of Physical Chemistry of Drugs, Faculty of Pharmacy, Comenius University Bratislava, Bratislava, Slovakia
[2]Department of Physiology, Jessenius Faculty of Medicine in Martin, Comenius University Bratislava, Martin, Slovakia

Pulmonary surfactant (PS) lines the interior of the lung alveoli and acts to lower the surface tension at air-liquid interface (Fig. 1a). PS is composed of lipids (~90 wt%) and specific surfactant associated proteins (~10 wt%). The absence of PS due to prematurity, or its damage, is treated by exogenous PS in neonatal medicine, and promising results are obtained also in ventilated Covid-19 patients. Curosurf® (Cur), an extract of porcine lung tissue, is one such clinically used replacement surfactant. It is composed of at least 50 different phospholipids and a small amount of the essential proteins SP-B and SP-C (~2 wt%). The hydrophobic protein SP-B generates oligo- and multi- lamellar organization of Cur. Combining techniques of small angle X-ray and neutron scattering (SAXS and SANS) we determined structural parameters of Cur bilayers, the repeat distance, d, and the thickness of lipid bilayer d_L (Fig. 1a).

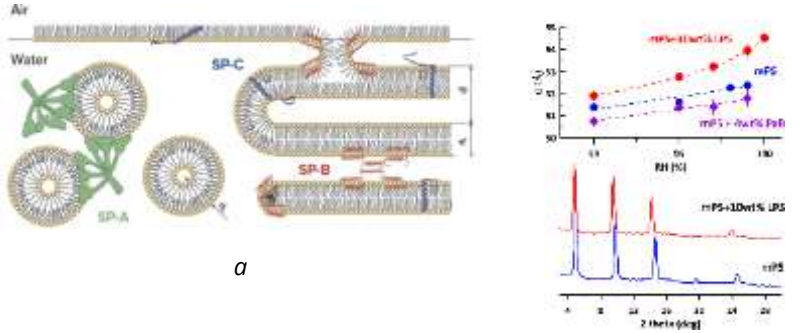

a *b*

Fig. 1. a) Illustration of pulmonary surfactant structure; b) SAND patterns of aligned lipid bilayers and extracted repeat distances (*d*) of exogenous PS in the presence of LPS and PxB, respectively.

Bacterial endotoxin, lipopolysaccharide (LPS), is the major component of the outer membrane of Gram-negative bacteria. At pulmonary infection, LPS interferes with PS and disturbs its structure and function [1]. Polymyxin B (PxB) is an antimicrobial peptide primarily used to treat infections by resistant Gram-negative bacteria. In addition, PxB improves the surface properties of exogenous PS and combined therapy (PxB-Cur) was found as benefiting at treatment of animal models [2]. We investigated structural changes of Cur and its model lipid system free of proteins (mPS) in the presence of LPS and PxB combining techniques of SAXS, SANS and small angle neutron diffraction (SAND). Differential scanning calorimetry was used to characterize the temperature (T_m ~ 30 ^oC) of gel to liquid-crystalline phase transition of lipid mixtures (Cur and mPS). We found that PxB affects d_L and induces a fusion of unilamellar vesicles of exogenous PS. SAND on the stacks of aligned mPS bilayers deposited on a silicon wafer and hydrated in vapors (at four different RH %) of 8 % D_2O

(representative diffraction patterns Fig. 1b) allowed to unravel the effect of both LPS and PxB on the PS bilayer thickness, d_L, in this complex system. Our structural findings accurately reflect the situation with a native lung surfactant as confirmed by recent *in vivo* study [2] and support the idea of PxB/PS combined therapy in neonatal medicine.

Acknowledgements. SAXS experiments were performed at BL11-NCD beamline at Alba Synchrotron with the collaboration of Alba staff. SANS experiments were performed at PAXY instrument of LLB CEA Saclay; SAND at D16 spectrometer of ILL, Grenoble. Experiments were supported by projects APVV-17-0250, JINR 04-4-1121-2021/2025 and VEGA 1/0223/20.

[1] M. Kolomaznik et al., Int. J. Mol. Sci. **2018**, 19, 1964
[2] A. Calkovska et al., Sci Reports **2021**, 11, 22

PL: Magnetic Nanoparticles for Solving Diagnostics - Therapeutic problems with COVID-19

A. Zelenakova[1], V. Zelenak[2], P. Hrubovcak[1], J. Szucsova[1], E. Benova[2], L. Nagy[1], M. Barutiak[1], J. Kosuth[3], Z. Sulinova[4], S. Vilcek[4]

[1]Department of Condensed Matter Physics, Pavol Jozef Šafárik University, Košice, SlovakiaCountry
[2]Department of Inorganic Chemistry, Pavol Jozef Šafárik University, Košice, Slovakia
[3]Institute of Biology and Ecology, P. J. Safarik University, Kosice, Slovakia
[4]Department of Epizootiology and Parasitology, University of Veterinary Medicine and Pharmacy, Komenského 73, 040 01 Kosice, Slovakia

Last two years have shown us our limits in the fight with global pandemic. The spread of COVID19 disease revealed our vulnerability and inefficiency when dealing with a kind of serious virus in general. Despite of a large effort of scientific community, many crucial questions regarding corona virus

disease are still remaining unaddressed. The most important is concern a fast and plausible diagnostics and effective treatment. In response to these challenges, we have developed nanocomposite systems based on Fe_3O_4 magnetic nanoparticles (NPs) for COVID19 diagnostics and therapeutic applications. Series of nanoparticle systems with magnetic core and amorphous silica (SiO_2) shell have been prepared and their surface has been modified by specific organic ligands (Fig.1). Owing to the ligands, the prepared NPs are capable of bonding either virus RNA or anti-virus drug. By the action of applied magnetic field, the NPs may be concentrated in a certain point (diagnostics) or delivered into the affected tissue (treatment). Feasible magnetic performance of the prepared nanoparticle systems is therefore crucial for their application.

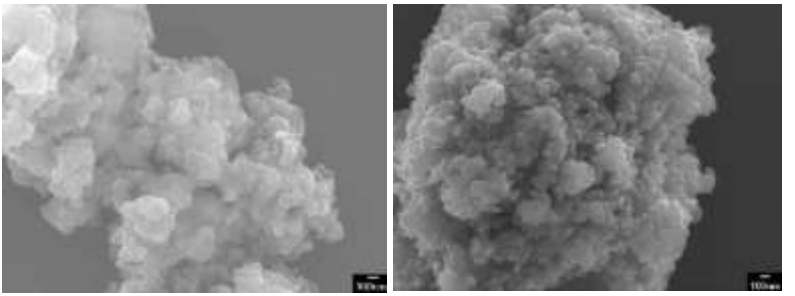

Fig.1. Structure of magnetic beads modiefied by organic ligands for RT-PCR diagnostics.

We have conducted series of magnetic measurements in order to distinguish between magnetic behavior of the pure nanoparticle system and systems with various coatings. We demonstrate the application of the fundamental models that have been modified in order to fit the experimental zero-field cooling magnetization data. We discuss the influence of the nanoparticle shell parameters (morphology, thickness,

ligands) on the overall magnetic performance of the systems. With the aid of magnetic data modeling along with the strong experimental support provided by other methods (electron microscopy, X-ray diffraction) we can conclude on nanoparticle structural and magnetic characteristics and the presence/absence of interparticle interactions. Accurate determination of nanoparticle system properties is essential for its further tuning towards the desired application.

Acknowledgments. This work was supported by the Operational Programme Integrated Infrastructure, project "NANOVIR", ITMS:313011AUW7, co-funded by ERDF and APVV-20-0512.

PL: The challenge of protecting cultural heritage assets: the HERACLES project vision and experience

G. Padeletti

CNR-ISMN Rome 1 – Research Area, Italy

Europe's significant cultural diversity together with exceptional ancient architectures and artefact collections attracts millions of tourists every year. These global assets are of incalculable value and have to be preserved for future generations. The effects of floods, extreme windstorms or rains on these assets are clearly identifiable but it should be worth to note that all these effects are seriously amplified on ancient and fragile assets where advanced techniques, commonly used for modern buildings and structures, cannot be applied to preserve their originality. In order to address all of the above challenges the European project HERACLES proposed a holistic, multidisciplinary, and multi-sectorial approach with the aim to provide an operative system and eco-solutions to innovate and to promote a strategy and vision for the

future of CH resilience. In this framework, HERACLES proposes a novel systematic approach to ensure the sustainable management and protection of the different CH typologies with respect to the CC impacts. The approach benefits from a multidisciplinary methodology that bridges the gap between the two different worlds: the CH stakeholders and the scientific/technological experts, which are both involved in the project

Invited and Oral Session (HALL 1)

T14-I: Environmentally friendly processes in electronics waste treatment technologies

H. Cesiulis[1,2]

[1]Dept. Phys. Chemistry, Vilnius University, Vilnius, Lithuania
[2]JSC Elektronikos Perdirbimo Technologijos, Vilnius, Lithuania

Waste from electrical and electronic equipment (WEEE) includes a large range of devices, and now is one of the fastest growing waste streams. This type of waste contains a complex mixture of materials, some of which are hazardous. These can cause major environmental and health problems if the discarded devices are not managed properly. In addition, modern electronics contain rare and expensive resources, which can be recycled and re-used if the waste is effectively managed. The main factors that currently limit the contribution of recycling to meet demand for raw materials in the EU can be summarized as: (1) recycling of many materials from end-of-life products and waste streams is currently not economically feasible; (2) there is a lack of suitable eco-friendly technologies available for recycling; (3) some

materials are embodied in products stocked in use for long time periods; (4) demand for many materials is growing.

Because of complexity WEEE composition, an entire treatment and recycling technological chain comprises a number of mechanical and chemical treatment processes in order to obtain metals in forms and compounds allowing them to be conveniently separated and obtained in pure metallic form.

The proposed chemical processes in WEEE treatment chain are focused on application the bio-compatible chemicals (such as citric acid, oxalic acid, glycine) to treat a main batch of mechanically treated WEEE. Actually, the metals dissolution processes are corrosion processes, therefore using appropriate even biocompatible ligands and oxidators it is possible to leach Sn, Cu, Pb, Ni, Zn, precious metals avoiding to use the big volumes of aggressive acids within 4-12 hours at 60-80 °C. Then it is possible to reduce precious metals and to obtain metal concentrate containing precious metals up to 5-10 %.

Afterwords, the residual base metals can be electrodeposited by electrowinning in the form of alloys on various cathodes, such as 3D graphite, “bateries” of cathodes closely located to each other, etc.

Acknowledgements. The study has partially received funding from the EU H2020 MSCA SMARTELECTRODES project, Nº 778357.

T14-O: Effects of ocean acidification on the morphology and structure of Hexaplex trunculus sea snail shell biomaterial revealed by Raman, XRD AND SEM-EDX data

G. Lazar[1], F. Nekvapil[1], I. Bajama[1], T. Tamas[2], M. Suciu[3], L. Barbu-Todoran[3], S. Grdan[4], S. Cinta Pinzaru[1], S. Dupont[5], A. Bratos Cetinic[4], L. Glamuzina[4]

[1]Biomolecular Physics Department, Babes Bolyai University, Kogalniceanu 1, RO-400084 Cluj-Napoca, Romania
[2]Department of Geology, Babeş-Bolyai University, Kogalniceanu 1, RO-400084 Cluj-Napoca, Romania.
[3]Advanced Research and Technology Center for Alternative Energy, National Institute for Research and Development of Isotopic and Molecular Technologies, Donat 67-103, 400293 Cluj-Napoca, Romania.
[4]Department of Applied Ecology, University of Dubrovnik, 20000 Dubrovnik
[5]University of Gothenburg, Kristineberg Marine Research Station, Kristineberg 566, 45178 Fiskebackskil, Sweden

Hexaplex trunculus (Linneaeus, 1758), also known as banded dye-murex, is a medium sized gastropod species belonging to the family Muricidae, famous for its purple dye content, one of the most valued resource in the ancient times. In the present work, the effect of a range of pH conditions relevant in the context of ocean acidification on the *H. trunculus* shells were studied using Raman Spectroscopy, Scanning Electron Microscopy (SEM), as well as X-Ray Diffractometry (XRD). Specimens originating from environments with the pH ranging from 8.1 to 7.4 were studied, to replicate the expected future ocean acidification. The snails are mainly composed of a $CaCO_3$ backbone, and organic pigments. In terms of the $CaCO_3$ polimorph, the *H. trunculus* is mainly composed of aragonite, both the Raman spectra and XRD data however, revelead specimens containing calcite traces, at pH 8.0-7.8. In order to

study the effect of pH on the morphology we compared the Raman and XRD spectral properties, of the snail individuals as a function of the environmental pH. Using these properties, we compared the relative crystallinity of the biogenic calcium carbonate at the various pH values. The crystallinity was relatively constant on the interior of the shells, with larger variations being visible on the exterior, suggesting a higher pH sensitivity on the exterior of the shells, as expected. Moreover, the XRD data suggests that the presence or absence of calcite in the crystalline structure does directly influence the crystallinity of the calcium carbonate. The SEM-EDX data was then correlated with the Raman spectra to accurately determine the pH influence on the morphology.

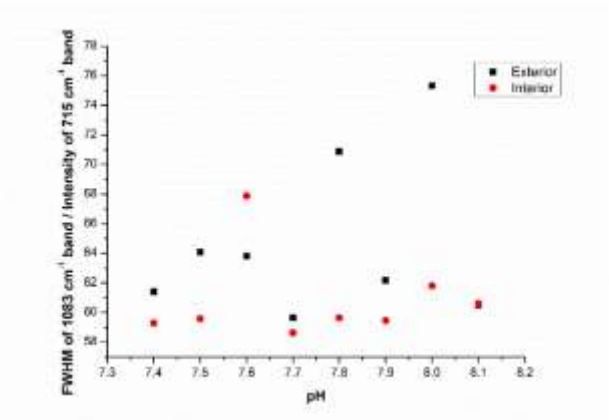

Fig. 1. 1083 cm^{-1} band FWHM and 705 cm^{-1} band intensity ratio as a function of pH, on spectra collected both from the interior and exterior of specimens.

Acknowledgements. This work was supported by a grant of the Romanian Ministry of Education and Research, CCCDI - UEFISCDI, project number PN-III-P2-2.1-PED-2019-4777, within PNCDI III.

T14-O: Lightweight carbonaceous materials derived from waste foam-like materials for oil spill remediation

M. Ignat[1], E. Turcu[1], P. Samoila[1], C. Cojocaru[1], L. Sacarescu[1], G. Predeanu[2], V. Harabagiu[1], F. Cosmulescu[3]

[1]"Petru Poni" Institute of Macromolecular Chemistry, 41A Grigore Ghica Voda Street, Iasi 700487, Romania
[2]Research Center for Environmental Protection and Ecofriendly Technologies, University Politehnica of Bucharest, 1-7 Gheorghe Polizu Str., 011061 Bucharest, Romania
[3]SC Cosfel Actual SRL, Griviței Rd., 95-97, Sector 1, 010705, Bucharest, ROMANIA

As well known, pyrolysis, a thermally induced chemical decomposition of organic materials, is still the key process in the production of nanocarbons. Nowadays, organic matter makes up a large portion of human, animal, and plant waste, and pyrolysis is used to safely dispose of waste polymers, whereas direct burning or combustion is harmful to the environment. Additionally, there are numerous uses for the solid carbon leftovers generated during the pyrolysis of waste materials, the process being explored the most in both industry and academia. Moreover, pyrolysis of waste foam-like materials including organic molecules could produce valuable lightweight carbonaceous materials since it is affordable, renewable, economical, easy to obtain, and produced in large quantities as raw materials.
In the present study, different foam-like materials such as corn and sunflower stalk pith, corn starch peanuts, and polyethylene foam used for packing were considered as carbon sources to create lightweight carbonaceous materials with a large surface area (Fig.1).

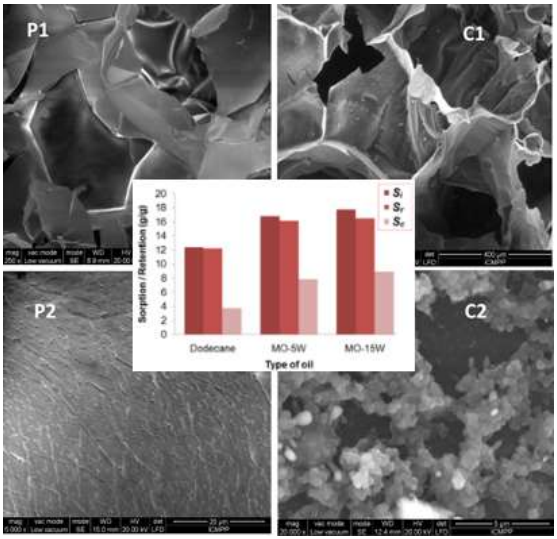

Fig. 1. SEM images for foam-like materials (P1, P2) and derived lightweight carbon materials (C1, C2); absorption capacity of the carbonaceous material towards various oils (inset).

Due to their inherent hydrophobic properties and great adsorption properties, the prepared monolithic carbon foams exhibit a prospective application for the adsorption and separation of oil or organics from water. Thus, they are proposed for use in a variety of oil and solvent spill treatments (Fig.1 inset).

Acknowledgments. The financial support of the European Fund for Regional Development, Competitiveness Operational Programme 2014-2020; POC/163/1/3 – Project 4WASTEUPGRADE (Contract no. 386/390062/4.10.2021, cod MySMIS: 120696) is gratefully acknowledged.

T14-O: Characterization of lignocellulosic biomass derived from agricultural wastes

D. Timpu[1], P. Samoila[1], V. Harabagiu[1], G. Predeanu[2], F. Cosmulescu[3]

[1] "Petru Poni" Institute of Macromolecular Chemistry, 41A Grigore Ghica Vodă Alley, 700487 Iasi, Romania;
[2]Research Center for Environmental Protection and Ecofriendly Technologies, University POLITEHNICA of Bucharest, 1-7 Gheorghe Polizu Str., 011061 Bucharest, Romania
[3] SC Cosfel Actual SRL, Griviței Rd., 95-97, Sector 1, 010705, Bucharest, Romania

This work is aimed to obtain an innovative and integrated pilot-technological line for the synthesis in the microwave field of some advanced carbonaceous materials (MCA) for niche applications in the field of water purification, through the valorization of some biopolymeric/lignocellulosic waste.
The technology proposes a new approach for obtaining designed materials and offers the possibility of an economically attractive production method.
The investigations included the inventory of the quality of the precursors: target lignocellulosic waste from fruit pits/peels, peach pits, olives, walnut shells, pulp from the pressing of pits (camelina, rapeseed, sunflower, safflower, grapes, etc.). A wide range of analysis techniques were used to monitor their characteristics depending on the requirements of the target processes: WAXD, DSC, DMA, ATG-IR, FT-IR, SEM, EDX, SPM, determination of surface properties (contact angle, porosity, etc.), chromatographic analyses.
The slideshow presents the main stages for the transformation of biopolymeric waste into a uniform material

suitable for analysis, respectively obtaining samples with a reduced and uniform particle size. Also, the complex characterization of raw materials by WAXD – Wide Angle X-Ray Diffraction, SEM – Scanning Electron Microscopy, EDX - Energy Dispersive Spectroscopy and FTIR - Fourier-transform infrared spectroscopy are shown.

Acknowledgments. The financial support of European Fund for Regional Development, Competitiveness Operational Programme 2014-2020; POC/163/1/3 – Project 4WASTEUPGRADE (Contract no. 386/390062/4.10.2021, cod MySMIS: 120696) is gratefully acknowledged.

T14-O: Screening of waste shell biomaterials for recycling as adsorbents for water-borne pollutants

F. Nekvapil[1,2,3], G. Lazar[1,2], M-L. Soran[1,3], M. Mihet[3], R. Hirian[1], A. Ciorita[3,4], S.B. Angyus[5,6], T. Kusovaca[7], M. Precanica[7] S. Cinta Pinzaru[1,2]

[1]Ioan Ursu Institute, Babeș-Bolyai University, Cluj-Napoca, Romania
[2]RDI Institute in Applied Natural Sciences, Babeș-Bolyai University, Cluj-Napoca, Romania
[3]National Institute for Research and Development of Molecular and Isotopic Technologies, Cluj-Napoca, Romania
[4]Electron Microscopy Centre, Babeș-Bolyai University, Cluj-Napoca, Romania
[5]Faculty of Chemistry, Babeș-Bolyai University, Cluj-Napoca, Romania
[6]National Institute for Research and Development of Optoelectronics INOE 2000 INCD Bucharest, Research Institute for Analytical Instrumentation, Cluj-Napoca, Romania
[6]Applied Ecology Department, University of Dubrovnik, Dubrovnik, Croatia

Crustacean shells are accumulating as a household, restaurant or fisheires industry waste, currently without a proper management and valorisation strategy. These shells represent

a complex biocomposite with 3D nanoarchitecture and biomolecular content [1, 2], beeing the subject of numerous studies [3]. The valuable components within shells are carotenoids, chitin and biogenic calcium carbonate.

We comparatively prospected the composition and morphology of Blue crab (*Callinectes sapidus*) and spider crab (*Maja squinado*) from Adriatic Sea in order to assess their suitability for production of adsorbents for water-borne pollutants. Considered samples were shells before and after carotenoids extraction. Additionally, shells of the european flat oyster (*Ostrea edulis*) were also analysed in equivalent manner (Fig. 1).

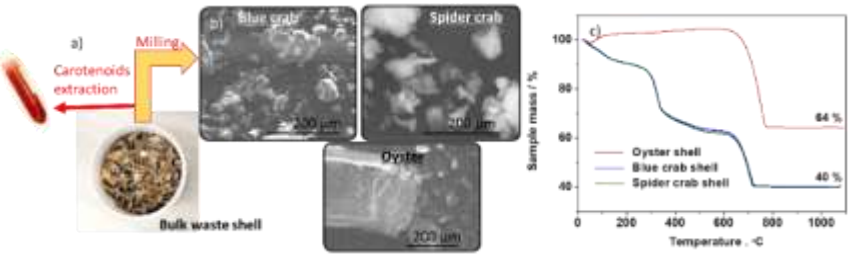

Fig. 1. (a) Waste crab shell stock from which carotenoid-depleted shell powder is obtained, b) SEM images, and c) TGA analysis of shell powder obtained from the blue crab, the spider crab and the oyster.

SEM imaging showed that all the shell powder particles feature extensively roughened surface (Fig. 1b), allowing large area available for pollutants adsorption. Raman and XRD revealed that crab shell biomineral matter consists of chitin and calcite, while oyster consists exclusively of calcite. Nitrogen physisorption measurements (BET) show that post-extraction crab shell powder features internal pore surface area of 32.9 m^2/g, up to 6 times more than native shells, while

the oyster shells do not feature internal porosity. Thermogravimetric analysis (TGA) showed two major mass loss events in crab shells, between 260 and 370°C and 620 and 740°C, while oyster shell featured only the latter event (Fig 1c). The current results show that the considered crab and oyster shells biocomposites could be recycling as potentially feasible adsorbents for pollutants.

Acknowledgements. This work was supported by the grant of the Ministry of Research, Innovation and Digitalization, CNCS-UEFISCDI, project number PN-III-P1-1.1-PD-2021-0477, within PNCDI III and by the grant of the Romanian Ministry of Eudcation and Research, CCCDI-UEFISCDI, project number PN-III-P2-2.1-PED-2019-4777, within PNCDI III.

[1] Nekvapil, F. et al., Sci. Rep.-UK, **2020**, 10, 3019.
[2] Nekvapil, F. et al., ACS Sustain. Chem. Eng. **2019**, 7, 16820.
[3] Lazar, G. et al., ACS Omega, **2021**, 6, 27781-27790.

T14-I-online: The production of electrical power from waste organic materials the key of circular economy

O. N. Ionescu [1,2,3], H. M. Bardeanu[3], M. P. Suchea[2]

[1]Petroleum and Gas University from Ploiesti, Ploiesti, Romania
[2]National Institute for Microtechnology IMT Bucharest, Voluntati, Ilfov, Romania
[3]Genesis Biotech, Filipesti, Romania

After decades of promoting a society based on excessive consumption the simultaneous threat of fossil fuel crisis, climate changing and not the last the last irresponsible political war games brought to general attention the absolute necessity of establishing a circular economy. In regard with inorganic materials, the selective waste management has

been a real success, however, the organic materials are still a large problem especially for the large urban area. One of the most sustainable methods of converting the organic waste in electrical power is to use the biogas production technology via anaerobic digestion. Although the biogas production based on biomass (corn silage) is a well-known technology the conversion of the old production capacity in an effective manner in order to process the organic waste is quite a challenging task. In this talk are presented the main challenges encountered in the conversion of a corn silage-based biogas production plant into a plant capable of using over 90% organic waste.

Invited and Oral Session (HALL 2)

T10-O-online: Portable Paper-based Plasmonic Biosensor for rapid detection of CEACAM5 using Metal Enhanced Fluorescence

L. Susu[1,2], S. Astilean[1,2], M. Focsan[1]

[1]Nanobiophotonics and Laser Microspectroscopy Centre, Interdisciplinary Research Institute on Bio-Nano-Sciences, Cluj-Napoca, Romania
[2]Biomolecular Physics Department, Faculty of Physics, Babes-Bolyai University, 1 M. Kogălniceanu str., Cluj-Napoca 400084, Romania

Rapid detection and quantification of cancer biomarkers plays a crucial role in early diagnosis, screening and treatment, especially in developing countries with limited resources. In consequence, there are still great challenges in designing multiplexed biosensors that are simple, inexpensive and efficient [1]. Although paper-based biosensors, in particular, have received a great interest than before due to the fact that

they meet the criteria for point-of-care (PoC) devices, the main drawbacks with these devices is the low sensitivity and efficiency in performing quantitative measurements [2]. Herein, we design a low-cost paper-based nanosensor through plasmonic calligraphy by directly drawing individual plasmonic lines on Whatman filter paper using a regular ballpoint pen filled with gold nanorods (AuNR)-as colloidal ink (Fig. 1a).

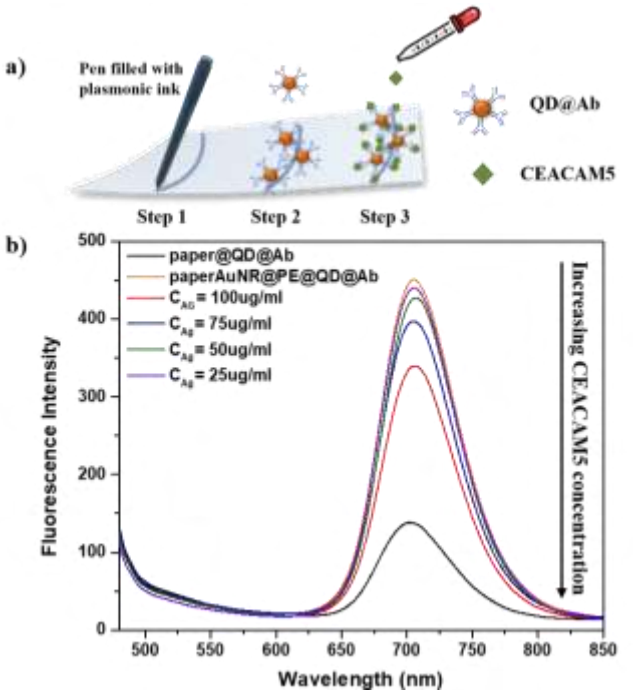

Fig. 1. a) Schematic illustration of the plasmonic calligraphy approach; b) Emission spectra of QD@Ab on bare paper (black spectrum), onto the plasmonic lines (orange spectrum) and after different concentrations of CEACAM5 were captured.

The as calligraphed plasmonic arrays were further successively coated with negatively and positively charged

polyelectrolytes layers employed as dielectric spacer to promote the enhancement of the emission of carboxyl-functionalized quantum dots (QD)−previously conjugated with specific antibodies (QD@Ab)−for qualitatively and quantitatively determination of Carcinoembryonic antigen-related cell adhesion molecule 5 (CEACAM5), a clinical biomarker for gastrointestinal cancers [3]. The efficiency as well as the sensitivity of our portable nanosensor was validated by monitoring the enhanced fluorescence intensity of the QD@Ab when different concentrations of CEACAM5 were added dropwise on the plasmonic arrays (Fig. 1b).

[1] T. Mahmoudi, M. de la Guardia, B, Baradan, Trends Analyt. Chem., **2020**, 125, 114842.
[2] S. Kesetsirikul, M.J. Shiddiky, N.-T. Nguyen, Microfluid. Nanofluidics, **2020**, 24, 17.
[3] A. Xiao, Y. Huang, J, Zheng, P. Chen, B.-O. Guan, ACS Appl. Mater. Interfaces, **2020**, 12, 1799-1805.

T11-O: Describing complex dielectric properties in ferroelectric-based composites by a new dynamic finite element method

L. Padurariu, L.P. Curecheriu, V.A. Lukacs, R.S. Stirbu, L. Mitoseriu

Dielectrics, Ferroelectrics & Multiferroics Group, Faculty of Physics, Al. I. Cuza University of Iasi, Blv. Carol I, 700506, Iasi, Romania

Since single-phase ferroelectric materials cannot accomplish all the technological requirements in applications, developing composite materials that combine the properties of the ferroelectrics with other constituent phases (linear dielectrics, magnetic materials, or other conductive/ semiconductor components) is a commonly proposed solution. Recently, it

has been shown by Finite Element Method (FEM) simulations that a major factor that influences the effective properties of composite materials is the local electric field inhomogeneity introduced by the interfaces. Based on this effect, we proposed the original concept local field engineering which involves the design of materials with controlled microstructures and, implicitly, an optimum inhomogeneity of the electric field to improve the functional properties [1,2].

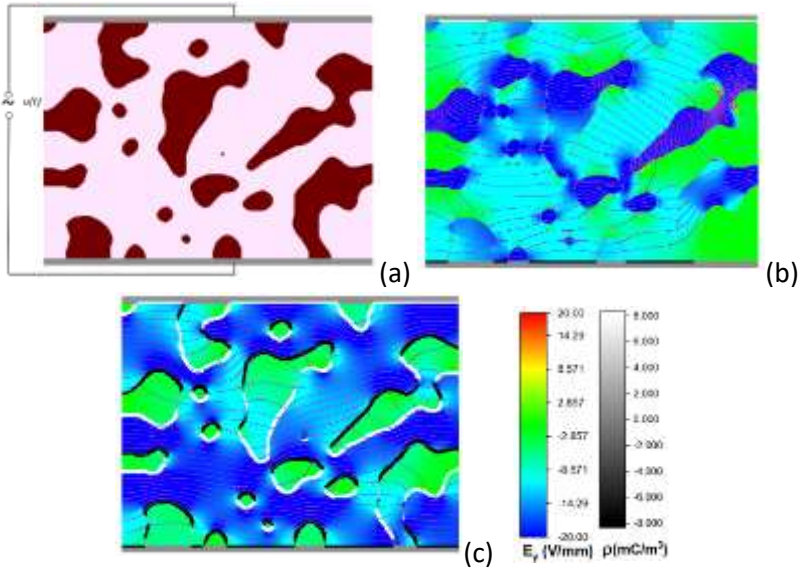

Fig. 1. A $BaTiO_3$-$CoFe_2O_4$ composite with a concentration of 30% for the magnetic phase (a) and the images of local electric field and charge densities simulated at a frequency of 10^6 Hz (b) and frequency of 1 Hz (c) corresponding to the amplitude (10V) of the ac signal- u(t).

Another important factor that influences the functional properties of composites is the accumulation of free charges at interfaces, but this has been neglected so far because it involves important computational difficulties. In this work we

propose a new modelling dynamic approach based on finite element method able to describe the complex impedance at any frequency in the range from 1Hz to 1MHz.
The approach allows us to explore the influence of free electric charges on the effective dielectric properties of real composite systems as ferroelectric-semiconductor, magnetoelectric, porous ferroelectrics, etc. For example, the simulated images of local fields and charge densities at different frequencies in a magnetoelectric composite are represented in Figs. 1(b-c).

Acknowledgments. This work was supported by the UEFISCDI Romanian project PN-III-P1-1.1-TE-2019-1929.

[1] L. Padurariu et. al., Appl. Phys. Lett. **2012**, 100, 252905.
[2] L. Padurariu et. al., Acta Mater. **2016**, 103, 724 .

T13-O: High-index contrast $LiNbO_3$ optical waveguides fabricated by High Vacuum Vapor-phase Proton Exchange

M. R. Sandu[1], L. Hrostea[1], A. P. Rambu[1], F. Doutre[2], V. Tiron[1], S. Tascu[1],

[1]Research Center on Advanced Materials and Technologies, Department of Exact and Natural Science, Institute of Interdisciplinary Research, Alexandru Ioan Cuza University of Iasi, Blvd. Carol I, no. 11, 700506 Iasi, Romania
[2]Universite Cote d'Azur, CNRS, Institut de Physique de Nice (INPHYNI), UMR 7010, Nice, France

Highly confining waveguides (Δn_e>0.1) and low propagation losses have been fabricated in lithium niobate (LN) by a new process called High Vacuum Vapor-phase Proton Exchange (HiVac-VPE) [1]. Index contrast and propagation losses of HiVac-VPE channel waveguides are investigated in view of

telecom applications. The results recommend HiVac-VPE as very promising technique for fabricating efficient nonlinear photonic integrated circuits in LN crystals. We present here the influence of the high vacuum drying effect on the optical features and quality of both planar and channel waveguides fabricated in benzoic acid vapor. The impact of high vacuum on the optical features of the waveguides and reproducibility of the process were tested over one year and a half by producing, in same conditions, more than fifty waveguides. HiVac-VPE process was performed on Z-cut LN optical grade samples in a hermetically sealed hourglass tube for different exchange durations *t(h)*. Prior to be sealed, the bottom part of the tube is filled with pure Benzoic Acid (BA) powder as vapor source. The sample to be processed is placed in the top part of the tube and then, by using a turbo pumping station, the tube is pumped down to a pressure as low as $p=3.4\pm0.1\times10^{-5}$ mbar. This very low pressure is 10^8 times lower compared to the first reports on vapor phase exchange [2] and 10^5 times lower compared to the ones reported by the literature for liquid phase exchange [3] and is imperative in order to diminish as much as possible any traces of water from the acid powder. In order to reconstruct the index profile of the planar waveguides, the effective indices of the propagation modes have been measured using a standard two-prisms coupling set-up at $\lambda=633$ nm [4]. The measured effective indices N_{eff} of TM guided modes as well as the values of mode depths calculated by IWKB [5] allow us to reconstruct the index profiles of waveguides fabricated for different exchange durations. As we can see on Fig. 1, the index profiles are a mix of a step and a gradient profile.

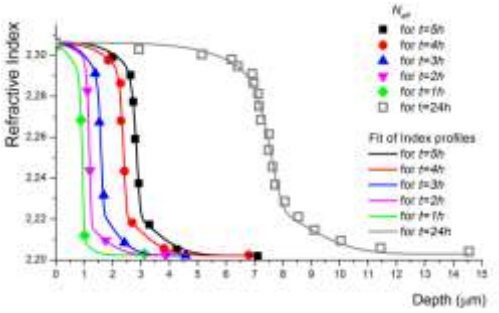

Fig. 1. Index profiles of Z-cut HiVac-VPE waveguides fabricated for different exchange durations. The symbols represent the measured N_{eff} of the propagating modes, except the IWKB surface indices on the ordinate.

Propagation losses in the HiVac-VPE channel waveguides have been measured by using the Fabry-Pérot cavity technique [6]. The best of our investigated channel waveguides exhibit propagation losses around 3.5±0.1 dB/cm.

Acknowledgements: This work was supported by a grant of the Romanian Ministry of Education and Research, CNCS—UEFISCDI, Project number PN-III-P4-ID-PCE-2020-0239, Contract number PCE 142/2021, within PNCDI III.

[1] A. P. Rambu, A. M. Apetrei, F. Doutre, H. Tronche, V. Tiron, M. de Micheli, S. Tascu, Photonics Res. **2020**, 8 (1), 8-16.
[2] P.J. Masalkar, M. Fujimura, T Suhara, H. Nishihara, Electron. Lett, **1997,** 33 (6), 519-520.
[3] O. Stepanenko, E. Quillier, H. Tronche, P. Baldi, M. De Micheli, J. Lightwave Technol. **2016**, 34 (9), 2206-2212.
[4] P. K. Tien, R. Ulrich, J. Opt. Soc. Am. **1970,** 60 (10), 1325–1337.
[5] J. M. White, P. F. Heidrich, Appl. Optics, **1976**, 15 (1), 151-155.
[6] D. Castaldini, P. Bassi, S. Tascu, G. Sauder, P. Aschieri, M. de Micheli, P. Baldi, K. Thyagarajan M. R. Shenoy, Opt. Eng. **2007**, 46 (2), 124601.

T13-O: Influence of high vacuum on the fabrication of proton exchanged lithium niobate waveguides

L. Hrostea, M. R. Sandu, A. P. Rambu, S. Tascu,

Research Center on Advanced Materials and Technologies, Department of Exact and Natural Science, Institute of Interdisciplinary Research, Alexandru Ioan Cuza University of Iasi, Blvd. Carol I, no. 11, 700506 Iasi, Romania

Precise control and reproducibility of optical waveguides fabrication are extremely important for efficient and compact devices for a wide range of photonics applications. Here we experimentally validate the excellent control and reproducibility of the index contrast and index profile of optical waveguides fabricated on Z-cut lithium niobate (LN) substrates by High Vacuum Proton Exchange (HiVacPE) technique [1]. Proton exchange processes for both high and low-vacuum conditions were performed in a hermetically sealed hourglass tube. The bottom part of the tube was filled with 16 g of Benzoic Acid (BA) and Lithium Benzoate (LB) powder mixture as proton source. Both high and low-vacuum waveguides (by HiVacPE and LoVacPE respectively) were fabricated by mixing the powders in concentration of ρ_{LB}=2.60±0.05%. The sample to be processed is placed in the top part of the tube and then the tube is pumped down to a pressure as low as $p_{HiVacPE}$= 3.5×10^{-5} mbar for the tubes destined to HiVacPE process [1] and $p_{LoVacPE}$= 3.5 mbar for LoVacPE process respectively [2]. In order to verify over the time the reproducibility of each process, at random moments during one year, twenty samples (ten pairs) were fabricated by using the above mentioned conditions. In order to reconstruct the index profiles of the planar waveguides, the effective indices of the propagation modes have been measured using

a standard two-prisms coupling set-up at λ=*633* nm [3]. The measured effective indices N_{eff} of TM guided modes as well as the values of mode depths calculated by IWKB [4] are presented on Fig. 1 (a), where, in order to avoid the redundant information, we present only the extreme shapes of the index profiles. For the other samples, the index profile shapes are located between the two extremes either for high or low-vacuum conditions. As it can clearly be seen in Fig 1. (a), the HiVacPE waveguides show an exponentially decreasing index profiles with low values of the index contrast distributed in a very narrow range of $\pm 0.01\times10^{-2}$ around the mean value of $\Delta n_e=2.34\times10^{-2}$.

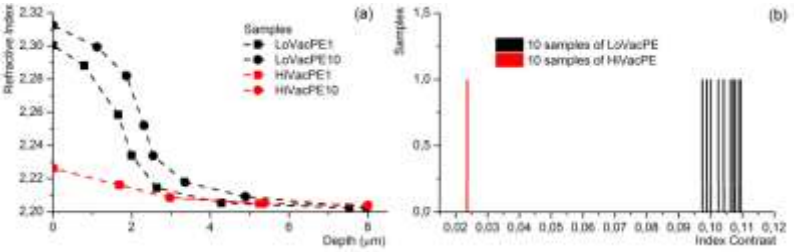

Fig. 1. (a) Extraordinary index profile for planar waveguides fabricated by using both HiVacPE and LoVacPE process. (b) Distribution histogram of refractive index contrast for both HiVacPE and LoVacPE samples.

In relative terms, the indices are spread in a very narrow range of ±0.01/2.34, i.e. 0.34 % relative to the mean value. On contrary, the index profile of LoVacPE waveguides is a mix of a step and a gradient profile with high values of the index contrast distributed in a large range of $\pm1\times10^{-2}$ around the mean value of $\Delta n_e=10.4\times10^{-2}$. In relative terms, the indices are spread in a wide range of ±1/10.4, i.e. ± 9.6 % relative to the mean value. So, there is an improvement of index contrast

reproducibility of two orders of magnitude. On Fig. 1 (b) is depicted the distribution histogram of refractive index contrast for both types of samples.
To summarize, the index contrasts of HiVacPE waveguides exhibit a very narrow distribution compare to the large distribution exhibited by the LoVacPE waveguides.

Acknowledgements. This work was supported by a grant of the Ministry of Research, Innovation and Digitization, CNCS/CCCDI-UEFISCDI, project number COFUND-QUANTERA-2-InQuRe, within PNCDI III.

[1] A. P. Rambu, A. M. Apetrei, F. Doutre, H. Tronche, M. De Micheli, S. Tascu, J. Lightwave Technol. **2018**, 36, 2675-2684.
[2] O. Stepanenko, E. Quillier, H. Tronche, P. Baldi, M. De Micheli, J. Lightwave Technol. **2016,** 34, 2206-2212.
[3] P. K. Tien, R. Ulrich, J. Opt. Soc. Am. **1970,** 60 (10), 1325–1337.
[4] J. M. White, P. F. Heidrich, Appl. Optics, **1976**, 15 (1), 151-155.

T13-O: Control of the growth of nanostructures by Oblique-Angle Deposition to create unique photonic designs

C. Marsal[1], E. Panchout[1], B. Giroire[1], C. Dupeyrat[2], T. Girardeau[1], F. Paumier[1]

[1]Institut de recherche Pprime, CNRS-Universite de Poitiers-ISAE-ENSMA-UPR 3346, Poitiers, France
[2]Safran Electronics & Defense, 26 Avenue des Hauts de la Chaume, Saint-Benoit, France

Nowadays, more and more innovative materials are sought to create unique photonic designs. Surface nanostructuration is a means of technological breakthrough and covers many application areas such as optics, sensors, optical fibers, and

medical imaging. Oblique-Angle Deposition (OAD) is a recognized and original technology for producing highly porous sculptured nanostructures. It allows a very precise control of the refractive index of the layers with the deposition conditions. Additionally, the film morphology can be modified by changing the substrate orientation during the deposition [1], allowing control of the complex refractive index in the three dimensions of the layer. The resulting layers are complex to characterize due to their anisotropies and porosity gradients. Therefore, deep investigations are required.

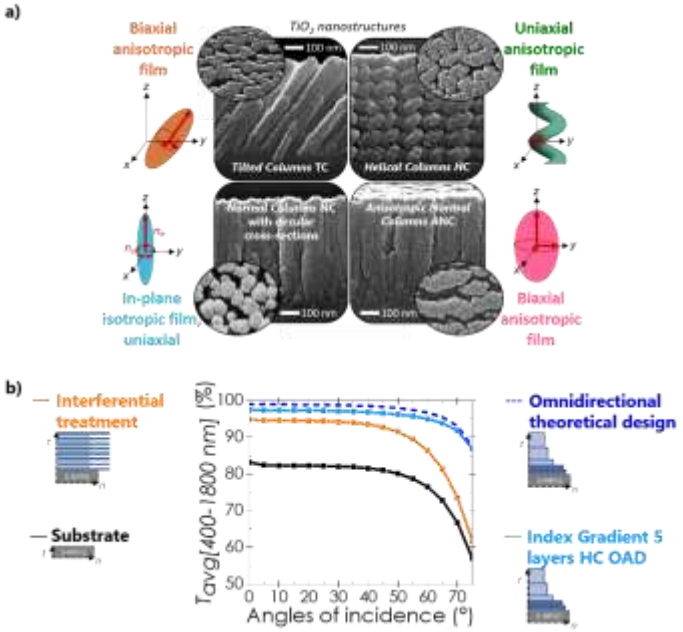

Fig. 1. Interests of the OAD technology: a) Nanostructures growth control; b) Development of ultra-high performance broadband omnidirectional antireflection.

New advanced morphologies (slanted columns, normal columns, anisotropic normal columns, and helical columns) have been fabricating using Oblique-Angle Deposition (Fig.1.a). Based on optical characterizations of both spectrophotometry and spectroscopic ellipsometry, a complex analytical optical model is established for each new morphology and confirmed by microstructural characterization, especially by Scanning Electron Microscopy. Perfect correlations have been demonstrated between nanostructures and optical properties. The diffusion of these new morphologies was also thoroughly investigated to optimize the performances of optical treatments. Helical columns were found to scatter less than all other morphologies, which was confirmed by finite element simulations. These results have enabled the development of ultra-high performance broadband omnidirectional antireflective coatings in the Visible-SWIR range (Fig.1.b) [2]. Finally, ongoing work proves that these helical columns and these anisotropic normal columns allow the fabrication of high performance polarimetric filters.

[1] Y. Zhao *et al.*, Chem. B **2003**, 5219 59–73.
[2] D. Poitras *et al.*, SPIE **2004**, 43 6 1286–1295.

T13-O: Potentialities of Oblique Angle Deposition (OAD) for linear and circular polarization

E. Panchout[1], C. Marsal[1], F. Paumier[1], T. Girardeau[1], B. Giroire[1], C. Dupeyrat[2]

[1]Insitut Pprime (SP2MI, University of Poitiers, CNRS) Poitiers, France
[2]Safran Electronics&Defense (Safran) 26 avenue des hauts de la chaume, Saint-Benoît, France

The growing interest in real-time augmented imaging (hyperspectral or polarimetric) has recently led to the development of DoFP (Division of Focal Plane) polarimeters with several polarimetric filters placed directly on top of the photometric sensor. Metallic wire-grids are generally used because of their small thickness to polarize the incident light for polarimetric imaging, and are deposited directly on the sensors, usually in a matrix of four pixels, in order to capture several polarization directions. Unfortunately, wire-grid polarizers suffer from a poor extinction coefficient and low transmitted flux compared to thicker polarizers. The use of a new type of polarizer, known as a Polarimetric Filter by Reflection (PFR), can in theory remove a technological lock and achieve a very high extinction coefficient and close to no flux loss. PFR can be realized by OAD (Oblique Angle Deposition), which enables the fabrication of porous and anisotropic thin films by controlling deposition parameters such as the deposition rate, the angle of incidence α or the azimutal rotation of the substrate φ (Fig. a). By finely controlling these parameters, it is possible to create thin films with different morphologies, such as Helical Columns (Fig. b) that exhibit properties for the circular polarization or Anisotropic Normal

Columns (Fig. c, d) that exhibit properties for the linear polarization.

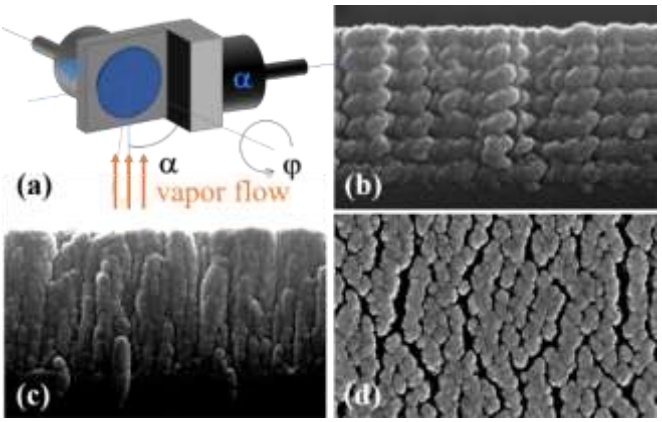

Fig: a) sample holder for OAD; b) cross section of Helical Columns; c) cross section and d) plane view of Anisotropic Normal Columns

In addition, with the control of the α angle we can precisely control the porosity, making a wide range of optical indices in the three dimensions of the layers. By studying the anisotropic properties of these different architectures with *in-situ* XRD and ellipsometry annealing, we have demonstrated that amorphous nanostructures exhibit crystallisation of the anatase phase. This transformation highly increases anisotropic behaviors, which enables the improvement of existing optical designs, to create planar, low-loss circular and linear polarizers.

T5-O: Magnetic properties of selected magnetoplasmonic nanoparticles

R. Bortnic[1], A. Szatmari[1], G. Souca[1], R. Hirian[1], R. Dudric[1], L. Barbu-Tudoran[2,3], V. Toma[4], R. Stiufiuc[4], E. Burzo[1], R. Tetean[1]

[1]Faculty of Physics, "Babes Bolyai" University, Kogalniceanu 1, 400084 Cluj-Napoca, Romania
[2]Electron Microscopy Center "Prof. C. Craciun", Faculty of Biology & Geology, "Babes-Bolyai" University, 5-7 Clinicilor St., 400006 Cluj-Napoca, Romania.
[3]Integrated Electron Microscopy Laboratory, National Institute for Research and Development of Isotopic and Molecular Technologies, 67-103 Donat St., 400293 Cluj-Napoca, Romania
[4]Department of Bionanoscopy, MedFuture Research Center for Advance Medicine,"Iuliu Hatieganu" University of Medicine and Pharmacy, Pasteur 4-6, 400337 Cluj-Napoca, Romania

We report the successful synthesis and a complete magnetic characterization of $CoFe_2O_4$@SiO_2@Au magnetoplasmonic nanoparticles. The $CoFe_2O_4$ magnetic nanoparticles were prepared by using the hydrothermal method. A subsequent SiO_2 shell followed by a plasmonic Au shell were deposited on the magnetic core creating magnetoplasmonic nanoparticles with a core-shell architecture. A spin glass type magnetism was shown at the surface of the $CoFe_2O_4$ nanograins. Depending on the external magnetic field, two types of spin-glasses were identified and analyzed in correlation with the exchange field acting on octahedral and tetrahedral iron sites. The reduced magnetizations of spin glass components follow a $m_g=(1-bH^{-1/2})$ field dependences. The *b* values are strongly correlated with the intensities of exchange interactions. The magnetization per formula unit of $CoFe_2O_4$ core is not changed in the case of $CoFe_2O_4$@SiO_2@Au nanocomposites. The gold nanoparticles creating the plasmonic shell, show a giant diamagnetic susceptibility, dependent on their crystallite sizes.

Sunday, September 11, 2022

9:30 **Excursion I: Three Island Cruise**

19:30 Dinner break

Monday, September 12, 2022

7:30 **Excursion II: Montenegro Highlights**

19:30 Dinner break

Tuesday, September 10, 2022

08:00	**Invited and Oral Sessions** HALL 1, HALL 2-University of Dubrovnik
10:10	**Coffee break**
11:50	**Plenary and Invited Session** HALL 1
12:40	**Lunch**
15:00	**Plenary and Invited Session** HALL 1
17:20	**Coffee break**
17:50	**Invited and Oral Sessions** HALL 1, HALL 2
18:30	**Excursion III** **Sunset and dinner on KARAKA boat**

T5-O: Investigation of atomic electric fields in 2D WSe_2 by STEM differential phase contrast

M. Groll[1], J. Buerger[1], J. K. N. Lindner[1]

[1] *Nanopatterning – Nanoanalysis – Photonic Materials, Department of Physics, Paderborn University, Paderborn, Germany*

Two-dimensional transition metal dichalcogenides (TMDs) are promising candidates for next generation optoelectronic devices such as single photon emitters or high-performance field effect transistors [1]. These applications exploit the exciting and layer-thickness dependent electronic and optical properties of 2D TMDs such as a direct band gap for a monolayer instead of an indirect one for the bulk form [2]. While TMD monolayers consist of covalently bond metal and chalcogen atoms, the stacked layers forming the 3D bulk material are only bond by weak van der Waals interaction. This layered structure facilitates a comparably easy fabrication of 2D thin films. Since the optoelectronic properties are dominated by the electronic structure of the individual layers and influenced by the electric field distribution around atoms and defects, investigations of the electric field and charge density distribution with subatomic resolution are crucial.

One of the techniques allowing the characterization of electric fields within a specimen is differential phase contrast (DPC) in scanning transmission electron

microscopy (STEM). In combination with state-of-the-art correction of lens aberrations, STEM DPC even enables to visualize and quantify electric field distributions around single atoms. DPC measurements are based on the detection of the center of mass (CoM) shift of the intensity distribution caused by the Coulomb interaction of the incident beam electrons with the electric fields inside the specimen [3]. These shifts are measured with a position sensitive detector such as a segmented or pixelated detector. For segmented detectors, accurate electric field magnitudes are obtained using the intensity differences of opposing detector segments and an adequate calibration.

In order to reveal the electric field and charge density distribution of 2D WSe_2 mechanically exfoliated flakes were transferred to TEM grids. STEM-DPC measurements on these 2D flakes are performed at an acceleration voltage of 80 kV using an eight-fold segmented detector. We show the electric field and charge density distribution of WSe_2 flakes of different thicknesses with subatomic resolution. Furthermore, a comparison of the electric field distribution of pristine and defective WSe_2 lattices is given as those defects have an influence on the optoelectronic behavior.

[1] J. An et al, Adv. Funct. Mater **2022**, 32, 2110119.

[2] J. Gusakova, et al, Phys. Status Solidi A **2017**, 214, 1700218.

[3] K. Müller, et al, Nat. Commun. **2014**, 5, 5653.

T1-O-online: Deposition and manipulation of carbon nanotube bundles on a CMOS-compatible platform

R. S. Singh[1,2], K. Takagi[2], T. Aoki[2], J. Moon[2], Y. Neo[2], F. Iwata[2], H. Mimura[2], D. Moraru[2]

[1]*Graduate School of Science and Technology, Shizuoka University, Japan*
[2]*Research Institute of Electronics, Shizuoka University, Japan*

The miniaturization of electronics pushes the dimensions of the key devices, Si transistors, well into the nanoscale [1], posing several fundamental challenges. Carbon nanotubes (CNTs), particularly single-walled CNTs (SW-CNTs), have been widely considered for future electronics due to their excellent transport properties, nanoscale dimensions, and flexibility [2]. SW-CNTs can be made more compatible with CMOS platforms by using appropriate deposition methods.

CNTs are typically grown or deposited by solution processing on the substrate, which does not allow adequate control of CNT density and/or local positioning. We look into the possibility of using an emerging technology called inkjet printing technology to deposit low-density SW-CNT bundles locally, intending to fabricate CMOS-compatible CNT-devices. In this work, we investigated the deposition conditions for low-density CNT-bundles and subsequent manipulation by an atomic force microscopy (AFM) technique. Proof-of-concept demonstrations of interruption of some CNT-bundles allows the deeper study of current through such low-density CNT networks.

First, we optimized the homogeneity and dispersion conditions of SW-CNTs using dimethylformamide (DMF) solvent for inkjet printing (or NMP in some cases). It is well

understood that obtaining a stable solution for a suitable dispersion is critical because van der Waals attractive forces between the CNTs can form nano-bundles, ropes, or agglomerates [3]. Long-time sonication was done to achieve good solution homogeneity on Si/SiO_2 surface. The objective of device fabrication is to deposit individual CNTs or CNT-bundles between Al electrodes on SiO_2 to form a transistor structure. In order to accomplish this, Al electrodes (approx. 100 nm thick) with gaps of 300-5000 nm were fabricated using a lift-off method. The CNT-bundles were deposited in the gap between Al electrodes by inkjet printing.

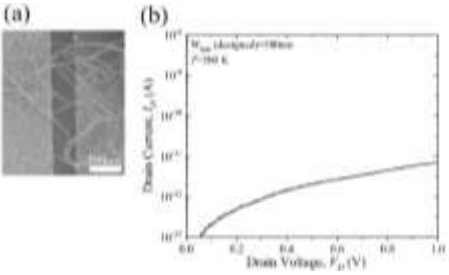

Fig. 1 (a) FE-SEM image of a CNT-bridge network deposited by inkjet printing in a gap (designed gap = 500 nm) between Al source and drain electrodes. (b) Room-temperature (T=300K) I_D-V_D characteristics for a CNT-FET, exhibiting low current via one or a few CNT-bridge(s).

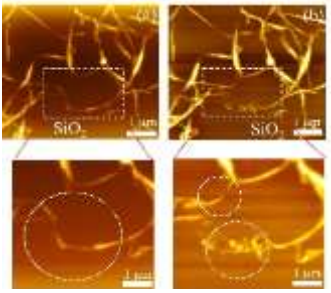

Fig. 2 (a) AFM image of CNT-structures deposited by pipette dropping from NMP solution on SiO_2 surface; (b) AFM image on the same area after applying AFM manipulation. Zoom-in images are shown below for clarity.

Figure 1(a) shows an FE-SEM image of a CNT-FET containing a few CNT-bridges deposited in the nano-gaps. Figure 1(b) shows room temperature output I_D-V_D characteristics for the same device [4]. Structure as shown in Figure 1 (a) can be formed by inkjet printing with higher control, but further

manipulation of CNT-bundles may allow optimization of the position, angle or coupling. Figures 2(a) and 2(b) show a proof-of-concept demonstration of the modification of CNT-bundles by the AFM tip (observed by comparing (a) and (b) in the marked region) [4-5].
With further optimization of the deposition, device fabrication, inkjet printing and manipulation processes can be expected to allow precise control of CNT-deposition on a CMOS-compatible platform. This work can open new pathways for basic studies of hybrid nano-electronics.

[1] M. M. Waldrop, Nature **2016,** 530, 144-147.
[2] R. Saito *et. al,* "Physical Properties of Carbon Nanotubes", Imperial College Press, London **1998**.
[3] R. P. Tortorich and J. W. Choi, Nanomaterials **2013,** 3, 453-468.
[4] R. S. Singh, K. Takagi, T. Aoki, J. Moon, Y. Neo, F. Iwata, H. Mimura and D. Moraru, Materials **2022**, 15, 4935-1-9.
[5] F. Iwata, Y. Ohashi, I. Ishisaki, L. M. Picco and T. Ushiki, Ultramicroscopy **2013,** 133, 88-94.

T1-O-online: Fabrication and characterization of Cd – free A_{II} - B_{VI} heterojunctions for sensing applications

A. M. Panaitescu[1], V. A. Antohe[1,2]

[1]University of Bucharest, Faculty of Physics, R&D Center for Materials and Electronic & Optoelectronic Devices (MDEO), 405 Atomistilor Street, PO Box MG-11, Bucharest-Magurele, 077125, Romania
[2]Universieé catholique de Louvain (UCLouvain), Institute of Condensed Matter and Nanosciences (IMCN), Place Croix du Sud 1, B-1348 Louvain-la-Neuve, Belgium

A cadmium (Cd) free substrate-type based on ZnSe/ZnTe heterojunction structure was obtained by evaporating onto optical glass 100 nm gold (Au) thin film representing the back

contact. Afterwards, a 500 nm ZnTe was sputtered followed by zinc selenide (ZnSe), zinc oxide and ITO, finally resulting the (Au/ZnTe/ZnSe/ZnO/ITO) submicrometric structure. All the ultra thin films were deposited via magnetron sputtering radio-frecquency regime (MS-RF) technique, apart from Au layer obtained by vacuum thermal evaporation (TVE). Subsequent structural chracterization through X-Ray diffraction (XRD) along with morphological investigation via scanning electron microscopy (SEM), and optical characterization by UV-VIS spectroscopy were performed on all structure's ultra thin films. The electrical measurements onto the Cd free structure revealed an asymmetrical dark current-voltage characteristics and good photovoltaic response at AM 1.5 illumination. Moreover, the Schokley mechanism was identified, along with the evaluation of its corresponding parameters, such as diode ideality factor, reverse saturation current, and series and shunt resistances of the device. A sensibility test for the 420 nm – 500 nm domain was performed by varying incident wavelength's intensity from 100 W/cm^2 down to 10 W/cm^2 and measuring the photocurrent electrical intensity. In addition, the action spectrum when illuminating the structure at AM 1.5 provided the sufficient information to consider the present ZnSe/ZnTe heterojunction – based submicrometric structure to be more suitable for the UV domain, potentially integrated into UV sensing devices.

T1-I: Application of Laser Processing for Controlling IV Group Semiconductors Properties: Si, Ge, SiGe, GeSn

P. Onufrijevs

Institute of Technical Physics, Faculty of Materials Science and Applied Chemistry, Riga Technical University, P. Valdena 3/7, Riga LV-1048, Latvia

Lasers are highly versatile in almost any solid material processing and have a wide range of applications. A new approach is proposed – to use a temperature gradient field induced by powerful pulsed laser radiation with the aim to generate and redistribute point defects and impurity atoms. In this case, there is a possibility to form a graded bandgap structure, form nano-cones, homo- and hetero-junction.

The most recent topic of investigation is related to overcoming the equilibrium solubility of Sn atoms in Ge and the relaxation of residual strain in GeSn epitaxial layers by laser radiation. The binary GeSn alloys on Ge/Si substrates are very promising candidates for mid-infrared Si photonics [1] due to the possibility of obtaining a direct bandgap semiconductor at more than 8% content of Sn atoms. However, the compressive strain [2] for such GeSn/Ge heterostructures plays a crucial role in the indirect-to-direct bandgap transition leading to the shift towards higher Sn concentrations. Unfortunately, the growth of a fully strain-relaxed GeSn epilayer with high Sn atoms content and high material quality is challenging due to several reasons: the high segregation coefficient on Sn inside the Ge; the lattice mismatch between α-Sn and Ge (Si) is 14.7% (19.5%), and the equilibrium solid solubility of Sn in Ge is less than 1%.

In this study, we applied post-growth femtosecond and nanosecond laser processing of Ge1-ySny (y=4-8%) alloys with

the aim to study strain relaxation of GeSn epilayers grown by MBE on Ge/Si substrates. In both cases, the RSM method revealed that laser processing has been leading to the partial compressive strain relaxation of GeSn epilayer depending on laser radiation intensities. The increase of Sn atomic concentration, revealed by TEM-EDS and XPS up to 14% at the surface layer, was obtained using nanosecond laser radiation and explained by the thermogradient effect [3]. At the same time, femtosecond laser radiation almost did not change the content of Sn atoms in the GeSn layers. SEM and AFM imaging provided evident microstructure changes and formation of LIPSS [3] at higher laser intensities, while slow carrier lifetime changes, determined by differential transmittivity, were not observed for nanosecond laser processing, indicating that laser irradiation does not generate defects that reduce the electronic quality of the material. However, infrared time-resolved pump-probe spectra revealed the reduction of fast relaxation decay times.

Acknowledjments. The study has been supported by the European Regional Development Fund within the Activity 1.1.1.2 “Post-doctoral Research Aid” of the Specific Aid Objective 1.1.1 “To increase the re- search and innovative capacity of scientific institutions of Latvia and the ability to attract external financing, investing in human resources and infrastructure” of the Operational Programme “Growth and Employment” (No. 1.1.1.2/VIAA/3/19/409).

[1] D. Schwarz, et al., 44th Int. Conv. Information, Commun. Electron. Technol., IEEE, **2021**, pp. 50–54.
[2] W. Dou, et al., Sci. Rep. **2018**, 8, 5640.
[3] P. Onufrijevs, et al., Opt. Laser Technol. **2020,** 128, 106200.

T1-I: Laser Processing for Enhanced Antibacterial Properties of Titanium Plates

L. Grase

Institute of Materials and Surface Engineering, Faculty of Materials Science and Applied Chemistry, Riga Technical University, Riga, Latvia

A laser is an important tool widely used to process surfaces of materials in order to control surface topography and phase composition thus influencing a variety of properties, including surface wettability, antimicrobial properties, and tribology. The controlled enhancement of antibacterial properties of titanium and its alloys can be achieved by using laser-induced micro-texturing of the surfaces [1]. Laser-induced periodic surface structures (LIPSS) play an important role in the production of antibacterial surfaces [2]. The development of the antibacterial properties of a surface depends not only on the parameters of obtained microstructure but also on certain types of bacteria. Therefore, the study aims to develop femtosecond (fs) laser technology to obtain enhanced antibacterial properties of titanium surfaces with LIPSS against *S. aureus* and *E. coli*. Titanium samples were irradiated by fs laser. The optimization of antibacterial properties was performed using different hatch spacings in micrometer range. The morphology and chemical composition of these surfaces were investigated by field emission scanning electron microscopy (FESEM), Energy Dispersive X-ray spectroscopy (EDS), X-ray photoelectron spectroscopy (XPS), Raman spectroscopy, and others. A drop shape analyzer was used to determine wetting properties. The antibacterial activity of samples was determined by ISO 22196:2011 standard using reference bacterial cultures of Gram-positive *Staphylococcus*

aureus (ATCC 25923) and Gram-negative *Escherichia coli* (ATCC 25922). After irradiation by fs laser the LIPSS are formed on the surface of Ti plates with periodicity in the range of about 300 – 850 nm, as well as changes in surface chemical composition took place, suggesting Ti (IV) oxides formation. The experimental results revealed that morphological and surface chemical composition changes of the titanium surface induced by fs laser radiation led to enhanced antibacterial properties against *S.aureus* by more than 99 % and *E.coli* more than 80% in comparison with non-irradiated Ti plate sample. The best results were obtained with hatch spacings 12 μm against *S.aureus* and 16 μm against *E.coli*. The difference in results could be explained by the difference of shape and cell wall structure of certain bacteria.

Acknowledgments. This work has been supported by the European Regional Development Fund within the Activity 1.1.1.2 "Post-doctoral Research Aid" of the Specific Aid Objective 1.1.1 "To increase the research and innovative capacity of scientific institutions of Latvia and the ability to attract external financing, investing in human resources and infrastructure" of the Operational Programme "Growth and Employment" (No.1.1.1.2/VIAA/4/20/638).

[1] I. Shivakoti et.al., Coatings, **2021**, 11, 124, 1 – 15
[2] B. Dashtbozorg et.al., Appl. Surf. Sci., **2021**, 565, 150594.

T1-I: Thin Composite Nanostructured Films for Electromagnetic Shielding of Modern Electronics

V. Barsukov[1], V. Khomenko[1], I. Senyk[1], Ya. Kuryptia[1], O. Butenko[1], O. Chernysh[1], V. Tverdokhleb[1], I.V. Tudose[2, 3, 4], K. Muratis[2], O.N. Ionescu[5], M. Suchea[2,5], E. Koudoumas[2]

[1]Department for Electrochemical Power Engineering and Chemistry, Kyiv National University of Technologies and Design/ Kyiv, Ukraine
[2]Center of Materials Technology and Photonics, School of Engineering, Hellenic Mediterranean University/ Heraklion, Crete, Greece
[3]Chemistry Department, University of Crete/ Heraklion, Crete, Greece
[4]Institute of Electronic Structure and Laser, Foundation for Research & Technology-Hellas/ Heraklion, Crete, Greece
[5]National Institute for Research and Development in Microtechnologies-IMT / Bucharest, Romania

We present results proving the exsistance of synergetic effect between carbon materials of different morphology, for example, between colloidal graphite and graphitized carbon black. The joint contribution of both components was found to result in higher shielding efficiency than that of the common arithmetic sum of their individual contributions (Fig. 1).

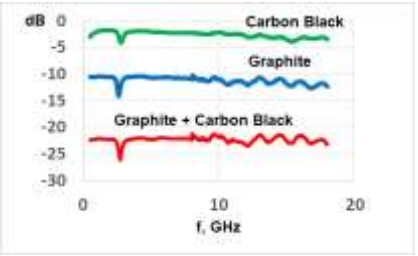

Fig. 1. Synergetic effect of carbon materials of different morphology

Our team has developed thin coatings based on composite paints, which ensure a shielding efficiency at the level of -30 - 50 dB in the frequency range from 50 MHz to 30 GHz.

Moreover, the use of other nanomaterials as fillers, e.g. graphene, carbon nanotubes, etc. allows to increase the shielding efficiency up to -50 dB at the frequency of 30 GHz.
In addition, the composition of the films enables to get a required ration between the reflection and absorbtion (Fig.2).

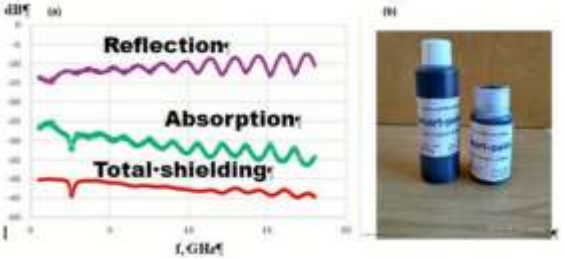

Fig 2. The reflection, absorption and total shielding efficiency (a) for developed paints (b).

To measure these performances, we used measuring complex from KEYCOM Corp. (Japan) based on the vector analyzer Anritsu MS 46122 A-020 and special TEM-cells, the results of the measurements corresponding to the ASTM ES7 and ASTM D4935 standards.
To this date, our coatings have been applied to the inner surface of around 5000 Ukrainian thermal scanners of ARCHER brend and 100 radiation measurement portable devices SVG.

Acknowledgements. The authors acknowledge the financial support from the NATO Science for Peace and Security Programme, grant G5477 “Nanostructured composite paints for electronics electromagnetic shielding”.

T1-O: Atomic electric fields in InAs measured by scanning transmission electron microscopy

J. Buerger[1], V.S. Kunnathully[1], T. Riedl[1], J.K.N. Lindner[1]

[1]*Paderborn University, Department of Physics, Warburger Straße 100, 33098 Paderborn Germany*

InAs quantum dots (QDs) are promising for quantum optic devices such as single photon emitters [1]. However, the crystalline quality is crucial for the device performance since defects influence the electronic properties of the InAs QDs. Among the electronic properties is the electric field distribution and in particular the electric field distribution around individual atoms. Differential phase contrast (DPC) in scanning transmission electron microscopy (STEM) is one of the techniques that allows the measurement of such electric fields and the derivation of charge densities [2]. In combination with state-of-the-art C_s-correction of lens aberrations, the visualization and quantification of electric fields is possible with a resolution far below the typical distance of atoms in a crystalline specimen. DPC is based on the measurement of transferred momenta imposed on the incident beam by the specimen's electrostatic potentials. As a rough approximation, the interaction with the electric field at each pixel of the scan can be assumed to be similar to that in a plate capacitor. This results in a rigid deflection of the beam or a redistribution of the intensity distribution measureable with a position sensitive detector. Therefore, the aim of this study is to investigate the atomic electric field distribution and charge densities in InAs QDs using DPC.

Quantum dots of InAs are heteroepitaxially grown on prepatterned GaAs substrates by molecular-beam epitaxy [3]. Nanosphere lithography combined with reactive ion etching is used to pre-pattern the GaAs substrate, resulting in GaAs pillars on whose tops InAs QDs are grown. A focused ion beam instrument is employed for the preparation of the TEM specimen. DPC characterizations are conducted on a probe-side C_s-corrected JEOL JEM ARM200f at an acceleration voltage of 200 kV using an eight-fold segmented detector and paired with conventional STEM dark-field imaging. In addition, multi-slice DPC image simulations are calculated for comparison.

We show sub-atomically resolved quantitative electric field maps of InAs QDs analysed in [110] zone axis orientation. The atomic electric fields as well as the charge densities are in good agreement to corresponding multi-slice image simulations. Measured electric field magnitudes are in a range of several tenth V/nm, also matching the electric field magnitudes of other III-V semiconductors such as GaN [2]. Crescent-like features in the electric field distribution of In atomic columns are observed, which are presumably due to bonding. Investigations of the electric field and charge density distributions at nanotwin boundaries reveal a reduction in electric field magnitude at the twin boundary.

[1] M.V. Rakhlin, et al., Sci. Rep. **2018**, 8, 5299.
[2] K. Müller-Caspary, et al., Ultramicroscopy **2017**, 178, 62-80.
[3] T. Riedl, et al., Adv. Mat. Interfaces **2022**, 9.11, 2102159.

T3-I-online: The Role of Surface Topography in Optimising Triboelectric Nanogenerator Performance

D. M. Mulvihill[1], G. Min[2], Y. Xu[1], R. Dahiya[2]

[1]Materials and Manufacturing Research Group, James Watt School of Engineering, University of Glasgow, Glasgow, UK
[2]Bendable Electronics and Sensing Technologies (BEST) Group, James Watt School of Engineering, University of Glasgow, Glasgow, UK

Triboelectric nanogenerators are a promising energy harvesting technology receiving significant global attention at present. However, results published in the literature have indicated that their output appears to be very sensitive to contact pressure. We demonstrate that the contact pressure dependence of TENG output arises because of the contact pressure dependence of the real contact area.

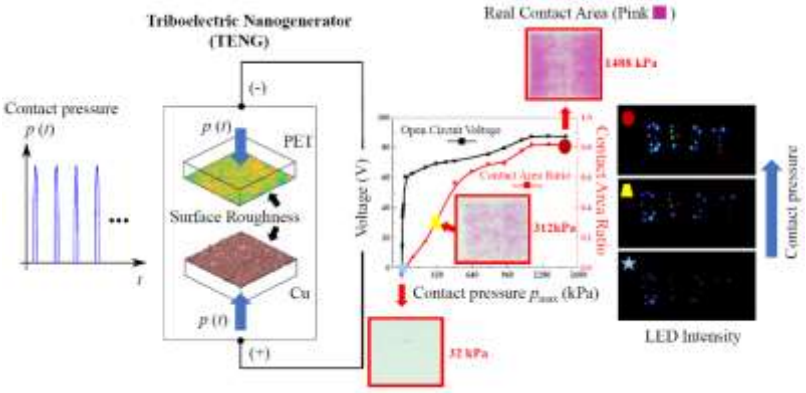

Fig. 1. Effect of surface topography and contact pressure on triboelectric nanogenerator output. Left to right: mechanical forcing function, rough surface TENG, TENG output voltage and contact area versus contact pressure and LED intensity with increasing contact pressure.

This is because, for surfaces with roughness (Fig. 1), real contact area is pressure-dependent.

We demonstrate this by concurrently measuring both TENG electrical output and real contact area over a wide range of pressures [1]. As shown in Fig. 1, the evolution of voltage output with contact pressure closely tracks the response of contact area with pressure. In fact, both electrical output and contact area appear to saturate at about the same pressure. TENG output increases with contact pressure and the LEDs in Fig. 1 become progressively brighter. We also explore applications and implications of the contact pressure sensitivity and put forward a new TENG model incorporating the mechanics of surface roughness with the electrostatics of TENGs to correctly predict the contact pressure-dependant TENG response observed in experiments [2]. The important implication is that surface topography and contact pressure must be carefully considered in the design of TENGs and their output can clearly be optimised by optimal selection of surface topography, mechanical properties of the contacting materials and contact pressure.

[1] G. Min, Y. Xu, P. Cochran, N. Gadegaard, D. M. Mulvihill, R. Dahiya, Nano Energy, **2021**, 83, 105829.

[2] Y. Xu, G. Min, N. Gadegaard, R. Dahiya, D. M. Mulvihill, Nano Energy, **2020**, 76, 105067.

T3-O-online: Preparation and characterization of new membrane-based on PVDF fibers loaded with TiO_2:Sm reinforced with graphene/graphene oxide for wastewater cleaning

P. Pascariu

"Petru Poni" Institute of Macromolecular Chemistry, 41A Grigore Ghica Voda Alley, 700487, Iasi, Romania

Currently, water pollution caused by industrialization, population growth, and global warming has determined the development of new methods for obtaining clean water. The textile and drug industries are the largest sources of water pollution [1].

New composite membranes based on PVDF fibers loaded with Sm doped TiO_2 (TiO_2:Sm) nanostructures [2] and graphene-based nanoparticles obtained by the electrospinning technique are reported. The addition of the inorganic nanostructures induced photocatalytic properties, while the graphene-based nanoparticles (G - graphene or GO - graphene oxide) improved the mechanical properties. The materials were evaluated in terms of crystalline structure (XRD), surface morphology (SEM), mechanical and adsorption/desorption properties. The membranes were used in photocatalytic assays for the degradation of methylene blue (MB) under visible light irradiation. To intensify the photocatalytic processes, the effect of hydrogen peroxide addition was also investigated. The results revealed that the PVDF-based membrane containing 15% TiO_2:Sm and 2.5% GO showed an optimal photocatalytic activity due to its high porosity, relevant adsorption capacity, and improved mechanical properties. The response surface methodology

was employed to optimize the experimental conditions of the photocatalytic process.

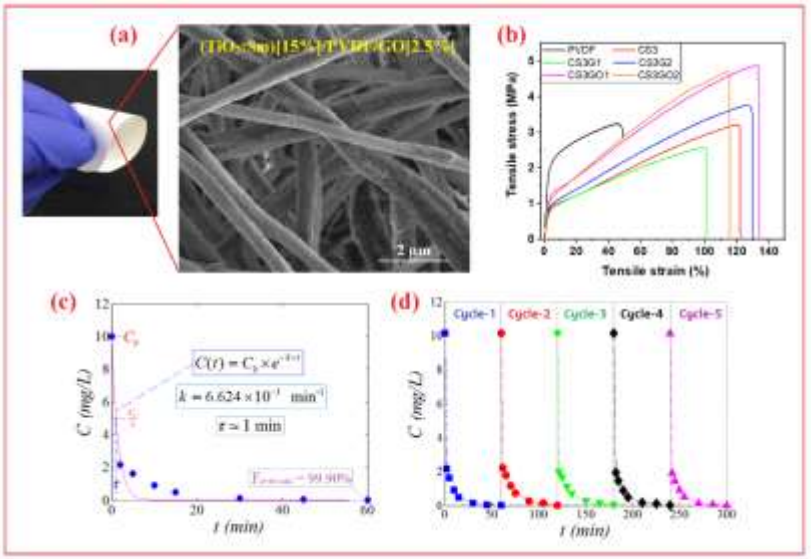

Fig. 1. High entropy alloys: a) SEM images of (TiO_2:Sm)[15%]/PVDF/GO[2.5%]; b) elongation at break and Young's modulus (%) for TiO2:Sm[10, 15, or 18%] doped PVDF samples before the addition of G or GO; c) kinetics of photocatalytic degradation (visible light) of MB dye recorded under optimal conditions; d) Recycling of MB dye degradation for five times under similar experimental conditions.

The addition of H_2O_2, significantly increased the rate constant of photodegradation reaction ($k=6.624 \cdot 10^{-1} min^{-1}$), disclosing a half-life of the reaction of about 1 min. This short half-life time represents a remarkable outcome for a photocatalytic process conducted under visible light irradiation. Also, good recycling capacity was observed for the optimal (TiO_2:Sm)[15%]/PVDF/GO[2.5%] composite membrane.

[1] M. Homocianu, P. Pascariu, J. Environ. Manage. **2022**, 311, 114817.
[2] P. Pascariu, C. Cojocaru, M. Homocianu, P. Samoila, J. Environ. Manage. **2022**, 316, 115317.

T3-O-online: Deposition of $Sr_xTi_yO_z$ thin films with controlled stoichiometric compositions using a combinatorial approach based on Chemical Beam Vapour Deposition for photocatalytic applications

V. Roge[1], C. Garlisi[1], P. Lunca Popa[1], K. Menguelti[1], M. Michel[1], C. Vergne J. Guillot[1], E. Wagner[2], W. Maudez[2], G. Benvenuti[2], B. R. Pistillo[1], E. Barborini[1]

[1]Materials Research and Technology (MRT) Department, Luxembourg Institute of Science and Technology (LIST), L-4422 Belvaux, Luxembourg
[2]3D-Oxides, F-01630 Saint Genis Pouilly, France

Perovskites materials with ABO_3 structure such as $SrTiO_3$ have been widely studied in the last decade for their remarkable physico-chemical properties and multiple application fields like ferroelectricity, sensing or photocatalysis for renewable energies production or environmental remediation [1, 2]. Although many synthesis methods have already been employed for the growth of $SrTiO_3$, the approach using a combinatorial deposition process like chemical beam vapour deposition (CBVD) paves the way to the understanding of their stoichiometric dependent properties [3].
In this work, we aim at presenting the relationship linking crystallinity, optical properties, and photocatalytic activity of $Sr_xTi_yO_z$ thin films to their composition. For example, as depicted on Fig. 1, the use of a proper deposition setup allows the growth of a compositionally graded thin film with Sr/Ti

ratios ranging from 0.2 to 1.3. Material with a sub-stoichiometric strontium composition (Sr/Ti = 0.2 – 0.4) shows an amorphous structure, whereas crystalline $SrTiO_3$ is observed at a Sr/Ti ratio close to 1. At intermediate values, crystalline and amorphous phases coexist.

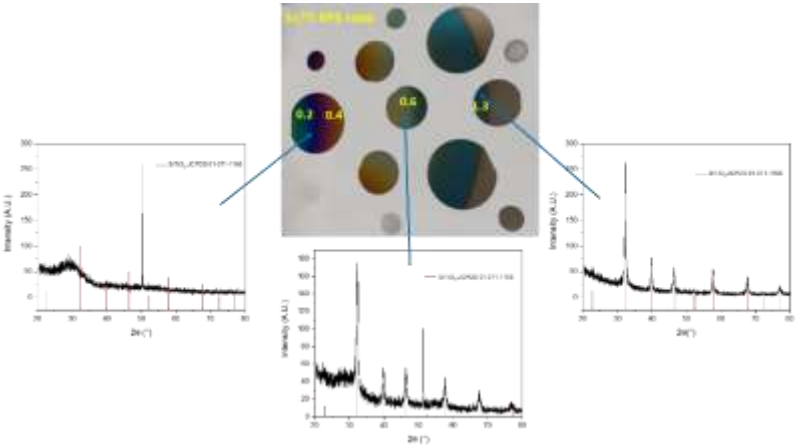

Fig. 1. Photographic image highlighting the compositionally graded $Sr_xTi_yO_z$ thin film, associated with XRD diffractograms and Sr/Ti ratios determined by XPS.

Optical properties of the different $Sr_xTi_yO_z$ thin films as well as results of photocatalytic activity, evaluated by the standard approach of decolourisation of methylene blue, will be shown. CBVD combinatorial approach enables effective study of the dependence of material features on stoichiometry in complex oxides, enabling in turn the fine-tuning of material properties in respect to the target applications.

[1] J. Chen, Z. He, G. Li, T. An, H. Shi, Y. Li, Appl. Catal. B: Environ. **2017,** 146-154.

[2] B.L. Phoon, C.W. Lai, J.C. Juan, P.L. Show, W.H. Chen, Intern. J. Energ. Res, **2019**, 43, 5151-5174.
[3] C. Garlisi, P. Lunca Popa, K. Menguelti, V. Roge, M. Michel, C. Vergne, J. Guillot, E. Wagner, W. Maudez, G. Benvenuti, B.R. Pistillo, E. Barborini, Nanomaterials (Basel) **2022**, 12, 1012.

T3-O-online: Synergistic effect of monoclinic and partially hydrated WO_3 in $Au/TiO_2/WO_3$-$WO_3 \cdot 0.33H_2O$ heterostructures for applications in heterogenous photocatalysis and SERS

I. Szekely[1,2], K. Saszet[1,2], Zs-R. Toth[2], T. Gyulavari[3], K. Magyari[1,2], M. Baia[1,2]

[1]Faculty of Physics, Babeș-Bolyai University, Cluj-Napoca, Romania
[2]Centre of Nanostructured Materials and Bio-Nano Interfaces, Institute for Interdisciplinary Research on Bio-Nano-Sciences, Cluj-Napoca, Romania
[3]Department of Applied and Environmental Chemistry, University of Szeged, Szeged, Hungary

Commercial TiO_2 is an efficient photocatalyst under ultraviolet light irradiation for degrading and mineralizing organic pollutants, like dyes, alkaloids, and pharmaceuticals [1,2]. However, due to its wide band gap of ≈ 3.2 eV, the photocatalytic efficiency of TiO_2 under visible light irradiation is modest. To remediate this issue, ternary $Au/TiO_2/WO_3$ heterostructures were developed to improve the commercial TiO_2's photocatalytic efficiency under visible and ultraviolet light irradiation to extend the applicability range of TiO_2 as sensing, adsorption, respectively hydrogen production.
In this work, $Au/TiO_2/WO_3$ heterostructures were synthesized, where two types of tungsten oxides were employed to prepare the composites. 12% (w/w%) monoclinic (WO_3); 12% hexagonal partial hydrate ($WO_3 \cdot 0.33H_2O$), and 76%

commercial TiO_2 (Evonik Aeroxide P25) were utilized to prepare the pH adjusted (pH = 1) TiO_2/WO_3-$WO_3 \cdot 0.33H_2O$ composites [3]. Gold nanoparticles were deposited on the TiO_2/WO_3-$WO_3 \cdot 0.33H_2O$ ternary composites surface employing a slightly modified Turkevich-Frens reduction method, thus obtaining the $Au/TiO_2/WO_3$-$WO_3 \cdot 0.33H_2O$ (pH=1) composite.

The presence of the Au nanoparticles was proved by SEM-EDX and UV-Vis DRS measurements. Fourier Transform Infrared Spectroscopy, Raman Spectroscopy, and X-ray diffraction measurements were employed to prove the presence of TiO_2, monoclinic WO_3, and hexagonal partial hydrate $WO_3 \cdot 0.33H_2O$ semiconductors in the composite (Fig.1).

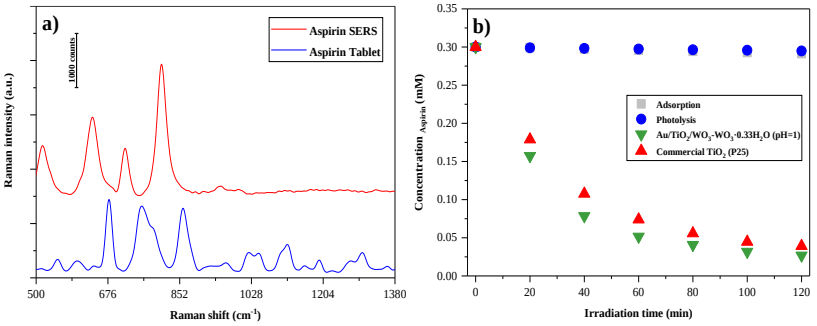

Fig. 1. Raman and SERS spectra of Aspirin (a); Photocatalytic removal of Aspirin under UV light irradiation (b).

The photocatalytic efficiency of the composite was evaluated by methyl orange, caffeine, and aspirin removal under UV and visible light irradiation, and its SERS applicability was assessed by detecting Aspirin and caffeine in small concentrations.

The novel composite showed improved UV light-driven photocatalytic efficiency compared to commercial TiO_2 for methyl orange, caffeine, and aspirin degradation and mineralization; as well as the composite is an efficient

photocatalyst under visible light irradiation, respectively it showed potential as a SERS material.

[1]C. Castaneda, J. J. Martinez, L. Santos, H. Rojas, S.M. Osman, R. Gomez, R. Luque, Chemosphere, **2022**, 288, 132506.
[2]I. Acosta, E. Moctezuma, K. Lopez de la O, E. Leyva, B. Zermeno, Top. Catal. **2022**.
[3]I. Szekely, M. Baia, K. Magyari, B. Boga, Z. Pap, Appl. Surf. Sci. **2019**, 490, 469–480.

T3-O: Metal-organic frameworks for energy applications

V. Zelenak, N. Kiraly

Department of Inorganic Chemistry, Faculty of Science, P.J. Safarik University in Kosice, Kosice, Slovakia

Creating an environmentally friendly and carbon-neutral society is currently a significant challenge. An emphasis on reducing the carbon footprint of human activities and efforts made to adopt sustainable and renewable energy sources resonate at various levels of society. The transport sector and the automotive industry represent significant challenges. The introduction and use of batteries and electric vehicles as well as hydrogen technologies is an important step toward reducing the carbon footprint of traffic.
Among the most challenging materials for energy storage are porous coordination polymers, also called metal–organic frameworks (MOFs). MOFs are two- or three-dimensional porous crystalline materials with infinite lattices. In our work we have prepared new MOFs, which were studied for hydrogen storage and also used as a host for sulphur, as a conductive part of cathode material of Li-S bateries.

We prepared a galium metal-organic framework $\{[Ga_2(H2TCPP)(OH)_2]\cdot 5DMF\cdot 2H_2O\}_n$ denoted as GaTCPP containing a porphyrinic base ligand was used as a host for sulphur. Lithium−sulphur batteries attract increasing interest due to their high theoretical specific capacity, advantageous economy, and "eco-friendliness". As a conductive part of cathode material, GaTCPP MOFs displayed successful sulphur capture and encapsulation proven by stable charge/discharge cycle performances (Fig. 1), high-capacity retention, and Coulombic efficiency. The electrodes with pristine GaTCPP showed a discharge capacity of 699 mAh g^{-1} at 0.2 C in the fiftieth cycle. However, the doping of GaTCPP by Ni^{2+} has a positive impact on the electrochemical properties, the capacity increased to 778 mAh g^{-1} in the fiftieth cycle at 0.2 C.

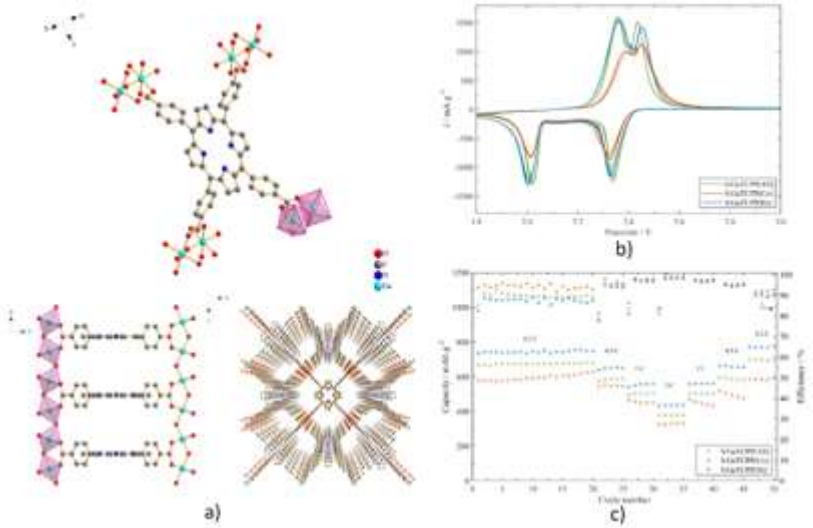

Fig. 1. a) Structure of GaTCPP; b) cyclic voltammograms at a scan rate of 0.1 mV s^{-1}; b) galvanostatic cycling at different C-rate.

In addition to battery application, we investigated porous MOF for hydrogen adsorption/storage. Safe and large storage of hydrogen is one of key factors for widespreading of hydrogen technologies. In our work we prepared novel holmium porous metal-porphyrin framework {[Ho(H_2TPPS)]·H_3O^+·4H2O}$_n$. The compound showed CO_2 and H_2 adsorption. Hydrogen adsorption was studied at -196 °C with hydrogen uptake 2.1 wt.% at 1 bar.

Acknowledgement. This work was supported by the Scientific Grant Agency of the Slovak Republic (VEGA) under Project No. 1/0865/21.

T3-O: Electrochromic polyamides featuring triphenylamine moiety modified with methyl and trifluoromethyl groups

C. P. Constantin, R. D. Radu, M. D. Damaceanu

Electroactive Polymers and Plasmochemistry Department, "Petru Poni" Institute of Macromolecular Chemistry, Aleea Grigore Ghica Voda 41A, Iasi - 700487, Romania

As part of our pursuit for new advanced materials capable of tackling current technological concerns, we developed the chemical blocks to build new polyamides viable as electrochromic (EC materials). Hence, we designed a novel TPA-functionalized diamine by combining several structural elements, each playing its part toward enhanced, highly stable EC response with suitable processability. We used the trifluoromethyl group to augment solubility and transparency, the ortho-connected methyl moiety to lower TPA's oxidation potential, and the dimethylamine unit to block its para position to avoid radical cation recombination and enhance

redox stability. Moreover, the latter was foreseen to provide an additional oxidation state which may enrich the overall optical and EC behavior of the resulting material [1,2]. Three new polyamides incorporating TPA units were prepared by using acid dichlorides as monomeric counterparts. Detailed structural characterization of the diamine and resulting polymers was carried out by spectroscopic tools, followed by comprehensive photo-optical investigation assisted by computational calculations. A close-up of the redox and electrochemical stability of the synthesized materials was also performed via cyclic voltammetry. The architectural variation in the polyamidic backbone imposed by the structural alteration in the diacid segment determined individual monitoring of the spectroelectrochemical behavior of each polymer to draw structure-function correlations, with an emphasis on electrochromic effect, stability, and efficiency.

Acknowledgments. This work was supported by a grant of the Romanian Ministry of Research, Innovation and Digitization, CNCS/CCCDI – UEFISCDI, Project PN-III-P2-2.1-PED-2019-3520, 438PED/2020, within PNCDI III.

[1] F.W. Li, T.C. Yen, G.S. Liou, Electrochim. Acta **2021**, 367, 137474.
[2] J.T. Wu, H.T. Lin, G.S. Liou, ACS Appl. Mater. Interfaces **2019**, 11 (16), 14902–14908.

T3-O: Combining TiO_2 & WO_3 with MoS_2 for efficient photo-/electrochemical water splitting

R. Levinas[1,2], N. Tsyntsaru[1,3], H. Cesiulis[1]

[1]*Department of Physical Chemistry, Institute of Chemistry, Faculty of Chemistry and Geosciences, Vilnius University, Vilnius, Lithuania*
[2]*Department of Catalysis, State research institute Center for Physical Sciences and Technology (FTMC), Vilnius, Lithuania*
[3]*Institute of Applied Physics, Chisinau, Republic of Moldova*

In the renewable energy field transition metal oxides (e.g., TiO_2 and WO_3) are often used as photoactive materials as they generate photoexcited electron-hole pairs at exposion to a light of sufficient energy. The electrons can be collected, whereas the holes can participiate in photoelectrochemical oxidation reactions. Thus, these materials act as photo- or photoelectrochemical catalysts. However, in order to lower their band gap and extend the range of absorbed wavelengths more towards visible light, they must be modified with other materials, e.g. MoS_2.

A practical method of producing TiO_2/MoS_2 and WO_3/MoS_2 composites is anodization. Anodization is a convenient and fast way to electrochemically form an oxide film: upon application of a sufficient anodic potential or current in corrosive media. As it dissolves, metal cations interact with hydroxide from water, and an oxide film is formed. This process can be further expanded by adding other materials into the anodization solution. In particular, the tetrathiomolybdate (MoS_4^{2-}) anion can anodically disproportionate into MoS_3. Thus, when anodization is carried out in an electrolyte containing MoS_4^{2-}, a composite of the metal oxide and a mixed-stoichiometry MoS_x is formed (Fig. 1).

The composites in this study were synthesized by different methods. TiO_2/MoS_2 was synthesized under controlled potentiostatic conditions in order to grow a structured nanotube morphology.

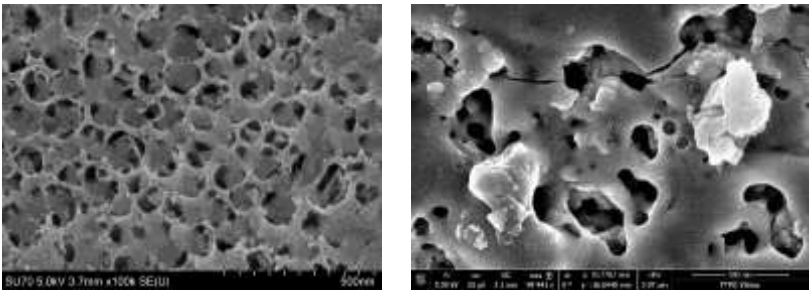

Fig. 2. SEM images of obtained by anodization composites: a) TiO_2/MoS_x; b) WO_3/MoS_x.

On the other hand, WO_3/MoS_2 was obtained by galvanostatic anodization, by setting a current density to reach enough voltage for plasma discharges to occur. Both materials were extensively characterized and applied for photoelectrochemical water splitting. It was found that the composites are more efficient that their respective base oxides.

Acknowledgements. This work has received funding from the European Union's Horizon2020 research and innovation programme under the MSCA grant №778357-SMARTELECTRODES and from the Vilnius University Junior Researcher project MSF-JM-6/2021.

T3-O: Emerging organic blends for ternary solar cells

L. Hrostea[1], L. Leontie[2]

[1]Research Center on Advanced Materials and Technologies (RAMTECH), Department of Exact and Natural Sciences, Institute of Interdisciplinary Research, Alexandru Ioan Cuza University of Iasi, Romania
[2]Faculty of Physics, Alexandru Ioan Cuza University of Iasi, Romania

Starting from the advantages of the binary blends of a donor (polymer) and an acceptor material (fullerene or non-fullerene) in the heterojunction-based solar cells and combining them with the strengths of tandem solar cells, this work presents a ternary blend photovoltaic structure (Fig. 1), involving a donor (D) and two acceptors (A_1 and A_2) materials. The studied blend is based on a chlorinated conjugated polymer (PBDB-T-2Cl), a non-fullerene (ITIC-F) and a fullerene (PCBM), in different weight ratios.

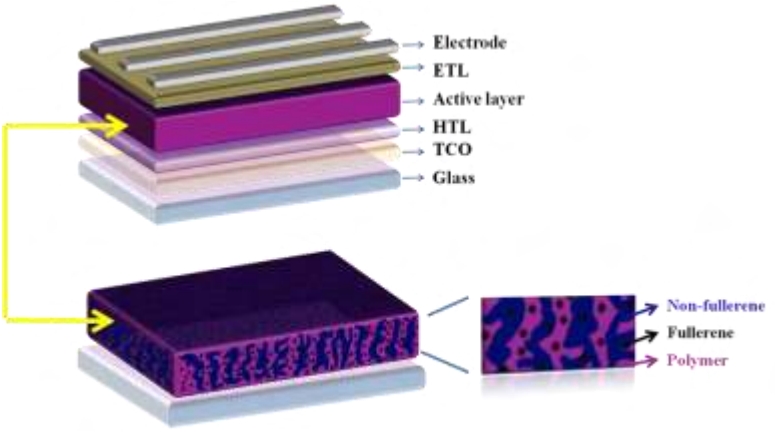

Fig. 2. Ternary organic solar cell (where ETL and HTL are electron, respectively hole transport layer, TCO is the transparent conductive oxide)

The optical, morphological and electrical properties attest that the proposed ternary blend guarantees: (i) a better overlap between the absorption spectrum of light-harvesting active layer and the solar spectrum by spectral complementarity of materials, (ii) improved charge carrier transport by appearance of a cascade-type energetics due to the alignment of different molecular orbital levels, and (iii) enhancement of electrical properties, which will be reflected in improved operating parameters of the device.

Acknowledgement: This work was supported by a grant of the Romanian Ministry of Research, Innovation and Digitization, CNCS - UEFISCDI, project number PN-III-P1-1.1-PD-2021-0394, within PNCDI III.

Plenary Session and Invited Session (HALL1)

PL: Advanced magnetic nanodevices as therapeutic agent

G.F. Goya[1,2,3], C. Marquina[1,2,3], J. A. Fuentes-Garcia[1,2,3], M. R. Ibarra[1,2,3]

[1]Instituto de Nanociencia y Materiales de Aragón (INMA), CSIC-Universidad de Zaragoza, Zaragoza 50009, Spain
[2]Laboratory of Advanced Microscopies, University of Zaragoza, Zaragoza 50420, Spain
[3]Departmento de Física de la Materia Condensada, Universidad de Zaragoza, Zaragoza 50009, Spain

Magnetic based nanodevices are considered as promising nanovectors for tumor treatment at the clinic and and also for therapeutic drug release [1]. The knowledge of the mechanisms triggering the cell dead using magnetic nanodevices as targeting vectors is relevant for the design of

these nanovectors for therapeutic purposes. For that objective several nanodevices as core-shell magnetic nanoparticles [2] and magnetic nanofibers [3] have been synthetized and tested in vitro using several cell lines (Fig.1).

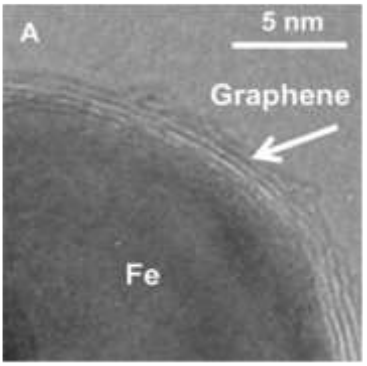

Fig. 1. Core&shell magnetic nanoparticles encapsulated in graphene cages

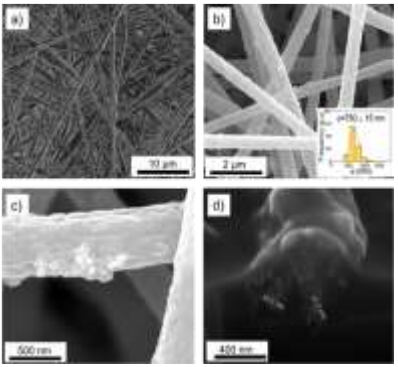

Fig. 2. SEM images of magnetic fibers: a) BES image; b) SE image and fiber diameter histogram (inset) c), close-up showing magnetic nanoparticles in the surface d), cross section of single magnetic fiber

Our first approach is based on the influence of the nanovector physical properties and its response to an applied electromagnetic field [1]. The drastic effect induced by magnetic hyperthermia is a key issue for the use of magnetic functional nanodevices in focused therapies. Our results in in vitro models demonstrate that a complex interplay of physical effects makes this technique a very promising alternative or adjuvant therapy for tumor treatment, first, due to the nanovector biocompatibility, (verified at cell level and in vivo), and second, because it is a localized treatment avoiding the side effects provoked by the currently used therapies.

Consequently, the optimization of the functional nanomaterials is very relevant for their application.
Other field of relevance among the applications of magnetic nanoparticles is the targeted drug release. In this field the use of our core@shell nanoparticles becomes relevant, due to their biocompatibility and their outstanding adsorption/desorption properties [4].

[1] H G.F: Goya, V. Grazu and M.R. Ibarra, Curr. Nanosci. **2008**, 4, 1-16.
[2] B. Sanz, M.P. Calatayud, E. De Biasi, E. Lima Jr., M. Vasquez Mansilla, R.D. Zysler, M.R. Ibarra, G.F. Goya. Scie. Rep. **2016.** 6, 38733.
[3] J.A. Fuentes-Garcia, B. Sanz, R. Mallada, M.R. Ibarra, G. F. Goya, submitted.
[4] B. Zhong, A, Mateu-Roldan, M. L. Fanarraga, W. Han, D. Munoz-Guerra, J. Gonzalez, L. T. Weng, M. R. Ibarra, C. Marquina, K.L. Yeung, Chem. Eng. J., **2022**, 435 134466.

PL: Superconducting spintronics with spin-orbit coupling and symmetry filtering

F. G. Aliev[1,2], C. Gonzalez-Ruano[1], D. Caso, P. Tuero[1], L. G. Johnsen[3], C. Tiusan[4,5], M. Hehn[5], I. Zutic[6], J. Fabian[7], J. Linder[3]

[1]Departamento Física de la Materia Condensada C-III, Universidad Autonoma de Madrid, Madrid 28049, Spain.
[2]Instituto Nicolas Cabrera (INC) and Condensed Matter Physics Institute (IFIMAC), Madrid 28049, Spain.
[3]Department of Physics, Center for Quantum Spintronics, Norwegian University of Science and Technology, 7491 Trondheim, Norway.
[4]Department of Solid State Physics and Advanced Technologies, Faculty of Physics, Babes-Bolyai University, Cluj-Napoca 400114, Romania.
[5]Institut Jean Lamour, Nancy Universite, 54506 Vandoeuvre-les-Nancy Cedex, France.

[6]Department of Physics, University at Buffalo, State University of New York, Buffalo, New York 14260, USA.
[7]Institute for Theoretical Physics, University of Regensburg, 93040 Regensburg, Germany.

Generation and control over long-range triplet (LRT) Cooper pairs is a key milestone for applications in superconducting spintronics. Here we overview fully epitaxial ferromagnet-superconductor hybrids with interfacial spin orbit coupling as a new platform for superconducting spintronics compatible with commercial spintronics [1-4].

We have studied all-epitaxial V/MgO/Fe junctions with competing in-plane and out-of-plane (OOP) magnetic anisotropies, and spin-orbit coupling (SOC) at the MgO interface. First, we experimentally demonstrated a thousand-fold increase in tunnelling anisotropic magnetoresistance below the vanadium critical temperature (T_C), which supports LRT formation depending on the magnetic configuration of the Fe layer [1]. Then we observed the predicted converse effect: the transformation of the in-plane and out-of-plane magneto crystalline anisotropies of the Fe layer driven by the superconductivity of vanadium through the SOC-bearing MgO interface [2] (Fig.1). The effective perpendicular magnetic anisotropy (PMA) is also enhanced, inducing a partial OOP magnetization reorientation without any applied field, and a reduction of the field required to induce a complete OOP transition [3]. We modelled our results in terms of an additional contribution to the free energy of the ferromagnet arising from the controlled generation of triplet Cooper pairs, which depends on the relative angle between the exchange field of the ferromagnet and the spin-orbit field. Finally, we discovered that V/MgO/Fe/MgO/Fe/Co junctions show record

high tunnelling magnetoresistance in the normal state (at room temperature), making them also applicable for high bias conventional spintronics [4]. Our findings offer the ability to tune magnetic anisotropies using superconductivity - a key step in designing future cryogenic magnetic memories.

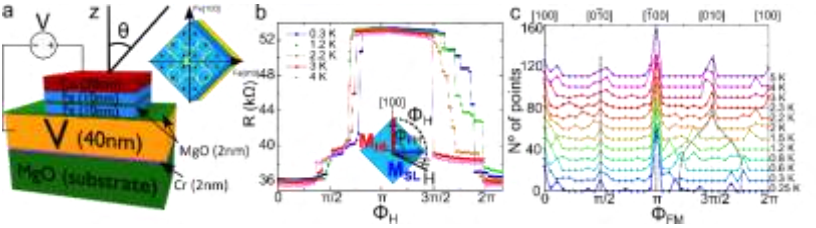

Fig. 1. Studied samples: a) sketch of the layer structure and in-plane magnetocrystalline anisotropy profile b) resistance during in-plane rotations of the magnetic field for several temperatures, from above to below T_C; c) calibrated angle between the two ferromagnetic layers during the rotations, showing the new stable configurations at 45º below T_C.

[1] I. Martinez et al., Phys. Rev. Appl. **2020** 13, 014030.
[2] C. Gonzalez-Ruano et al., Phys. Rev. B, **2020** 102, 020405(R).
[3] C. Gonzalez-Ruano et al., Scientific Reports 11, **2021** 19041.
[4] C. Gonzalez-Ruano et al., Adv. Elect. Materials, **2021** 8, 2100805.

T4-I: Magnetic skyrmions for neuromorphic and qubit applications

C. Tiusan[1], R. One[2], S. Mican[3], A. G. Cimpoesu[4]

[1]*Department of Solid-State Physics and Advanced Technologies Faculty of Physics, Babeș-Bolyai University Cluj-Napoca, Romania*
[2]*Doctoral School of Physics, Faculty of Physics, Babeș-Bolyai University Cluj-Napoca, Romania*
[3]*Department of Solid-State Physics and Advanced Technologies Faculty of Physics, Babeș-Bolyai University Cluj-Napoca, Romania*
[4]*Faculty of Physics, Babeș-Bolyai University Cluj-Napoca, Romania*

One of the most recent magnetic paradigms in the information technologies is based on the use of magnetic skyrmions. These solitons are vortex-like swirling topological defects in the magnetization texture [1] with diameters in the nanometer-range suitable for classical, neuromorphic or quantum spintronics applications.
In this paper we illustrate our results of multiple scale modelling, from ab-initio to micromagnetic simulations. They were performed to identify the phase diagrams of materials parameters allowing either to stabilize skyrmionics ground states or to write them from initially saturated state using the spin-transfer torque of a pulsed perpendicular current in nanometer-size disks based on magnetic materials with electric field tuneable perpendicular magnetic anisotropy and Dzyaloshinskii–Moriya interactions (DMI) (Fig.1). Moreover, the temperature dependence of skyrmion stability has been analysed to point out the main/critical material properties allowing to get stable skyrmions beyond cryogenic conditions, towards the room-temperature goal.

Following these material issues, we illustrate and briefly discuss some current advances in the underlying Physics and potential applications of skyrmions as classical bits in racetrack memories [2], as artificial neurons in neuromorphic architectures and devices [3] and helicity qubits [4].

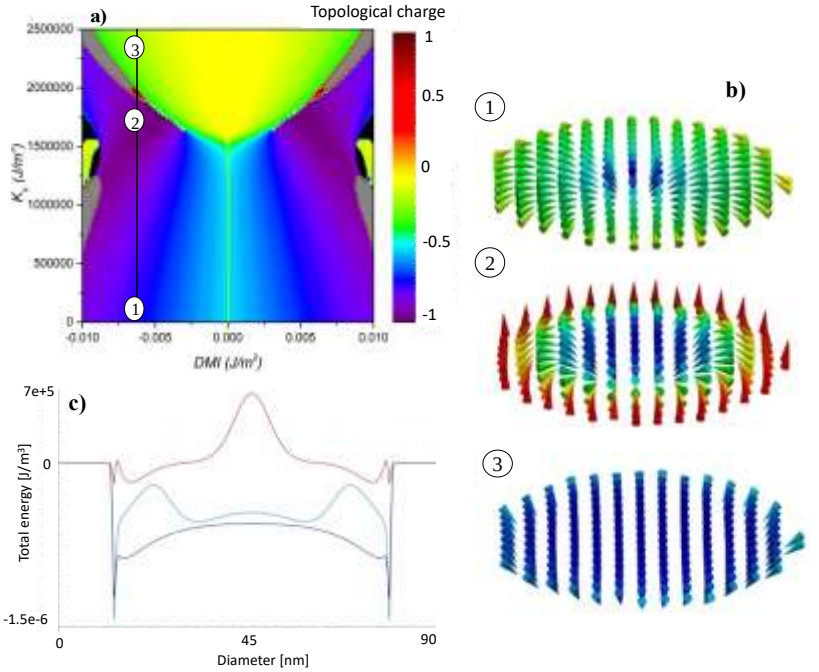

Fig. 1. a) Calculated phase diagram: PMA-DMI-Topological charge illustrating skyrmionics the regime (topological charge$Q = -1$, $Q = \frac{1}{4\pi}\int d^2x\ \vec{m}\cdot\left(\frac{d\vec{m}}{dx}\times\frac{d\vec{m}}{dy}\right)$). b) vortex, skyrmionics and perpendicular saturation configuration and corresponding total energy (c).

[1] A. Fert et al, Nature Reviews Materials, **2017,** 2, 17031.
[2] Tomasello et al, Sci Rep **2014**, 4, 6784 .
[3] Sai Li *et al* **,** Nanotechnology **2017,** 28 31LT01
[4] [C. Psaroudaki et al, Phys. Rev. Lett. **2021**,127, 067201.

T4-I: Intercalation enhanced superconducting response in hyper-expanded hybrid iron chalcogenides

A. Deltsidis,[1,2] L. Simonelli,[3] G. Vailakis,[1,2] I. Capel Berdiell,[1] G. Kopidakis,[1,2] E.S. Bozin,[4] A. Lappas[1]

[1]*Institute of Electronic Structure and Laser, Foundation for Research and Technology - Hellas, 71110 Heraklion, Greece*
[2]*Department of Materials Science and Technology, University of Crete, 70013 Heraklion, Greece*
[3]*ALBA Synchrotron Light Source, 08290 Cerdanyola del Vallés, Spain*
[4]*Condensed Matter Physics and Materials Science Department, Brookhaven National Laboratory, 11973 New York, USA*

2D iron chalcogenides offer a rich playground where structural and electronic correlations can be tuned by intercalation chemistry [1]. Electron donor molecules co-intercalated with alkalis in the β-FeSe (Fig. 1b) impact the electronic structure of the parent phase as the intercalation increases the interlayer separation and leads to a five-fold rise of the superconducting critical temperature (T_c~ 44 K). We have developed low-T solvothermal routes that afford the high-T_c $Li_x(C_5H_5N)_yFe_{2-z}Se_2$ system (Fig. 1a) in order to understand the parametrization of T_c with structure-property aspects probed by high-resolution synchrotron X-ray based tools. Total scattering experiments, combined with quantitative pair distribution function (PDF) analysis uncovers that high-T_c in these materials relates to the tetragonal $ThCr_2Si_2$-type average structure. However, in-situ PDF study of the [Li-C_5H_5N-FeSe] reaction pathway over time, uncovers local distortions, involving the $FeSe_4$ edge-sharing units that swell as a consequence of the electron donating [Li-C_5H_5N] moieties being accommodated in the interlayer space [2]. Motivated by such findings, element-specific (Fe & Se K-edge) X-ray absorption (XAS) and emission (XES) spectroscopies (T= 20-300 K) were utilised to find that (a) $FeSe_4$ units carry a slightly

reduced local Fe magnetic moment, while (b) doping-mediated local lattice modifications, delved by conventional T_c-optimization measures (cf. anion height and $FeSe_4$ tetrahedra regularity), become less relevant when layers are spaced far away [3]. EXAFS analysis, recognizes that such distortions are compensated by a softer Fe-network that relates to Fe-site vacancies, while DFT calculations corroborate that Fe-site deficiency of isolated $Fe_{2-z}Se_2$ (z, vacant sites) planes occurs at low energy cost, giving rise to stretched Fe-sheets, in accord with the experiments. The work provides insights on the interplay of electron donating spacers and the iron-selenide layer's tolerance to defect chemistry, offering a tool to favorably tune the Fermi surface properties and engineer robust superconducting states at elevated temperature.

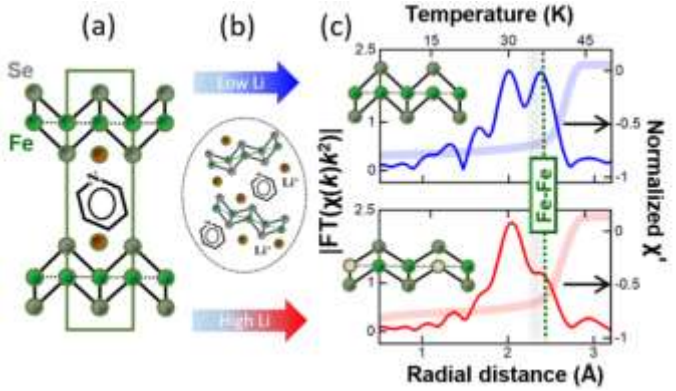

Fig. 1. 2D hybrid iron-selenides, with large interlayer separation (a), are investigated by high-resolution synchrotron X-ray tools to find that increasing Fe-vacancy concentration with Li-level (b), retains a robust superconducting response, T_c~ 44 K (c).

[1] H.K. Vivanco and E.E. Rodriguez, J. Solid State Chem. **2016**, 242, 3-21.

[2] I. Capel Berdiell, E. Pesko, E. Lator, A. Deltsidis, A. Krztoń-Maziopa, A.M.M. Abeykoon, E.S. Bozin, A. Lappas, Inorg. Chem. **2022**, 61, 4350-4360.
[3] A. Deltsidis, L. Simonelli, G. Vailakis, I. Capel Berdiell, G. Kopidakis, A. Krztoń-Maziopa, E.S. Bozin, A. Lappas, Inorg. Chem. **2022**, 61, 12797-12808.

Plenary Session and Invited Session (HALL1)

PL: Kinetic Monte Carlo simulations of the epitaxial growth of 2D materials

J-N. Aqua, K. Wang[1], G. Prevot[1], Z. Ben Jabra[2], M. Koudia[2], M. Abel[2], I. Berbezier[2]

[1] INSP, Sorbonne Universite, Paris, France
[2]IM2NP, Aix-Marseille Universite, CNRS, Marseille, France

The recent discovery of two-dimensional materials (2DM) has revolutionized solid-state physics and opened up novel potential applications thanks to their ability to confine carriers. Graphene (Gr) and transition metal dichalcogenide (TMDC) are particularly studied as regards their outstanding and promising electronic, optical but also spintronic properties. Nevertheless, a technological lock for their industrial applications lies in their synthesis. Since exfoliation has intrinsic limitations regarding the size and quality of the 2D crystals, epitaxy is the most suitable and reliable technique. Today's of the materials homogeneity thence requires further fundamental investigation to understand and control their growth mechanisms during van der Waals (vdW) epitaxy.
To model these systems, kinetic Monte-Carlo simulations are the most appropriate tool in order to include and describe

atomistic process, yet making prediction for mesoscopic or macroscopic time and space scales. We will discuss kinetic Monte-Carlo simulations dedicated to describe the dynamics of epitaxial growth, see Fig. 1 and Ref. [1]. The out-of-equilibrium dynamics is based on stationary markovian processes related to both deposition, diffusion and attachment/detachment of adatoms. We consider for this purpose lattice models that renormalize the atomic vibrations defining the characteristic scale of the elementary processes. The transition rates associated with the escape from a metastable state are dominated by the Boltzmann factor of the binding energy. It is approximated by two contributions related to the in-plane and out-of-plane neighbors.

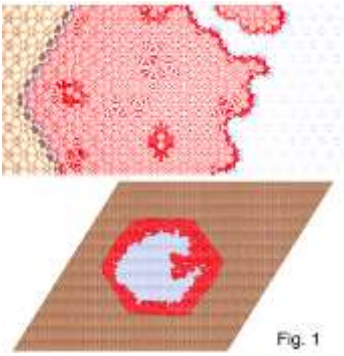

Figure 3 : kinetic Monte-Carlo simulations of Si on Gr

We will show the application of this formalism to two systems, consisting of silicene on graphene (Gr) and silicene on Ag(111). In the first case [1], in addition to the previous general model, we added surface effects on the energy barriers. These effects are at work in these highly asymmetric systems where van-der-Waals and covalent bonding have different strengths depending on the atomic position. We included this effect and rationalized the growth of large silicene flakes that were recently found on high-quality Gr [1]. The model correctly reproduces the growth dynamics where (i) relatively large 2D crystal can grow and (ii) a bead grows on its boundary. This mode can be rationalized by a dynamic dewetting effect. On the other hand, we also

produced an analysis of the growth of Si on Ag(111) substrate. In this case, experiments revealed the importance of alloying effect even though Ag and Si are not miscible at these temperatures. Yet, Si islands can form inserted 2D islands in the substrate surface plane, expelling Ag atoms that accumulate at step edges. By including extra alloying processes in the Monte-Carlo modeling, we could reproduce this growth and found relatively good quantitative comparison between theory and experiments.

[1] Z. Ben Jabra, M. Abel, F. Fabbri, J-N. Aqua et al, ACS Nano **16** (2022) 5920.

PL: Vibrational Spectroscopies of Nanoscale Semiconductor Structures

D. R. T. Zahn

Semiconductor Physics, Chemnitz University of Technology, Company) Chemnitz, Germany

Ternary (I-III-VI) and quaternary (I-II-IV-VI) metal-chalcogenides like $CuInS_2$ or $Cu_2ZnSn(S,Se)_4$ are among the materials currently most intensively investigated for various applications in the area of alternative energy conversion and light-emitting devices. They promise more sustainable and affordable solutions to numerous applications compared to the well-known II-VI and III-V semiconductors. Potentially superior properties are based on an unprecedented tolerance of these compounds to non-stoichiometric compositions and polymorphism. However, if not properly controlled, these merits can also lead to an undesirable coexistence of different compounds in the lattice and huge concentrations of point

defects. Raman spectroscopy of phonons has become one of the most powerful tools of structural diagnostics and probing physical properties of bulk and micro- or nanocrystalline I-III-VI and I-II-IV-VI compounds. The interpretation of the vibrational spectra of these compound nanocrystals (NCs) and conclusions about their structure can be complicated compared to bulk counterparts because of size and surface effects as well as emergence of new structural polymorphs that are not realizable in the bulk. In this talk, the present knowledge in the field of I-III-VI and I-II-IV-VI NCs regarding their phonon spectra is reviewed.

PL: Silicon clathrate films for optoelectronic and photovoltaic applications

T. Fix[1], R. Vollondat[1], D. Stoeffler[2], J.-L. Rehspringer[2], A. Slaoui[1]

[1] *Cube laboratory, CNRS and University of Strasbourg, Strasbourg, France*
[2] *Institut de Physique et Chimie des Matériaux de Strasbourg (IPCMS), CNRS and University of Strasbourg, Strasbourg, France*

Several forms of silicon are used in industry, mainly crystalline, multicrystalline and amorphous silicon. Here we propose to investigate a novel form of silicon films, namely silicon clathrates. They are in a way similar to carbon fullerenes as they form hollow spheres (Fig. 1). The electronic and optical properties of some of these clathrates are strongly different to the “standard” silicon (direct bandgap) and can pave the way for novel applications in electronics and optoelectronics [1-3]. Only a very narrow range of conditions enables the formation of silicon clathrates. The fabricated Si clathrate films are analyzed in terms of structural, optical,

electrical, surface properties by a wide range of techniques (Fig. 1). In particular, not only the size of the clathrates but also the presence of doping atoms can dramatically modify their properties. Ion implantation is used to modify the properties of the clathrates. We investigate the potential of these materials for solar energy applications. In this work we show using surface photovoltage spectroscopy that photocarriers can be generated in type II silicon clathrate films, with a direct bandgap around 1.9 eV. We compare our experimental results with ab initio electronic structure calculations. We also show that the resistivity of type II silicon clathrate films is tunable over 4 orders of magnitude by varying the guest Na atom concentration in the cages.

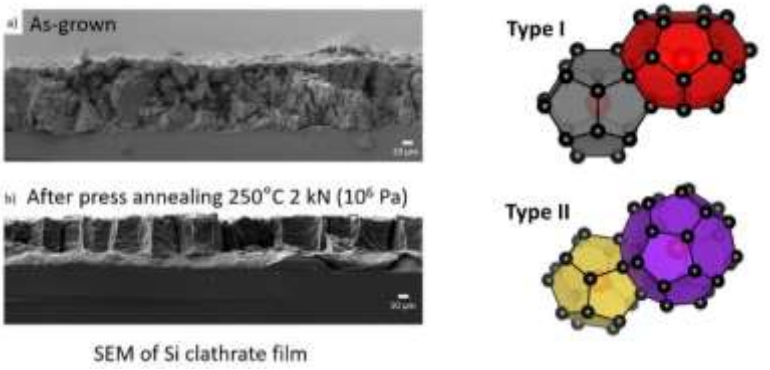

Fig. 1. (left) silicon clathrate film on c-Si (001) before and after press annealing. (right) schematics of type I and type II silicon clathrates.

We would like to thank the x-ray and microscopy platforms of IPCMS and the C3Fab platform of ICube. We also thank C. Chevalier from INL France. This project has received financial support from the CNRS through the 80|Prime program, through the MITI interdisciplinary programs, and is currently funded by a French ANR grant EXOSIL.

[1] T. Kume, F. Ohashi, S. Nonomura, Jpn. J. Appl. Phys. **2017**, 56, 05DA05.
[2] T. Fix, R. Vollondat, A. Ameur, S. Roques, J.-L. Rehspringer, C. Chevalier, D. Muller, and A. Slaoui, J. Phys. Chem. C **2020**, 124, 14972–14977.
[3] R. Vollondat, S. Roques, C. Chevalier, J. Bartringer, J. L. Rehspringer, A. Slaoui, T. Fix, J. Alloy Comp. **2022**, 903, 163967.

PL: Contribution of atomic force microscopy to the nanoscale analysis of ferroelectric films (for photovoltaic applications)

S. Colis, X. Henning, L. Wendling, A. Dinia, M.V. Rastei

Institut de Physique et Chimie des Materiaux de Strasbourg (IPCMS), CNRS and University of Strasbourg, France

The asymmetric distribution of charges in the unit cell of ferroelectric (FE) materials induces a directional spontaneous polarization that can be switched by applying an external electric field. This process can be exploited for different type of applications such as sensors, actuators, memories, spintronic devices, capacitors or solar cells, where FE materials are mostly used in the form of thin films. In the case of solar cells, photon absorbers made of ferroelectrics can be particularly interesting because of the intrinsic internal field brought by the polarization of the material and which is very efficient for exciton splitting. The potential interest of FE Bi_2FeCrO_6 (BFCO) for photovoltaic devices was already demonstrated [1,2] but the reproducibility of the results is rather limited. In order to have a better understanding of the ferroelectric photovoltaic effect, in-depth local FE, conductive and opto-electronic analyzes are needed. Nanoscale

investigations can unveil in a more accurate way the fundamental working mechanisms at stake in these materials. For this purpose, an AFM coupled with an external light source seems an ideal characterization tool. Besides the FE character and the polarization switching mechanism particularly important in applications (as related to the stability of the ferroelectric domain structure) [3,4], we will discuss the possibility of correlating the conductive properties with the polarization state of BFCO (Fig.1). Finally, conductivity measurements under illumination will be presented as a function of different parameters (polarization state, wavelength, light power...).

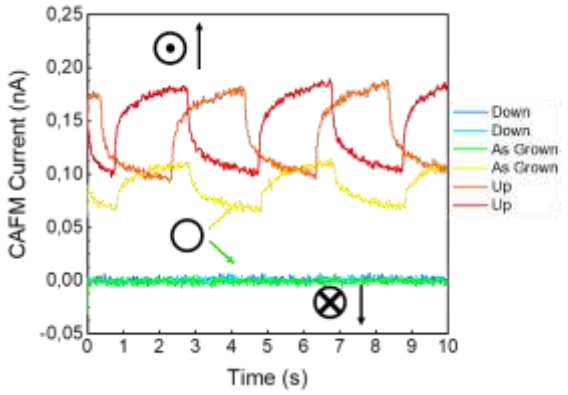

Fig. 1. Photocurrent variation recorded on two grains upon illumination (on/off; 450 nm) for Bi_2FeCrO_6 films polarized up, down and in the as-grown state.

Acknowledgments. This work was supported by the French National Research Agency (ANR) through the Programme d'Investissement d'Avenir under contract ANR-11-LABX-0058 - NIE

and ANR-17-EURE-0024 within the Investissement d'Avenir program ANR-10-IDEX-0002-02.

[1] R. Nechache, C. Harnagea, S. Li, L. Cardenas, W. Huang, J. Chakrabartty, F. Rosei, Nature Photonics **2015**, 9, 61–67.
[2] A. Quattropani, A. Makhort, M.V. Rastei, G. Versini, G. Schmerber, S. Barre, A. Dinia, A. Slaoui, J.L. Rehspringer, T. Fix, S. Colis, B. Kundys, Nanoscale **2018**, 10, 13761.
[3] M.V. Rastei, F. Gellé, G. Schmerber, A. Quattropani, T. Fix, A. Dinia, A. Slaoui, S. Colis, ACS Appl. Energ. Mater. **2019**, 2, 8550-8559.
[4] L. Wendling, X. Henning, F. Roulland, M. Lenertz, G. Versini, L. Schlur, U. Chung, A. Dinia, S. Colis, M. Rastei, Thin Solid Films **2022**, 757, 139384.

T10-I: New development of gas sensor devices based on black coating

J. More-Chevalier[1], M. Hruska[2], D. Prokop[1], M. Novotny[1], P. Fitl[2], M. Poupon[1], C. A. Correa[1], P. Pokorny[1], L Fekete[1], P. Hruska[1], L. Volfova[1], J. Lancok[1]

[1]Institute of Physics of the Czech Academy of Sciences, Na Slovance 1999/2, 182 21 Prague, Czech Republic.
[2]Department of Physics and Measurements, University of Chemistry and Technology Prague, Technicka 5, 16628 Praha 6, Czech Republic

A gas sensor is a device able to detect the presence of gases in the atmosphere. The gas concentration produces a corresponding potential difference by changing the sensor's resistance, which can be measured as an output voltage. The acoustic-based gas sensor is one of the different types of sensor which detects a mass variation per unit area by measuring the change in the resonance frequency. The

relation between the shift of the resonant frequency and the mass increment is described by Sauerbrey's equation [1]. The sensor efficiency is correlated with the number of sensitive particles to the active surface of the sensor. In order to improve the mass sensitivity of a sensor, a black metal (BM) layer can be deposited onto the active surface of the sensor. BMs are metals with highly porous surfaces [2]. Their surface properties result from the combined effect of nanostructural, microstructural, and macrostural features. In this work, BM layers were deposited onto Quartz crystal microbalance (QCM) sensors to improve this mass sensitivity. BM layers were deposited by PVD techniques and investigations were performed on structures, defects, and nanoscopic porosities in the films. Moth-eye-like surface morphologies with antireflective properties were obtained for these BM layers. Impedance measurements were carried out on BM coated QCM sensors and compared with blank QCM sensors. Effects of the BM coatings on the resonance frequencies were reported confirming this potential to improve the mass sensitivity of QCM sensors.

[1]G. Sauerbrey, Zeitschrift fiir Physik. **1959**, 155, 206–222.
[2]J. More-Chevalier, M. Novotny, P. Hruska, L. Fekete, P. Fitl, J. Bulir, P. Pokorny, L. Volfova, S. Havlova, M. Vondracek, J. Lancok, RSC Adv. 2020, 10, 20765–20771.

Wednesday, September 14, 2022

08:00	**Poster Session I** HALL 1-University of Dubrovnik
10:00	**Poster Sessions II and Coffee break**
12:00	**Lunch**
15:00	**Invited and Oral Sessions** HALL 1
17:00	**Coffee break**
17:00	**Invited, Oral Session and Poster Session III (online)** HALL 1, HALL 2
20:00	**Gala Dinner**

T1-P: Transition Metal-Oxynitride Thin Film Structures for Supercapacitor Applications

J. Som[1], M. Roy[1], K. Sarkar[1], B. Smith[1], D. K. Dare[3], X. Lu[2], D. Kumar[1]

[1]Mechanical Engineering Department, North Carolina A & T State University, Greensboro, North Carolina, USA
[2]Department of Applied Engineering Technology, North Carolina A & T State University, Greensboro, North Carolina, USA
[3]Cornell Center for Materials Research, Cornell University, Ithaca, New York, USA

Electrocatalytically highly active titanium oxynitride (TiNO) thin films were fabricated on commercially available titanium metal plates using a pulsed laser deposition method for energy storage applications. The elemental composition and nature of bonding were analyzed using x-ray photoelectron spectroscopy (XPS) to reveal the reacting species and active sites responsible for the enhanced electrochemical performance of the TiNO electrodes. A study of the SEM images before and after electrochemical cycling showed a negligible degradation of TiNO sample, suggesting the TiNO electrodes are stable under the cycling conditions. Symmetric supercapacitor devices were fabricated using two TiNO working electrodes separated by ion transporting layer to analyze their real-time performance. The galvanostatic charge-discharge studies on the symmetric cell have indicated that TiNO films deposited on the polycrystalline titanium plates at lower temperatures are superior to TiNO films deposited at higher temperatures in terms of storage characteristics. For

example, TiNO films deposited at 300 °C, exhibited the highest specific capacity of 69 mF/cm^2 at 0.125 mA/cm^2 with an energy density of 7.5 Wh/cm^2.
The performance of this supercapacitor (300 ^{o}C TiNO) device is also found to be ~ 22 % better compared to that of 500 ^{o}C TiNO supercapacitor with a capacitance retention ability of 90% after 1000 cycles. The difference in the electrochemical storage and capacitance properties is attributed to the reduced leaching away of oxygen from the TiNO films by Ti plate at lower deposition temperatures, leading to higher oxygen content in the TiNO films, and consequently, a high redox activity at the electrode/electrolyte interface.

T1-P: Optical characterization of HfO_2 and ZrO_2 thin films grown by pulsed laser deposition

L. Badea[1,2], D. Craciun[3], G. Dorcioman[3], P. Garoi[3], R. Udrea[1,4], M. D. Mihai[5,6], V. Craciun[3,7]

[1]*Faculty of Physics, University of Bucharest, Măgurele, Romania*
[2]*National R&D Institute for Non-Ferrous and Rare Metals, Pantelimon, Romania*
[3]*National Institute for Laser, Plasma & Radiation Physics, Măgurele, Romania*
[4]*APEL LASER SRL, 15 Vintilă Mihăilescu Street, 077135 Bucharest, Romania*
[5]*Horia Hulubei Natl Inst Phys & Nucl Engn IFIN HH, 077125 Magurele, Romania*
[6]*University Politehnica of Bucharest, RO 060042, Romania*
[7]*Extreme Light Infrastructure for Nuclear Physics, Măgurele, Romania*

HfO_2 and ZrO_2 have multiple uses from high k dielectrics in microelectronics to protective and thermal diffusion barriers in high temperature engines. In all these applications the working temperatures will also depend on surface morphology and optical properties. We investigated the

optical surface properties of thin films deposited by the pulsed laser deposition technique. This laboratory technique has a great utility for research purposes: by changing the deposition conditions, films possessing different stoichiometry, structure and surface morphology could be obtained.

We used an ArF laser to grow films under various oxygen pressures. After deposition, the thickness and stoichiometry were investigated using non-Rutherford backscattering spectrometry, the structure using grazing incidence X-ray diffraction and chemical bonding using X-ray photoelectron spectroscopy. The chemical composition of the deposited films was investigated by non-Rutherford backscattering spectrometry with alpha particles having a 3.040 keV energy, which corresponds to an oxygen resonance. Typical examples of the acquired spectra are displayed in Fig. 1 for two HfO_x films deposited under two different oxygen pressures. The oxygen to hafnium composition was varied from 1.72 to 2.40, while for oxygen to zirconium it varied from 1.75 to 2.14.

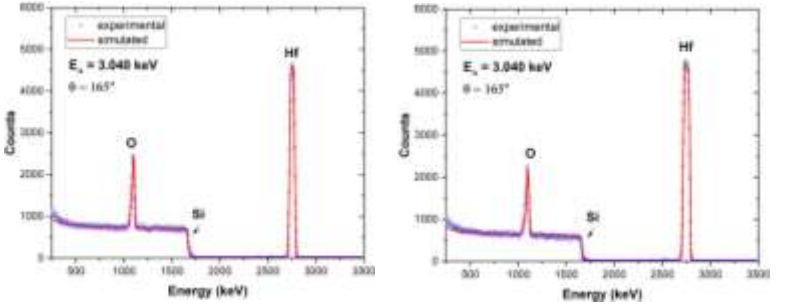

Figure 1. Non-Rutherford backscattering spectrometry of HfO_2 thin films deposited under different O_2 pressures.

The effect of stoichiometry on the optical emissivity was measured from room temperature up to 800 °C using an

optical pyrometer. The optical constants were also studied at room temperature using optical transmittance and spectroscopic ellipsometry.

Acknowledgments**.** This work was supported by a grant of the Ministry of Research, Innovation and Digitization, CNCS – UEFISCDI, project number PN-III-P4-PCE-2021-1158, project number PN-III-P2-2.1-PED-2021-2659, ELI 04/01.10.2020, within PNCDI III, POC 361-SMIS 122040 and Nucleu programme LAPLAS VI, no. 16N/2019

T1-P: Raman microscopy and spectroscopy studies of V_2O_5 grown by spray pyrolysis method

C. Pachiu[1], I. V. Tudose[2,3], C. Romanitan[1], O.A. Brincoveanu[1], E. Koudoumas[2], M. P. Suchea[1,2*]

[1] National Institute for Research and Development in Microtechnologies (IMT-Bucharest), 126A Erou Iancu Nicolae Street, Voluntari 077190, Romania
[2]Center of Materials Technology and Photonics, School of Engineering, Hellenic Mediterranean University, 71410 Heraklion, Crete, Greece
[3]Chemistry Department, University of Crete, 70013 Heraklion, Greece

V_2O_5 is the most stable vanadium-oxide composition due to its large O/V ratio. As a consequence, V_2O_5 is the most common compound resulting in nature from aging of vanadium-oxides by oxygen absorption from the atmosphere. V_2O_5 can be described as layers of distorted VO_6 octahedra stacked together and held by weak bond interactions. V_2O_5 is widely used as a catalyst, and very promising in optoelectronics applications due to its electrochromic properties [1-3]. Vanadium oxide thin-films with a specific stoichiometry are often obtained by adequately choosing a lattice-matching substrate and adjusting several parameters including the

deposition technique, precursor deposition rate, pressure and temperature.

In the present study we have examined the surface morphology of V_2O_5 thin films grown by spray pyrolysis onto different substrates, as deposited and after thermal treatment, by using Raman spectroscopy as well as imaging by Raman mapping. Raman mapping is quite remarkable in following the relative intensity change of the bands related to the material structure, before and after any treatment. Raman mapping has been applied successfully to characterize the microstructural transformation of the amorphous V_2O_5 films to a crystalline form after postdeposition thermal treatment. The results have shown that using Raman spectroscopy and mapping as a powerful combination for in-depth analysis of V_2O_5 thin films characterization helps to reveal significant information regarding their structuring (Fig.1).

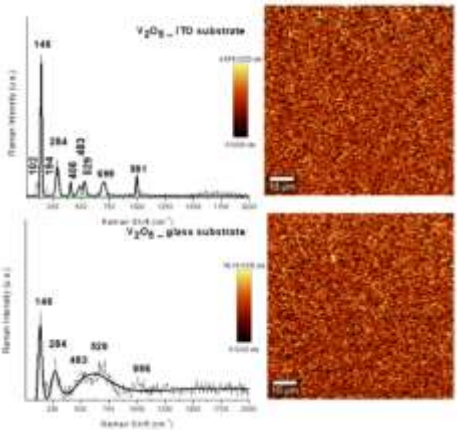

Fig. 1. Examples of Raman spectra and Raman imaging of V_2O_5 thin films grown on two different substrates.

Acknowledgments. This research was partially financed by "MICRO-NANO-SIS PLUS" core Programme and MicroNEx,

Contract nr. 20 PFE din 30.12.2021, financed by the Ministry of Research, Innovation and Digitalization through Program 1—Development of the National R & D System, Subprogram 1.2—Institutional Performance—Projects for Institutional Excellence.

[1] K. Mouratis, V. Tudose, C. Romanitan, C. Pachiu; O. Tutunaru, M. Suchea, S. Couris, D. Vernardou, K. Emmanouel, Materials, **2020**,13, 3859.
[2] C. Pachiu, M. Carp, K. Mouratis, I.V. Tudose, C. Romanitan, O. Tutunaru, S. Couris, E. Koudoumas, M.P. Suchea, International Semiconductor Conference (CAS), **2020,** pp. 191-194.
[3] K. Mouratis, I.V. Tudose, Bouranta, A. C. Pachiu, C. Romanitan, O. Tutunaru, S. Couris, E. Koudoumas, M. Suchea, Nanomaterials, **2020** 10 (12), 2397.

T1-P: Area-selective wet chemical etching of ferroelectric zirconium-doped hafnium oxide ultra-thin films for high-frequency electronics

L. A. Dinu[1], M. Aldrigo[1], C. Romanitan[1], F. Nastase[1], S. Vulpe[1], R. Gavrila[1], A.B. Serban[2]

[1]National Institute for R&D in Microtechnologies, 126A Erou Iancu Nicolae Street, 077190 Voluntari (Ilfov), Romania
[2]Extreme Light Infrastructure-Nuclear Physics (ELI-NP), 'Horia Hulubei' National R&D Institute for Physics and Nuclear Engineering (IFIN-HH), 30 Reactorului Street, 077125 Măgurele, Ilfov, Romania

The use of high-permittivity nanoscale ferroelectric materials, such as zirconium-doped hafnium oxide (HfZrO), brings an important contribution to the downscaling of electronic devices. The performances of state-of-the-art HfZrO-based electronic devices are currently investigated using continuous HfZrO films deposited on the whole wafer surface. This paper goes beyond the actual state-of-the-art applications relying on

ferroelectric HfZrO thin films, by providing selective patterned areas of HfZrO ultra-thin film, using the wet etching (WE) technique.

The microfabrication process started with the deposition of TiN and HfZrO, and then the wafers were subjected to a photolithographic process to pattern the areas for selective etching of HfZrO, illustrated in Fig 1A. For the WE of thin HfZrO films, a diluted 1% HF solution was used. Several HfZrO pieces have been immersed in etchant for different periods of time to select the optimum time to etch the 6.8-nm-thick layer of HfZrO. The top-view SEM micrographs of the non-etched and etched structures are depicted in Fig 1B.

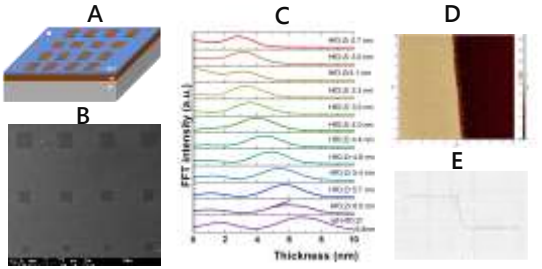

Fig 1. A) Illustration of wet etched test structures of HfZrO on TiN layer; B) SEM image of etched area for MIM fabrication; C) FFT analysis for the investigated HfZrO films with the obtained thicknesses; D) AFM scan; E) AFM profile of non-etched and etched areas.

To quantify the effects of the WE process at different stages, X-ray reflectivity (XRR) investigations were performed. The layer thickness varied from 6.8 nm for the unetched film up to 2.7 nm when the immersion time was 120 s. The corresponding thickness in each case can be found in Fig. 1C. From the AFM measurements we were able to discriminate between non-etched and etched areas (Fig 1D and E). The successful WE

process was investigated also by XPS, where no reaction products, such as fluorides, have been observed.
A well-controled etching process allowed the patterning of HfZrO ultra-thin films only in selected areas. This process will benefit the integration of ferroelectric-based devices, such as capacitors, phase shifters or ferroelectric tunnel junctions, into a much more complex electronic platform for CMOS-compatible next-generation high-frequency electronics.

Acknowledgement. This work was supported in part by the Romanian Ministry of RID, CCCDI-UEFISCDI, under Project PN-III-P2-2.1-PED-2019-0052, within PNCDI III, and in part by the European Project NANO-EH, Grant. No. 951761.

T-P: Chemical States and Bandgap Energy of Titanium Nitride Thin Films

M. Roy[1], K. Sarkar[1], J. Som[1], A. Odusanya[1], M. A. Pfeifer[2], D. K. Dare[2], V. Craciun[3], D. Kumar[1]

[1]Mechanical Engineering Department, North Carolina A & T State University, Greensboro, North Carolina, USA
[2]Cornell Center for Materials Research, Cornell University, Ithaca, New York, USA
[3]National Institute for Laser, Plasma and Radiation Physics, Magurele, Romania

Single crystalline titanium nitride (TiN) and partially oxidized titanium nitride ($TiNO_x$) thin films have been grown in a rock-salt structure on sapphire substrates using high vacuum conditions during pulsed laser deposition (PLD). The film thickness was varied from a few unit cells to several unit cells by changing number of pulses from 150 to 5000 pulses. X-ray photoelectron spectroscopy (XPS) analysis has shown that

oxygen content of the $TiNO_x$ films increases with film thickness (or deposition time), which in turn, affects the exposure time of the ablated materials to the residual oxygen in the deposition chamber (the source of TiN oxidation). The lattice constant of the $TiNO_x$ films, measured using XRD, is found to increase with the oxygen content in the film, which confirms previous density functional theory (DFT) calculations. The lattice constant increase is explained by enhanced electrostatic repulsion between O^{2-} orbitals near vacant Ti^{3+} sites; to maintain charge neutrality within the lattice, one Ti^{3+} cation vacancy must be created for every three substitutions of N^{3-} ions by O^{2-} ions. We have observed an asymmetric 'V' shape variation in the optical bandgap energy as a function of film thickness. The bandgap values decreased from 3.89 eV to 3.30 eV as the number of pulses (thickness) increase from 150 to 750 (1.5 to 4 nm) and then increased from the minimum of 3.30 eV to 3.87 eV as the number of pulses increased from 750 to 5000 (thickness 4 nm to 30 nm). The bandgap variation following the left arm of the V-curve is attributed to the quantum confinement effect, while the variation of the bandgap following the right arm of the V-curve is believed to be associated with the increased defects density of the Ti^{3+} cations that is caused by the charge imbalance in the $TiNO_x$ lattice due to partial substitution of N^{3-} by O^{2-} ions.

T1-P: Colloidal solution based BaTiO3 thin films

V. Mykhailovych[1,2], G. Caruntu[5], I-M. Risca[3], A. Graur[1], A. Diaconu[1], A. Rotaru[1]

[1]FIESC & Research Center MANSiD, USV, Suceava, Romania
[3]Department of General Chemistry and Material Science, Yuriy Fedkovych Chernivtsi National University, Chernivtsi, Ukraine,

[2]Faculty of Forestry & Research Center MANSiD, USV, Suceava, Romania
[4]Department of Chemistry and Biochemistry, CMU, Mt. Pleasant, USA
[5]Science ofAdvanced Materials (SAM) Program, CMU, Mt. Pleasant, USA

Modern development of technology increasingly requires the obtaining and improving of materials with high dielectric constant for practical application as active components for capacitors, field effect transistors, sensors, etc. One of the bright representatives of materials with perspective dielectric properties are perovskite BaTiO3 nanoparticles. This type of compound are already known as high-k material, and for example, based on 10-12 nm sized high-k BaTiO3 nanocrystals with cubic morphology Parizi et al fabricate flexible field effect transistor and capacitor with a value of dielectric permittivity 220 [1]. In another work Caruntu et al synthesized monodisperse titanium-based perovskite colloidal nanocrystals with a size from 5 to 78 nm for cubes [2]. However, the nanoparticles above 80 nm with a cubic-like morphology for $BaTiO_3$ have not been obtained till now, and it is of primary interest as the dielectric constant increase with particle size [3] and in combination with a cubic morphology allow them to assembly uniformly.

This study is devoted fabrication of thin film based on cuboidal BaTiO3 nanocrystals with a size above 100 nm, which were synthesized at this scale for the first. Nanoparticles of $BaTiO_3$ were obtained by modifying the previously reported syntheses by Adireddy [4]. Two solutions containing Ba(NO3)2 and 1-BuOH solution containing $Ti(Bu)_4$ and oleic acid in BuOH were regularly mixed with each other and 12.5 mmol NaOH resulting in a white creamy solution which was stirred for 15 min. The resulting white mixture was subsequently

thermal treated for 96 hours in a 200 mL Teflon-liner autoclave. Synthesized powders were collected by decantation and washed by ethanol. Finally, $BaTiO_3$ nanocrystals were dispersed in toluene to form the colloidal solution with a different concentration.

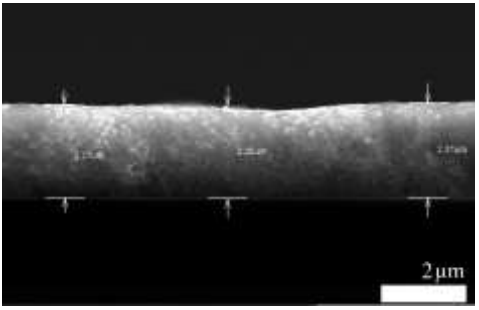

Fig. 1. Thin film based on cubic $BaTiO_3$ nanocrystals.

At final step the thin films were obtained by drop casting on the silver coated glass, see Fig. 1. The obtained films are about 2.3 µm thick with a high density. Cubic nanoparticles are uniformly distributed which allow the formation of uniform continues film.

Acknowledgements. This work was supported by the Romanian Research Grant (PN-III-P4-ID-PCCF-2016-0175: HighKDevice). VM acknowledges the financial support through the project "PROINVENT", Contract no. 62487/03.06.2022 - POCU/993/6/13 - Code 153299, financed by The Human Capital Operational Programme 2014–2020 (POCU), Romania.

[1] G. Caruntu et al., Mater. Adv., **2022**, 3, 6474-6484.
[2] D. Caruntu et al., Nanoscale, **2015**, 7, 12955-12969.
[3] T. Shaw, et al., Annu. Rev. Mater. Res, **2000**, 30, 263.
[4] S. Adireddy, et al., Chem. Mater., **2010**, 22, 1946-1948.

T1-P: High-k $ZnCr_2O_4$ nanoparticles: from synthesis to nanoelectronic devices fabrication

V. Mykhailovych[1,2], G. Caruntu[4,5], M. Mykhailovych[1], A. Diaconu[1], P. Fochuk[4], I. Fodchuk[5], A. Rotaru[1]

[1]*FIESC & Research Center MANSiD, USV, Suceava, Romania*
[2]*Department of Chemistry and Biochemistry, CMU, Mount Pleas-ant, USA*
[3]*Science of Advanced Materials Program, CMU, Mount Pleasant, USA*
[4]*Department of General Chemistry and Material Science, Yuriy Fedkovych Chernivtsi National University, Chernivtsi, Ukraine*
[5]*Physical, Technical and Computer Science Institute, Yuriy Fedkovych Chernivtsi National University, Chernivtsi, Ukraine*

Intensive progress of micro and nano electronics requires the developments and improvements of the active elements of modern devices. One of the wide class of materials with a promising and unique properties for practical application is spinel type materials [1] as they are perspective in various technological applications [2-4]. In this work we present the synthesis of high-k dielectric $ZnCr_2O_4$ spinel type nanocrystals with various sizes and morfologies. Nanoparticle's morphology progress and dielectric properties were investigated as a function of gradual annealing temperature. Morphology changes are ranging from 10 nm sized "seeds" to regular octahedral with an average size of 350 nm. The physical and chemical properties of the synthesized nanoparticles were investigated by several methods such as: Field Effect Scanning Electron Microscopy, X-ray diffraction, Raman spectroscopy, Energy Dispersive X-Ray analyses and Broadband Dielectric Spectrometry. The real part of the dielectric permittivity increases with the size of the nanoparticles. The dielectric permittivity for octahedral 350 nm sized $ZnCr_2O_4$ nanocrystals was found in the range of 400 at high frequency (1 MHz) and 1500 at low frequency (100 Hz). Thin films

of $ZnCr_2O_4$ were fabricated by drop-casting method from colloidal solution.

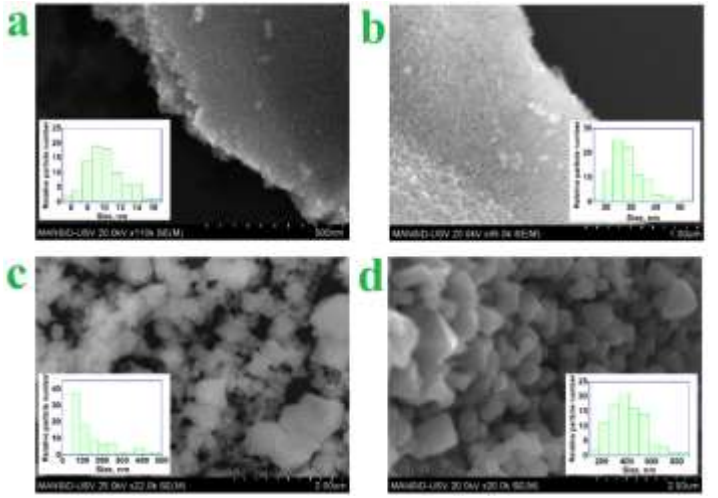

Fig. 1. FE-SEM micrographs recorded on ZnCr2O4 after thermal treatment at 500 °C - (a), 700 °C - (b), 800 °C - (c) and 900 °C - (d) respectively.

Acknowledgements. This work was supported by the Romanian Research Grant (PN-III-P4-ID-PCCF-2016-0175: HighKDevice). VM acknowledges the financial support through the project "PROINVENT", Contract no. 62487/03.06.2022 - POCU/993/6/13 - Code 153299, financed by The Human Capital Operational Programme 2014–2020 (POCU), Romania.

[1] Q. Zhao, et al., Chem Rev, **2017**, 117, 10121-10211.
[2] M.G. Bellino, et al., JACS, **2007**, 129, 3066-3067.
[3] M.Y. Park, et al., J. Mater. Chem. A, **2022**, 10, 11917-11925.
[4] X. Xu, J. Gao, W. Hong, RSC Advances, **2016**, 6, 29646-29653.

T1-P: Size dependent strain relaxation of InAs quantum dots grown atop GaAs(111)A nanopillars

V. S. Kunnathully, T. Riedl, A. Trapp, T. Langer, D. Reuter, J.K.N. Lindner

Dept. of Physics and Center for Optoelectronics and Photonics Paderborn (CeOPP), Paderborn University, 33098 Paderborn, Germany

InAs quantum dots (QDs) are nanostructures with potential for commercial applications such as lasers, IR photodetectors and single photon emitters due to their narrow bandgap and 3D quantum confinement [1]. In this regard, InAs QDs grown on GaAs(001) substrates have been well studied but, there is a paucity of information concerning the same with GaAs(111)A substrates. The major impediment for InAs QD growth on GaAs(111)A arises from dislocation mediated plastic lattice relaxation at the early stage of growth. This has been recently overcome by low temperature InAs molecular beam epitaxy (MBE) on nanopillar-patterned GaAs(111)A substrates [2]. Such a result opens new possibilities such as reduced strain volume and lower Ga diffusion into InAs QDs [3,4]. In this contribution the strain relaxation of InAs QDs resulting from MBE deposited InAs film thicknesses of 15, 5 and 2 nm on GaAs(111)A pillars are studied. The size dependence of strain within the QDs synthesized is probed by employing high-angle annular dark-field scanning transmission electron microscopy (HAADF-STEM). Geometrical phase analysis (GPA) and peak-pairs analysis (PPA) are performed to evaluate strains from the HAADF-STEM images. Additionally, the strain relaxation mechanisms based on the observed results are verified theoretically using molecular static simulations. HAADF-STEM

images indicate a critical QD diameter of ≈10 nm below which 60° misfit dislocations are absent in the investigated InAs QDs as seen in Fig.1. This critical diameter marking the transition towards a fully coherent strain state is also corroborated by estimated plastically accomodated strain extracted from effective Burgers vector along the heterointerface, indicated in Fig.1.

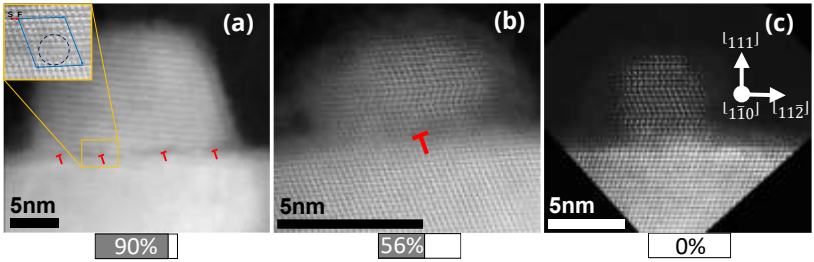

Fig. 1. a), b) and c) are HAADF-STEM images showing InAs islands on GaAs(111)A nanopillar tops resulting from nominally deposited InAs film thicknesses of 15, 5 and 2 nm, respectively. The locations of 60° misfit dislocations are indicated where present. The contribution of misfit dislocations towards strain relaxation is indicated below each image. All images were acquired along the $[1\bar{1}0]$ zone axis direction.

Examination of the HAADF-STEM image intensities reveal the confinement of misfit dislocations to the InAs/GaAs(111)A heterointerface. Further, the experimental strain maps indicate the presence of 1.2 nm and 0.4 nm wide strained regions at the heterointerface for the coherent and dislocated islands, respectively, in agreement with molecular static simulations. A significant outcome of this analysis is the effectiveness of free surfaces at elastically relieving lattice misfit strain which, together with the restricted adatom diffusion, enables the formation of InAs QDs on GaAs(111)A nanopillar tops [5].

T2-P: Sub threshold electrical measurements using Langmuir Probe method

S. A. Irimiciuc[1], R. Udrea[2], P. Garoi[1], D. Craciun[1], V. Craciun[1,3]

[1]*INFLPR, 409 Atomistilor street, Magurele, RO-077125, ROMANIA*
[2] *Physics Faculty, University of Bucharest, Bucharest-Magurele, Romania*
[3]*Extreme Light Infrastructure for Nuclear Physics, Romania*

Recent developments in the newly developed high-power system from ELI-NP have been closely related to the intense research on providing the adequate characterization/diagnostic tools to ensure the correct performance of all adjacent systems. One of the core drawbacks which was identified while using these high-power laser systems is the relatively short life-time of optical components due to damage and stress induced by the laser beam-mirror interaction. the ability to have a real time feedback loop from the beam line becomes mandatory as structural and functional changes should be signaled before permanent damage is induced. Permanent damage on the optical components is defined as observable post-ablation at surface level, and thus the ablation threshold is a clear, quantifiable limit of these component.
The aim of this work is centered on developing based on an electrical diagnostic system a flexible, in situ monitoring tool for sub threshold measurements during laser matter interaction that can span fs up to ns irradiation regimes. For sub threshold ablation conditions, the pre-plasma vapor cloud which consists mostly of electrons and ions has a wide energy distribution with a wide cumulative peak defining this state.

With the increase of laser fluence, fast narrow distributions are induced on the LP signal accompanied by a luminous structure, which signals the plasma ignition fluence. Analyzing the charge particle distribution as a function of the laser fluence we were able to predict the ablation threshold fluence. Further investigations provided information on the ablation mechanism involved in this fluence regime and on the properties of the ejected cloud, the so called pre-plasma state of the ablated vapor.

Our results reflect well the existing data from literature and provides an extra layer of understanding as we are able to prove the existence of an energetic plateau around the ablation threshold. The plateau strongly depends on the nature of the target and defines the fluence range where structural changes are occurring at the surface. SEM and XPS investigations of the irradiated area provided information about the morphological and surface chemistry process induced during irradiation in the threshold range.

Acknowledgment. This work was supported by Romanian Ministry of Education and Research, under Romanian Nat. Nucleu Program LAPLAS VI –n. 16N/2019 and ELI-RO_2020_12.

T3-P: Processing of Continuouslly Compositionally Graded Kesterite Layers for Photovoltaic Applications

B.S. Vasile[1], I. Boerasu[2], R.D. Trusca[1], V.A. Surdu[1], O.R. Vasile[1]

[1]Department of Science and Engineering Of Oxide Materials and Nanomaterials, Facultu of Chemical Engineering and Biotechnologies, University Politehnica of Bucharest, Romania

[2]National Research Center for Micro and Nanomaterials, University Politehnica of Bucharest, Romania

To boost the challenge of the 2050' global energy demend, two main limitations have to be overpassed in the remained time window. Firstlly, to identify new alternative energy sources to replace the nowadays energy sources that's are in a critical natural decline. The second limitation is raised up by the industry imposed 2050's climate neutrality objective. Nowadays, photovoltaics based on crystalline Si represent the worldwide matured renewable energy technologies. Manly due to the high production cost/watt, this technology has to be replaced by another stable, costly-efficient and environment friendly technology, such as those based on Cu2ZnSnS4 (CZTS) Kesterite.

Herein, we report our result on processing of high quality innovative CZTS absorbers with a continuously compositional gradient (CCG). The aim of our research is to tune the CZTS's optical and photoelectrical properties by the adjustment of Cu/(Zn+Sn) ratio. If so, the absorber's Eg can be engineered leading to a cell with a graded bandgap through a compositionally graded CZTS absorber. In this perspective, our approach was to keept the Cu mol% constant at 1.6, while modifying the ratio of the concentration of the Zn to Sn (Zn/Sn) across the absorber. Three different CZTS compositions were synthetized by an enviorement friendly technique. C0 - stoiochiometric, C1 at Zr/Sn=0.9, and C2 at Zr/Sn =0.8. The CCG structure were obtained by depositing 3 layers of each composition in the followeeng order in respect to the used Mo-SLG substrate. The solution was placed spin-coating at 3000 rpm for 30s and two step pyrolysis in air: at 160°C and at 400°C. The final CCF structure was crystallized by clasic thermal annealing at 400°C in Ar athmosfere.

The x-ray analysis (XRD), performed on the set of samples, shows the presence of the pure kesterite phase. Based on the recorded XRD patterns and on the Rietveld refinement algoritm, it was concluded that the degree of the cristalinity is increasing with the decreasing of the concentration gradient, and the average crystallite diameter is decreasing by almost half in respect to the stoiochiometric sample, as depicted in Table 1.

Table 1.

C0		C1		C2		M1	
a [Å]	5.4225	a [Å]	5.4239	a [Å]	5.3998	a [Å]	5.4257
b [Å]	5.4225	b [Å]	5.4239	b [Å]	5.3998	b [Å]	5.4257
c [Å]	10.843	c [Å]	10.838	c [Å]	10.843	c [Å]	10.844
Mean [Å]	68.71	Mean [Å]	30.20	Mean [Å]	28.21	Mean [Å]	29.95
Stdev	17.71	Stdev	10.45	Stdev	11.21	Stdev	15.02
Cryst. [%]	55.99	Cryst. [%]	63.49	Cryst. [%]	63.73	Cryst. [%]	63.73

Scanning electron microscopy (SEM) technique was involved to investigate the top and cross-section morphology of the as processed set of samples. According to the recorded images, the deposited set of layers ar fully covering the substrat, and no pin-holes or cracks were observed. The final thickness of the CCG structure was estimated to 542 nm (Fig.1).

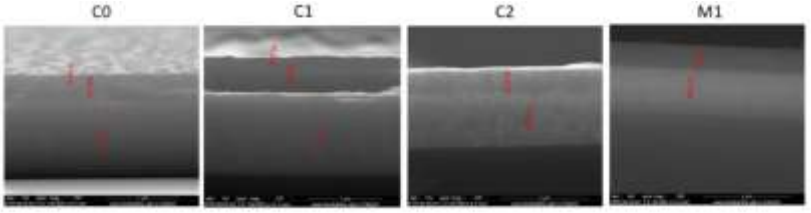

Figure 1.

It is observed in the recorded SEM cross-section images, that the film thickness is increasing from 359 nm to 542 nm as the Cu/(Zr+Sn) ratio is decreasing. The UV-VIS spectra of the

samples indicate a strong absorbance in the visible range, with the presence of a less intense band at ~260 nm, in the UV range. The extension to long wavelengths, +800 nm indicates the possibility of absorbing IR radiation (with applicability in making special windows for low energy consumption). Also, the good absorption presented in the visible range recommends the samples for devices that accumulate solar energy (solar cells).

T3-P: Graphene and nanosilicon based films for high voltage lithium-ion capacitors with ionic liquid electrolytes

V. Khomenko, D. Patlun, V. Barsukov

Department for Electrochemical Power Engineering and Chemistry, Kyiv National University of Technologies and Design/ Kyiv, Ukraine

Lithium-ion batteries (LIBs) and electrochemical capacitors (supercapacitors) dominate the energy supply for portable electronics. Nanotechnology has opened up a new opportunity for the fabrication of high-performance electrodes. In this work, we demonstrate the development of advanced lithium-ion capacitors (LIC). LIC contains a negative electrode, which is similar to LIB anode, and a positive electrode, which is similar to a supercapacitor. In this research we present a binder-free approach to forming electrodes of LIC. Graphene and silicon-based films on the current collector were obtained by Plasma Enhanced Chemical Vapor Deposition (PECVD). A novel approach was made to fabricate LIC having silicon–graphene composite anode (Fig.1) and graphene-based cathode (Fig.2) in ionic liquid electrolytes. The total electrode thickness was less 2 microns.

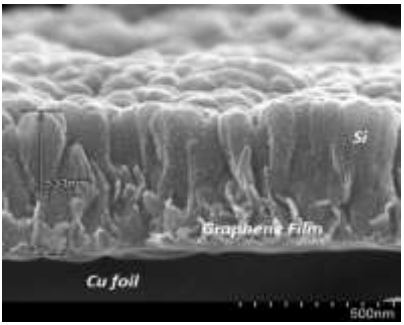

Fig. 1. Microstructure of the Si-graphene composite on Cu foil.

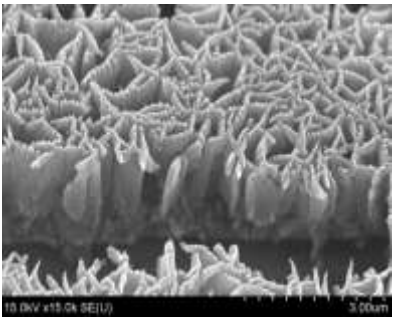

Fig. 2. Microstructure of the graphene film on Al foil.

Electrolyte formulation remains a fundamental element of these state-of-the-art systems. 1-Butyl-1-methylpyrrolidinium bis(trifluoromethylsulfonyl)imide (electronic grade) so-called Pyr14TFSI with 0.1 M LiTFSI has chosen them for LIC. Fig. 3 shows the CV of LIC based on nanomaterials.

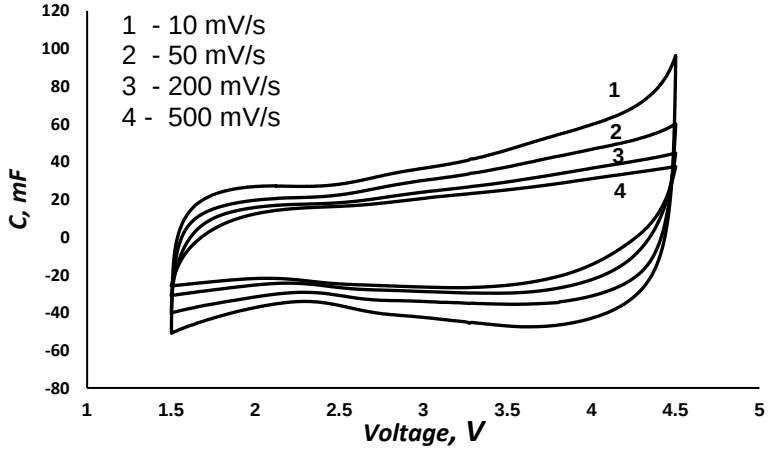

Fig. 1. Electrochemical performance (CV) of lithium-ion capacitor with ionic liquid electrolyte (Pyr14TFSI) contained 0.1M LiTFSI.

According to Fig. 3, LIC with 4.5V working voltage showed excellent rate capability, with almost 80% of the original capacitance retained when the charge-discharge capacitor rate was increased from 10 to 500 mV/s. Our prototype cells already reach high specific energies of ~80 W·h/kg, while maintaining a specific power of up to 1 kW/kg and cycling stability of over 1000 cycles. Owing to high energy density, LIC based on nanomaterials exhibit great potential as high-performance energy sources for advanced technologies where high power and energy density are required.

Acknowledgements. The authors acknowledge the NATO Science for Peace and Security Programme, which supports this work under grant SPS G5772.

T3-P: Influence of the Preparation Conditions on the Catalytic Efficiency of CoPt Catalyst for MOR

O-G. Dragos-Pinzaru[1], G. Stoian[2], F. Borza[3], N. Lupu[4]

[1]*National Institute of R&D for Technical Physics, Iasi, Romania*
[2]*National Institute of R&D for Technical Physics, Iasi, Romania*
[3]*National Institute of R&D for Technical Physics, Iasi, Romania*
[4]*National Institute of R&D for Technical Physics, Iasi, Romania*

Air pollution is the most important environmental risk to human health, and it is seen as a major concern at both national and international level. The World Health Organization (WHO) has found that nine out of ten people are breathing air that exceeds WHO guideline limits containing high levels of pollutants, which is killing an estimated seven million people every year. The pollution index in Romania

gradually increased from 50.5 in 2016 to 58.42 in 2021. If we're going to make a serious dent in climate change and other environmental problems, we need to substitute more clean energy sources for fossil fuels. Renewable energy is one promising option.

The DMFC (Direct Methanol Fuel Cell) technology allows to produce electricity directly from high density liquid methanol fuel trough electrochemical reactions, working at the same time at low temperatures. In DMFC, a mixture of methanol and water is directly introduced to the anode where the methanol is directly oxidized on a catalyst, to carbon dioxide, using the methanol oxidation reaction (MOR). One of the important class of conventional materials used as catalysts for MOR in a DMFC is represented by CoPt alloy, due to their exceptional performance in terms of activity and selectivity.

In this study, experiments were carried out in order to optimize the catalytic properties of CoPt nanowires by controlling the electrodeposition parameters. The CoPt nanowires electrodeposition uses a stable hexachloroplatinate solution. It will be shown that the crystalline structure of the CoPt nanowires can be controlled by adding saccharine like organic additives into the electrochemical bath. At the same time, it will be demonstrated that the composition and the catalytic properties of the CoPt nanowires arrays with a diameter of 200 nm can be tuned out by controlling the electrodeposition conditions.

In order to study the electrocatalytic properties of the CoPt alloys as catalysts for the MOR we have used cyclic voltammetry (CV) in aqueous solution of 2.0M CH_3-OH and 0.1M H_2SO_4 at a scan rate of 100 mV/s.

Fig. 1a presents an example of the cross-section of the AAO template, filled with CoPt nanowires electrodeposited at -0.8 V from the solution containing saccharine at pH 2.5, while Fig. 1b present the catalytic behaviour for methanol oxidation reaction in acidic medium of the CoPt alloys, prepared at pH2.5.

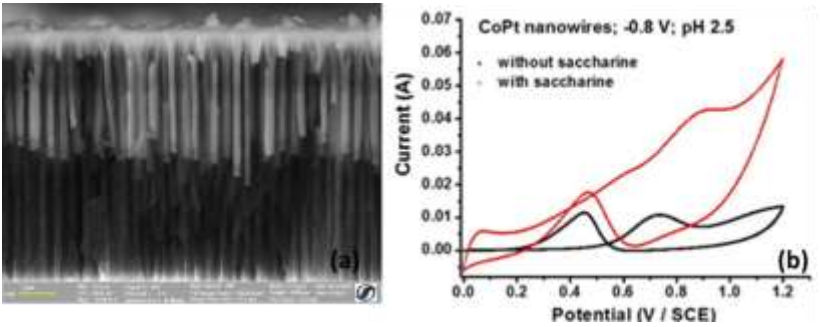

Fig. 1. (a) *Cross-section SEM micrograph of the AAO template filled with CoPt nanowires and* (b) *CV curves for methanol oxidation on the CoPt nanowires catalysts in aqueous solution of 2.0 M CH_3-OH and 0.1 M H_2SO_4*

Acknowledgments. This work was supported by the Romanian Executive Agency for Higher Education, Research, Development, and Innovation (UEFISCDI), contract number 110PCE/2022 (Project PN-III-P4-PCE-2021-1395/GreenEn).

T3-P: Improvement of the performance of Sb_2Se_3 solar cell by TiO_2 layer treatment

V. Pakstas[1,2], R. Kondrotas[1], A. Drabavicius[1], A. Naujokaitis[1], M. Franckevicius[1], A. Meshalkin[3], H. Cesiulis[2,4]

[1]*Center for Physical Sciences and Technology, Vilnius, Lithuania*
[2]*JSC "Elektronikos Perdirbimo Technologijos", Vilnius, Lithuania*
[3]*Institute of Applied Physics, Chisinau, Moldova*
[4]*Faculty of Chemistry and Geosiences, Vilnius University, Vilnius, Lithuania*

Thin-film solar cells with absorber layers of CdTe, $CuInGaSe_2$ (CIGS) or $CuInSe_2$ (CIS) have already achieved a power conversion efficiency (PCE) up to 20%. However, these semiconductors contain indium and gallium, which are scarce in the earth's crust, or are toxic like cadmium. Less than a decade ago, antimony selenide was proposed as an excellent material for a cheap, non-toxic absorber. Sb_2Se_3 is rapidly becoming a sustainable light-absorbing material for thin-film solar cells with a conversion efficiency of over 10% [1].

To achieve high PCE for solar cells with Sb_2Se_3 light-absorbing layers, several drawbacks need to be considered. The main problems are related to the loss of open circuit voltage (V_{OC}), the back-contact barrier, the compatibility of the electron transport layer with the absorber and its quality. It is also known that surface adhesion defects of coatings can occur at the buffer layer/absorber interface, but most researchers ignore this and focus on the large absorber defects.

Here, we studied the growth process of Sb_2Se_3 on TiO_2 substrates using the vapour transport deposition (VTD) method. TiO_2 layers were prepared on conductive fluorine-doped tin oxide (FTO)-coated glass substrates. A compact layer of titanium dioxide with anatase structure of 30-150 nm was deposited at 320-550 °C by spray pyrolysis of acetylacetone (200 µL) and titanium isopropoxide (300 µL) dispersed in ethanol (4.5 ml) [2].

In order to evaluate the influence of TiO_2 layers on the parameters of $FTO/TiO_2/Sb_2Se_3$ solar cell, the following settings have been explored: 1) The thickness of the TiO_2 layer - from 30 to 150 nm; 2) The heat treatment - from 320°C up to 550°C; 3) The chemical treatment of TiO_2 in a $TiCl_4$ solution with additional annealing. The appropriate treatment of the TiO_2 layer allows to increase the V_{OC} of the Sb_2Se_3 solar cell and to improve the voltammetric properties.

Acknowledgment. This work has received funding from the European Union's Horizon 2020 research and innovation programme under the Marie Sklodowska-Curie grant agreement Nº 778357- SMARTELECTRODES.

[1] R. Tang, X. Wang, W. Lian, J. Huang, Q. Wei, M. Huang, Y. Yin, Ch, Yiang, Sh. Jang, G. Xing, Sh. Chen, Ch. Zhu, X. Hao, M.A. Green, T. Chen, Nature Energy **2020**, 5, 587–595.
[2] D. Prochowicz, M. Franckevičius, A.M. Cieslak, S.M. Zakeeruddin, M. Gratzel, J. Lewinski, J. Mater. Chem. A **2015**, 3, 20772-20777.

T4-P: Effects of Silicon addition on magnetic properties of MM-Fe-B ribbons

M. Lostun, H. Chiriac, M. Porcescu, G. Stoian, N. Lupu, M. Grigoras

National Institute of Research & Development for Technical Physics, 700050 Iasi, Romania

Currently, the market for permanent magnets is dominated by 90% of Nd-Fe-B-based magnets, which are critically dependent on the rare earth metal Nd / Pr / Dy / Tb. Due to the high price and low supply of neodymium (Nd), many researchers have attempted to replace Nd by using the low-priced rare earth metals, such as Ce or La [1, 2]. On the other hand, environmental pollution from extraction process of rare-earths is severe [3]. Replacing Nd with Misch-metal (MM) can lead to a balanced use of rare earth elements and will reduce environmental pollution. Misch-metal (MM) with the nature ratio (25–35 wt % La, 45–55 wt % Ce, 4–10 wt % Pr, 14–18 wt % Nd) is a typical representative of the mixed rare-earth elements coexisted in the mines. However, the total replacement of critical rare earth with MM leads to a lower Curie temperature (Tc) of about 17 % [4] and also to a

significant decrease in coercivity (Hc) and, consequently, of the energy product (BH)max. The magnetic properties can be improved by using a substitute element to replace some of the Fe in MM-Fe-B. In this work, we report the effect of Fe substitution by Si on the hard magnetic properties of $MM_{14}Fe_{80-x}Si_xB_6$ ribbons, where, $0<x<1$. The crystal structures, magnetic properties, intergranular exchange interactions and phase transition temperatures of annealed $MM_{14}Fe_{80-x}Si_xB_6$ ribbons were investigated. A critical amount of Si enhanced the magnetic properties of the alloys by partially decreasing the formation of paramagnetic $MMFe_2$ phase and by refining the grains. The analysis of Henkel plots confirmed that the exchange interaction among grains was greatly improved for the optimized doping of Si. The optimized magnetic properties of coercivity Hc=8.7 kOe, remanence magnetization Mr=81 emu/g and Curie temperature Tc= 247 ºC were obtained for annealed $MM_{14}Fe_{79.2}Si_{0.8}B_6$ ribbons.

Acknowledgement. This work was supported by a grant of the Ministry of Research, Innovation and Digitization, CCCDI - UEFISCDI, project number PN-III-P2-2.1-PED-2021-1386, within PNCDI III.

[1] M. Grigoras et al, J. Magn. Magn Mater. **2017**, 432, 119.
[2] Z Y Zhang et al, Mater. Res. Express **2017**, 4, 086503.
[3] Le. Zhou, Jianping Ge, The Extractive Industries and Society, **2021,** 8, 340–354.
[4] R. Li, et al. AIP Advances **2017**, 7, 056207.

T4-P: Synthesis of α''-$Fe_{16}N_2$ powders with elongated particles prepared by high-pressure gas atomization technique

M. Grigoras, M. Lostun, M. Porcescu, G. Ababei, G. Stoian, N. Lupu

National Institute of Research & Development for Technical Physics, 700050 Iasi, Romania

Rare-earth permanent magnets (PMs) are currently widely employed in various applications. The demand for high-performance permanent magnets is constantly growing, primarily due to the accelerated development of motors in electric/hybrid vehicles and wind turbine generators [1, 2]. Currently, the best PMs are all made of rare earth, such as Sm-Co, and Nd-Fe-B. Rare earth metal is non-renewable, and source reserves are dwindling. Moreover, the mining, refining, recycling of rare earth are harmful to the environment, generating soil, air, and water pollution [3]. Therefore, there is a strong global effort to replace or reduce the critical elements of rare earths with more abundant and less expensive ones. Iron-nitrogen magnets based on α''-$Fe_{16}N_2$, with possible giant magnetization, can be a promising candidate for replacing rare-earth permanent magnets. In addition, both Fe and N are abundant, much cheaper than rare-earth elements, and completely non-polluting. The saturation magnetization reported on films, foils and powder is very scattered, from 230 to 315 emu/g due to the difficulty in synthesizing α''-$Fe_{16}N_2$ [4]. Additionally, the manufacture of bulk magnet with reasonable magnetic properties is still an obstacle that has not been overcome, primarily due to low coercivity. The highest reported coercivity for powders (PMs precursors) was as 2.2 kOe [5]. High coercivity can be achieved by either the

materials intrinsic high magnetocrystalline anisotropy, fine particle/grain size, or shape anisotropy.

Here, we report the effect of particle size and shape on the morphology, structure, and magnetic properties of Fe-N powders prepared by high-pressure gas atomization of pure iron ingots in a high purity nitrogen atmosphere. Atomization is carried out by using a nitrogen gas high-pressure to break a molten iron into fine droplets, and then condensing it into a collector to obtain a fine iron nitride powder. By controlling the parameters involved in the gas atomization process, such as atomization pressure, the diameter of the ejection nozzle, the angle between the gas jet and the molten iron jet, and the diameter of the gas nozzle, we managed to control the size and shape of the particles. Thus, we found that: (i) the particle size decreases as the atomizing pressure increases and / or the diameter of the gas nozzle decreases, (ii) the particle shape changes from sphere to ellipsoid for an angle between the gas jet and the molten iron jet less than 45 degrees, (iii) the α''-$Fe_{16}N_2$ phase content of the powders increases with increasing breaking gas pressure and ejection temperature. Fe-N particles prepared in an elongated shape and with a diameter of less than 50 μm have a high potential to be used for the production of high performance α''-$Fe_{16}N_2$ anisotropic magnets.

Acknowledgement. This work was supported by a grant of the Ministry of Research, Innovation and Digitization, CNCS - UEFISCDI, project number PN-III-P4-PCE-2021-0298, within PNCDI III.

[1] B. Zhou, Z. Li, C. Chen, Minerals, **2017**, 7, 203.
[2] T. A. Huynh, M. F. Hsieh, Energies, **2018**, 11, 1385.

[3] Le. Zhou, Jianping Ge, The Extractive Industries and Society, **2021,** 8, 340–354.
[4] J. Cui et al. Acta Mater., **2018**, 158, 118-137.
[5] T. Ogi et al. Adv. Powder Technol., **2016**, 27, 2520–2525.

T4-P: Magnetocaloric effect of iron nanoparticles embedded in titanium nitride thin film heterostructure

K. Sarkar[1], V. Jones[2], D. Kumar[3]

[1]Department of Mechanical Engineering, North Carolina A&T State University, Greensboro, North Carolina, USA
[2]Department of Physics, North Carolina A&T State University, Greensboro, North Carolina, USA
[3]Department of Mechanical Engineering, North Carolina A&T State University, Greensboro, North Carolina, USA

There is a strong need to develop new material systems with efficient refrigeration capability that reduce energy consumption and leave minimum footprint on the environment. Magnetic refrigeration is an excellent candidate to achieve this goal due to their potential for high energy efficiency. The magnetic refrigeration process is based on the magnetocaloric effect (MCE). It is a magneto-thermodynamic phenomenon in which an adiabatic change in temperature of a magnetocaloric material (MCM) is caused by exposing the thermally isolated material to a magnetic field. Most of the work on the MCE is focused on bulk magnetocaloric materials (MCMs) containing rare earth elements since the entropy change scales with magnetic moment per atom, which is high for rare earth elements. But with limited availability and high cost, many efforts are being taken to explore rare earth-free MCMs. Nanoparticles and heterostructure systems can be used as an alternative to traditional bulk MCE materials due to

control over the entropy change across the magnetic phase transition that can be maneuvered by varying particle size. In this work, nanostructures comprising of iron (Fe) particles embedded in a titanium nitride (TiN) thin-film matrix in a TiN/Fe/TiN multilayered pattern have been fabricated using a pulsed laser deposition method. The 2□□XRD diffraction pattern recorded from the Fe-TiN multilayer sample grown on single-crystal c-Al_2O_3 substrates reveals TiN peak which is textured with respect to (111) planes. Scanning electron microscopy (SEM) and atomic force microscopy (AFM) were used to determine the particle size of iron nanoparticles. The magnetic properties of Fe-TiN systems were investigated using Vibrating Sample Magnetometer (VSM) attached to a Physical Property Measurement System (PPMS). Magnetization versus field (M vs. H) curves were recorded for in-plane fields. High angle annular dark-field images in conjunction with dispersive energy analysis, recorded using scanning transmission electron microscopy, show a clear presence of alternating layers of Fe and TiN with a distinct atomic number contrast between Fe particles and TiN. Quantitative information about the isothermal entropy change (□S) and the MCE in the multilayer Fe-TiN system has been obtained by applying Maxwell relation to the magnetization versus temperature data at various fields. A MCE with sizable isothermal entropy change (□S) maintained over a broad range of temperatures (10 K < T < 300 K) is reported for a rare earth-free nanoparticle Fe-TiN heterostructure. At lower applied fields, the positive entropy change (inverse MCE) peaks in the vicinity of field-dependent blocking temperature giving □S as high as 1.4×10^3 J/Km^3 at an applied field as low as 0.075 T at 10K. On the other hand, with the dynamic magnetic hysteresis absent above the

blocking temperature, the negative □S as high as 4.18×10^3 J/Km^3 (normal or forward MCE) is obtained for 3 T at 300 K. The refrigeration capacity (RC) at various applied fields have also been evaluated with the realization of a maximum of RC values of 7.4 × 10^5 J/m^3 (~94 J/kg) at 3 T. With a combination of a broad range of usable□□S and easy accessibility, the Fe-TiN material system can give us insight for the fabrication and design of novel MCMs with improved refrigeration efficiency needed for next-generation solid-state cooling.

T4-P: Properties of 3D Printed Magnets, Obtained Using $SmCo_5$/Fe Magnetic Nanocomposite Powders

R. Hirian[1], F. Popa[2], R. Bortnic[1], G. Souca[1], I. Balasz[1], V. Pop[1]

[1]Faculty of Physics, Babeş-Bolyai University, Cluj-Napoca, RO-400084 Romania

[2]Materials Science and Engineering Department, Technical University of Cluj-Napoca, Cluj-Napoca, RO-400641 Romania

Nearly thirty years ago, the potential of obtaining an energy product of 1 MJ/m^3 in hard-soft exchange coupled nanocomposites (spring magnets) was first shown [1]. Since then, even though there has been much advancement in this area of research, the 1 MJ/m^3 energy product still proves elusive. The best result obtained so far is approximately 400 kJ/m^3 (close to $Nd_2Fe_{14}B$ magnets) in thin films [2]. One of the great challenges in this field is producing an anisotropic magnet, as the nanostructured materials is difficult to obtain in an aligned form.

In recent years, additive manufacturing by 3D printing has come to the forefront as an affordable and efficient manufacturing method. This technique brings with it the

possibility of 3D printing isotropic polymer bonded magnets with complex shapes. To this end a 3D printer filament, composed of small magnetic particles incased in a polymer matrix, is used. As these materials are isotropic (in most cases), it would be a good application case for spring magnet particles. The theoretically higher energy product of the exchange coupled nanocomposites makes them very attractive, as it could allow for the loading of a lower magnetic powder fraction into the polymer, which in turn should make the printing process easier.

In this work magnetic 3D printer filaments (Nylon + magnetic powder) were produced, using $SmCo_5$/Fe nanocomposites (obtained by mechanical milling and subsequent annealing) as the magnetic powder. For comparison, filaments were also made using commercial $SmCo_5$ powders. At this point of the study, the produced magnetic filaments were used to 3D print some cylindrical bonded magnets. The microstructure of the printed magnets was investigated by Scanning Electron Microscopy, and their magnetic properties (saturation magnetization, coercive field and energy product) were investigated at room temperature, in order to assess the feasibility of using exchange coupled nanocomposite powders in the production of 3D printed magnets.

[1] R. SkomskiJ. Appt. Phys. **1994**, 76, 7059-7064

[2] V. Neu, S. Sawatzki, M. Kopte, Ch. Mickel, L. Schultz, IEEE Trans. Magn. 48 (2012) 3599-3602.

T5-P: Comparison of magnetic properties and magnetocaloric effect in in nano- and polycrystalline $La_{0.7}Ba_xCa_{0.3-x}MnO_3$ manganites

R. Atanasov[1], E. Brinza[1], R. Bortnic[1], R. Hirian[1], L. Barbu[2], I.G. Deac[1]

[1] Faculty of Physics, Babeș-Bolyai University Cluj-Napoca, Str. Kogalniceanu 1, 400084 Cluj-Napoca, Romania

[2] National Institute for Research and Development of Isotopic and Molecular Technologies, Donath 67-103, P.O. Box 700, 400293 Cluj-Napoca, Romania

Structural, magnetic properties and magnetocaloric effect of $La_{0.7}Ba_xCa_{0.3-x}MnO_3$ bulk and nanocomposite powders have been investigated. Bulk polycrystalline compounds were produced by solid-state reaction and nanoparticles were synthesized by sucrose Sol-Gel method. The structural properties were investigated by X-ray diffraction and Rietveld refinement. A change from rhombohedral to orthorhombic structure is observed for $x > 0.25$ level in both systems, as well as diminishing lattice size with increasing substitution level. Both Williamson-Hall method and Rietveld refinement were used for crystallite size determination. Morphological properties were investigated with an optical microscope for the bulk system and with Transmission Electron Microscopy (TEM) for the nanoparticles. Grain sizes for the bulk samples was found to be in the range 1-3 μm. TEM shows that the average size of the nanoparticles is 40-50 nm. Magnetic measurements were done by using a Vibrating Sample Magnetometer in the range 4-300 K and they revealed ferromagnetic order below TC which systematically decreases with increasing the substitution level. In order to determine the type of phase transition, Arrott plots were constructed and

investigated. All samples exhibit second order phase transition. Magnetic enthropy change was determined from magnetic isotherm measurements for each compound. Nano-sized compounds present a wider temperature range in effective magnetocaloric effect with a lower peak compared with the same bulk compound. Critical temperatures of each compound were determined. The lowest values were found to be 260 K and 130 K at x=0.25 for the bulk and nanoparticles, respectively. The saturation magnetization at 4 K was about 3.7 μB / f.u. for large particles and 0.9 μB / f.u. (x = 0.25) for nanoparticles. The magnetocaloric effect is the most intense for x = 0.25 doped bulk sample, with a magnetic entropy change of 7.0 J/kg K at 270 K while for the nano-samples it reaches 1.3 J/kg K at 220 K, when x = 0.2, for μ0ΔH = 4 T. In spite of the small values of the magnetic entropy change, for the nano-particle samples, the relative cooling power (RCP) is much larger than in the case of bulk polycrystalline samples. Further comparison and future prospects in advantages of nano-sized compounds are discussed.

T5-P: FePt heterostructures with tailored electro-optical properties

C. Leostean[1], O. Pana[1], S. Macavei[1], M. Stefan[1], D. Toloman[1], A. Popa[1], C.M. Teodorescu[2]

[1]National Institute for Research and Development of Isotopic and Molecular Technologies, 67-103 Donat, 400293 Cluj-Napoca, Romania
[2]National Institute of Materials Physics, Atomistilor str. 405A, Magurele - Bucharest, Romania

Multiferroic heterostructures with coupled ferroelectric and ferromagnetic elements have attracted an ever-increasing

amount of interest recently due to their strong magnetoelectric coupling at room temperature. The magnetoelectric coupling leads to electric field control of magnetism, or magnetic field manipulation of polarization, which provides a wide variety of applications in spintronics and electronic devices.

Barium titanate ($BaTiO_3$) is well known as a ferroelectric material that is used in capacitors, electromechanical transducers and nonlinear optics. In the last decade, there is groing interest in $BaTiO_3$ based heterostructures with 3d metals or alloys [1-4].

Half-metallic FePt (L10) is well known for its magnetic properties that is foreseen for high density magnetic data storage. Its development is currently driven to exchanging coupling [5,6].

The successful deposition of high- quality films strongly depends on reliable and optimal fabrication techniques. It is known that through the use of PLD technique, even for complex materials, the stoichiometry of the target is preserved within the deposited film. First, FePt thin films were grown on Al_2O_3(0001) substrare by using 9600 pulses at 5 Hz laser repetition rate with 370 mJ energy in Ar atmosphere at 700^{o}C. Then, on the optimized FePt thin films, a $BaTiO_3$ layer was deposited by using 9600 pulses at 5 Hz laser repetition rate with 250 mJ energy in Ar atmosphere at 600^{o}C. In the final step, the deposited thin film was the annealied in O_2 atmosphere at 650^{o}C for 30 min.

Structural, morphological, optical and magnetic properties of the prepared heterostructures were investigated for both fundamental and applicative point of view.

Acknowledgments. This work was supported by the Romanian Ministry of Research, Innovation and Digitalization, Core Programme, Project PN19 35 02 03.

[1] T. T. Xiao, M. J. Casanove, C. Z. Cai et al., Mater. Res. Express **2016**, 3, 086404
[2] Haffer S, Lüder C, Walther T, et al., Micropor. Mesopor. Mat. **2014**, 196, 300–4
[3] S. Geprägs, A. Brandlmaier, M. Opel, et al., Appl. Phys. Lett. **2010**, 96, 142509
[4] M. Lee, H. Choi, Y. C. Chung, J. Appl. Phys. **2013**, 113, 17C729
[5] J. Yu, T. Xiao, X. Wang, et al., Nanomaterials **2019**, 9(1), 53
[6] S. Gutoiu, C. Leostean, M.L. Soran, et al., AIP Advances **2020**, 10, 055215

T5-P: MoS_2/FePt thin films on Mg (100) substrates with tailored properties

S. Macavei[1], O. Pana[1], M. Stefan[1], D. Toloman[1], A. Popa[1], C. Leostean[1], S. Cinta Pinzaru[2], S. Colis[3]

[1]National Institute for Research and Development of Isotopic and Molecular Technologies, 67-103 Donat, 400293 Cluj-Napoca, Romania
[2]Faculty of Physics, Babes-Bolyai University, Mihail Kogălniceanu 1, 400084 Cluj-Napoca, Romania
[3]University of Strasbourg, Institute of Physics and Chemistry of Materials, PCMS-DCMI, 23 rue du Loess, 67034 Strasbourg, France

MoS_2 thin films are currently being developed for sensing, photocatalysis and supercapacitors aplications [1-3]. Their bandgap cand be tailored by varying the layer thickness [4]. Half-metallic FePt (L10) is well known for its magnetic properties that is foreseen for high density magnetic data

storage. Its development is currently driven to exchanging coupling [5,6]. When a semiconductor is interfaced with a half-metal there is a charge transfer across the interface which involves only spin polarized states coming from or going to the Fermi level of the half-metal. Depending on the oxidation energy or work functions of both half-metal and SC, three arrangements of energy bands and charge/spin transfers at the interface are possible. MoS_2/FePt thin films are foreseen for applications in the spintronics technology as magnetic sensors, spintronics couplers, and magnetic random access memory (MRAM), magnetic tunnel junctions (MTJs), domain wall race-track memories etc.

The successful deposition of high- quality films strongly depend on reliable and optimal fabrication techniques. It is known that through the use of PLD technique, even for complex materials, the stoichiometry of the target is preserved within the deposited film. First, FePt thin films were grown on MgO(001) substrate by using 9600 pulses at 5 Hz laser repetition rate with 362 mJ energy in Ar atmosphere at 700^{o}C. Then, on the optimized FePt thin films, a MoS_2 layer was deposited by using 2400 pulses at 5 Hz laser repetition rate with 295 mJ energy in Ar atmosphere at 700^{o}C.

XRD patterns and Raman spectroscopy E_{2g} and A_{1g} vibration modes of MoS_2, indicate the growth of crystalline MoS_2 layers. Using UV-Vis spectroscopy as well as UV-excited photoelectron spectroscopy (UPS) the band alignment at the MoS2/FePt interface was determined. The magnetic properties of the prepared heterostructures were investigated. It can be seen that the MoS_2 film, at high temperatures, becomes a ferromagnet and is exchange coupled with the FePt film. As the temperature decreases, this coupling decreases thus the

magnetization behavior below ~30K being the characteristic of the FePt film. This analysis is important from both fundamental and applicative point of view.

Acknowledgments. The authors would like to express appreciation to the Romanian Ministry of Research, Innovation and Digitization for the financial support through Projects PN 19 35 02 03 (Core Program) and ELI_17/16.10.2020.

[1] Neetika, A. Kumar, et al., Thin Solid Films **2021**, 725, 138625
[2] Y.-F. Huang, K.-W. Liao, et al., Catalysts **2021**, 11, 1295.
[3] R. Wang, D. Jin, Y. Zhang, et al., J Mater Chem A. **2017**, 5, 292
[4] Y. Zhang, Y. Kuwahara, et al., Nanoscale **2020**, 12, 11908
[5] J. Yu, T. Xiao, X. Wang, et al., Nanomaterials **2019**, 9(1), 53
[6] S. Gutoiu, C. Leostean, M.L. Soran, et al., AIP Advances **2020**, 10, 055215

T5-P: Highly efficient photocatalyst based on MWCNT and $CoFe_2O_4$ nanoparticles

M. Stefan[1], C. Leostean[1], A. Popa[1], D. Toloman[1], I. Perhaita[2], A. Cadis[2], S. Macavei[1], O. Pana[1]

[1]National Institute for Research and Development of Isotopic and Molecular Technologies, 67-103 Donat, 400293 Cluj-Napoca, Romania
[2]"Raluca Ripan" Institute for Research in Chemistry, "Babes-Bolyai" University, Fântânele st. 30, 400294, Cluj-Napoca, Romania

MWCNT-$CoFe_2O_4$ nanocomposites were prepared in sequential synthesis steps by decorating $CoFe_2O_4$ nanoparticles on the surface of functionalized MWCNT. Initially, the $CoFe_2O_4$ nanoparticles were obtained by chemical precipitation and subsequently, the obtained $CoFe_2O_4$

nanoparticles were anchored on functionalized MWCNT through polymer wrapping. The thermal analysis approaches namely, evolved gas analysis (EGA) coupled with FT-IR spectra were involved in highlighting the sequential steps mechanism for obtaining MWCNT-$CoFe_2O_4$ nanocomposites. The composite formation was proved by X-ray Diffraction (XRD), Scanning Transmission Electron Microscopy (STEM), FT-IR spectroscopy, X-ray Photoelectron Spectroscopy (XPS). The influence of $CoFe_2O_4$ content on the magnetic and textural properties (surface area and porosity measurements) of the obtained nanocomposites was evidenced. Depicting the importance of thermal stability of nanomaterials in different industrial applications, the thermal behavior of MWCNT and $CoFe_2O_4$ was pointed out. Furthermore, the photocatalytic activity against organic pollutants such as Rhodamine B (RhB) and oxytetracicline (OTC) were evidenced. Additionally, the electron spin resonance spectroscopy (ESR) coupled with spin trapping technique was used to evidence the generation of reactive oxygen species (ROS). The obtained results suggest the efficient anchoring of $CoFe_2O_4$ on MWCNT through polymer linkage resulting in a thermal stable magnetic recoverable photocatalyst. The photocatalytic mechanism was discussed in terms of ROS generations acting as oxidants that cause the degradation of organic pollutants molecules. During the irradiation superoxide anion ($O_2^{\cdot-}$), hydroxyl (•OH) radical and nitroxide were detected. Generally, higher the amount of cobalt ferrite nanoparticles, higher the efficiency of the photocatalytic process.

Acknowledgments. The authors would like to express appreciation to the Romanian Ministry of Research, Innovation

and Digitization for the financial support through Projects PN 19 35 02 03 (Core Program) and ELI_17/16.10.2020.

T5-P: ZnO based nanostructures with modulable optical properties for photocatalytic applications,

M. Stefan, A. Falamas, D. Toloman, A. Popa, C. Leostean, S. Macavei, L. Barbu, O. Pana

National Institute for Research and Development of Isotopic and Molecular Technologies, 67-103 Donat, 400293 Cluj-Napoca, Romania

The development of new materials having tailored architecture that can easily meet the requirements of modern industrialization has the target of researchers all over the world. In the last decade, the environmental pollution caused by release in air, water and soil of harmful contaminants has been exploited [1,2]. This may not be an easy task since these poluttants are toxic for human health and aquatic environment.

As it is well known, semiconductor based photocatalysis is consider an efficient green way to remove dyes, antibiotics or other drugs from waste water since it use inoffensive photocatalysts and solar energy as inexpensive and regenerable energy source [3,4]. One of the most frequent problems was that the commonly used photocatalysts are insufficient visible light absorption, fast charge recombination of charge carriers, poor textural properties and recovery of photocatalysts. Several attractive methods have been designed to overcome these drawbacks, by either modifying the surface of ZnO nanostructures or by combining ZnO with metals, non-metals, or organic molecules.

Considering these, different ZnO based nanocomposites (ZnO-Au and/or ZnO-$NiFe_2O_4$) were synthesized and tested for water depollution under visible irradiation.

The ZnO-Au nanocomposites were prepared by decorating gold on preformed ZnO nanoparticles by reducing hydrogen tetrachloroaurate(III) in the presence of hydrazine. The ZnO-$NiFe_2O_4$ heterostructures were synthesized through a two-stage process: initially magnetic $NiFe_2O_4$ nanoparticles were obtained by chemical coprecipitation method, followed by obtaining ZnO nanoparticles by the sol-gel process.

The nanocomposites were characterized by using XRD, TEM/HRTEM, XPS, Uv-Vis, TG/DTG/DTA, FT-IR, and VSM to highlight its properties.

Photocatalytic activity against Rhodamine B under visible irradiation was evaluated and the photocatalytic mechanism was elucidated based on the reactive oxygen species (ROS) generated by the samples and trapping experiments.

This work not only offers a controllable method for the fabrication of semiconductor based composites structure but also provides an effective and conveniently photocatalyst for the practical application in the purification of wastewater.

Acknowledgments.This work was suppotred by two grants of the Ministry of Research, Innovation and Digitalization, CNCS – UEFISCDI, project number PN-III-P1-1.1-TE-0836 and PN-III-P1-1.1-TE-2019-1141, within PNCDI III.

[1] J D. B. Miklos, C. remy, M. Jekel, K. G. Linden, J. E Drewes, U. Hubner, Water Res. **2018**, 139, 118-131.

[2] A.L. Garcia-Costa, A. Alves, L.M. Madeira, M.S.F. Santos, J. Environ. Chem.Eng. **2021**, 9, 104709.

[3] E. Evgenidou, A. Ofrydopoulou, N. Malesic-Eleftheriadou, C. Nannou, N.M. Ainali, E. Christodoulou, D.N. Bikiaris, G.Z. Kyzas, D.A. Lambropoulou, Sci. Total Environ. **2020**, 741, 140394.

[4] A. A. H. Bukhari, Des.Water Treat. **2021**, 212, 143-151.

T5-P: SERS barcoding of widespread pathogens assisted by machine learning classification models

N. E. Dina[1], L. Stăncioiu[2], K. Wieland[3], C. Haisch[3]

[1]National Institute for Research and Development of Isotopic and Molecular Technologies, Cluj-Napoca, Romania
[2]Faculty of Physics, Babeș-Bolyai University, 400084 Cluj-Napoca, Romania
[3]Analytical Chemistry Chair, Technische Universität München, Munich, Germany

Surface enhanced Raman scattering (SERS) sensing, in particular for 'real-life' applications is now aided by supervised complex models for bis dataset analysis and classification, such as machine learning (ML) models.

This work focuses on the use of simple, single-step and effective protocol to create a gold thin layer-based SERS-active substrate for pathogens' detection. The thin gold films deposited on glass provided a semitransparent detection window for top illumination inside microchannels filled with bacteria.

Spectral data acquired were evaluated in terms of signal quality and the detection process was optimized by using different thicknesses for the gold films. All raw data between 600 – 1700 cm^{-1} were preprocessed as shown in Figure 1 to ensure reliability and reproducibility. Classification of SERS spectra recorded for three bacterial species was assessed by using 6 ML models.

The ready-to-use SERS-active substrates herein proposed enable the label-free detection and identification of widespread bacteria by deploying adapted machine learning models. Additionally, the employed design consists of ten

separate microchannels enabling multiplex, ultra-sensitive detection on one chip.

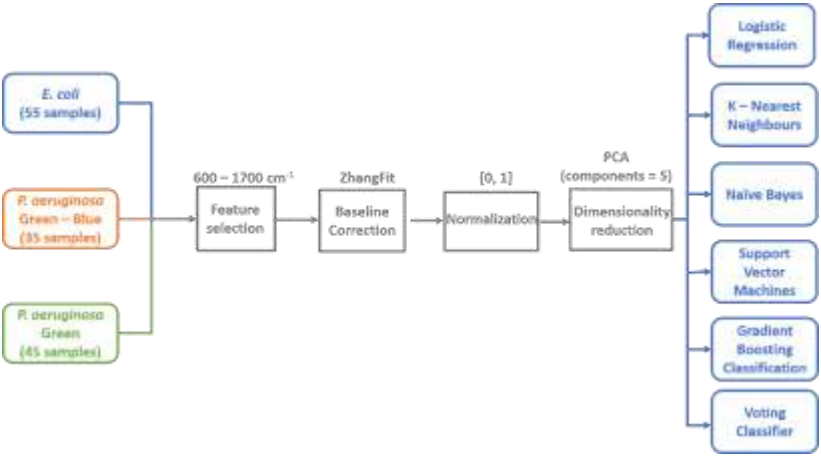

Fig. 1. A schematic representation of the pre-processing steps used before deploying the Machine Learning models.

Acknowledgements: This work was supported by a grant of the Romanian the Ministry of Research, Innovation and Digitization, CNCS – UEFISCDI, project numbers PN-III-P1–1.1-TE-2019–0910, and through the Core Program, Project No. PN 19 35 02 01.

T5-P: Superparamagnetic $Ga_{0.9}Fe_{2.1}O_4$ nanoparticles for biomedical applications

A. Mesaros[1], M. Năsui[1], T. Marinca[2], B. S. Vasile[3], O. Pana[4]

[1]Physics and Chemistry Department, C4S Center, Technical University of Cluj-Napoca, Cluj-Napoca, Romania
[2]Materials Science and Engineering Department, Technical University of Cluj-Napoca, Cluj-Napoca, Romania
[3]Department of Science and Engineering of Oxide Materials and Nanomaterials, University Politehnica of Bucharest, Bucharest, Romania

[4]National Institute for Research and Development of Isotopic and Molecular Technologies, 67-103 Donat, 400293 Cluj-Napoca, Romania

Over the past two to three decades, the synthesis and characterization of metal substitute magnetite, $Fe_{3-x}M_xO_4$ (M = Mn^{2+}, Co^{2+}, Zn^{2+}, Ni^{2+}, Al^{3+}, Ga^{3+}, etc.) have been intensively researched both for their fundamental scientific interest and for their multiple applications, such as: magnetic storage media [1], biosensing applications [2], medical application – targeted drug delivery [3] as contrast agents in magnetic resonance imaging (MRI) [4], and magnetic inks for ink jet printing [5]. To date, different chemical strategies have been developed to synthetize magnetic ferrite nanoparticles, such as co-precipitation, hydrothermal, sol-gel, micro-emulsions, or polyol method, proving that the physical and chemical properties are strongly dependent on the used synthetic route.

The goal of this work was to synthesize free of agglomeration and crystalline $Ga_{0.9}Fe_{2.1}O_4$ nanoparticles by solvothermal (ST) method and to study their structure, morphology and magnetic properties. Up to now, there have been no reports on the synthesis of nanometric size gallium ferrite with this specific stoichiometry Ga:Fe:O = 0.9:2.1:4. In the present research, we obtained the gallium ferrite stable colloidal solutions using a single compound, triethylene glycol (TEG) as solvent and capping agent. A narrow size distribution of the nanoparticles, below 10 nm, was achieved through well-defined processing conditions to control nucleation and growth, i.e. temperature, dwell time, heating rate and decomposition process. The chemical composition, structure, morphology and magnetic properties of the obtained

nanoparticles have been investigated. The composition and expected spinel structure were confirmed and a superparamagnetic behavior at room temperature was also shown. Due to their morphology and superparamagnetic behaviour the $Ga_{0.9}Fe_{2.1}O_4$ nanoparticles present a promising potential for biomedical applications as theranostic agents for diagnosis and drug delivery or as thermal seeds for magnetic hyperthermia.

Acknowledgments. This work was suppoted by a grant of the Ministry of Research, Innovation and Digitalization, CNCS – UEFISCDI, project number PN-III-P4-PCE-2021-1561, within PNCDI III.

[1] M. M. Miller, G. A. Prinz, S. F. Cheng, and S. Bounnak, Appl. Phys. Lett. **2002**, 81, 2211.
[2] T. K. Jain, M. A. Morales, S. K. Sahoo, D. L. Leslie-Pelecky, and V. Labhasetwar, Mol. Pharm. **2005**, 2, 194.
[3] I. Chourpa, L. Douziech-Eyrolles, L. N. Okassa, J. F. Fouquenet, S. C. Jonathan, M. Souce, H. Marchais, and P. Dubois, Analyst **2005**, 130(10), 1395.
[4] A. Akbarzadeh, M. Samiei, and S. Davaran, Nanoscale Res. Lett. **2012**, 7, 144.
[5] E. Solano, L. P. Mirabet, F. M. Julian, R. Guzman, J. Arbiol, T. Puig, X. Obradors, R. Yanez, A. Pomar, S. Ricart, and J. Ros, J. Nanopart. Res. **2012**, 14(8), 1034–1049.

T5-P: High-efficient separation of photoinduced charge carriers in magnetic heterostructures

A. Popa, M. Stefan, D. Toloman, D. Silipas, C. Leostean, L. Barbu, O. Pana

National Institute for Research and Development of Isotopic and Molecular Technologies, 67-103 Donat, 400293 Cluj-Napoca, Romania

Water pollution is currently one of the most important problems of international community. Research addressing the water cleaning issue is increasing and aims to settle these problems in a less costly and more efficient way. A wide variety of methods are used for pollutant removal from wastewater [1]. Among them, photocatalysis represents one of the most economical and environmentally friendly approach. This method is based on the generation under light irradiation of reactive oxygen species (ROS) which can oxidize the pollutant, converting them into non-hazardous forms [2]. A major challenge imposed by the practical applications is the development of highly photoactive materials with assured long-lifetime activity and which can be easily separated from the suspension to avoid the ecotoxicological risk of the residual nanoparticles. The magnetic photocatalysts can substitute heterogeneous catalysts due to its separation capability and high levels activity. The spinel compounds have been extensively studied in various applications of different fields including photocatalysis due to its low production cost, high coercivity, chemical stability and narrow band gap [3].
To improve the efficiency and recycling capacity of photocatalysts, in this study, we developed a magnetically recoverable photocatalyst based on ZnO nanoparticles decorated on $CoFe_2O_4$. This composite is expecting to have an

enhanced the photocatalytic efficiency because of the synergic effects of transition metal oxide and spinel ferrite. The coexistence and crystallinity of $CoFe_2O_4$ and ZnO was verified using X-ray powder diffraction (XRD). Transmission electron microscopy depicts the attachment of ZnO nanoparticles on $CoFe_2O_4$ surface. The photocatalytic removal of Rhodamine B was tested under visible light irradiation. The generation of ROS species was evidenced by electron paramagnetic resonance coupled with spin trapping technique.

Acknowledgments. This work was suppotred by a grant o fthe Ministry of Research, Innovation and Digitization, CNCS – UEFISCDI, project number PN-III-P1-1.1-TE-0836, within PNCDI III and 5/5.1/ELI-RO/17.

[1] M.N. Chong, Water Res. **2010**, 44, 2997-3027.
[2] X. Wang et al. Chem. Eng. J. **2022,** 429, 132270-1332275.
[3] A. Syed et al. Colloids Surf. A Physicochem. Eng. Asp. **2021** 629 127449-127459.

T5-P: Transition metal ions as a tool for controlling the photocatalytic activity of MWCNT-TiO_2 nanocomposites

D. Toloman, M. Stefan, O. Pana, T. D. Silipas, C. Leostean, L. Barbu, A. Popa

National Institute for Research and Development of Isotopic and Molecular Technologies, 67-103 Donat, 400293 Cluj-Napoca, Romania

Industrial effluents containing organic pollutants such as dyes are highly toxic and difficult to biodegrade. These pollutants are genotoxic and can disturb endocrine systems even at low concentrations; therefore, they are dangerous to human health [1]. Decolorisation and complete mineralization are

difficult because of the dyes' complex structure. In order to reduce the risk of pollution and allow water recycling, it is required to remedy industrial wastewater before its sewerage. Advanced Oxidation Processes (AOPs) are considered a promising technique for removing organic pollutants. Semiconductor photocatalysis, an AOP technique, has gained more recognition because of its properties like nontoxicity, chemical, biological stability, and low cost [2]. For this purpose, MWCNT decorated with undoped and Cu or Mn-doped TiO_2 nanoparticles were synthesized. PXRD patterns show the diffraction plans specific to MWCNT, anatase, and rutile phases of TiO_2. The ratio between anatase and rutile phases differs from sample to sample. Through EPR spectroscopy, the defect and the valence states of the dopant ions in the TiO_2 lattice were shown and correlated with XPS results. The morphology of the samples was analyzed by SEM and TEM. The photocatalytic activity of the samples was evaluated against RhB aqueous solution under UV irradiation. The sample containing Cu^{2+} ions has the best photocatalytic performance. The photocatalytic mechanism was explained based on the correlation of structural characteristics, optical properties, ROS species generation, and scavenger experiments. Industrial effluents containing organic pollutants such as dyes are highly toxic and difficult to biodegrade.

Acknowledgments. The authors would like to express appreciation to the Romanian Ministry of Research, Innovation and Digitization for the financial support through Projects PN 19 35 02 03 (Core Program).

[1] D. Neena, et al, Sci. Rep. **2018**, 8, 10691
[2] N. Sharotri, D. Sud, Sep. Purif. Technol. **2017**, 18, 3382–391.

T5-P: Photoactive ZnO-$ZnFe_2O_4$ heterostructures for water depollution under visible irradiation

D. Toloman, A. Petran, A. Popa, M. Stefan, D. Silipas, C. Leostean, L. Barbu, O. Pana

National Institute for Research and Development of Isotopic and Molecular Technologies, 67-103 Donat, 400293 Cluj-Napoca, Romania

Water is the source of life and an essential resource for human survival. With fast socio-economic development and increasing population worldwide, the water environment crisis has drawn widespread concern for humanity nowadays [1]. An improvement of water supply and sanitation, and better management of water resources, especially in terms of water reuse, can significantly contribute to poverty reduction and boost economic growth in low-income countries. Responding to these requirements, adopting new ecologically and environmentally friendly technologies is necessary [2]. Photocatalytic degradation has rapidly emerged as one of the most attractive advanced oxidation processes (AOP) for the destruction of organic, inorganic, and microbial pollutants due to a number of advantages it bears over other water treatment protocols. Such merits include its versatile nature in terms of the type of pollutants that can be removed and the medium in which the process is applicable [3]. The method is based on use of semiconductors as photocatalysts which, under UV or visible irradiation, may produce the degradation of most organic pollutants leading to the formation of non-toxic carbon dioxide and water, thereby eliminating the problem of sludge formation which otherwise cause secondary pollution [4]. In this scope, ZnO-$ZnFe_2O_4$ heterostructures were synthesized and used as photocatalyst

for water depollution under visible irradiation. The samples were prepared using solvothermal method. Structural, morphological, optical and magnetic properties of the prepared heterostructures were investigated. Photocatalytic activity against Rhodamine B under visible irradiation was evaluated and the photocatalytic mechanism was elucidated based on the reactive oxygen species generated by the samples and trapping experiments.

Acknowledgments. This work was suppotred by a grant o fthe Ministry of Research, Innovation and Digitization, CNCS – UEFISCDI, project number PN-III-P1-1.1-TE-0836, within PNCDI III.

[1] J. Sun, et al, J. Mater Res. Technol. **2020**, 9, 4951-4967.
[2] R. Banos, et al, Sustain. Energy Rev. **2011**, 15, 1753–1766.
[3] Y. Li, Z. Zhang, L. Pei, X. Li, T. Fan, J. Ji, M. Ye, Appl. Catal. B Environ. **2016**, 190, 1.
[4] M. Cao, P. Wang, Y. Ao, C. Wang, J. Hou, J. Qian, J. Colloid Interface Sci. **2016**, 467, 129.

T5-P: Toxicity effects of Manganese-Doped Copper Oxide Nanoparticles on malignant cells

S Gutoiu[1], O Pana[1], S Macavei[1], C Leostean[1] O Grad[1], G Blanita[1], M Suciu[1]
National Institute for Research and Development of Isotopic and Molecular Technologies, 67-103 Donat, 400293 Cluj-Napoca, Romania

In recent years, due to the intensification of research in areas such as nanomaterials with applications in theranostics, it has been possible to develop alternative therapies. These often involve the synthesis of composite materials, with specific properties and architectures that are designed to target a certain cells responsible for a specific disease. The tendency is

to combine materials from several classes (magnetic, genetic, oxides, etc.) so in the end to obtained platforms with multifunctional characteristics, such as the possibility to transport the drug to the cells, to target a certain malignant cells types and in end to release the transported drug into the cells. Achieving these objectives often required the development of new synthesis methods, which are attained in several stages, each of them partially contributing to the formation of multifunctional platforms.

This work proposes the obtaining of Manganese-Doped Copper Oxide nanoparticles (Mn-CuO-NPs) that are well known for their cytotoxicity. In part their toxicity has been attributed to the release of copper ions and manganese ions from Mn-CuO-NPs in malignant cells. Here we obtained the desired nanoparticles employing the hydrothermal method and chloride reagents as precursors. The synthesis aqueous mixture was transferred in Teflon autoclave and maintained at 180℃ after night. The black precipitate obtained was washed with water and dried in oven. The elemental composition of materials was determined by XPS measurements, the structure and microstructure was checked by XRD and TEM analyses. The qualitative and quantitative elemental analysis was performed using X-ray excited electron spectroscopy, using the XPS Spectrometer (SPECS) with the Mg anode (1253.64eV). The sample was subjected to successive corrosions with accelerated Ar ions at a voltage of 1kV and a total time of 90 minutes. The spectra were interpreted using the CasaXPS program. XPS spectra corresponding to the Mn2p line and the Cu2p line are shown in figure 1.

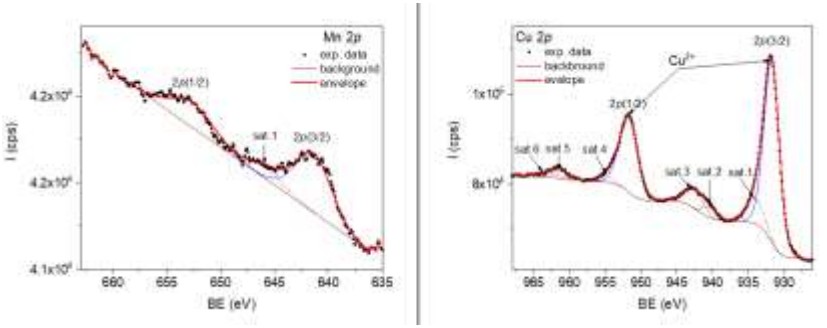

Fig 1. XPS spectra of Mn2p and Cu2p lines

The therapeutic potential of Coper Oxide and Manganese Doped Copper Oxide was proved by analyzing the cytotoxic effect was of two cancer cells lines.

Acknowledgments. This work was carried out through the Core Programme project no. PN19 35 02 03, developed with the support of the Ministry of Research, Innovation and Digitization, CNCS – UEFISCDI, project number PN-III-P2-2.1-PED-2019-3484, within PNCDI III and 5/5.1/ELI-RO/17.

T6-P: Microwave-controlled oxidation of graphite using different intercalation agents

M. Ignat[1], I. Salaoru[2], F. Iacomi[3]

[1]Faculty of Chemistry, Alexandru Ioan Cuza University of Iasi, 11 Carol I Bvd., Iasi, 700506, Romania
[2]Emerging Technologies Research Centre, De Montfort University, Hawthorn Building, The Gateway, Leicester LE1 9BH, UK
[3]Faculty of Physics, Alexandru Ioan Cuza University of Iasi, 11 Carol I Bvd., Iasi, 700506, Romania

As well known, carbon is one of the most abundant material, next to oxygen, in the environment. In the last decades, considering its sutainability, the potential of carbon based

materials has been recognized by recent findings on fullerene, carbon nanotubes and graphene [1]. Due to its excellent electronic, optical, thermal and mechanical properties, graphene cought the attention of many researchers worldwide makes the subject of numerous publications fore more than a decade [2]. Usualy, the synthesis procedure of graphene is based on the reduction of graphene oxide. Nevertheless, the basal plane of graphene is destroyed by oxidation, thus limiting its application in electronics or electronically reinforced composites [3]. Therefore, efforts were made to produce controlled oxidation that will be strong enough to break Van der Waals bonds while yet protecting graphene domains. Hence, using piranha etching solution with intercalated graphite for the controlled oxidation of graphite particles via microwave heating is one such method [4]. The result is solution processable clean, highly conductive graphene sheets with less oxygen quickly and directly (in only a couple of seconds) involving microwaves. In contrast to graphene oxide and pristine graphene sheets, these highly conductive graphene sheets contain distinctive chemical architectures. They can be dispersed without the use of surfactants or stabilizers in both aqueous and organic solvents. Because functional graphene-based materials could offer a promising alternative to other classes of materials as the active core for memory devices, we expect the prepared graphene oxide will improve the performance and make it possible to create reliable and controllable memory cells.

Acknowledgments. This work is part of IES\R3\203157 collaboration project.

[1] M. Matsumoto, Y. Saito, C. Park, et al. Nature Chem. **2015** 7, 730–736.
[2] X. Xie, Y. Zhou, K. Huang, Front. Chem. **2019** 7:355.
[3] A.K. Jehad, K. Kocabas, M. Yurddaskal, J. Mater. Sci.: Mater. Electron. **2020** 31, 7022–7034.
[4] J. Lin, Y. Huang, S. Wang, G. Chen, Ind. Eng. Chem. Res. **2017** 56 (33), 9341-9346.

T7-P: Crown ether - modified polyimides with environmental tuned light-emission ability

A.P. Chiriac, M. D. Damaceanu

"Petru Poni" Institute of Macromolecular Chemistry, Electroactive Polymers and Plasmochemistry Laboratory, Aleea Gr. Ghica Voda 41A, Iasi 700487, Romania

Polymers containing imide cycles form one of the most important classes of heterocyclic polymers with practical applications, being also known as high performance polymers. Aromatic polyimides are considered to be high performance due to some important characteristics, such as thermo-oxidative stability, excellent insulating properties, high mechanical strength, dimensional stability, low dielectric constant and resistance to chemicals, which make them useful for use in a wide field of advanced technologies, from aerospace industry and (opto)electronics to biological field [1,2]. By incorporating different functional groups in the chemical structure of polyimides, versatile materials with particular properties and high applicative potential can be obtained. Due to their fluorescence ability and good performance, polyimides have recently attracted wide interest as novel, thermally stable, and luminescent materials [3].

The peculiar properties of polyimides are the result of their rigid polymer chains, highly polar groups, and strong intermolecular interactions. The interactions induced by the intra- and inter-chain charge transfer complex (CTC) formation and electronic polarization make them attractive as photo-optical materials. Thus, the charge transfer processes in polyimides can control their absorption, fluorescence, or other photoactive properties. However, the solid state fluorescence quantum yield of fully aromatic polyimides derived from aromatic dianhydrides and diamines is generally lower than 0.01. But this can be improved through chemical alteration of polyimide structure. For instance, the introduction of polar groups or strong electron donor or electron acceptor groups in the polymer chains can tune the donor-acceptor behavior, and subsequently the CTC formation, with direct consequence on the polyimide light-emitting ability.

On the other hand, crown ethers are well known for their affinity for alkali metal ions and chemical species, being largely exploited as building blocks for molecular sensors. A smart fluorescent compound containing a crown ether moiety can be developed as optical sensor for metal ions, anions and other bio-molecules [4]. Crown ethers have high thermal stability and good organo- solubility, but are chemically unstable. Thus, they were often incorporated into a wide range of polymers [5].

Along these lines, here we report on the development of some polyimides modified with 15-crown-5 moiety in the side chain. Beside the structural identification, a detailed study with regard to their physico-chemical behavior is reported, with focus on UV-Vis absorption and fluorescence properties. We evidenced the presence in these polymers of a ground-state

intermolecular charge transfer (CT) complex between the crown ether electron donor and the acceptor diimide segment, which endowed the studied polyimides with strong variable light emission in the green to yellow spectral range, which is contingent on surroundings.

Acknowledgements. This work was supported by a grant of the Romanian Ministry of Research, Innovation and Digitization, CNCS/CCCDI– UEFISCDI, Project PN-III-P2-2.1-PED-2019-3993, contract no. 485PED/2020, within PNCDI III.

[1] D.J. Liaw, K.L. Wang, Y.C. Huang, K.R. Lee, J.Y. Lai, C.S. Ha, Prog. Polym. Sci. **2012**, 37, 907–974.
[2] P. Ma, C. Dai, H. Wang, Z. Li, H. Liu, W. Li, C. Yang, Compos. Commun. **2019**, 16, 84–93.
[3] M. Nara, R. Orita, R. Ishige, S. Ando, ACS Omega **2020**, 5(24), 14831–14841.
[4] J. Li, D. Yim, W.D. Jang, J. Yoon, Chem. Soc. Rev. **2017**, 46, 2437–2458.
[5] E.M. Maya, A.E. Lozano, J.G. Campa, J. Abajo, Macromol. Rapid Commun. **2004**, 25, 592–597.

T7-P: Composite materials based on nitrile-containing polyimide and MWCNTs for energy applications

A.P. Chiriac, I. Butnaru, M. Asandulesa, M.D. Damaceanu

"Petru Poni" Institute of Macromolecular Chemistry, Electroactive Polymers and Plasmochemistry Laboratory, 41A Grigore Ghica Voda Alley, Iasi, Romania

Composite materials have drawn the attention due to their wide range of applications in high-tech branch of modern industries such as aerospace, energy, engineering, construction, instrumentation, or medicine. Since various

limitations of traditional micrometer-scale polymer composites have been identified, tremendous research efforts were undertaken to develop new polymer nanocomposites which are able to overcome the shortcomings of the former composites [1]. One challenge of nanotechnology is represented by the success in organizing the composite constituents in a certain way as to obtain new materials or devices able to maintain their performances under various stressing factors such as very high or low temperatures, chemical agents, radiation, tensile stress, etc. [2].

Polyimides belong to high performance polymers class and are among the most suitable polymer matrix for various fillers due to their unique and appealing properties [3]. The synergistic combination of polyimides having outstanding mechanical, electrical, thermal, optical or electrochemical features with CNTs which possess attractive caracteristics like excellent mechanical, electrical, thermal and magnetic properties, chemical stability and high aspect ratio enables the design of versatile PI-CNTs nanocomposites. Thus, the homogeneous dispersion of CNTs into polyimide matrix endows the corresponding composites with overall improved physical properties compared with the pristine polymer, thereby extending their field of applications [4-8].

Herein we present several strategies approached for the homogeneous dispersion of 2 wt% MWCNTs (pristine and functionalized) into a polyimide matrix containing nitrile, ether and fluorene units. The corresponding flexible PI-MWCNTs films were characterized by mechanical tests, morphology investigations, thermal analysis and dielectric spectroscopy, and the results were compared to those registered on the

pristine polyimide film to establish the benefit of MWCNTs on the overall polyimide properties and applications.

Acknowledgements. This work was supported by a grant of the Ministry of Research, Innovation and Digitization, CNCS/CCCDI – UEFISCDI Romania, project no. PN-III-P1-1.1-TE-2021-1110, contract no. TE 83/2022, within PNCDI III.

[1] M. Ishigami, H.J. Choi, S. Aloni, S.G. Louie, M.L. Cohen, A. Zettl, Phys. Rev. Lett. **2004**, 93, 196803.
[2] P. Ma, C. Dai, H. Wang, Z. Li, H. Liu, W. Li, C. Yang, Compos. Commun. **2019**,16, 84–93.
[3] Z. Xu, Z. L. Croft, D. Guo, K. Cao, G. Liu, J Polym Sci. **2021**, 59, 943–962.
[4] M. H. D. A. Farahani, D. Hua, T.-S. Chung, Sep. Purif. Technol. **2017,** 186, 243-254.
[5] N. Zindy, C. Aumaitre, M. Mainville, H. Saneifar, P. A. Johnson, D. Bélanger, M. Leclerc, Chem. Mater. **2019**, 31, 8764−8773.
[6] Y. Jeong, J. Park, J. Lee, K. Kim, I. Park, ACS Sens. **2020**, 5, 481−489.
[7] Y.-Y. Wang, Z.-H. Zhou, C.-G. Zhou, W.-J. Sun, J.-F. Gao, K. Dai, D.-X. Yan, Z.-M. Li, ACS Appl. Mater. Interfaces **2020**, 12, 8704−8712.
[8] N. K. Han, Y. C. Choi, D. U. Park, J. H. Ryu, Y. G. Jeong, Compos. Sci. Technol. **2020**, 196, 108212.

T7-P: Influence of the nature of carbon filler on the electrical conductivity of acrylic polymer-based composites

V. Barsukov[1], I. Senyk[1], Ya. Kuryptia[1], V. Khomenko[1], O. Butenko[1], O. Chernysh[1], V. Tverdokhlib[1], Z. Zakhozhai[2], M.P. Suchea[3,4], E. Koudoumas[3]

[1]Department for Electrochemical Power Engineering and Chemistry, Kyiv National University of Technologies and Design/ Kyiv, Ukraine
[2]V.I. Vernadskii Tavria National University/ Kyiv, Ukraine
[3]Center of Materials Technology and Photonics, School of Engineering, Hellenic Mediterranean University/ Heraklion, Crete, Greece
[4]National Institute for Research and Development in Microtechnologies-IMT / Bucharest, Romania

The dependence of specific conductivity of the acrylic polymer-based composites on the content of the following carbon fillers with different morphologies: carbon black N330 (ASTM D1765-19) from Kremenchug Technical Carbon Plant, Ukraine; carbon fibers T300 from Toray Composite Materials America, Inc., USA; dry colloidal graphite preparations S-1 (DCGP S-1) from Zavalie Graphite, Ukraine; battery grade graphite GAK-1 from Zavalie Graphite, Ukraine, was investigated. Fig.1 shows a sharp influence of the filler nature and morphology on the percolation threshold, which changes from ca 6-15 to 35-50% for these fillers.

Besides, the experimental values correspond well to the calculated curves. Composites with binary fillers DCGP S-1/carbon black, carbon fibers/carbon black, GAK-1/carbon black demonstrate a sufficient synergistic effect in the range of 50-70 vol. % (Fig. 2). This range is quite beyond of the percolation threshold.

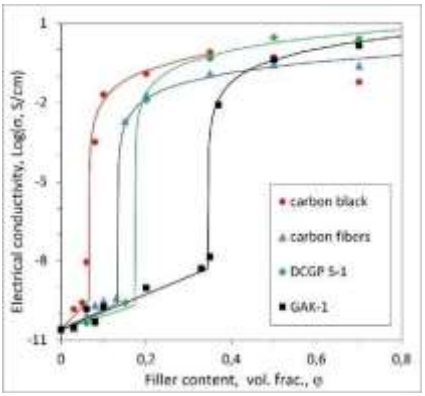

Fig.1. Dependence of specific conductivity of acrylic polymer-based composites on the content of carbon filler. Dots - experimental values. Lines - calculation according to the Equation $\sigma=\sigma 0\ (\phi-\phi c)t$ [1], where t is the critical index, σ0 is the conductivity parameter that describes the percolation curve after the percolation threshold ($\phi > \phi c$), ϕ is the volume content of the filler (vol. fr), ϕc is the volume content of the filler at the percolation threshold.

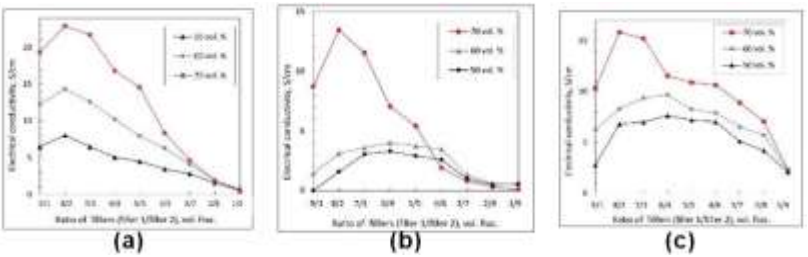

Fig 2. Dependence of electrical conductivity vs ratio of filler components for the following binary fillers: DCGP C-1/carbon black (a), GAK-1/carbon black (b), carbon fiber/carbon black (c).

An interesting feature of carbon black is that at a certain ratio of carbon components of the binary filler system is the formation of additional local chains of "cluster" arrays of nanosized carbon black particles between particles of more conductive graphite or carbon fibers (long-distance charge

transporters). This combination of fillers leads to synergy of the system - the formation of a highly branched percolation network with high electrical conductivity. The developed conductive polymer coatings can be useful for electromagnetic shielding, battery materials and some other applications.

Acknowledgments. M.P.S. contribution was partially financed by the Romanian Ministry of Research, Innovation and Digitalisation thorough „MICRO-NANO-SIS PLUS" core Programme and MicroNEx, Contract nr. 20 PFE din 30.12.2021.

[1] A. L. Efros, B. I. Shklovskii, Physica Status Solidi, **1976**, 76(2), 475.

Poster Session II (near HALL 1)

T7-P: Tailorable photophysiscal behavior of Schiff base polymers containing electron donor and acceptor segments

C.P. Constantin, M.D. Damaceanu

Electroactive Polymers and Plasmochemistry Department, Petru Poni Institute of Macromolecular Chemistry, Iasi - Romania

Schiff base polymers (polyimines or polyazomethines) serve as high-performance macromolecular frameworks for a broad arrangement of commercially-relevant features like π-conjugation, semiconducting behavior, high thermal stability, interesting optical activity, therapeutic conduct, liquid crystalline demeanor a.o. [1].
They also represent perfect substitutes for vinlyene polymers, to which they are bound by a similar opto-electronic

performance and an isoelectronic character. The complex set of characteristics that can be tailored *via* clear-cut amendment of the macromolecular architecture qualifies polyimines as ideal polymers for developing structure-property connections and as extensive functional materials [2].

The present work evaluates the effects of incorporating electron-donating and electron-withdrawing units within a Schiff base-type macromolecular construct and the envisaged fine-tuning possibilities offered by the generated electronic push-pull system. Such a medley was accessed by the polycondensation of specific monomers embedding phenoxazine (the push unit), and oxadiazole and fluorene-based segments (the pull units).

The use of distinct heterocycles enables a precise adjustment of the opto-electronic characteristics, in terms of electronic density, HOMO and LUMO energy levels, emission color and quantum yield in solution and in solid state.

Acknowledgements: This work was supported by a grant of the Ministry of Research, Innovation and Digitization, CNCS/CCCDI – UEFISCDI, project PN-III-P2-2.1- PED-2019-3993, contract no. 485PED/2020, within PNCDI III.

[1] A. Iwan, D. Sek, Prog. Polym. Sci. **2008**, 33, 289-345.
[2] C.P. Constantin, M.D. Damaceanu, J. Phys. Chem. C **2017**, 121, 6300-6313.

T7-P: Organic polymeric blends for solution-processed white organic light-emitting diodes

R. D. Rusu, C.P. Constantin

Electroactive Polymers and Plasmochemistry Department, Petru Poni Institute of Macromolecular Chemistry, Iasi - Romania

Since the first white organic light-emitting diode (WOLED) was pioneered in 1995, WOLEDs generated a tremendous upturn in technological progress and found their way from great promise to commercial certainty in the display and lighting markets [1]. The vacuum-deposited WOLEDs are in the research spotlight, with power efficiencies surpassing fluorescence tubes. The alternative, solution-processed WOLEDs is believed to be superior in terms of cost, area, and flexibility but is still considered a major challenge due to materials-related issues and new, improved, emissive products are a major target [2].

The present work is focused on identifying the proper medley of carefully-designed chemical building blocks to develop various dyes and polymeric materials capable to emit light of a certain color. We synthesized and optimized various small organic and macromolecular products embodying active elements which were used as monochrome species in combination with structural tools adding superior processing and/or charge transport.

Further on, solution-processed, hybrid polymeric materials were developed by physically mixing monochrome blue-emitting polymers with the complementary organic dyes in a single layer able to emit each individual color. By judicious adjustment of the nature and ratio of each component, white emission was unlocked, both in solution and solid state.

Acknowledgements: This work was supported by a grant of the Ministry of Research, Innovation and Digitization, CNCS/CCCDI – UEFISCDI, project PN-III-P2-2.1- PED-2019-3993, contract no. 485PED/2020, within PNCDI III.

[1] N. U. Islam et al, ECS J. Solid State Sci. Technol. **2021**, 10, 106004.
[2] B. Van der Zee et al, Adv. Mater. **2022**, 34, 2108887.

T7-P: Surface chemistry of polydopamine and its derivates

T. Radu, A. Petran

National Institute for Research and Development of Isotopic and Molecular Technologies, 67 – 103 Donat St., 400293 Cluj-Napoca, Romania Country,

One of the easiest and most versatile ways to functionalizing material surfaces is represented by polydopamine inspired by the adherent nature of catechol and amine functional groups in mussel adhesive proteins. Functionalized surfaces of different materials like metal oxides, noble metals and carbon materials by polydopamine and its derivatives exhibit a variety of interesting properties for cell culture, energy storage devices, microfluidics, artificial photosynthesis, drug delivery, encapsulation, etc. In order to better understand the electrical properties and surface chemistry of polidopanine (PDA) and its derivatives (PDL) an XPS study was conducted on three different samples: Glass@PDL, Glass@PDA and bulk polidopamine. C, O, and N XPS spectra from Glass@PDL and Glass@PDA sample surfaces were measured and compared to the bulk polymer. In the coating polymerization process PDL provides less quinonic moieties than OH groups compared to PDA based on the C=O/C-O ratio 1.8 vs 2.4 in Glass@PDL vs. Glass@PDA. Moreover, zeta potential measurements showed

that adsorption process is at least in part due to the difference in electrostatic potential between the surface (+30mV) and polydopamine (-20mV). Contact angle measurements were also conducted to determine the hydrophilicity of the sample surfaces.

T8-P: ZnO Sodium Alginate Based scaffolds for tissue regeneration

O. R. Vasile[1,2], A. Stanciulescu[2], R. D. Trusca[2], E. Vasile[2], B. S. Vasile[2]

1Academy of Romanian Scientists, Ilfov Str. No. 3, 50044 Bucharest, Romania
2National Research Center for Micro and Nanomaterials, University Politehnica of Bucharest, 060042 Bucharest, Romania

Nowadays, cells and support matrices are widely used for skin tissue regeneration. The used materials for the design of the matrices (normaly natural polymers, synthetic polymers or hybrid materials) have to have the following properties: (i) good bioactivity and biocompatibility; (ii) mechanical properties that are similar to the tissue (iii) to have supporting role, (iv) and to produce optimal circumstances for the adhesion and proliferation of the cells that are part of the regeneration process. [1]
The aim of the study is to synthetise composite materials with antibacterial properties for improving the healing process. Thus, composite fibroin-sodium alginate-hyaluronic acid matrices were obtained, starting from: sodium alginate powder (purity 99.98%, Sigma-Aldrich), hyaluronic acid (Sigma-Aldrich), silk fibroin solution concentration 50mg / mL (20mL, Sigma-Aldrich). For the antibacterial materials, we used zinc oxide covered with essential oils. The synthesis of zinc oxide

was obtained starting from zinc acetate dihydrate (purity 98%, Sigma-Aldrich), sodium hydroxide (purity 98%, Sigma-Aldrich) and absolute ethyl alcohol, using a green method of synthesis. Oregano essential oil (DoTerra), clove essential oil (DoTerra) was used as esential oil.

The choise of the natural polymers materials includes silk fibroin for superior mechanical properties, sodium alginate for swelling properties, hyaluronic acid that helps with tissue regeneration. The efficiency of the obtained materials was compared in terms of the antibacterial effect.

The obtained materials were characterized in what concerns their morpho-structure, swelling, and antibacterial properties using specific characterization methods.

SEM micrographs are revealing a uniform distribution of zinc oxide in the matrix for all concentration used (1, 3, 5% of functionalized ZnO). Fig. 1.

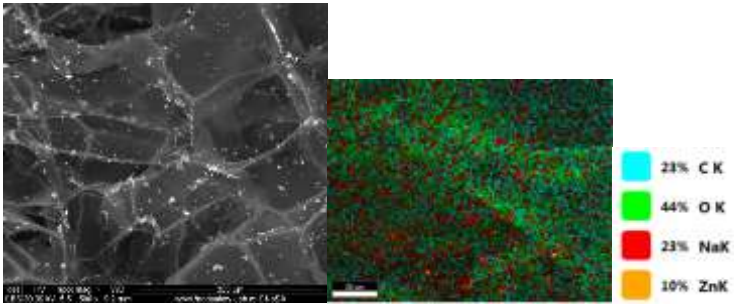

Fig. 1. a) SEM microstructure and elemental distribution of ZnO.

Antimicrobial activity was the best as the concentration of functionalized ZnO increased. The most efficiency was obtained for sodium alginate / hyaluronic acid / silk fibroin matrix with 5% ZnO functionalized with clove essential oil.

[1] Z. Li and J. Guan, “Hydrogels for cardiac tissue engineering,” Polymers (Basel)., vol. 3,

T8-P: Study the mechanism to form inclusion complex of β-cyclodextrin with quaternary ammonium compound by spectroscopic, calorimetric and molecular modeling approaches

A. Pirnau[1], M. Mic[1], C. G. Floare[1], M. Miclaus[1], I. Kacso[1], M. Palage[2], Cs. Molnar[1], B. M. Tihauan[3]

[1]Affiliation (Department, University, Company) City, Country, e-mail1National Institute for Research and Development of Isotopic and Molecular Technologies, 67- 103 Donat, Cluj-Napoca 400293 Romania
[2]Department of Pharmaceutical Chemistry "Iuliu Haţieganu" University of Medicine and Pharmacy, 41 Victor Babeş, Cluj-Napoca 400012 Romania
[3]Sanimed International Impex, 2A Bucuresti-Giurgiu, Călugăreni, Romania

Spectroscopic investigation supported by molecular modeling methods has been used to describe the inclusion complex of β-cyclodextrin (β-CD) with 1-Methyl-1-({2-[4-(trifluoromethyl)phenyl]-1,3-thiazol-4-yl}methyl) piperidinium chloride (1MPTMPC) in solution and in solid state. Solution-state complexation between the 1MPTMPC and β-CD was established using 1H NMR spectroscopy and isothermal titration calorimetry (ITC). From the 1H NMR spectroscopic studies, 1:1 complex stoichiometry was deduced with an association constant (K) of 925 M−1. The ITC technique provides the thermodynamic parameters ΔH, ΔS and ΔG which reveals driving forces involved during complex formation. The formation of the solid inclusion compound was confirmed by X-ray powder diffraction and differential scanning calorimetry. The most probable conformation of the inclusion complex obtained through a molecular docking investigation corroborates well to ROESY experiment.

Acknowledgments. Financial support from the Project PN-III-P2-2.1-PTE-2021-0303.

T8-I: Copolymers synthesized in solid phase for the formation of fluorescently-labelled pH-sensitive micelles suitable for drug delivery applications

C. M. Al-Matarneh[1], R. Ghiarasim[1], C. E. Tiron[2], A. Tiron[2], M-G. Dimofte[2].

[1]Centre of Advanced Research in Bionanoconjugates and Biopolymers, "Petru Poni" Institute of Macromolecular Chemistry, Iasi, Romania
[2] TRANSCEND Centre, Regional Institute of Oncology, Iasi, Romania

Micelles have gained significant attention in recent years as a potent drug delivery method for the treatment of malignancies. As drug delivery systems, micelles have a number of benefits, including ease of chemical structure synthesis and modification, nanoparticle size, improved drug solubility in water, prolonged circulation time, increased accumulation in tumor sites, lowered side effects, and improved drug bioavailability and efficiency [1]. Particularly, peptide-based micelles with a stimuli responsive behavior torwards pH changes are of particular interest. [2]. Histidine-based micelles are pH-responsive due to the imidazolyl group's protonation and deprotonation properties. Additionally, poly(amino acids) also have strong biodegradability, biocompatibility and an abundance of chemically changeable side groups that can be used to create functional micelles. As a result, the use of basic amino acids for medication delivery is quite diverse [3].

The primary goal of this study was to look into the possibility of designing and synthesis using solid phase peptide synthesis (SPPS) of poly(ethylene glycol)-polyhistidine-lysine sequences able to self-assemble into micelles and to evaluate the ability of the

corresponding micelles to be labeled with fluoresceine-isothiocianate (FITC), together with investigation of drug release profiles at pH levels similar to those found in a malignant extracellular environment.

The designed and assembled free and FITC-loaded micelles were physico-chemically characterized, and their cytotoxicity was tested on a human breast cancer cell line (MDA-MB-231) while the cellular areas where micelles disassembled and released FITC were assessed using immunofluorescence.

We came to the conclusion that using SPPS to create polyhistidine diblock copolymers produced sequences that exhibited behavior resembling that of the copolymeric sequences created via ring opening polymerization, whereas the benefits of SPPS may provide simple tailoring of the histidine site or the adsorption of a wide range of useful compounds.

Acknowledgment: The research leading to these results has received funding from the EEA Grants 2014-2021, under Project contract no. 37/2021.

[1] L. Xie, R. Liu, X. Chen, M. He, Y. Zhang, S. Chen, Front. Bioeng. Biotechnol. **2021**, 9, 744657.

[2] R. Augustine, D.-K. Kim, H. A. Kim, J. H. Kim, I. Kim, J nanosci nanotechnol **2020,** 20, 6959–6967.

[3] R. Ghiarasim, C.E. Tiron, A. Tiron, M.-G. Dimofte, M. Pinteala, A. Rotaru, Nanomaterials **2022**, 12, 1798.

T8-P: Investigations of high entropy alloy thin films grown by pulsed laser deposition

E. A. Laszlo[1,2,3], D. Craciun[2], G. Dorcioman[2], G. Craciun[3], V. Geanta[4], I. Voiculescu[4] D. Cristea[5], J. C. Mirza-Rosca[6], V. Craciun[1,7]

[1]*Faculty of Physics, University of Bucharest, Măgurele, Romania*
[2]*National Institute for Laser, Plasma & Radiation Physics, Măgurele, Romania*
[3]*National Institute of R&D for Microtechnologies, Voluntari, Romania*
[4]*Faculty of Material Science and Engineering, Polytechnic University of Bucharest, Bucharest, Romania*
[5]*University of Transylvania, Faculty of Materials Science and Engineering, Brașov, Romania*
[6]*Univesity of Las Palmas de Gran Canaria, Mechanical Eng. Dept., Las Palmas de Gran, Canaria, Spain*
[7]*Extreme Light Infrastructure for Nuclear Physics, Măgurele, Romania*

Solid solutions of $AlCoCrFeNi_x$ high entropy alloys (HEAs) produced by vacuum arc remelting method with molar ratio, x, ranging from 0.2 to 2.0, were used as targets to grow protective thin HEAs and high entropy nitrides (HENs, (AlCoCrFeNix)N) films with the aid of a Pulsed Laser Deposition (PLD) system. Three targets with Ni chemical molar ratio x equal to 0.4, 1.2 and 2.0, corresponding, respectively, to HEA having a body centered cubic (BCC), mixed BCC and face centered cubic (FCC), and finally FCC structure were used for thin film depositions using a KrF excimer laser. The depositions were performed in residual low vacuum (10^{-7} mbar) or under N_2 (10^{-4} mbar) at room temperature on Si, polished Ti and glass substrates. The films' structure was investigated using grazing incidence XRD, their surface morphology, thickness and elemental composition was

investigated by Scanning Electron Microscopy (SEM), EDS and X-Ray Photoelectron Spectroscopy (XPS), respectively. A homemade four-point probe (4PP) set-up was used to determine films electrical resistivity, while X-Ray Reflectometry (XRR) was used to estimate their density. Nanoindentation was employed to test films mechanical properties. The electrochemical behavior of films under simulated physiological conditions was investigated by Open Circuit Potential (OCP) and Electrochemical Impedance Spectroscopy (EIS). The solution used in experiments was a simulated body fluid. For OCP measurements the working electrodes were kept in solution for 24 hours. AC impedance data were collected at different potentials using a PAR 263 A potentiostat coupled with a PAR 5210 lock-in amplifier. The AC potential amplitude was set at 10 mV and single sine wave recordings were performed at frequencies in the range of 10^{-1} and 10^{5} Hz for all specimens.

XRD results showed that all deposited films, regardless of the initial structure of targets, were mostly FCC structured. EDS and XPS results showed that the elemental composition of films was rather close to that of the targets. Deposition under a N_2 atmosphere resulted in the inclusion of 4-10 at% nitrogen into films in a metallic nitride type compound, which may explain the higher electrical resisitivity. The OCP value measured for the deposited films increased over time implying that a passive layer is forming on the surface of the material. It was observed that all films tend to passivate in Ringer's solution, and the film deposited under nitrogen from the target having x=1.2 exhibited the highest increase. The highest repassivation potential (the potential at which the passive layer is again intact) was exhibited by the same film,

implying that it has the highest stability range of all analyzed films. Impedance measurements indicated high corrosion resistance values for 3 samples with Ni content x=1.2.

Aknowledgment. This work was supported by a grant of the Ministry of Research, Innovation and Digitization, CNCS – UEFISCDI, project number PN-III-P4-PCE-2021-1158, project number PN-III-P2-2.1-PED-2021-2659, PN-III-P2-2.1-PED-2019-4926, within PNCDI III and Nucleu programme LAPLAS VI, no. 16N/2019.

T8-P: Eptifibatide-functionalized silver nanoparticles – A new aproach in cardiovascular medicine

I. Inkielewicz-Stepniak[1], E. Megiel[2]

[1]*Department of Pharmaceutical Pathophysiology, Medical Univeristy of Gdansk Medical University of Gdansk, Poland*
[2]*Department of Chemistry, University of Warsaw, Poland*

In 2021, according to World Health Organization, 17.9 million people (30% of all global deaths) died from cardiovascular diseases [1]. Of these deaths the majority (13.7 million) were due to myocardial infarction and stroke [1,2] Thus, thromboembolic diseases are major causes of morbidity and mortality worldwide and therefore, there is the urgent need for novel, more effective therapies.
Methods: In the search for new drug delivery platforms for cardiovascular diseases and coating of medical devices, we design and synthesized eptifibatide-functionalized silver nanoparticles (AgNPs-EPI) and examined the antiaggregation effectiveness on blood platelets and antimicrobial as well as antibiofilm properties. Spherical AgNPs linked to eptifibatide were synthesized and characterized. Hemocompatiblity was

measured on endothelial cells (HUVEC), platelets and red blood cells. The antiplatelet effect of AgNPs-EPI was measured by quartz crystal microbalance with energy dissipation under flow condition. Antimicrobial and antimicrobial activity was assessed on a wide range of pathogens, including clinical strains and expressed by minimal inhibitory concentrations (MIC) and the minimum biofilm eradication concentration MBEC, respectively. Result: The synthesized NPs are spherical, narrow dispersive with an average diameter of metalcore 12.3 nm. AgNPs-EPI exibit hemocompatible properties, exert antiaggregation effect on platelets under flow condition and cause prolongation of the occlusion time in the presence of collagen/ADP and collagen/adrenaline. AgNPs-EPI had antimicrobial and antibiofilm properties against pathogens associated with catheter-related bloodstream infections.
Conclusion: AgNPs-EPI synthesized by our group have antiaggregation effect on blood platelets, antimicrobial and antibiofilm activity and a better biosafety profile than uncoated AgNPs of similar size. AgNPs-EPI exert more effective antiaggregation effect on platelets compare to EPI. Those observations are of critical importance for the future *in vivo* investigations and the potential application of AgNPs-EPI as platform for antiplatelets drug and in medical devices for human use.

Acknowledgments. This work was funded by grant HARMONIA (2017/26/M/NZ7/01030) from the Polish National Science Center.

T8-P: Investigation of graphene oxide nanoflakes as optical imaging agents inside tissue-like phantoms via multimodal confocal microscopy

M. Potara[1], S. Suarasan[1], A-M. Craciun[1], M. Focsan[1], A-M. Hada[1,2], S. Astilean[1,2]

[1]Nanobiophotonics and Laser Microspectroscopy Center, Interdisciplinary Research Institute in Bio-Nano-Sciences, Babes-Bolyai University, Cluj-Napoca, Romania
[2]Faculty of Physics, Babes-Bolyai University, Cluj-Napoca, Romania

Graphene oxide (GO) can be spectroscopically discriminated from the tissue through well-defined fingerprint Raman bands as well as intrinsic visible and near-infrared (NIR) photoluminescence (PL), which make it appropriate as contrast agent for imaging of tumor in tissues with high photostability [1]. However, the biomedical use of GO nanoflakes as contrast agents is to some extent hindered by the intrinsic low emission efficiency especially at neutral pH. The present study is focused on proving the enhancement of PL properties of GO in aqueous solution by the effect of polyvinylpyrrolidone (PVP) coating and assessing the performance of as-fabricated PVP-GO compound as reliable contrast agents in tissue-like agarose-phantoms by confocal Raman/fluorescence microscopy. The formation and stability of PVP-GO are analyzed by UV–Vis-NIR spectroscopy, Raman spectroscopy, dynamic light scattering (DLS) and zeta potential measurements. The PL emission properties of PVP-GO at pH values relevant for biomedical applications are investigated via steady-state and time-resolved fluorescence measurements. Finally, GO and PVP-GO compounds are tested for dispersibility and photostability inside tissue-like agarose-

phantoms with regard to their performance as visible and NIR contrast agents. The combination of three non-invasive microscopic techniques, here confocal Raman microscopy, Re-scan confocal fluorescence microscopy and two-photon-excited fluorescence lifetime imaging microscopy performed under visible and NIR excitation, reveals that PVP-GO exhibits a superior performance than GO as Raman/PL contrast agent inside biological phantoms at both 2D and 3D levels. Notably, PVP coating empowers GO nanoflakes not only with enhanced PL properties, but also with excellent dispersibility inside tissue-like phantoms.

Acknowledgements. This work was supported by a grant of Ministry of Research and Innovation, CNCS-UEFISCDI, project number PN-III-P4-ID-PCCF-2016-0142, within PNCDI III.

[1] K.P. Loh, Q. Bao, G. Eda, M. Chhowalla, Nat. Chem. **2010**, 2, 1015–1024.

T8-P: Study of the structural and morphological proprieties of collagen scaffold with cannabis sativa oil. Wound healing applications

O. Brincoveanu[1,2], I. C. Marinas [2,3], C. Romanitan [1], V. Tucureanu[1]

[1]National Institute for R&D in Microtechnology - IMT Bucharest, Romania
[2]Research Institute of the University of Bucharest – ICUB Bucharest, Romania
[3]Research & Development for Advanced Biotechnologies and Medical Devices, SC Sanimed International Impex SRL, Călugăreni, Romania

Wounds represent a major healthcare problem especially for chronic wounds associated with poor blood circulation, diabetes or a weak immune system. Nowadays, biomaterials with therapeutic molecules play an active role in each stage of wound healing. Collagen-based biomaterials are broadly used

to treat wounds due to its biocompatible and biodegradable properties [1]. *Cannabis sativa* extract, is known for its anti-inflammatory and analgesic effects, possesses antioxidant activity and successfully improved the biocompatibility. Thus, demonstrating the efficacy of cannabis-based therapies for treating wound-related pain, inflammation, and wound healing [2,3].

The aim of the study was to evaluate the structural and morphological properties of the collagen scaffold supplemented with *C. sativa* hydroalcoholic extract and the kinetics' release of active antioxidant compounds (phenol content, DPPH and FRAP assays) with good hemocompatibility. The scaffold was prepared by mixing *C. sativa* inflorescence extract with collagen sponge. Before homogenization, collagen was cross-linked with glutaraldehyde to ensure phenolic compounds binding in presence of phosphate buffer saline (pH= 7.4). For the cross-linked collagen, 50% ethanol was used instead of the extract. The surface proprieties of collagen and functionalized material was studied by SEM and the structural proprieties were performed by XRD and AFM. Also, the kinetics of the active principles were evaluated by Folin–Ciocalteu method and through monitoring the antioxidant activity over time. The antioxidant activity was maximum in the initial stage of release, after which it decreases as the contact time increases. The hemocompatibility has shown compliance with the requirements of ISO 10993 family of standards for medical devices. The hemolysis index was below 5% for both the crosslinked collagen and for the one functionalized with *C. sativa* extract, thus complying with the international

regulations regarding the hemocompatibility of medical devices [4].

Acknowledgments. This work is funded by the Ministry of Research Innovation and Digitalization through Program 1 - Development of the National R & D System, Subprogram 1.2 - Institutional Performance - Projects for Excellence Financing in RDI, CCCDI-UEFISCDI Grant 328/10.08.2020 (project number PN-III-P2-2.1-PED-2019-1300), within PNCDI III, and MCID Grant 14N/2019 - IMT core program MICRO-NANO-SIS PLUS, project 19160102.

[1] S. Lo, M. B. Fauzi, Pharmaceutics, **2021**13(3), 316.
[2] E. Sangiovanni, M. Fumagalli, B. Pacchetti, S. Piazza, A. Magnavacca, S. Khalilpour, G. Melzi, G. Martinelli, M. Dell'Agli, Phyther Res., **2019,** 33(8), 2083.
[3] K. Shao, C. Stewart, J.M. Grant-Kels, Clin Dermatol., **2021,** 39 (5), 784.
[4] ASTM F756–00, Standard Practice for Assessment of Hemolytic Properties of Materials.

T8-P: Laser micromarking of dental implants for improved traceability

D. Craciun[1], G. Dorcioman[1], P. Garoi[1], R. Udrea[2,3], S. A. Savencu[3], M. N. Selagea[3], D. Budei[4], J. Marza-Rosca[5], V. Craciun[1,6]

[1]National Institute for Laser, Plasma & Radiation Physics, Măgurele, Romania
[2]Faculty of Physics, University of Bucharest, Măgurele, Romania
[3]APEL LASER SRL, Bucharest, Romania
[4]DENTIX MILLENNIUM SRL, Sabareni, Giurgiu, Romania
[5]Univesity of Las Palmas de Gran Canaria, Mechanical Eng. Dept., Las Palmas de Gran Canaria, Spain
[6]Extreme Light Infrastructure for Nuclear Physics, Măgurele, Romania

The manufacturing of dental implants is one of the major fields of biomedical engineering with a history of more than 60 years. An important part of the manufacturing of these implants is their traceability. First of all, the knowledge of the producers ensures that adequate quality medical implants, manufactured from known origin raw materials will be used. Secondly, if there is discovered that a systemic problem with a batch of implants exists, then corrective measures could be immediately and efficiently taken for all patients that received those implants.

The traceability of medical implants can be obtained by marking the products with a specific alpha-numeric code or serial number. We investigated the laser marking of dental implants since it is a mature technology having many advantages: it can mark any type of material, possess a micrometer size resolution, it is clean, vacuum or clean room compatible and biocompatible. Using a Coherent PowerLine Pico system (equipped with a Coherent RapidNX laser source: fundamental center wavelength: 1064.5 ±0.5 nm, repetition rate: 50 kHz to 1 MHz, output energy: 7 μJ at 1064nm, 1 MHz) we irradiated both flat Ti disks and Ti implant samples.

We first investigated the laser system parameters (wavelength, pulse duration, focusing, fluence, gas atmosphere, repetition rate) that will make the process rapid and economically viable. Secondly, we investigated the laser marking areas characteristics to observe changes in surface morphology, structure, chemical composition, corrosion resistance, mechanical properties and biocompatibility. The laser irradiated area was investigated using scanning electron microscopy, grazing incidence X-ray diffraction, X-ray photoelectron spectroscopy, nanoindentation, Open Circuit

Potential (OCP) and Electrochemical Impedance Spectroscopy. The results are encouraging, the properties of the laser irradiated areas being similar to the original ones. Examples of the laser marking results performed at different laser fluences and repetition rates are presented in Fig. 1. It is clear that the markings are both visible and legible.

a) b) c)

Figure 1. Optical microscope images of the laser marked areas

T8-P: Electron Paramagnetic Resonance fingerprinting of yeast cells overexpressing metal-binding peptides.

A.M. Rostas[1], D. Toloman[1], I. Farcasanu[2]

[1]Physics of Nanostructured Systems, ITIM,Cluj-Napoca, Romania
[2]Organic Chemistry, Biochemistry and Catalysis, University of Bucharest, Bucharest, Romania

In this work, we aim to develop an efficient and reliable method to monitor intracellular proteins by Electron Paramagnetic Resonance (**EPR**) spectroscopy. For this purpose, a cellular model expressing Green Fluorescence Protein (GFP) tagged with an array of metal-binding oligopeptides (MeBPep) designed to trap EPR-responsive metal ions, such as Mn(II) or Cu(II) is used. This model

develops EPR spectroscopy as a toolbox for comparative profiling of cells – both standard and expressing metal-binding peptides - in the absence or the presence of heavy metals, both essential and not essential for life.

Heavy metals such as Cu, Fe, Mn, and Zn have a dualistic behavior when interacting with the living systems, both benefic and harmful, depending on their concentration. Heavy metals are essential for life in trace amounts. They act as cofactors for various enzymes or bind to and stabilize the tridimensional structure or the electronic cargo of biomolecules. However, in the opposite situation, when the concentration of heavy metals gets higher than the physiological threshold, they become toxic because they bind non-specifically to biomolecules.

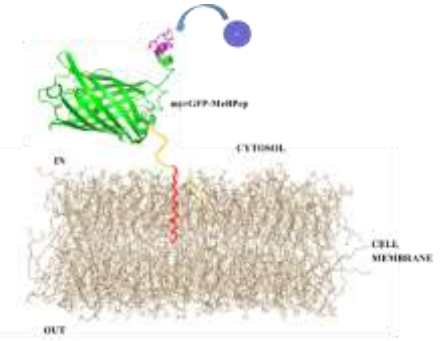

Fig. 1. Cartoon representing the binding of the myrGFP-MeBHxP to the inner face of the plasma membrane, shown here for myrGFP-D6. The elements shown in this cartoon do not represent the correct size ratios.

As a result, they interfere with other metal homeostasis or overwhelm the innate transport systems across membranes [1-3]. Moreover, the harmful effect of excess metals can result

from an increased free radical formation within the cell due to Fenton-like reactions [4].

Metal-accumulating organisms with potential biotechnology applications (bioremediation, bioextraction, biosynthesis of metallic nanoparticles, etc.) using *Saccharomycescerevisiae* cells were obtained. The budding yeast *Saccharomycescerevisiae* represents a versatile model organism used in both fundamental and applicative research due to easy growth and manipulation, non-pathogenicity, and extraordinary genetic amenability [5].

Starting from the observation that some strains expressing GFP-MeBPephyper accumulated Mn(II) or Cu(II) resulted from metal sequestration by MeBPep (Fig.1), we tested if such MeBPep could be used to trap EPR-active cations for the analysis ofMeBPep-tagged proteins by EPR.

Acknowledgments. This work was supported by a grant of the Ministry of Research, Innovation and Digitalization, CNCS – UEFISCDI, project number PN_III_P1-1.1-PD-2021-0024, within PNCDI III

[1] Z.L. He, X. E. Yang, P.J. Stoffella, J Trace Elem Med Biol. **2005**, 19, 125-140.

[2] H.S. Kim, Y.J. Kim, Y.R. Seo, J Cancer Prev. **2015**, 20, 232-240.

[3] A. T. Jan, M. Azam, K. Siddiqui, A. Ali, I. Choi, Q. M. Haq. Int J Mol Sci. **2015**, 16, 29592-29630.

[4] H. Kozlowski, P. Kolkowska, J. Watly, K. Krzywoszynska, S. Potocki, Curr. Med. Chem. **2014**, 21, 3721-3740.

[5] H. Feldmann, Yeasts in Biotechnology. Wiley-Blackwell; **2011**. p. 347-371. ISBN: 978-3-527-64486-5

T8-P: PH dependent fluorouracil release from novel composite drug based on biogenic calcium carbonate

G. Lazar [1,2], F. Nekvapil [1,2], R. Hirian [3], B. Glamuzina[4], T. Tamas [5], L. Barbu-Tudoran [6,7], S. Cinta Pinzaru [1,2]

[1] *Babes Bolyai University, Biomolecular Phys. Dept., Kogalniceanu 1, RO-400084 Cluj-Napoca,Romania;*
[2] *Institute for Research, Development and Innovation in Applied Natural Science, Fântânele 30, 400327, Cluj-Napoca, Romania.*
[3] *Babes Bolyai University, Faculty of Physics, Kogalniceanu 1, RO-400084 Cluj-Napoca, Romania;*
[4] *Department of Aquaculture, University of Dubrovnik, Ćira Carića 4, 20 000, Dubrovnik, Croatia;*
[5] *Department of Geology, Babeş-Bolyai University, 1 Kogălniceanu, 400084 Cluj-Napoca, Romania;*
[6] *Electron Microscopy Centre, Babeș-Bolyai University, Clinicilor 5-7, 400006 Cluj-Napoca, Romania;*
[7] *Advanced Research and Technology Center for Alternative Energy, National Institute for Research and De-velopment of Isotopic and Molecular Technologies, Donat 67-103, 400293 Cluj-Napoca, Romania*

The ever growing demand for cheaper and more efficient drugs, has put targeted drug delivery to the forefront of scientific research. Research efforts are being focused on the development of new, biocompatible materials from industrial byproducts, following the Blue Bioeconomy concepts. Due to its porous structure, the shell of the blue crab [1] is used as carrier for fluorouracil (5-FU), a drug widely used for the treatment of colorectal cancer. In our previous work [2] we have proven the viability of the concept by demonstrating the adsorption of 5-FU in the nanopores of the blue crab shell, followed by the slow release of the drog from the carrier,

using spectroscopic techniques, such as Raman Spectroscopy, X-Ray Diffraction or Surface Enhanced Raman Scattering (SERS).

In order to investigate the 5- FU release from the composite drug, in environmental conditions compatible with the gastro-intestinal tract, the drug realease was measured in acidic pH conditions replicating the GI tract environment. The characteristic 5-FU SERS spectral signature was used in order to build a calibration curve, spectral intensity as a function of 5-FU concentration, which was then used to quantify the released amount.

Acknowledgements: This work was supported by a grant of the Romanian Ministry of Education and Research, CCCDI - UEFISCDI, project number PN-III-P2-2.1-PED-2019-4777, within PNCDI III.

[1] F. Nekvapil, S. Cinta Pinzaru., L. Barbu–Tudoran, et al. Sci.Rep **2020**, 10, 3019.

[2] G. Lazar, F. Nekvapil, R. Hirian, B. Glamuzina, T. Tamas, L. Barbu-Tudoran, S. Cinta Pinzaru, *ACS Omega* **2021**, 6, 42, 27781–27790.

T8-P: The physics of microwaves vaporization of metallic wires

V. Craciun [1,2], D. Craciun[1], P. Garoi[1], M. Mogildea[3], G. Mogildea[3] S. I. Zgura[3]

[1]*National Institute for Laser, Plasma and Radiation Physic, Magurele, Romania*

[2]*Extreme Light Infrastructure for Nuclear Physics, ELI-NP, IFIN-HH, Magurele, Romania*

[3]*Institute for Space Science, Magurele, Romania;*

It has been experimentally found that metal oxide nanoparticles can be synthesized based on microwaves vaporization of metallic wires in air or a gaseous atmosphere. Nanoparticles characterization using advanced techniques such as grazing incidence X-ray diffraction, scanning and transmission electron microscopy and X-ray photoelectron spectroscopy showed that the nanoparticles are single crystals and stoichiometric oxides [1]. To obtain the metal wire vaporization, the output of a commercial 800 W microwave generator is coupled through an antenna to a cylindrical wave guide cavity, which acts as a focusing device for the microwaves In its nodal point, indicated by 6 in Fig. 1 below, where a high-power density is achieved, a metal wire (7 in Fig. 1) is placed, which will strongly absorb the microwaves, resulting in its rapid heating, vaporization and finally a plasma plume formation (see Fig.2).

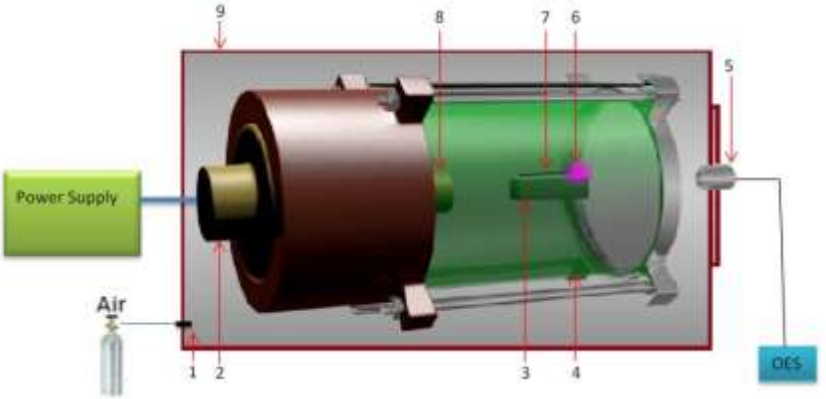

Fig. 1. Design of the microwave generator: 1 - air connector, 2- magnetron, 3 - ceramic support, 4 - TM011 waveguide cavity, 5 - the optical fiber of the spectrometer, 6 - the focal point of the waveguide, 7 - metallic wire, 8- magnetron antenna, 9- pressure chamber.

Optical emission spectroscopy investigations indicated that atoms from the wire were exited and ionized, along with atoms

from the gas. The attained high temperature can promote chemical reactions between these excited atoms and the grow of nanoparticles, which are collected near the cavity wall.

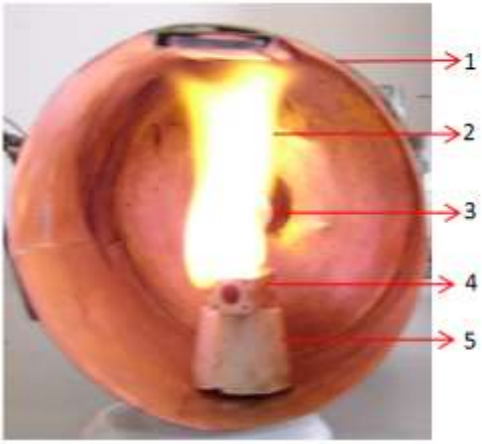

Fig. 2. Plasma generated by a Fe wire in interaction with microwaves: 1- TM waveguide, 2- plasma, 3- magnetron antenna, 4- ceramic support, 5 – plastic support.

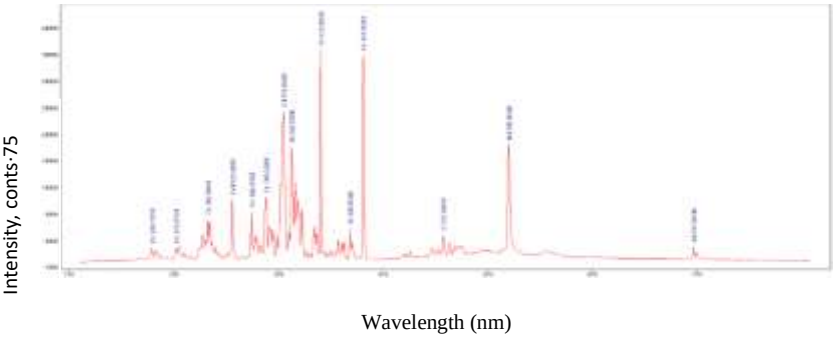

Fig.3. The optical emission spectrum of plasma generated by the Fe wire when exposed to 250 W microwaves power.

The fact that a thin metal wire can efficiently absorb microwaves is counterintuitive. The theoretical analysis of the microwaves plasma generation indicated that the physical parameters such as electric conductivity, magnetic permeability, dimension of the metallic wires and power of the microwaves play a key role in plasma initiation process.

Acknowledgments. This work was supported by a grant of the Ministry of National Education and Scientific Research by project code PN-III-P2-2.1-PED-2021-0957 and Nucleu programme LAPLAS VI, no. 16N/2019.

[1] D. Craciun, P. Garoi, M. Mogildea, G. Mogildea, S. I.Zgura, B. S. Vasile, V. Craciun, Appl. Surf. Science, **2022**, 575, 151788.

T9-P: Effect of WC-Co cermet positioning and Ni-Cr interlayer on the microstructure and mechanical response of WC-Co / AISI 304 L rotary friction joint

B. Cheniti[1], B. Belkessa[1], B. Maamache[1], N. Ouali[1], M. Hakem[1]

[1]Research Center in Industrial Technologies CRTI, P.O. Box 64, Chéraga. Algeria

Joining WC-Co cermet to steel is combining the high hardness, wear and thermal resistance of the ceramic based composite (WC-Co) to the tough and ductile steel [1]. In petroleum industry, the drill tool (drill bit) is often composed of two main parts: the steel body and the WC-Co cermet active part (bit). This later is joined to the former with brazing process using a soft Ag-Cu based alloy in order to avoid a brutal interface and insure propriety gradient at the junction between the dissimilar materials [2,3]. The interfacial reaction between WC-Co cermet and a given filler material is dependent on the

design of filler metal and the control of working temperature [4]. In the present work, interaction between Ni-Cr interlayer, deposited on WC-Co cermet surface by oxyacetylene process, and the base materials in WC-Co/Ni-Cr/AISI 304L joint using RFW process was investigated. Two welding configurations (Fig. 1) were considered i.e., WC-Co cermet was fixed in rotary side (RS) and in feeding side (FS) and that with and without Cr-Ni interlayer to evaluate their effect on the microstructure, micro-mechanical properties (hardness and Young's modulus) and bonding strength of the weld joints. Similar microstructure across the weld joints was obtained of the different welding configurations that produced similar behavior in hardness and elastic modulus (Fig. 2). A diffusion zone was formed at the weld interface as a result of the mutual inter-diffusion of both cermet (W and Co) and steel elements (Fe, Cr and Ni) that enhanced with the insertion of the interlayer when the cermet was fixed in rotary side.

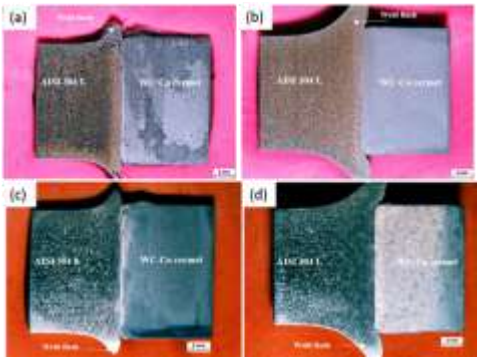

Fig. 1. Macrographic images of the as-welded friction joints: (a): WC-Co in FS WOI (b): WC-Co in RS WOI, (c): WC-Co in FS WI and (d): WC-Co in RS WI,

The introduction of the NiCr interlayer was beneficial to relax the residual stresses and improving the shear strength of the WC-Co cermet/AISI 304L steel joints, which is promising technology for drilling tools industries.

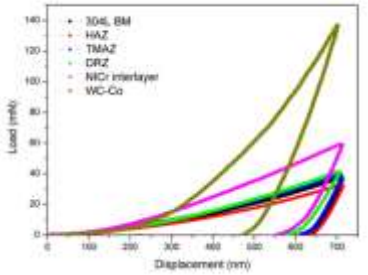

Fig. 2. L-D curves of the different regions in the WC-Co/AISI 304L steel joints

[1]. M. N. Avettand-Fenoel, T. Nagaoka, H. Fujii, R. Taillard, J. Manufact. Proces. **2018**, 31, 139.
[2]. B. Cheniti, D. Miroud, R. Badji, D. Allou, T. Csanádi, M. Fides, P. Hvizdos, Int. J. Refract. Metals Hard Mater. **2017**, 64, 210.
[3]. B. Cheniti, D. Miroud, P. Hvizdos, J. Balko, R. Sedlak, T. Csanadi, B. Belkessa, M. Fides, Mater. Chem. Phys. **2018**, 208.
[4]. H. Hao, Y. Wang, Z. Jin, and X. Wang, Journal of Materials Science **1995**, 30, 4107.

T9-P: Effect of microstructure and intermetallic precipitates on the electrochemical behavior of dissimilar AA6061-T6/ER5183/AA5086-H32 aluminum TIG-weld

M. Hakem[1], S. Mathieu[2], B. Belkessa[1], M. Djama[1], N. Ouali[1]; B. Cheniti[1]

[1]Research Center in Industrial Technologies CRTI. P.O.Box 64, Cheraga 16014, Algeria.
[2]Université de Lorraine, CNRS, Institut Jean Lamour – CNRS, F-54000 Nancy, France.

In the present work, dissimilar tungsten inert gas (TIG) welding of AA6061-T6 to AA5086-H32 has been conducted using pulsed and alternative welding current. Microstructure examination revealed that the extent of the HAZ in pulsed weld joint is narrower than the one obtained by alternative current. EDS analysis showed that, regardless the welding process, both alloys contained Fe-rich intermetallic precipitates (IMPs) in BM and HAZ. Besides, only β-phase is detected in 6061 while Al3Mg2 was found in 5086 alloy. The electrochemical behaviour of each zone of the weldments is evaluated in ASTM G69 media according to two setups where the open circuit potential is affected, a second setup is used to check the results. The results showed that the polarization curves of BM and HAZ of both alloys overlap each other and the entire curves exhibit a cathodic plateau with constant current density while the lowest resistance polarization was obtained in WM of both assemblies. AFM and SEM micrographs of the exposed surface suggest that all specimens suffer from localized corrosion and the IMPs act as nucleation sites for corrosion.

T9-P: Fabrication and optimization of tunable ZnO thin films on flexible substrates for SERS detection

A. Colnita[1], D. Marconi[1], I. Brezestean[1,2], M. Suciu[1,3], L. Barbu[1,3]

[1]Molecular and Biomolecular Physics Department, National Institute for Research and Development of Isotopic and Molecular Technologies Cluj-Napoca, Romania

[2]Babeș-Bolyai University, Faculty of Physics Cluj-Napoca, Romania

[3] Electron Microscopy Centre, Faculty of Biology and Geology, Babes-Bolyai University, 44, Republicii Str., 400015 Cluj-Napoca, Romania

Recently, the fabrication of novel surface-enhanced Raman scaterring (SERS) substrates based on micro/nanostructured semiconductor films have become popular as important analytical tools for fundamental and technological research [1]. In the case of semiconductor materials, the SERS enhancement has been demonstrated to arise from the charge transfer between the substrate and the analyte through the conduction band of the semiconductor [2]. Zinc oxide (ZnO) is an n-type semiconductor material with very promising SERS activity mainly assigned to the different crystal facets which allows different atomic arrangements and electronic structures [3,4]. In this work we focused on the optimization of the deposition process of ZnO films on flexible substrates using magnetron sputtering technique. Several experimental parameters, such as deposition time, distance substrate-target and thickness have been optimized based on scanning electron microscopy (SEM) images. We have also assesed the growth mode of the films, the roughness and overall the quality of the deposition. Several film thicknesses have been evaluated in order to find the optimal one in terms of adherence on the plastic substrate, stability and crystalite

dimension. Our final aim was to use the optimal ZnO thin films as intermediate layer in the fabrication of ZnO-Ag hybrids with application in ultrasensitive, SERS detection nanoplatforms of biomolecules.

Acknowledgement. This work was supported by a grant of the Ministry of Research, Innovation and Digitization, CNCS - UEFISCDI, project number PN-III-P1-1.1-TE-2021-0753, within PNCDI III.

[1] T.T. Doanh, N. Van Hieu, T.N.Q. Trang, V.T.H. Thu, J. Sci.: Adv. Mater. Devices **2021**, 6(3), 379-389.
[2] C. Wang, G. Qiu, W. Ye, Y. Li, R.A. Harris, C. Jiang, Anal. Chem. **2021**, 93, 3403−3410.
[3] A. Pimentel, B.J. Coelho, D. Nunes, M.J. Oliveira, M.J. Mendes, H. Aguas, R. Martins, E. Fortunato, Materials **2017**, 10, 1351 (19 pag).
[4] F. Lu, Y. Guo, Y. Wang, W. Song, B. Zhao, Spectrochim. Acta, Part A **2018,** 197, 83-87.

T9 P: Effect of ageing on microstructure and corrosion resistance of LDX 2101 Lean duplex stainless steel

B. Belkessa, N. OualiB. Cheniti, B. Maamache, M. Hakem

Research Center in Industrial Technologies, CRTI Cheraga, Algiers 16014, Algeria

In the present paper, the precipitation behavior in Lean Duplex Stainless Steel (LDX) 2101 was investigated. The precipitates were detected by XRD and confirmed to be mainly Cr2N, together with some M23C6 particles.
After solution treatment at 1050°C, the Lean duplex alloy presents a typical ferritic-austenitic duplex structure.

Isothermal ageing treatments were carried out at 720°C for the period between 10 min and 240 hours.
The precipitates at δ /γ interface preferentially nucleated and grew into the ferrite phase, when increasing isothermal ageing times.
The hardness value of austenite was higher than that of ferrite, which is caused by the solid solution strengthening.
The ferrite/austenite (δ/γ) interface migrated from the precipitate particles into δ phase, leaving the precipitates behind along the original interfaces, which could increase the size of the secondary austenite phase and decrease the hardness values of both austenite and ferrite.
During aging, a relationship between microstructure and a corrosion resistance was revealed which was associated to the formation of chromium- and molybdenum depleted zones around the precipitates.

T9-P: Hybrid SERS heterostructured substrate using ZnO@Ag films as highly sensitive platform

I.A. Brezestean[1,2], D. Marconi[1], N.E. Dina[1], M. Suciu[1,3] A. Colnita[1]

[1] Department of Molecular and Biomolecular Physics, National Institute of R&D of Isotopic and Molecular Technologies, Cluj-Napoca, Donath 67-103, 400293 Romania

[2] Department of Biomolecular Physics, Faculty of Physics, Babeș-Bolyai University, Cluj-Napoca, Kogălniceanu 1, 400084, Romania

[3] Electron Microscopy Centre, Faculty of Biology and Geology, Babes-Bolyai University, 44, Republicii Str., 400015 Cluj-Napoca, Romania

Surface-enhanced Raman spectroscopy (SERS) is one of the most versatile and powerful analytical techniques for the ultra low-level detection of complex molecules due to the coupling of Raman scattering of a molecular system with the localized

plasmon resonance of silver nanostructures. Zinc oxide (ZnO) - based nanostructures are unique materials exhibiting semiconductor and piezoelectric dual properties [1], being proven to be suitable as SERS substrates [2].
In this work, we investigated the contribution of zinc oxide (ZnO) intermediate layer in hybrid ZnO@Ag films on the SERS performance of the bilayered substrate. The topography of metallic nanostructures was assessed by using Scanning Electron Microscopy (SEM). The reliability and reproducibility of the SERS signals of relevant biomolecules were monitored by SERS measurements. This study provides a new strategy to improve the overall SERS potential of ZnO - based materials by depositing thin layers with controllable parameters.

Acknowledgements: This work was supported by a grant of the Ministry of Research, Innovation and Digitization, CNCS - UEFISCDI, project number PN-III-P1-1.1-TE-2021-0753, within PNCDI III.

[1] Z. L. Wang, J. Phys. Condens. Matter, **2004**, 16 (25) R829–R858.
[2] Y. Wang, W. Ruan, J. Zhang, B. Yang, W. Xu,B. Zhao, J.R. Lombardi, **2009,** 40, 1072-1077.

T9-P: Implementation of advanced processed in the framework of SMARTELECTRODES project

I. Linnik[1]

[1] *JVSC plant Topaz, Chisinau, Republic of Moldova*

Within the framework of SMARTELECTRODES project, JVSC “TOPAZ” carried out a number of research works on study of the physicochemical properties of the coatings synthesized in the near-surface layer of parts made of aluminum alloys, titanium alloys, heat-resistant and stainless steels.

Main goal of these works was to obtain durable coatings that allow protecting specified surface of electrodes and parts used in an equipment operating on principles of electrophysical processing methods (technologies of electrochemical processing, electrolytic-plasma polishing, micro-arc oxidation, electro-spark alloying).
The obtained results were applied in the design and production of the following equipment manufactured by JVSC "TOPAZ":
1.Electrochemical complex "ЭХК-МК", in which a principle of applying protective coatings made of durable insulating material based on composite resins on the specified surface of the electrode-tools was used. These coatings ensure that the surfaces of parts are not etched during the electrochemical processing.
2.Installation for electro-spark alloying "МЭИЛ-14М", in which the principle of applying hard-alloy coatings to specified surfaces of parts was used. Applied coatings allow increasing the wear resistance and service life of parts made of titanium and heat-resistant steels.

T9-P: Effect of Aging Temperature on the Microstructure and Local Mechanical Properties of a UNSS32750 Super Duplex Stainless Steel.

B. Maamache, B. Cheniti, B. Belkessa, N. Ouali

Research Center in Industrial Technologies CRTI, P.O. Box 64, Cheraga, Algeria

In this paper, the effect of aging temperature on the microstructure, local mechanical properties of a UNS S32750 super duplex stainless steel is investigated. A massive preferential precipitation of σ phase and Cr_2N is detected at

the periphery of ferrite with an increase in their extent as aging temperature increases. Simultaneously, the δ phase decomposition is accentuated with temperature and reaches its maximum at 850°C. This behavior results in an enhancement in hardness and Young's modulus accompanied by a higher plasticity ratio. Figure 1(a) shows the load–displacement curves of ferrite, austenite and sigma phases of the sample aged at 750°C. It can be seen in the unloading segment of the curves that the slope is steep in σ phase than that in the other phases, suggesting its higher stiffness value. In the most often cases, the hard phases demonstrates high Young's modulus [1], as for σ phase (8.8 and 250 GPa for H_{IT} and E_{IT}, respectively), whereas the lowest values are recorded in austenite with 5.9 and 230 GPa for H_{IT} and E_{IT}, respectively (see Fig. 1a).

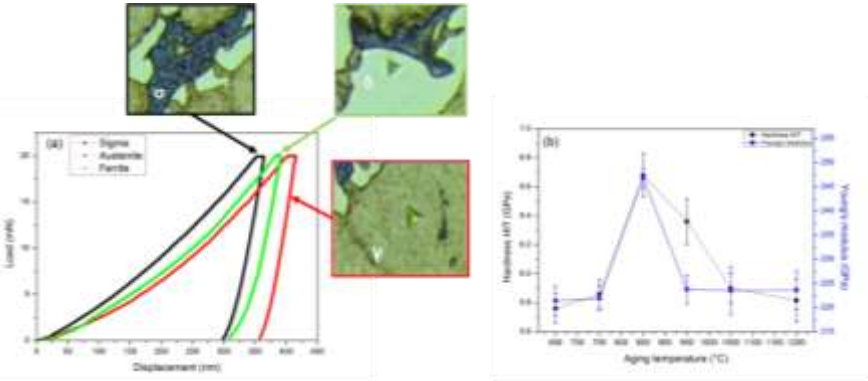

Fig. 1: Local-mechanical properties of the aged samples: (a)- load-displacement curves of different phases in the sample aged at 750°C and (b)- Hardness (HIT) and Young's modulus (EIT) values as a function of aging temperature.

These values are in coherence with those obtained by Argandona et al. [1] and significantly higher than those

presented by previous research works [2,3]. The main reason to this difference can be attributed, on the one hand, to the indentation size effect (ISE), i.e., the higher the applied load, the lower the hardness; and, on the other hand, to the surface characteristics (scratches, oxides) and the emplacement of the indentation into the microstructure (grain boundary) that may strongly influence the measurements [4]. The volume fraction of δ and σ phases changes with annealing temperatures. Knowing the hardness and elastic modulus of each phase with their respective volume fractions, the global mechanical properties (H_{IT} and E_{IT}) of the aged samples can easily be calculated as depicted in Fig. 1b.

In this study, the elastic strain to failure (H/E) so-called plasticity index, is measured to rank the aged samples according to their limit of elastic behavior to provide a close agreement in terms of wear resistance. Thereby, it is recommended to select these temperatures (750-950°C) when hardness, and high elasto-plasticity properties as well as wear resistance [5] are the most important requirement.

[1] A. Leyland and A. Matthews, Wear, **2000**, 246, 1–11
[2] G. Argandona, J.F. Palacio, C. Berlanga, V. Biezma, P.J. Rivero, Metals (Basel), **2017**, 7(6), 219.
[3] B. Yasuhiro, Trans. ISIJ, **1983**, 23, 240–246
[4] B. Cheniti, D. Miroud, R. Badji, P. Hvizdo, M. Fides, T. Csanadi, B. Belkessa, M. Tata, Mater.Sci. Eng., A, **2019**, 758, 36–46.
[6] T.L. Oberle, J. Met., 1**951**, 3, 438–439

T9-P: Obtaining and mechanical properties of Co-W coatings deposited from concentrated electrolytes

Zh. Bobanova[1], V. Petrenko[1], A. Dikusar[1]

[1]*Institute of Applied Physics, Chisinau, Moldova. MD-2028*

Recently Co-W coatings with high wear- and the corrosion resistance, deposited from gluconate electrolytes are of great interest [1]. Such electrolytes with rather low concentranion of main components-procursors containing atoms of Co and W have low operating life. Special investigation has been made to estimate the possibility to exploit electrolytes with much higher consentration of main components as well as with proportional increase in concentration of all conponents. Concentrations were increased up to 10 times.

An increase in the efficiency and durability of the used gluconate electrolytes is possible as a result of an increase in the incoming components concentration. In this case, it is preferable to increase the concentration of precursors - salts containing metals that are part of the deposited alloy. The increase concentration of every electrolyte component is less effective.

High-quality coatings from Co-W alloys were obtained at high CE = 96-98% from electrolytes with a high content of precursors 0.1 - 0.25 M at a concentration ratio of ligand and alloy-forming components (5-2): 1

The tungsten content of the coating decreases with an increase in the concentration of precursors from 0.1 M to 0.25 M at a constant ligand concentration. A similar change with ligand concentrations increases in the tungsten concentration from 20 at% to 30 at%.

Changing the concentration of the main components in the solution from 0.05 M to 0.5 M and the C_{Glu}/C_{Pre} ratio from 1:1 to 10:1 makes it possible to adjust the tungsten content from 8% to 30% and obtain coatings of various phase compositions.

X-ray structural studies have shown that alloys are formed both as polycrystalline substitutional solid solutions and thermodynamically stable Co_3W compounds, which, depending on the content of the alloying element W in the alloy, can be polycrystalline or finely crystalline.

Regardless of the method of changing the concentration of the components of the solution at a current density of 1 A/dm^2, the alloys are deposited with a high current efficiency and are characterized by a polycrystalline structure and high microhardness.

The microhardness of alloys increases with a decrease in current density and a change in the concentration of cobalt and tungsten salts in the range of 0.05 M–0.1 M and amounts to 800–750 kg/mm^2 at 1 A/dm^2.

Maximum deposition rates, tungsten content in coatings, their microhardness can be achieved using electrolytes with basic components concentration 3-5 higher then in standard ones. Correlation between pH and component concentration of gluconate electrolyte used and deposition rate, coating content, their structure, microhardness may be explained as the result of formation of high-molecular complexes in electrolyte solution under corresponding conditions that is confirmed by means of gel filtration chromatography [2].

Acknowledgements. The study has partially received funding from the EU H2020 MSCA SMARTELECTRODES project, Nº 778357.

[1]. D. P. Weston, P. H. Shipway, S. J. Harris, M. K. Cheng, Wear **2009**, 267, 934-943.
[2] A. I. Shulman, S. S. Belevskii, S. P. Yushchenko, A. L. Dikusar, Surf. Eng. Appl. Electrochem. **2014**, 50 (1), 9-17.

T9-P: Nontoxic antifouling coatings by engineered microtopography on PDMS surface for application in the marine environment

E. Manea, M. Purica, C. Parvulescu, I. Cernica, A. Dinescu

National Institute for R&D in Microtechnologies - IMT Bucharest, Romania

It is known that surfaces immersed in seawater are subject to the covering/accumulation of marine organisms (micro-organisms, algae, plants, mollusks, etc.) known as biofouling. Anti-fouling (AF) coatings have been developed to prevent surface contamination with biodeposits. Currently, one of the nontoxic AF strategies is to physically disrupt the adhesion of marine micro-organisms by using microtopographic surfaces, as used by natural marine organisms – such as shark skin, mollusk shells and which discourages the deposition of biofouling on them, [1].
Our work is focused on the design and realization of microtopographical surfaces by molding technique in silicon molds and replication in PDMS (poly(dimethylsiloxane)) substrates [2].
Engineered microtopographies to reduce the settlement of marine micro-organism are shown in Fig.1a, b, c.
As can be seen from Fig. 1, the dimensions of the elements in the microtopographies are in the range of 2-12 μm.

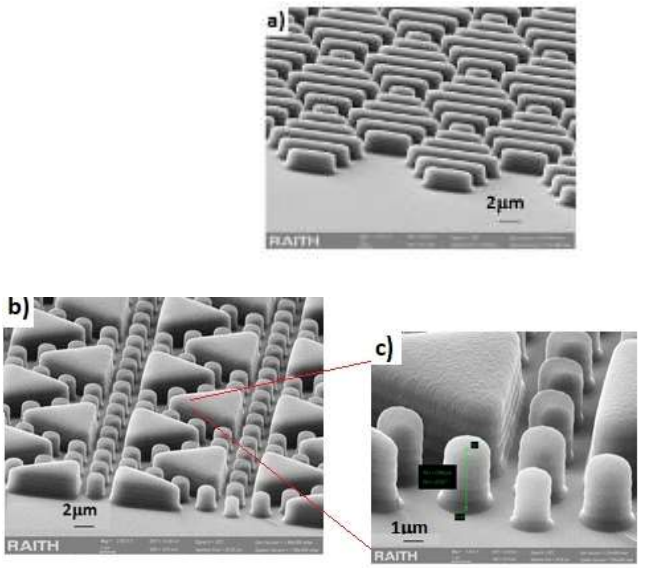

Fig. 1. The SEM images show two examples of micro-topographies made in PDMS: a) imitation of shark skin made of ribs of combined lengths of 2, 4, 8, 12 μm and separation widths of 2 μm and heights of 3 μm; b) equilateral triangles with a side of 10 μm surrounded by circular pillars with a diameter of 2 μm and a height of 3 μm; c) detail of the component elements.

Considering these dimensions, the change in surface wettability due to surface micro-texturization and according to the mechanism that adhesion strength is related to the number of attachment points, the obtained AF microtopographies are useful for reducing the settlement of marine micro-organisms with size from a few microns to a hundred (algal spores (5−10, diatoms (3−15 μm)) considered to be the major microfouling organisms.

Acknowledgments. This work was supported by IMT Bucharest Core Programme MICRO-NANO-SIS PLUS, project *PN19160302* (2019-2022).

[1] M. Pereira, C. Ankjaergaard, Advances in Marine Antifouling Coatings and Technologies; Woodshead Publishing: Cambridge, U.K. **2009,** p. 240
[2] E. Manea, C. Parvulescu, M. Purica, E. Budianu, C. Tibeica, DDF, **2016**, 369, 65-70.

T9-P: Residual stresses analysis in Lean duplex stainless steel welds using X-Ray Diffraction method

N. Ouali, B. Belkessa, B. Cheniti, K. Amara, W. Bedjaoui

Research Center in Industrial Technologies, CRTI Algiers, Algeria.

The effect of heat input on lean duplex stainless steel welded joints was studied. The weldments were subject to microstructural and mechanical characterization using optical and scanning electron microscopy. Residual stresses were measured on surface and in thickness directions by X-ray diffraction technique using $Sin^2\psi$ method.
The residual stresses were developed in the weld metal and the heat affected zone particularly for the lowest and highest heat input, which is due to a significant textured structure. No precipitation of carbides or intermetallic components was detected in the weld metals of the three specimens.
Duplex stainless steel with a microstructure comprised of nearly equal proportions of δ-ferrite and austenite γ, combine the attractive properties of ferritic and austenitic stainless steels. Owing of the high cost of nickel, the lightened range as lean duplex stainless steels (LDSSs) have been developed enabling partial or complete replacement of expensive Ni

used [1]. These are widely used in such industries as petrochemical, pharmacy, marine and many other fields. [2-3]. However, a number of undesirable phases such as carbides, nitrides and intermetallic compounds may appear in δ ferrite areas and δ/γ interfaces if the manufacturing processes are not carefully respected and residual stresses are too induced [4].

The present work is an attempt to study this material experimentally in welding process conditions to evaluate the heat input effect on residual stresses magnitude.

The base metal used in this work was a lean duplex stainless steel, LDX 2101(UNS S32101). The material was received in a plate form of 6.5 mm thickness and dimensions of 80x60mm^2. A multipass gas tungsten arc welding process (GTAW) was employed to join the specimens (Fig.1), using a duplex filler metal (ER2209).

In order to observe the microstructural evolution that occurs during welding, metallographic sections transverse to the welding direction were prepared and etched with Beraha reagent (0.7 g K2S2O5, 20 ml HCL, and 80 ml H2O). The ferrite volume fraction was estimated using a Fischer ferrite meter (MP30E).

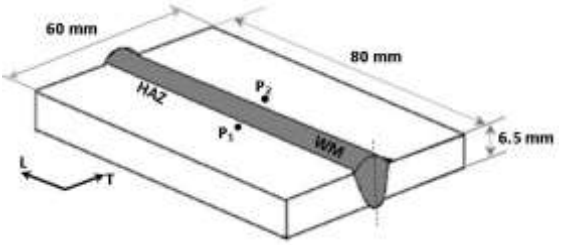

Fig. 1 Weld design with residual stresses measurement location

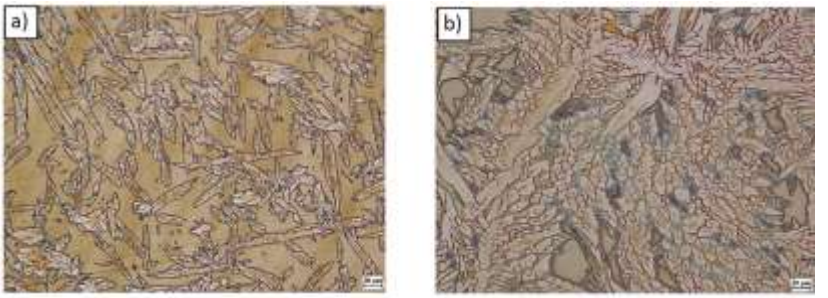

Fig. 2 Optical micrographs showing the microstructure of the weld region: a) low heat input, b) high heat input

Microstructural analysis of the LDX 2101 fusion zone as shown in Figure 2. revealed that the weld region contained more austenite than the parent material. The solidification mode is fully ferritic as the Creq/Nieq ratio is greater than 1.95 [5-6], the microstructure is characteristic for the welded duplex SSs which consist of δ-ferrite phase and reformed austenite phase.

The residual stresses were measured by XRD, using a four-circle XRD 3003 PTS Seifert goniometer with Cr-Kα radiation as X-ray source, whith wavelength k = 2.289 Å. The diffraction angle 2θ ranges from 149° to 161°. The measurements were made on the {211} atomic plane. The residual stress analysis was carried out on the basis of the sin2ψ method, which is employed for polycrystalline materials and several types of Welding process.

The longitudinal and transverse residual stresses (RSs) on the weld surface for the samples locations were all compressive. In the same time, they are higher in the longitudinal direction than in the transverse one [7].

This result is explained by the restrained and unrestrained cooling phenomena that take different directions along and perpendicular to the weld seam respectively.

Due to its effect on the weld thermal cycle, the heat input has been shown to have a significant influence on the phase balance of the welded lean duplex stainless steel, where the austenite content increases with heat input increases.

The welding heat input and has great effect on residual stresses, the weld superficial residual stresses measured by mean of sin2ψ method shows a compressive character, while they decrease as the heat input increases. In the machined welds, the residual stresses were compressive for lowest and highest heat input just near the heat affected zone and in the weld zone, due to a significant textured structure.

[1] D. J. K. John C. Lippold, Welding Metallurgy and Weldability Of Stainless Steels, Willey, **2005.**

[2] R. Gunn, Duplex Stainless Steels: Microstructure, Properties and Applications," Abingt. Publ., **1997**, p. 219.

[3] Z. Brytan, J. Niagaj, J. Sci., **2013**, 40 (5), 923–937.

[4] J. Pilhagen, R. Sandstrom, Mater. Sci. Eng. A, **2014**, 602, 49–57.

[5] S. Kumar, A. S. Shahi, Mater. Des., **2011**, 32 (6), 3617–3623.

[6] E. M. Westin, PhD thesis, Royal Inst. **2008**.

[7] N. Syahida, M. Nasir, M. Khairul, A. Abdul, S. Mamat, M. Iqbal, J. Eng. Appl. Sci., **2016**, 11 (9) 6166–6175.

T10-P: Hydrophilic oxidized carbon nanohorns/PVP/KCl nanohybrid for chemiresistive humidity sensor

B-C. Serban[1], O. Buiu[1], N. Dumbravescu[1], V. Avramescu[1], M. Brezeanu[2], C. Pachiu[1], M-R. Marinescu[1], M. Bumbac[3], C. Nicolescu[3]

[1]National Institute for Research and Development in Microtechnologies (IMT Bucharest), Voluntari, Romania

[2]Faculty of Electronics, Telecommunications and IT, University Politehnica of Bucharest

[3]Faculty of Sciences and Arts, Valahia University of Targoviste, Targoviste, Romania

In recent years, oxidized carbon nanohorns (CNHox) and their nanocomposites with different polymers and semiconducting metal oxides were employed as sensing layers in the design of several chemiresistive relative humidity sensing structures [1, 2]. This paper reports on a resistive sensor's RH sensing response, employing a ternary nanohybrid composite as sensing layers, comprising CNHox, PVP (Polyvinylpyrrolidone), and KCl; these were prepared at different w/w/w ratios (7:2:1, 6.5:2:1,5 and 6:2:2), and named K1, K2, and K3 respectively. The sensing structure includes a silicon substrate, a SiO_2 layer, and interdigital transducer (IDT)-like electrodes. The sensing film was deposited via the drop-casting method on the sensing structure. The sensing layers' morphology and composition were investigated through Scanning Electron Microscopy (SEM) and RAMAN spectroscopy. The RH capability of the manufactured sensors was investigated by applying a constant current between two IDH electrodes and measuring the voltage at different values of RH. Measurements performed showed that the resistance for one of the sensors

(K1) has a linear behavior with the variation of the RH (see Fig. 1), except for the first cycle (RH= 0 up 100 down 0). The response to the RH variations in time was determined using a commercially available state-of-the-art capacitive sensor as a reference (see data plotted in Fig. 2). Two types of sensing mechanisms responsible for the measured RH sensing behavior were identified, which can be discussed in terms of the Hard and Soft Acids and Bases (HSAB) theory.

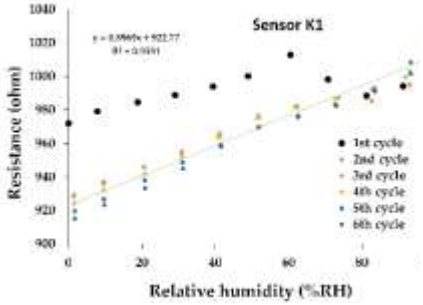

Fig. 1. RH response of chemirestive sensor K1 employing CNHox/PVP/KCl (7:2:1 w:w:w ratio) as sensing layer.

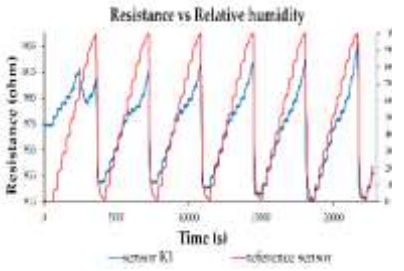

Fig. 2. Functional response, in time, of the K1 sensor (six complete cycles of RH variation).

Acknowledgments.The authors affiliated with IMT Bucharest and Valahia University of Targiviste would like to acknowledge the financial support through contract no 364PED-23/10/2020 (UEFISCDI project code PN-III-P2-2.1-PED-2019-5248 – "CASTOL").

[1] B.C. Serban et al., Coating, **2021**, 11(5), 530.
[2] B.C. Serban et al., Materials, **2022**, 14 (11), 2705.

T10-P: Testing the sensing potential of Ag/TiO_2/rGO nanocomposites by SERS

G. C. Olar[1], L. C. Cotet[2,3], C. I. Fort[2,3], C. Salagean[1,3], L. Baia[1,3], M. Baia[1,3]

[1]Faculty of Physics, Babes-Bolyai University, M. Kogalniceanu 1, 400084, Cluj-Napoca, Romania.
[2]Faculty of Chemistry and Chemical Engineering, Babes-Bolyai University, Arany Janos Str., 400447, Cluj-Napoca, Romania.
[3]Institute for Research-Development-Innovation in Applied Natural Sciences, Babes-Bolyai University, Fântânele Str. 30, 400294 Cluj-Napoca, Romania

The rapid development of science and technology together with the growth of urbanization and industrialization have led to the emergence of very serious environmental problems. Due to this fact, the chemical decontamination by semiconductor photocatalysis has become a hot field of research in recent years. The well-known material with high photocatalytic activity, which is also low cost, stable and non-toxic is TiO_2 that can degrade organic pollutants from water into non-toxic molecules. Separation and recombination of photogenerated electron-hole pairs play an important role in photocatalytic performance. To diminish the recombination of electron-hole pairs, the contact of TiO_2 nanoparticles with those of noble metals, such as Pt, Au, or Ag, was involved [1]. Moreover, rGO was also used to obtain multiple-component composites with improved photocatalytic performances [1,2]. On the other hand, metal nanoparticles such as Ag generate the localized surface plasmon resonance and contribute to the enhancement of the Raman signal of the molecular species adsorbed on their surface by SERS. Thus, in order to extend the applicability spectrum of photocatalysts, in the present

work, nanocomposites based on Ag, TiO_2 and rGO were prepared by hydrothermal method [3] by using different Ag concentrations. The samples' morphology was evaluated by SEM and their SERS activity was investigated by using rhodamine 6G as test molecule (Fig. 1). The obtained results indicate that the as prepared nanocomposites can be promising multifunctional materials exhibiting both photocatalytic and detection capabilities and could be used for sensor development.

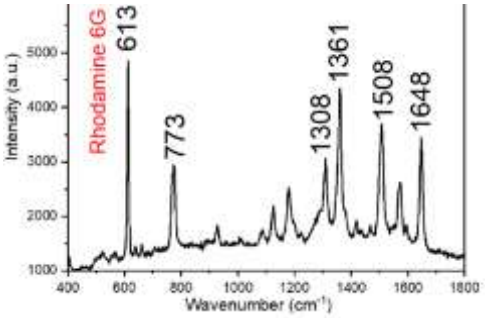

Fig. 1. SERS spectrum of Rhodamine R6G adsorbed on Ag/TiO_2/rGO hydrothermal nanocomposites

[1] Y. Liu, Y. Zhou, L. Yang , Y. Wang , Y. Wu , C. Li,J. Lu. J. Nanopart. Res. **2016**,18, 283.

[2] T. Wang, T. Tang, Y. Gao, Q. Chen, Z. Zhang, H. Bian, Physica E Low Dimens. Syst. Nanostruct. **2019**,112,128-136.

[3] J. Li, Q. Wu, J. Wu, M. Handbook of Nanoparticles. Aliofkhazraei, M. (eds), Springer, **2015**, p.1-28.

T10-P: Optimal geometrical conceptualization of IDEs for biosensors development based on multiphysics modeling and simulation

I. Turcan, T. A. Filip, M. A. Olariu

Department of Electrical Measurements and Materials, Faculty of Electrical Engineering, Technical University of Iasi, Iasi, Romania

Interdigitated electrodes (IDEs) based sensor in comb-like electrodes structure are attractive candidates for dielectrophoretic (DEP) trapping of particles and biological entities such as cells and bacteria within biosensing devices, owing to its simple structural design [1-3]. The sensitivity of IDEs can be improved based on geometric parameters of the electrode array [3]. Hence, the purpose of this study is to design and characterize the dielectrophoretic (DEP) microelectrodes with various array structure arrangements in order to produce optimum non-uniform electric field for particle capture. Finite element analysis software, COMSOL Multiphysics was used to study the effect of the electrodes geometry (fingers shape, gap sizes and width of fingers) on the induced electric field. Simulations indicated that IDEs with non-linear fingers (castellated, saw-teeth like and semi-circled) can generate higher electric field, i.e. larger DEP forces in comparison to interdigitated linear electrodes at the same operating voltage.

Acknowledgement: The study is funded from the research project of the Academy of Romanian Scientists "Evaluating the dielectrophoretic electromanipulation and electrical characterization capacity of biological targets with the help of all-in screen-printed interdigitated microelectrodes".

[1] H. Zhu, X. Lin, Y. Su, H. Dong, J. Wu, Biosens. Bioelectron. **2015**, 63, 371–378.
[2] A. F. M. Mansor, S. N. Ibrahim, IEEE Int. Conf. Semicond. Electron. Proceedings, ICSE **2016**, 169–172.
[3] L. Q. Jun, G. W. Bin Djaswadi, H. F. Bin Hawari, M. A. B Zakariya, Int. Conf. Intell. Adv. Syst. ICIAS **2018**, 1–6.

T10-P: Protein adsorbent based on kaolinite thin films

L. N. Dumitrescu[1], F. Andrei[3], E-R Ionita[2], R. Birjega[1], A. Lazea-Stoyanova[2], M-D Ionita[2], A-M. Banici[1], S. Brajnicov[1], A. Matei[1], G. Epurescu[1]

[1]Lasers Department, National Institute for Lasers, Plasma and Radiation Physics, 409 Atomistilor Street, 077125 Magurele, Romania
[2]Sources for Plasma and Applications Group, Low Temperature Plasma Laboratory, National Institute for Lasers, Plasma and Radiation Physics, 409 Atomistilor Street, 077125 Magurele, Romania
[3]Innovation Center in Photonics and Plasma for Advanced Materials and Technologies FOTOPLASMAT, National Institute for Lasers, Plasma and Radiation Physics, 409 Atomistilor Street, 077125 Magurele, Romania

Sensitive detection of allergens in a large variety of food matrices has become increasingly important considering the emergence of functional foods and new food manufacturing technologies. The significant allergens from egg white—ovalbumin (54% of egg white proteins) and ovomucoid (11%) have many potential applications in food processing or as nutraceutical and pharmaceutical agents. Although good manufacturing practices are implemented in the industry and labeling rules impose precise specifications of eggs or egg proteins present in the composition of food products, the potential for accidental contamination remains (e.g., by inadequate cleaning of production lines). Appropriate

analytical control of egg proteins is crucial to ensure the safety and quality of products. Highly oriented crystalline lamellar Kaolinite films were successfully prepared by laser techniques and used as a coating for the working electrode in electrochemical sensors. Thin films of lamellar cationic clays as kaolinite were obtained by laser methods (matrix-assisted pulsed laser evaporation (MAPLE), pulsed laser deposition (PLD)). Investigation of the adsorption process of allergen proteins on the deposited films by means of structure and morphology of the obtained kaolinite lamellar coatings were investigated morphologically using the Atomic Force Microscopy (AFM) and Scanning Electron Microscopy (SEM) methods, for structural characterization using the X-ray diffraction (XRD) and for the chemical surface properties by X-ray Photoelectron Spectroscopy (XPS) techniques. We achieved super hydrophilic lamellar coatings that can be produced using these two deposition methods. Kaolinite-modified electrodes were loaded with proteins and detected by voltammetry. Our results showed that a textured kaolinite thin film could be used as active surfaces in electrochemical sensing.

T12-P: Directed Self-Assembly of Polystyrene Nanosphere Lithography Masks Using Additively Printed Templates

A. Wolff[1], Y. Bauckhage[2], A. Heinrich[2], J.K.N. Lindner[1]

[1]Paderborn University, Department of Physics, Warburger Straße 100, 33098 Paderborn, Germany
[2]Zentrum für Optische Technologien – Hochschule Aalen, Anton-Huber-Straße 21, 73430 Aalen, Germany

Regular arrays of almost arbitrarily designed nanoobjects can be fabricated on large substrate areas using nanosphere lithography (NSL) [1]. For this, a self-assembled mono- or doublelayer of hexagonally ordered nanospheres is used as a shadow mask after tuning the size and shape of triangular mask openings by either a thermal or plasma or ion beam treatment. By depositing or eroding material at the substrate surface with a directed beam of atoms or ions while tilting and rotating the mask covered substrate, positive or negative objects can be fabricated at the surface at each mask opening in a highly parallelized way [2]. While NSL is a fast and versatile low-cost nanopatterning approach, the two major drawbacks are the limited perfection or 2D order of NSL masks (originating from the statistical nature of the self-assembly process) and the lack of control of the position and directional orientation of the masks on a planar surface. These drawbacks may be overcome using template assisted patterning approaches. However, while previous work has demonstrated that spheres can be selectively deposited and reproducibly arranged in trench- or box-shaped surface troughs of commensurable size (e.g. [3,4]), little is known if raised surface structures can be used to control the arrangement and order of nanospheres on surfaces.

In this investigation, a 6D-processing platform is used to fabricate different polymer line structures on glass substrates based on a microprojection stereolithography double patterning approach [5]. The patterns have either the shape of letter “W” or consist of arrays of open parallel or zigzag lines and are between 0.25 and 1.2 µm tall. A convective self-assembly technique employing a doctor blade is used to spread a suspension of 2 µm diameter polystyrene beads in water on the prepatterned surfaces and initiate the self-assembly process. Sphere arrangement and order are studied by light microscopy combined with numerical image analysis tools.

An improved order of spheres aligned with the edges of deposited polymer prepatterns can be observed on the lee side of open lines as exemplarily shown in Fig. 1, but a long-range effect on the order of spheres in a mask is not yet achieved.

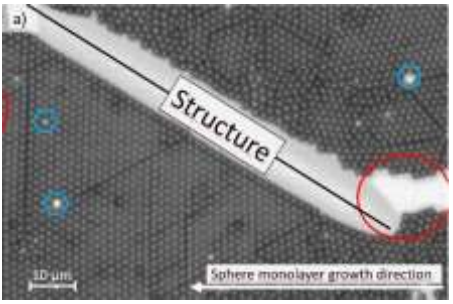

Fig. 1. Light microscopy image of spheres arranged next to a printed line structure.

[1] C. L. Haynes, R. P. Van Duyne, J. Phys.l Chem. B **2001**, 105, 5599.

[2] C. Brodehl, S. Greulich-Weber, J. K. N. Lindner, Mater. Today: Proc. **2017,** 4, S44.

[3] G. A. Ozin and S. M. Yang, Adv. Funct. Mater. **2001**,11, 95.

[4] K. Brassat, F. Assion, U. Hilleringmann, J.K.N. Lindner, phys. stat. sol. A **2013**, 210, 1485, and references within.

[5] Y. Bauckhage and A. Heinrich, Proc. SPIE 11294, **2020**, https://doi.org/10.1117/12.2545711.

T12-P: Low-keV Ion Beam Modification of Polystyrene Nanosphere Lithography Masks

J.S.C. Weiss[1], P. Hodges[1], J.K.N. Lindner[1]

[1]*Department of Physics, Paderborn University, 33098 Paderborn, Germany*

Nanosphere Lithography (NSL) [1] is a well-established low-cost technique to create regular patterns of tailor-made nanoparticles on large-area surfaces. It uses self-assembled, hexagonally close-packed mono- or doublelayers of colloidal nanospheres as a shadow mask on a substrate to create nanoobjects by either depositing or eroding material at the open interstices between triples of neighboring spheres. By tilting and rotating the substrate during material deposition it is possible to write objects with an atom beam, where the periodicity of objects is given by the nanosphere diameter, the shape is determined by the tilting and azimuthal deposition angles and the size and width of objects is determined by the distance of the mask opening and its width [2]. Therefore, it is important to control the size and shape of mask openings in NSL masks.

This can be achieved by either thermal or plasma or ion beam treatment of NSL masks. The effects of ion beams on NSL masks have been previously studied using ion masses from that of He to Au and energies from few ten keV to several MeV

[3]. It has been found that a beam parameter dependent interplay of mechanisms such as ion beam hammering sphere deformation, charging induced sphere displacement, sputter erosion and ion beam induced sintering of spheres [4] is active, the latter driven by the minimization of capillary surface forces among nanospheres which are getting viscous at the surface under irradiation.

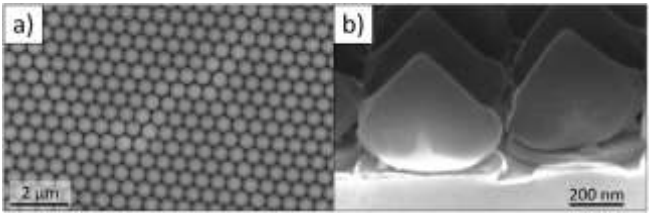

Fig. 1. SEM plane view (a) and cross-sectional image (b) of a NSL mask prior to (a) and after ion irradiation (b).

In this presentation we investigate for the first time the modification of self-organized NSL masks made from polystyrene (PS) spheres at particle energies as low as 1 keV, where the penetration depth of ions of only few nanometers is small compared to the diameter of spheres (600 nm). Both, $^{14}N^{+}$ and $^{40}Ar^{+}$ ions from a Kaufman ion source are used in a fluence range of 1-50 x 10^{16} cm^{-2}, both at normal and tilted angles of incidence. The shape modification of NSL masks is studied by field-emission scanning electron microscopy (SEM) in plane and cross-section view. The spheres deform into pyramidal dome structures at the irradiation pole and shrink both horizontally and vertically at the bottom side (Fig. 1). It is demonstrated that in addition to sputter erosion and ion beam induced sintering, the formation of ripples and the redeposition of material sputtered off the spheres play a

significant role in the controlled shape modification of masks. Monte-Carlo simulations are performed to support the interpretation of results.

[1] C. L. Haynes, R. P. Van Duyne, J. Phys. Chem. B **2001**, 105, 5599.
[2] C. Brodehl, S. Greulich-Weber, J. K. N. Lindner, Mater. Today: Proc. **2017,** 4, S44.
[3] V. Lotito, T. Zambelli, Adv. Col. Interf. Sci. **2022**, 304, 102642.
[4] J.K.N. Lindner, D. Kraus, B. Stritzker, Nucl. Instr. Meth. B **2007**, 257, 455.

T12-P: Arragement and alignment of lamellar block copolymer nanodomains in metallic antidot films

D. Kool[1,2], H. Venugopal[1,2], J.K.N. Lindner[1,2]

[1]Nanostructuring, Nanoanalysis and Photonic Materials Group, Dept. of Physics, Paderborn University, Paderborn, Germany
[2]Center for Optoelectronic and Photonics Paderborn CeOPP, Paderborn, Germany

Block copolymer lithography was intensively studied in the last two decades and has become an economically viable and competitive alternative to electron beam lithography or deep UV lithography for producing periodic nanopatterns on large areas [1]. Block copolymers consist of two immiscible polymer species which are covalently bonded, here poly(styrene) (PS) and poly(methyl methacrylate) (PMMA). By using certain polymer chain lengths and block length ratios of the two species in the BCP, different nanostructures can be created exploiting the self-assembly (SA) during nanophase separation, e.g. cylindrical, lamellar, gyroidal or spherical nanopatterns with feature sizes in the sub-10 nm range [2].

Here we exploit the SA of a lamella forming BCP with a block length ratio of 50:50, which results in repetitive PS and PMMA nanodomains of 11 nm width and spacing.

To guide the lateral alignment of lamellar nanodomains a metallic antidot prepattern is used, similar to a previous study [3] with cylindrical nanodomains. The antidot pattern is created by convective SA of PS nanospheres from a colloidal suspension on a SiO_2/Si substrate, leading to a hexagonally close-packed monolayer of nanospheres. Spheres are shrunk by reactive ion etching (RIE) and subsequently used as a shadow mask during vapor deposition of a thin gold film. After mask removal the antidot pattern is obtained, i.e. a gold thin film on SiO_2 with circular holes in hexagonal arrangement. This is used as substrate for the SA of lamella forming PS-*b*-PMMA BCP.

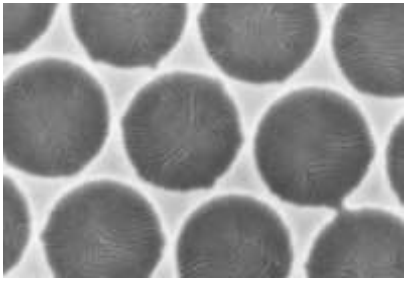

Fig. 1. SEM image of nanophase separated (PS-*b*-PMMA) BCP in gold antidots created by nanosphere lithography.

We demonstrate that by using this hierarchical SA technique of NSL and BCP lithography the alignment of BCP domains can be controlled (Fig. 1). This is achieved by tuning the dimensions of the antidot prepattern and adjusting the polymer film thickness inside the antidots. Furthermore, we

show that not only the total film thickness or film thickness difference of the resulting BCP film influences the lateral alignment and vertical orientation of the nanophase separated BCP nanodomains but also the film thickness gradient. By adjusting the geometry of the antidot pattern and the amount of deposited BCP one can adjust the shape of the BCP/air interface. This interface determines the film thickness gradient which strongly guides the lateral alignment of the lamellar BCP domain orientation.

[1] R. Ruiz et al., Science **2008**, 321, 936.
[2] T. Seshimo et al., Sci. Rep. **2016**, 6, 19481.
[3] K. Brassat et al., Nanoscale **2018**,10, 10005.

T12-P: Modification of self-organized nanosphere lithography masks using the Stoeber process

C. Zietlow[1], C.L. Wessel[1], J.K.N. Lindner[1]

[1]*Paderborn University, Department of Physics, 33098 Paderborn, Germany*

Nanosphere lithography (NSL) provides an easy and cost-efficient method to pattern large surfaces on the nanoscale by utilizing self-organizing properties of the spheres [1]. It allows producing billions of similar particles per square centimeter in a single processing step. However, due to the limited geometry of the openings between three neighboring spheres only triangle-shaped particles of a given size (depending on the sphere diameter) can be produced unless the mask openings are modified.
With a prior silica coating of the sphere mask and the application of the well-known Stoeber process [2], the openings can be shrunk in size by growing material radially on

top of the nanospheres [3]. These semi-closed mask openings can be used as pencils for drawing well-suited particles of different shapes and sizes, simply by tilting a sample with this modified NSL mask around two rotational axes during a PVD process [4] (Fig. 2a).

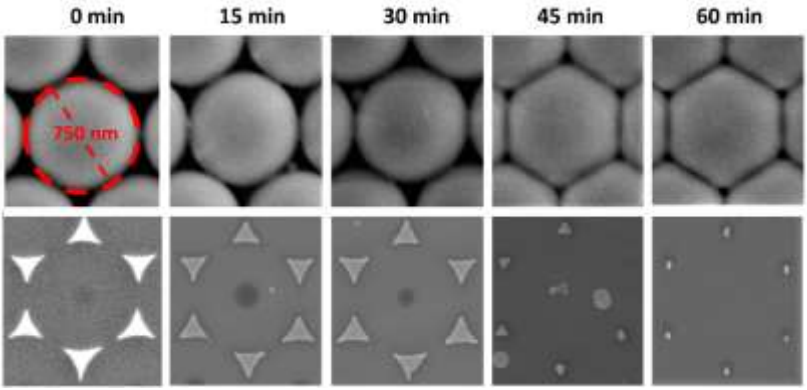

Fig. 1. Time series of the mask modification via the Stoeber process. The upper row shows the closing of the polystyrene nanosphere mask in the course of time. The used nanospheres have a diameter of 750 nm. The lower line shows the orthogonal projection of 20 nm Au on 5 nm Ti through the respective mask via electron beam vapor deposition.

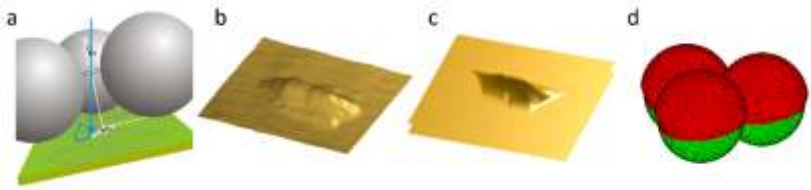

Fig. 2. a) Schematic of the double angle resolved nanosphere lithography [4]. b) AFM image and corresponding c) simulation of an exemplary particle. d) Nanomask (green) with additional material (red) clogging it during the electron beam evaporation.

In this contribution, the authors focus on the process itself from the creation of the nano mask to the final particle and show the applicability and the limits of the process by means of resulting particle size distributions (PSD). Both, the mask modification and the particle formation are accompanied by corresponding ray-trancing simulations (Fig. 2b-c), which also take into account the inherent clogging of the nanomask during the lithography process (see Fig 2d).

[1] C. L. Haynes and R. P. Van Duyne, J. Phys. Chem. B **2001**, 105 (24), 5599–5611.
[2] W. Stöber, A. Fink and E. Bohn, J. Colloid Interface Sci. **1986**, 26, 62-69.
[3] D. L. J. Vossen, J. J. Penninkhof, A. van Blaaderen, Langmuir **2008**, 24, 5967-5969.
[4] C. Brodehl, S. Greulich-Weber, J. K. N. Lindner, Mater. Today: Proc. **2017,** 4, S44.

T13-O: Potentialities of Oblique Angle Deposition (OAD) for linear and circular polarization

E. Panchout[1], C. Marsal[1], F. Paumier[1], T. Girardeau[1], B. Giroire[1], C. Dupeyrat[2]

[1]Insitut Pprime (SP2MI, University of Poitiers, CNRS) Poitiers, France
[2]Safran Electronics&Defense (Safran) 26 avenue des hauts de la chaume, Saint-Benoît, France

The growing interest in real-time augmented imaging (hyperspectral or polarimetric) has recently led to the development of DoFP (Division of Focal Plane) polarimeters with several polarimetric filters placed directly on top of the photometric sensor. Metallic wire-grids are generally used because of their small thickness to polarize the incident light

for polarimetric imaging, and are deposited directly on the sensors [1], usually in a matrix of four pixels, in order to capture several polarization directions. Unfortunately, wire-grid polarizers suffer from a poor extinction coefficient and low transmitted flux compared to thicker polarizers. The use of a new type of polarizer, known as a Polarimetric Filter by Reflection (PFR), can in theory remove a technological lock and achieve a very high extinction coefficient and close to no flux loss. PFR can be realized by OAD (Oblique Angle Deposition), which enables the fabrication of porous and anisotropic thin films by controlling deposition parameters such as the deposition rate, the angle of incidence α or the azimutal rotation of the substrate φ (Fig. a). By finely controlling these parameters, it is possible to create thin films with different morphologies, such as Helical Columns (Fig. b) that exhibit properties for the circular polarization [2] or Anisotropic Normal Columns (Fig.1. c, d) that exhibit properties for the linear polarization.

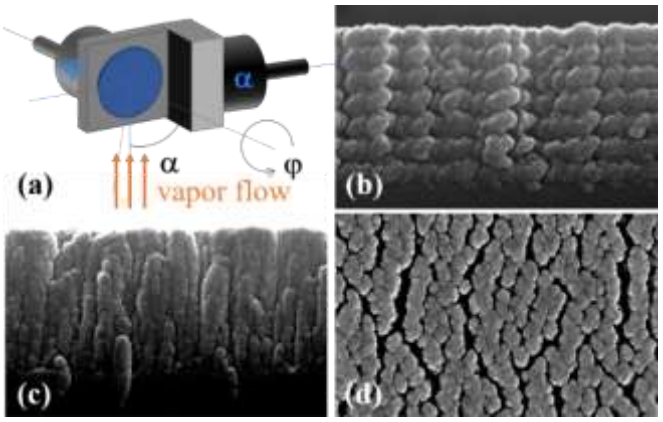

Fig.1. a) Sample holder for OAD; b) cross section of Helical Columns; c) cross section and d) plane view of Anisotropic Normal Columns

In addition, with the control of the α angle we can precisely control the porosity, making a wide range of optical indices in the three dimensions of the layers. By studying the anisotropic properties of these different architectures with *in-situ* XRD and ellipsometry annealing, we have demonstrated that amorphous nanostructures exhibit crystallisation of the anatase phase. This transformation highly increases anisotropic behaviors, which enables the improvement of existing optical designs, to create planar, low-loss circular and linear polarizers.

[1] K. Sasagawa, S. Shishido, K. Ando, et al. Optics express, **2013,** 21 (9) 11132-11140.
[2] A.C. Van Popta, M.J. Brett, J.C. Sit. Journal of Applied Physics. **2005**, 98, 083517.

T13-P: Techology for SMART anti-counterfeit labels with integrated RFID tag fabrication

C. Parvulescu[1], R. Tomescu[1], B. Comanescu[2], M. Pelteacu[2], D. Cristea[2]

[1]National Institute for Research and Development in Microtechnology – IMT Bucharest, 126A, Erou Iancu Nicolae Street, 077190, Voluntari, Ilfov, Romania
[2]S.C. Optoelectronica 2001 S.A., 35 Lacului Street, Ilfov, 077125 Magurele, Romania

One of the largest sources of organized crime revenue in the world is the counterfeit goods commerce [1]. Some of the most faked things are from domaines like clothing, coins / banknotes, fuels, automotive components, pharmaceuticals and microelectronic components [2]. In addition to being a major economic problem, counterfeiting poses a risk to human and national security. An effective solution to these

problems is to attach on the product/box SMART anti-counterfeit tags with RFID element. optimized

In this paper we propose a technology for the fabrication SMART security labels used mainly to protect products against counterfeiting and monitoring in the suplay chain.

The level of security of these multilayer structures is given by the integration of nano-text type security elements, metal micro-particles and a passive RFID element (with unique identification code) with a holographic background. The latter contains security features with optical effects (flip flop, guilloche lines, true color, channel switching, etc.) and consists of diffractive optical elements (DOE). The RFID assembly contains an antenna and an RFID chip. Metal micro-particles are an additional level of security due to the diversity of shapes and colours, but also due to the process of integration with the label represented by a non-deterministic method of deposition.

Fig. 1 Final intelligent multilayer holographic tag with a high level of security.

The process steps optimized for the fabrication of the proposed SMART tag are: i) Exposure of the holographic

structure layer using holographic lithography; ii) Exposure of the nanotext security key using the direct laser lithography equipment; iii) Development; iv) DC sputtering deposition of a 50 nm thin silver film for good electrical conductivity required for electrochemical deposition of nickel; v) Electrochemical deposition of Ni layer; vi) Metal microparticles with diffractive optical elements are randomly deposited on the holographic label's surface; vii) configuring\exposure of the RFID antenna on a PET foil using optical lithography, followed by gluing of a UHF RFID chip; viii) Both the holographic tag and the RFID tag are glued so that they form an intelligent multilayer holographic tag with a high level of security (Fig.1).

The developed process is simple and low-cost and alow the fabrication of complex and multilayer tag with a large number of security elements embedded in its layout. The small dimensions of the security elements embedded in the holographic label, and the untraceable coordinates after which are placed on top of the diffractive optical elements of the background make the identification significantly hard with the naked eye.

Acknowledgments. This work was supported by a grant of the Ministry of Research, Innovation and Digitization, CCCDI - UEFISCDI, project number PN-III-P2-2.1-PTE-2021-0646, within PNCDI III

[1] L. Chavarria, Q. Walker, D. Bahamon, Euromonitor International, **2020**

[2] Alison Smith, J. Mater. Chem. C., **2017**, 5. 3207 – 3215.

T13-P: Nanosphere lithography tests for metamaterials with applications in fluorescence improvement

R. Tomescu, V. Anastasoaie, C. Parvulescu, O. Brincoveanu, A. Dinescu, D. Cristea

National Institute for Research and Development in Microtechnology – IMT Bucharest, 126A, Erou Iancu Nicolae Street, 077190, Voluntari, Ilfov, Romania

In this paper we present the nanosphere lithography process optimization to obtain metamaterials suitable for applications in optical biosensensors. This type of sensors can detect an analyte from the external environment using various methods: interferometry, fluorescence (FL), refractive index change, surface-enhanced Raman scattering, [1, 2]. We focused on fluorescence (FL) based biosensors because are reliable, fast, and low-cost [3]. A method to increase the fluorescence intensity is to employ metamaterials. These types of materials are arrays of nano-antennas of various shapes and sizes much smaller than the wavelength so they can be considered homogeneous.

Here we propose a low-cost method to obtain nanostructured surfaces which can offer a significant fluorescence improvement. The main steps for obtaining the desired metamaterials are: deposition of the polystyrene nanospheres (PSn) on a substrate, metal deposition by e-beam method and lift-off.

To optimize these technology processes, we experimented different deposition methods for the PSn, substrate (silicon and glass) and nanosphere functionalizations.

Table 1 presents the technological parameters employed in PSn deposition for a set of 9 samples. The substrate was prepared by immersion in SurPass 4000 for 2 minutes.

SurPass 4000 is an advance aqueous based priming agent which provides maximum adhesion to a wide range of substrate materials [4]. PSn were functionalized by mixing a solution of Triton-X diluted in methanol 1:400 with PSn in water solution (2.5 wt%) to increase de adhesion to the Si substrate.

Table 1. Technological parameters employed in the substrate preparation and PSn deposition

No.	PSn/H_2O : Triton X	PSn deposition by spinning	PSn diameter
P1	2:1 (6 ml/3 ml)	200 rpm/2 sec; 500 rpm/6 sec; 800 rpm/20 sec	670 nm
P2	2:1 (6 ml/3 ml)	200 rpm/5 sec; 500 rpm/6 sec; 900 rpm/20 sec	670 nm
P3	2:1 (6 ml/3 ml)	200 rpm/2 sec; 500 rpm/6 sec; 900 rpm/9 sec; 1200 rpm/10 sec	640 nm
P4	2:1 (6 ml/3 ml)	200 rpm/2 sec; 500 rpm/6 sec; 900 rpm/5 sec; 1200 rpm/10 sec; 1500 rpm/10 sec	650 nm
P5	2:1 (6 ml/3 ml)	500 rpm/3 sec; 900 rpm/5 sec; 1200 rpm/4 sec; 1500 rpm/5 sec; 2000 rpm/6 sec	650 nm
P6	3,3:1 (1 ml/0,3 ml)	500 rpm/3 sec; 900 rpm/5 sec; 1200 rpm/2 sec; 1500 rpm/3 sec; 2000 rpm/6 sec	190 nm
P7	3,3:1 (1 ml/0,3 ml)	500 rpm/3 sec; 900 rpm/3 sec 1200 rpm/2 sec; 1500 rpm/3 sec; 2000 rpm/6 sec	180 nm
P8	3,3:1 (1 ml/0,3 ml)	Droplet	180 nm
P9	3,3:1 (1 ml/0,3 ml)	Droplet	690 nm

After the fabrication, the test structures were morphologically investigated using: i) Scanning electron microscope (SEM); ii) Atomic force microscope (AFM) and an optical microscope. The investigations shows that single layer of PSn with the best uniformity can be obtained usin a multi-step spinning process (500 rpm/3 sec; 900 rpm/5 sec; 1200 rpm/4 sec; 1500 rpm/5 sec; 2000 rpm/6 sec), medium size PSns functionalized with PSn/H_2O:Triton X 2:1. This uniformity is necessary for

obtaining metasurfaces with a good distribution of the metallic nanostructures attained after metal deposition and lift-off, and consequently a significant fluorescense improvement (up to 20 folds).

Acknowledgement. This work is funded by the Ministry of Research Innovation and Digitalization through Program 1 - Development of the National R & D System, Subprogram 1.2 - Institutional Performance - Projects for Excellence Financing in RDI, project MicroNEx, Contract no. 20 PFE/ 30.12.2021 and CCCDI-UEFISCDI Grant 328/10.08.2020 (project number PN-III-P2-2.1-PED-2019-1300), within PNCDI III.

[1] S. Rodionov, M. Remnev, V. Klimov, Sens.Bio-Sens. Res, **2019**, 22, 100263.
[2] P. Damborsky, J. Svitel, J. Katrlik, Essays Biochem., **2016**, 60 (1), 91–100.
[3] Qu, H., Fan, C., Chen, M. et al., J Nanobiotechnol, **2021**, 19, 403.
[4] Surpass 4000 DisChem inc., Data Sheet.

T14-P: Low Density Polyethylene Nano/Microfragments Interaction with Cyanobacteria

R. Forfota[1,2], M. Bocaneala[1,3], A. Ciorita[1,2], S. G. Macavei[4], S. Cinta Pinzaru[5,6], L. Barbu-Tudoran[1,2]

[1]Electron Microscopy Centre, Faculty of Biology and Geology, Biology and Geology Faculty, Babeș-Bolyai University, Cluj-Napoca, Romania
[2]Integrated Electron Microscopy Laboratory, National Institute for Research and Development of Isotopic and Molecular Technologies, Cluj-Napoca, Romania
[3]Department of Molecular and Biomolecular Physics, National Institute for Research and Development of Isotopic and Molecular Technologies, Cluj-Napoca, Romania

[4]*Physics of Nanostructured Systems Department, National Institute for Research and Development of Isotopic and Molecular Technologies, Cluj-Napoca, Romania*
[5]*RDI Laboratory of Applied Raman Spectroscopy, RDI Institute of Applied Natural Sciences (IRDI-ANS), Babeş-Bolyai University, Cluj-Napoca, Romania*
[6]*"Ioan Ursu" Institute, Babeş-Bolyai University, Cluj-Napoca, Romania*

Low Density Polyethylene (LDPE) is the largest plastic polutant found everywhere in the environment. Artificially fragmented to nano- and micrometer sizes LDPE was kept in contact with Arthrospira platensis and Coelomorun pussilum for 23 days. The metabolically relevant properties of cyanobacteria (optical density of the culture, concentration of chlorophyl, carotenoids, phycoerithrin, phycocyanin and exopolysacharides) were measured by spectrophotometry and the morphology was analysed by scanning and transmission electron microscopy. Results show that nanoLDPE stick to cyanobacteria cells but do not interfere significantly with their metabolism and morphology. MicroLDPE offer support for attachment. Both nano and microLDPE attach to cyanobacteria in the first few days of contact and may be uptaken in the trophic web by species feeding on cyanobacteria.

Aknowldegment. Part of this study was financially sustained from PN-III-P2-2.1-PED-2019-4777 awarded to SCP.

T14-P: SERS assessment of Cylindrospermopsin Cyanotoxin in environmental waters from Transylvania, Romania, and in fish tissue

Cs. Molnar[1,2], S. Cinta Pinzaru[2]

[1]National Institute for Research and Development of Isotopic and Molecular Technologies, 400293 Cluj-Napoca, Romania
[2]Ioan Ursu Institute of Physics, Babeş–Bolyai University, 400084, Cluj Napoca, Romania

Cylindrospermopsin (CYN), a cyanotoxin occurring in environmental waters as a cyanobacteria metabolite, has recently raised increased interest both in the scientific community and the environment, food control, and health care stakeholders. The primary source of exposure is either drinking water or ingestion of toxin-contaminated food and by inhalation and dermal contact during recreational activities in toxic waterbodies. A tolerable daily intake of 0.02 μg/kg body weight/day for human exposure was calculated based on acute toxicity studies in mice [1]. Here we present a fast and sensitive detection method based on surface-enhanced Raman scattering (SERS) of toxins in solutions and in fish tissue and we assess the capability of the SERS technique to detect the toxin in some environmental water bodies collected from Cluj area, Romania.

SERS analysis of toxins in environmental water bodies relies on robust reference data for fast and efficient monitoring and screening applications. In this work, the toxin was found to chemisorb on silver nanoparticles and the SERS signature is slightly dependent on concentration. Quantitative SERS analysis for concentrations range from 2.18 μM to 0.218 nM in

aqueous solution is achived. We used the SERS intensity ratio (Fig. 1) of the key SERS bands of CYN to build a calibration curve for a range of concentrations comprising four orders of magnitude, from micro- to sub nanomolar values [2]. The results open reliable perspectives for SERS translation as an effective method for toxin environmental monitoring.

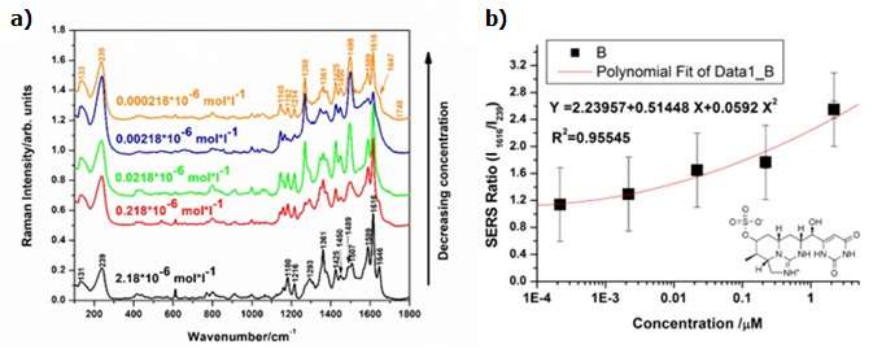

Fig. 1. a) SERS spectra of CYN at different concentrations, from 2.18 μ mol l-1 to 0.218 n mol l-1 as indicated on each spectrum; b) Plot of the relative intensity ratio of the SERS bands at 1616 cm-1 and 239 cm-1 as a function of CYN concentration. Error bars indicate standard deviation. A polynomial regression of second order best described (R2=0.955) the fitted data.

Aknowledgments. The financial support for this work was provided by the P1-1.1-PD-2019-0562 Program, Project

[1] R. Guzman-Guillen, et al, Environ. Toxicol. Chem. **2012**, 31, 2233–2238

[2] Article under review: Cs. Molnar, S. Cinta Pinzaru, V. Chis, I. Feher, B. Glamuzina, Spectrochim. Acta A: Molec. Biomolec. Spectrosc.

T14-P: A sustainable plastic waste initiative from macro- to microplastics based on Raman spectroscopy technique

I. Marica, I. Nesterovschi, S. Cinta Pinzaru

[1]Babeș-Bolyai University, Physics Faculty, Kogălniceanu 1, RO-400084 Cluj-Napoca, Romania

Nowadays, a world without plastics seems impossible due to their numerous benefits for a wide range of applications. Unfortunately, plastics (both macro- and micro) are worldwide recognized as one of the most serious threats to the planet's environment because of the pollution they create. It has become imperative to tackle this challenge of reducing plastic pollution by finding new, innovative ways to improve the plastic waste management strategies. The plastic waste recycling process, which first includes sorting, is an important strategy for plastic waste minimization according to the principles of circular economy. Raman Spectroscopy is known as a method of choice in plastics identification and sorting [1] based on their unique spectral fingerprint (Fig.1). However, in the natural environment, macro-plastic wastes are exposed to continuous degradation processes until they are eventually collected for recycling resulting in the formation of smaller plastic fragments (<5 mm) known as secondary microplastics.

Here, aiming to support a sustainable plastic waste management initiative based on Raman Spectroscopy technique we analyzed a high stock of plastic waste samples degraded for years in the natural environment comprising the 6 most common plastic types (Fig.1).

We determined the molecular changes seen in their Raman signals, changes related to natural degradation factors, such as long term solar atmospheric or seawater exposure, biofilm

deposit or other aggressive agents and, on other hand, due to intrinsic factors such as pigments.

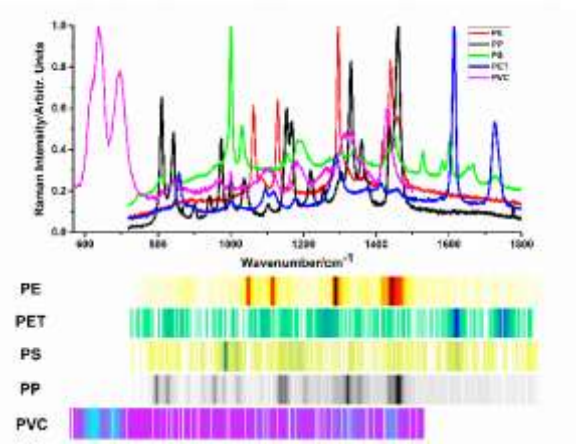

Fig. 1. Normalized Raman spectra of the main used plastic materials: PE (LDPE/ HDPE), PP, PET. PVC and PS and their specific Raman barcode [2].

. Regarding the pigments influeneces, special attention was paid to the Pigment Blue 15 (PB15) whose Raman unique fingerprint was very often found in our Raman signals of macro- an microplastics samples. Thus, in this study we also focused on the PB15 Raman signal, especially when a sorting algorithm of mixed plastic waste relying on Raman spectroscopy is considered, as well as when analytical tasks to promptly identify microplastic in environment, food products, drinking water and macro- and microorganisms are of interest.

[1] H. Kawazumi, A. Tsuchida, T. Yoshida, Y. Tsuchida, in *Progress in Sustainable Energy Technologies Vol II: Creating Sustainable Development*, **2014**.

[2] I. Marica, M. Aluas, S. Cinta Pinzaru, Waste Manag. **2022**, 144, 479.

T14-P: Low Density Polyethylene Release and Fragmentation in the Environment

M. Suciu[1,2], A. Ciorita[1,2], A. Tarta[1], M. Bocaneala[1,3], A. Rostas[4], S. G. Macavei[4], I. Kacso[4], M. Potara[5], I. Marica[6], C. S. Moldovan[7], R. I. Stiufiuc[7,8], S. Cinta Pinzaru[6,9], L. Barbu-Tudoran[1,2]

[1]Electron Microscopy Centre, Faculty of Biology and Geology, Biology and Geology Faculty, Babeș-Bolyai University, Cluj-Napoca, Romania
[2]Integrated Electron Microscopy Laboratory, National Institute for Research and Development of Isotopic and Molecular Technologies, Cluj-Napoca, Romania
[3]Department of Molecular and Biomolecular Physics, National Institute for Research and Development of Isotopic and Molecular Technologies, Cluj-Napoca, Romania
[4]Physics of Nanostructured Systems Department, National Institute for Research and Development of Isotopic and Molecular Technologies, Cluj-Napoca, Romania
[5]Nanobiophotonics and Laser Microspectroscopy Center, Interdisciplinary Research Institute on Bio-Nano-Sciences, Babes-Bolyai University, Cluj-Napoca, Romania
[6]RDI Laboratory of Applied Raman Spectroscopy, RDI Institute of Applied Natural Sciences (IRDI-ANS), Babes-Bolyai University, Cluj-Napoca, Romania
[7]Medfuture - Research Center for Advanced Medicine, "Iuliu Hatieganu" University of Medicine and Pharmacy, Cluj-Napoca, Romania
[8]Department of Pharmaceutical Physics & Biophysics, Faculty of Pharmacy, "Iuliu Haţieganu" University of Medicine and Pharmacy, Cluj-Napoca, Romania
[9]"Ioan Ursu" Institute, Babes-Bolyai University, Cluj-Napoca, Romania

Polyethylene can be found everywhere in the environment in present times and it degrades to smaller fragments given sufficient amount of time. Our study shows that low density polyethylene (LDPE) can reach nanometer sizes in short time and these dimensions domain is small enough to interact with the base of the food chain. Scanning Electron Microscopy

(SEM) and Dynamic Light Scattering (DLS) showed that 240 hours of UVC exposure produced nm LDPE fragments. Raman spectroscopy and Fourier Transformed Infra-Red (FTIR) spectroscopy confirmed the chemical degradation of the UVC-exposed LDPE by a decrease of crystallinity. LDPE closely interacts with Escherichia coli and Arthrospira platensis after only 72 hours of interaction. Our study indicates that nanoplastics are likely to be present in the environment in a "stealth mode".

Aknowldegment: part of this study was financially sustained from PN-III-P2-2.1-PED-2019-4777 awarded to SCP. We thank Elta'90MR for the images and access to NikonAXR confocal microscope during the workshop.

T14-P: Doxycycline hyclate loaded in porous biogenic carbonate: new drug formulation and characterization using Raman spectroscopy techniques and XRD

I. Bajama[1], G. Lazar[1], T. Tamas[2], S. Cinta Pinzaru[1,2]

[1]Ioan Ursu Institute, Babes-Bolyai University, 1 Kogalniceanu 400084 Cluj-Napoca, Romania.
[2]Department of Geology, Babes-Bolyai University, 1 Kogalniceanu 400084 Cluj-Napoca, România.

Doxycycline hyclate (C22H24N2O8H2O) is a derived drug from oxytetracycline group, with excipients such as magnesium stearate, microcrystalline cellulose, colloidal silicon dioxide, and some may contain titanium dioxide. It is commercially available as powder or colored capsules. Doxycycline is known to have low affinity for calcium binding. Like any other antibiotic administration, in doxycycline hyclate administration it is advised on avoiding food products containing calcium. In

veterinary administration, biogenic calcium carbonate from waste seafood (bivalve, crustaceans shells) is considered beneficial.

a)

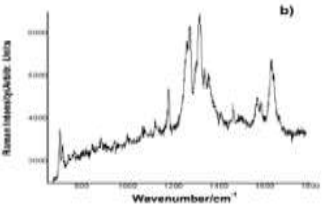

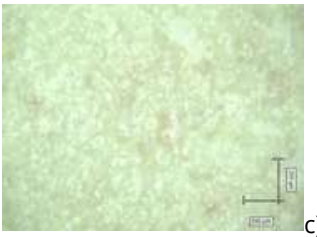

c)

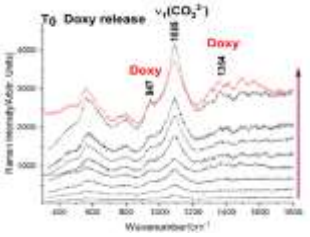

d)

Fig. 1 (a) Image of tablet formulation by loading doxycycline hyclate in biogenic calcite powder; (b) Raman spectrum of the doxycycline hyclate. Excitation: 632 nm; c) micrograph of the talet surface (scale bar 10 μm); d) a series of SERS spectra from the solution obtained immediately after tablet suspension in water (moment T_0): From fresly prepared SERS sample to a time course of 10 min, the SERS slowly indicated (as showed by arrow) the occurrence of doxycycline bands. Excitation: 532 nm.

Here we propose a new formulation of doxyclicline by loading antibiotic solution into porous biogenic carbonate from crustaceans, recently described [1] as a highly ordered 3D-nanostructure of pores and channels, suitable for efficient adsorption and slow release [2]. Powder of shell from the blue crab *C. sapidus*, with preserved nanoporosity was used to load the antibiotic solution and tablets formulation (Fig. 1). Surface

screening of tablets using Raman spectroscopy indicated a signal from biogenic calcite with preserved natural pigments. XRD diffractogram of the dried composite indicated calcite mineral, the drug adsorbed in pores being under the detection limit. The release of the antibiotic from the tablets has been investigated using SERS technique in a time course of 6 hours, measuring its release every 10 minutes. The SERS spectra (Fig. 1d) indicated a broaden, main band from carbonate Raman mode (1085 cm^{-1}) and slightly increasing SERS bands of doxycycline in time.

Acknowledgements. This work was supported by a grant of the Romanian Ministry of Education and Research, CCCDI-UEFISCDI, project nr. PN-III-P2-2.1-PED-2019-4777, acronym BluBioSustain.

[1] F. Nezval, S. C. Pinzaru, .et al. Sci. Rep 2020, 10, 3019 (2020).
[2] G. Lazar, S C. Pinzaru et al, ACS Omega 2021, 6, 42, 27781–27790.
[3] I. Bajama, S. C. Pinzaru et. al. Asian Journal of Physics Vol. 31, No 2 (2022) 355-364

T5-P: A new route to obtain silver doped titania nanoparticles with antimicrobial activity

R–C. Suciu[1], M. Stefan[1], A. Popa[1], D. Toloman[1], D. C. Vodnar[2], C. Grosan[1], O. Pana[1]

[1]National Institute for Research and Development of Isotopic and Molecular Technologies, Donat Street, No 67-103, 400293, Cluj-Napoca, Romania
[2]University of Agricultural Sciences and Veterinary Medicine, Faculty of Veterinary Medicine, 3-5 Calea Mănăştur Str., 400372 Cluj-Napoca, Romania

Silver doped titania photocatalyst has shown an important role in the removal of a wide range of pollutants in aqueous solutions under UV and visible light, including anionic and cationic dyes, organic and pharmaceutical compounds, metal

ions, and bacteria [1-3]. In this study we report the successful fabrication and characterization of novel silver doped titanium dioxide with antibacterial propert. Stable silver doped TiO_2 nanoparticles with different Ag^+/Ti^{4+} atomic ratio were synthesized by sol-gel method, using titanium (IV) n-butoxide, propionic acid, silver nitrate as precursors and the L(+)-ascorbic acid, as reducing agents. Calcinations at 450°C for 2h in air was applied to convert prepared gels to Ag - TiO_2 crystalline powder. UV - Vis spectroscopy, Fourier transform infrared spectroscopy (FT-IR), electron paramagnetic resonance spectroscopy (EPR) and Raman spectroscopy, fluorescence spectroscopy (PL), Scanning Electron Microscopy (SEM) and X – ray diffraction (XRD) was used to characterize the as – prepared Ag – TiO_2 nanopowder. The unit cell parameters of the TiO_2 anatase phase, the effective crystallite mean size, D_{eff} (nm) and the root mean square (rms) of the microstrains, $<\varepsilon^2>^{1/2}_{hkl}$, were calculated by Rietveld refinement analysis. The antimicrobial activity of powder was studied in darkness and in the presence of UV light, against Escherichia coli (abbreviated as E. coli) as a model for Gram-negative bacteria and Staphylococcus aureus (abbreviated as S. aureus). In the absence and in the presence of UV, the reduction in viable cells was observed. The results suggest that Ag doped TiO_2 nanonanoparticles can be used as effective growth inhibitors in various microorganisms, making them applicable to medical devices and antimicrobial control systems.

Acknowledgments.The authors would like to express appreciation to the Romanian Ministry of Research, Innovation and Digitization for the financial support through Projects PN 19 35 02 03 (Core Program) and ELI_17/16.10.2020.

[1] H. Chakhtouna, H. Benzeid, N. Zari, A. el kacem Qaiss, R. Bouhfid, Environ. Sci. Pollut. Res. **2021**, 28, 44638–44666
[2] A. Ajmal, I. Majedd, R. N. Malik, H. Idriss, M. A. Nadeem, RSC Advances **2014**, 4, 37003 -37026
[3] N. A. Narewadikar, K. Y. Rajpure, Nanotechnol. Russia **2022**, 17, 39 – 58.

T2-P: Understanding Damage Threshold Limit in Fs irradiation regime via target current measurements

S. A. Irimiciuc[1], R. Udrea[2], G. Bleotu[3], A. Dumitru[3], E. Stroici[1], P. Garoi[1], D. Ursescu[3], D. Craciun[1], V. Craciun[1,3]

[1]INFLPR, 409 Atomistilor street, Magurele, RO-077125, Romania
[2] Physics Faculty, University of Bucharest, Bucharest-Magurele, Romania
[3]Extreme Light Infrastructure for Nuclear Physics, Romania

With the current development of new and very powerful laser sources, understanding the behavior of optical components in high power irradiation regimes becomes crucial. Extending the life-time of key components for systems like ELI-NP is strongly connected to understanding their behavior below the laser induced damage threshold (LIDT). Our work is focused on providing insight into the material behavior below the LIDT by implementing a simultaneous dual analysis by means of Target Current (TC) and Floating Langmuir Probe (FLP) measurements. Several materials in bulk and thin film form (Ti, HfO_2, ZrO_2) for were irradiated by a gausiian fs laser bean (wavelength 800 nm, repetition rate 10 Hz, pulse duration 100 fs) on a wide range of fluences. Both TC and FLP signals are in good agreement with the existent theoretical description of fs-laser matter interaction.

Our proposed approach for LIDT monitoring system manages to provide measurable signals for fluences below LIDT with clear signature when damage is induced on the irradiated materials. This approach has great promise for scalability and implementation of the proposed diagnostic in high-power laser facilities. The recorded temporal current traces are complex, presenting multiple maxima above the ablation threshold and are discussed in terms of fundamental mechanisms involved and the nature of material.

Acknowledgments. This work was supported by the Ministry of Research, Innovation and Digitization, CNCS - UEFISCDI, project number PN-III-P4-PCE-2021-1158; PN-III-P2-2.1-PED-2021-2659; PN-III-P2-2.1-PED-2021-0957; program 5/5.1/ELI-RO, contract ELI_04/01.10.2020.

Invited and Oral Session (HALL 1)

T5-I-online: DFT+Σ_2 method for electron correlation effects at transition metal surfaces, heterostructures and nano-devices

M. M. Radonjic[1], A. Droghetti[2], A. Halder[2], I. Rungger[3], L. Chioncel[4]

[1]*Institute of Physics Belgrade, University of Belgrade, Pregrevica 118, 11080 Belgrade, Serbia*
[2]*School of Physics and CRANN, Trinity College, Dublin 2, Ireland*
[3]*National Physical Laboratory, Hampton Road, Teddington TW11 0LW, United Kingdom*
[4]*Theoretical Physics III, Center for Electronic Correlations and Magnetism, Institute of Physics, and Augsburg Center for Innovative Technologies, University of Augsburg, 86135 Augsburg, Germany*

We present a computational approach for electronically correlated metallic surfaces, interfaces and two-terminal

devices. The method combines density functional theory (DFT) and dynamical mean-field theory (DMFT) using a multiorbital perturbative solver for the many-body problem. Our implementation is designed to describe the electronic properties of ferromagnetic metallic thin films on a substrate and the electronic and linear-response transport properties of two-terminal nanoscale devices and hetero-structures. Capabilities and performances are assessed in detail for two prototypical nanoscale systems.

Firstly, we compare the calculation of a Fe monolayer on a W(110) substrate with the photoemission experimental data. Our method displays significant qualitative and quantitative improvements in the spectral function with respect to the results of density functional theory within the local spin density approximation. In particular, the spin splitting of the d states drastically reduces, and at the same time, their spectral width becomes narrower.

Secondly, we apply the method to the metallic junctions presenting alternating Cu and Co layers, exhibiting spin-dependent charge transport and giant magnetoresistance (GMR) effect. The electron-electron correlations on the Co d orbitals strongly suppress coherent transmission below the Fermi level due to finite lifetime. The transmission above the Fermi level is slightly reduced since it is mostly determined by s electrons. At the Fermi energy, in accordance with the Fermi-liquid behaviour, the reduction of the transmission predicted by DMFT is entirely due to the shifts of the energy spectrum induced by the electron correlations. Consequently, the resulting change in the transmission and GMR is only moderate.

[1] A. Droghetti, M. M. Radonjic, A. Halder, I. Rungger, L. Chioncel, Phys. Rev. B **2022**,105, 115129.
[2] A. Droghetti, M. M. Radonjic, A. Halder, L. Chioncel, I. Rungger, arXiv:2201.13118 (2022)

T11-I-online: The Phase Diagram of Kitaev Models under Arbitrary Magnetic Field Strengths and Orientations

F. Yilmaz[1], S. K. Yip[2,3], A. P. Kampf[1]

[1]*Theoretical Physics III, Center for Electronic Correlations and Magnetism, Institute of Physics, University of Augsburg, Augsburg 86135, Germany*
[2]*Institute of Physics, Academia Sinica, Taipei 115, Taiwan*
[3]*Institute of Atomic and Molecular Sciences, Academia Sinica, Taipei 115, Taiwan*

The Kitaev model is an exactly solvable bond anisotropic spin model within the real fermion language. Despite numerous studies along special field directions such as [001] and [111], there is a limited knowledge on the complete field angle dependence of possible phases, which can provide valuable information on the existence of fractionalization. To fulfill this purpose, we first extend the present studies on the field angle response of the anti/ferromagnetic Kitaev model. Yet, the realistic Kitaev materials, within the edgesharing octahedra paradigm, arise with the additional exchange terms. The studies on the candidate materials indicates the presence of a large spin-orbit Γ term along with perturbative Γ' and the Heisenberg J terms. It is therefore not reliable to depend on the topological properties of the pure Kitaev model as the only source of the thermal Hall conductivity experiments and it demands an understanding of these models with a complete field response.

Investigating the zero-field phase diagram of the realistic (K,Γ,Γ′) models, we identify conventional antiferromagnetic

zigzag and (partially) polarized spin phases as well as two exotic Kitaev(-Γ) spin liquid phases. The arbitrary magnetic field response of these phases provides a rich phase diagram hosting mainly the extended versions of the zero-field phases. We observe a partially fractionalized intermediate region with a finite Chern number and a vanishing gauge flux. This phase is concluded to be an extended phase of Kitaev-Γ spin liquid phase, which resides between the ZZ and the polarized phases. To comply our findings with the experiments and to verify the power of our method, we reproduce the narrow or extended regions of the intermediate phase depending on the field directions, $\theta=\pm 60$ in the ac plane, naturally. We finally revisited the relation between the topological GS and the anti/symmetric thermal conductivity tensor and further clarified our findings in this aspect.

T5-I: Crystal phase effects in group IV nanowire polytypes

M. Amato

Laboratoire de Physique des Solides (LPS)
Université Paris-Saclay, Centre scientifique d'Orsay, F91405 Orsay cedex

Crystal structure and interface engineering are acquiring an increasing importance in nanoscience because of their enormous potential to conceive new properties and functionalities [1]. As for nanowires (NWs), the emergence of new stable polytypes of common semiconductors promises to have a crucial impact in materials design [2].
Recent experimental investigations have confirmed the possibility to synthesize and exploit polytypism in group IV nanowires. Indeed, while the crystal structure of Si and Ge nanowires (NWs)

at standard conditions usually takes a well-defined cubic-diamond phase (as for their bulk counterparts), in the last few years several experimental observations of NWs exhibiting other phases — i.e. the hexagonal- diamond one — have been reported [2]. Other studies have instead succeeded in growing Si and Ge NWs containing both the cubic-diamond and the hexagonal-diamond phases opening the way to the fabrication of well-ordered group IV polytype homojunctions [3].
Driven by this promising evidence, here I will discuss recent first-principles calculations of the electronic and optical properties of hexagonal-diamond and cubic-diamond Si and Ge NWs as well as their homojunctions [4-8]. I will outline how a change in the crystal phase can strongly modify the electronic, optical and doping properties of the NW inducing novel and fascinating properties.

[1] D. Jacobsson, F. Panciera, J. Tersoff, M. C. Reuter, S. Lehmann, S. Hofmann, K. Dick, F. Ross, Nature **2016**, 531, 317-322.
[2] E. Fadaly, A. Dijkstra, J. Suckert, et al. Nature **2020**, 580.
[3] L. Vincent, G. Patriarche, G. Hallais, C. Renard, C. Gardès, D. Troadec, D. Bouchier, Nano Lett. **2014**, 14, 4828-4836.
[4] M. Amato, T. Kaewmaraya, A. Zobelli, M. Palummo, R. Rurali, Nano Lett. **2016**, 16, 5694-5700.
[5] T. Kaewmaraya, L. Vincent, M. Amato, J. Phys. Chem. C **2017**, 121, 5820-5828.
[6] C. Fasolato, M. De Luca, D. Djomani, L. Vincent, C. Renard, G. Di Iorio, V. Paillard, M. Amato, R. Rurali, I. Zardo, Nano Lett. **2018**, 11, 7075
[7] M. Amato, S. Ossicini, E. Canadell, R. Rurali, Nano Lett. **2019**, 19, 866.
[8] M. Amato, T. Kaewmaraya, A. Zobelli, J. Phys. Chem. C, **2020**, 124, 17290.

T5-I: Interface charge/spin transfer in layered ZnS/FePt/MgO thin films prepared by PLD

O. Pana[1], M. Stefan[1], D. Toloman[1], S. Macavei[1], C. Leostean[1], A. Popa[1], C. M. Teodorescu[2], S. Colis[3]

[1]Natl. Inst. for R&D. of Isotopic and Molec. Technol. 67-103 Donat, 400293 Cluj-Napoca, Romania
[2]Natl. Inst. of Mater. Phys., Atomiștilor 405A, 07715 Măgurele–Ilfov, Romania
[3]University of Strasbourg, Institute of Physics and Chemistry of Materials, PCMS-DCMI, 23 rue du Loess, 67034 Strasbourg, France

In recent years, considerable efforts have been devoted to the design and control fabrication of nanostructured magnetic composite materials with tailored structural, optical, electric, magnetic and surface properties [1]. Beyond the chemical composition or structure, a composite can be engineered through combined dimensionality and proximity effects. Thus, magnetic nanoscaled composite materials do not simply combine properties of the original components but also possess novel properties which are not seen in the original constituents [2,3]. By interfacing at nanoscale a half-metal with a semiconductor a polarized charge/spin transfer will result through the interface.
In most cases, through a double exchange mechanism, the semiconductor becomes ferromagnetically polarized and couples with the half-metal. The process depends of the energy bands setup at the interface. In the present work the FePt (L10) half-metal films covered with ZnS chalcogenide layers are prepared by PLD and investigated in order to determine some new emerging properties. This effect is driven by the energy band alignment at the interface. The charge/spin transfer may go from the semiconductor into the

magnetic core, thus leading to an increased overall magnetization or in the reverse way producing the decrease in the μB/f.u. number.

First the FePt thin films on MgO(100) substrates were deposited by PLD method at 5 Hz laser repetition rate in vacuum at 700 °C. Then a series of 5 samples of ZnS/FePt/MgO thin films were prepared by changing the number of pulses for zinc sulfide deposition at 5 Hz laser repetition rate.

The samples were characterized by XRD, XRR, UV-Vis, UPS and SQUID measurements. The XRD was used for crystal phase identification. The measurements were done in out of plane configuration – Brag Brettano, while reflectivity for thin film thickness and roughness were done in parallel beam configuration. The radiation source used is Cu Kα1. $L1_0$ (tetragonal) type structures for FePt and blende type for ZnS were identified, respectively.

The X-Ray reflectrometry (XRR) method was used to determine the layers thicknes of multistrat samples. For the FePt epitaxial layer (L10) a thickness of 12.2 nm resulted while thicknesses of ZnS layer were found between 5 and 28 nm for samples prepared with a number of pulses between 1200 and 4800 respectively. The alignment of energy bands at the interface was determined by UPS (valence band setup) combined with UV-Vis spectroscopy.

All these investigations are correlated with the transfer process of electrons with polarized spin at the half metal/semiconductor interface and the formation of the ferromagnetic phase inside the semiconductor. In general, due to the spin polarization of the energy bands at the Fermi level, half-metal ferromagnets interfaced with other nanoscale materials represent a rich source of very interesting new

physical phenomena both from a fundamental and applied point of view.

Acknowledgments. This work was suppotred by a grant o fthe Ministry of Research, Innovation and Digitization, CNCS – UEFISCDI, project number PN-III-P1-1.1-TE-0836, within PNCDI III and 5/5.1/ELI-RO/17.

[1] R.G. Chaudhuri, S. Paria, Chem. Rev. **2012**, 112, 2373–2433.
[2] M. Stefan, C. Leostean, O. Pana, M.-L. Soran, R.C. Suciu, E. Gautron, O. Chauvet, Appl. Surf. Sci. **2014**, 288, 180–192.
[3] S. Gutoiu, C. Leostean, M.-L. Soran, M. Stefan, S. Macavei, D. Toloman, A. Popa, A. Stegarescu, O. Pana, AIP Advances **2020,** 10, 055215

T5-O: Structural, morphological and magnetic study of $Co_{1-x}M_xFe_2O_4$ (M = Ni, Zn, Mn) obtained through a green, sucrose based, sol-gel method

A. Szatmari[1], R. Bortnic[1], R. Hirian[1], F. Nekvapil[1,2], L. Barbu[2], R. Tetean[1]

[1]Faculty of Physics, Babes-Bolyai University, Cluj Napoca, Romania
[2]National Institute for Research and Development of Isotopic and Molecular Technologies, Donat 67-103, P.O. Box 700, 400293 Cluj-Napoca, Romania

$CoFe_2O_4$ nanoparticles in which Cobalt has been substituted with Zn, Ni, Mn, $Co_{1-x}M_xFe2O4$ (where x = 0.02, 0.05, 0.1) were synthetized trough a green Sol-Gel method, using sucrose as a poly-condensation agent and pectin from animal origin as a chelating agent. The stoichiometric quantity of each precursor was separately dissolved in Milli-Q water and vigorously stirred. A sucrose solution was prepared. This sucrose solution was then added to each precursor solution. After, the precursor solutions were mixed together and thoroughly

homogenized. Pectin (1:5 wt. % pectin:sucrose) was added, and after the complete dissolution of pectin, the pH of the solution was lowered to approximately 1.5-2. This final solution was poured into a ceramic capsule and placed on a sand bath having the temperature of 200 ^{o}C until all the water was evaporated and a solid spongy gel was formed. This gel was thermally treated at 700 ^{o}C for 2 hours in order to eliminate all of the organic parts. Ultimately, the final form of the material was a magnetic black fine powder.

The X-ray measurements shown that all the obtained samples were single phase, having cubic structure with Fd3-m, specific to $CoFe_2O_4$ spinel structure. Rietveld refinement done on the X-Ray patterns reveal the average crystallite size to be approximately 55 nm. Raman Spectroscopy showed the variation of the cation occupancy on the tetrahedral sites as a function of dopant concentration. Transmission electron microscopy measurements show that the average crystallite size is approximately 50 nm.

The magnetic properties of the produced nanoparticles were studied at room temperature. The variation of the saturation magnetization as a function of dopant concentration and the variation of the coercivety were obtained from hysteresis curves measured at fields of up to 7 T.

T5-O: Spectroscopic Insight into the Steady-State and Time-Resolved Optical Properties of ZnO Nanoparticles

A. Falamas[1], I. Marica[2], A. Popa[1], F. Nekvapil[1,2], M. Stefan[3], C. Farcau[1]

[1]Molecular and Biomolecular Physics Department, National Institute for Research and Development of Isotopic and Molecular Technologies, 67-103 Donat, 400293, Cluj-Napoca, Romania

[2] Babeș-Bolyai University, 1 Kogalniceanu, 400084, Cluj-Napoca, Romania
[3]Physics of Nanostructured Systems Department, National Institute for Research and Development of Isotopic and Molecular Technologies, 67-103 Donat, 400293, Cluj-Napoca, Romania

This study presents a spectroscopic insight into the structural and optical properties of ZnO nanoparticles (NPs) [1] of different sizes and morphologies, synthesized using simple chemical methods. A complex investigation of their morpho-structural, steady-state and time-resolved optical properties was performed and the analysis focused on evidencing the interdependencies between these properties [2]. The calculated band gap presented a general inverse dependence on the particles diameter, irrespective of the morphology and method of preparation, while an increase of the intensity ratio between the UV and visible emission bands was observed with increasing the size of the particles. The time-resolved fluorescence investigation, namely time-correlated single photon counting (TCSPC), revealed the existence of three emissive states and the fluorescence lifetimes presented an overall decrease with increasing the particles diameter.
Several applications of the synthesized ZnO NPs were tested. Firstly, the photocatalytic activity was investigated for the degradation of two water pollutants, Rhodamine B (RhB) and oxytetracycline (OTC). The results showed that the structural and optical properties of ZnO NPs are related to their photocatalytic activity, reflecting important information associated to the electronic structure, as well as to the impurities and surface defects that influence their photocatalytic capacity. The presence of surface defects delayed the recombination of the photogenerated charges and led to an increase of the photocatalytic activity.

Secondly, we explored the potential of ZnO NPs and hybrid nanomaterials based on ZnO decorated with Au NPs as substrates for surface enhanced Raman scattering (SERS) and surface enhanced fluorescence (Fig.1) [3]. The nanomaterials were deposited as thin films using a simple drop deposition technique. Fluorescence enhancement was observed for Rhodamine 6G (R6G) adsorbed on ZnO NPs embedded in a polyvinyl alcohol (PVA) matrix, while a slight quenching was detected for the dye adsorbed on the Au decorated ZnO nanocomposites. Lifetime measurements indicated that neither the ZnO NPs nor the Au decorated ones modify substantially the decay rates of the dye when they were embedded in a PVA matrix, however, when R6G was adsorbed directly to the surface of the nanoparticles, a substantial decrease was identified. Surface enhanced Raman measurements

The substrates were further tested for Raman signal enhancement of R6G. The Au decorated ZnO nanocomposites presented a larger enhancement compared to the ZnO NPs.

Acknowledgment. This work was supported by a grant of the Romanian Ministry of Education and Research, CNCS - UEFISCDI, project number PN-III-P1- 1.1-TE-2019-1141, within PNCDI III and PN-III-P1-1.1-TE2021-0048.

[1] A.B. Djurisic, Y.H. Leung, Small **2006**, 2, 944-961

[2] A. Falamas, I. Marica, A. Popa, D. Toloman, S. Pruneanu, F. Pogacean, F. Nekvapil, T.D. Silipas, M. Stefan, Mat. Sci. Semic. Proc. **2022**, 145, 106644

[3] I. Marica, F. Nekvapil, M. Stefan, C. Farcau, A. Falamas, Beilstein J. Nanotechnology **2022**, 13, 472-490

T9-O: Grain size effects on the functional properties of $BaTiO_3$-based ceramic systems

V.A. Lukacs, L.P. Curecheriu, L. Padurariu, L. Mitoseriu

Dielectrics, Ferroelectrics & Multiferroics Group, Faculty of Physics, "Al. I. Cuza" University of Iasi, Iasi, Romania

Size and scale dependent phenomena in ferroelectric materials attract extensive interest due to the continuous trend of miniaturization in electronic systems. Alongside preserving the functional properties, comparative to bulk material, when reducing dimensions to nanoscale, a particular interest regards the maximization of dielectric, piezoelectric and ferroelectric properties at some specific ceramic grain sizes. In the case of $BaTiO_3$ ceramics, the researchers dedicated mainly to the critical grain size (GS) of around 1 μm, where enhanced properties have been found, irrespective of the synthesis procedure and sintering method [1,2]. Studies on scale-dependent properties performed in $BaTiO_3$-based ceramics are scarce [3] and no critical size with enhanced functional properties has been reported to date.

Therefore, this study is dedicated to the investigation of 5%Zr-$BaTiO_3$ (BZT) ceramics with variable GSs, prepared through classical sintering, in order to check for a similar possible critical value characterized by enhanced properties. The BZT ceramic system displays enhanced values of permittivity, in a broad critical range of GSs (1.5 – 15 μm), in the orthorhombic and tetragonal phases. The room temperature P(E) hysteresis loops, together with the DC-tunability behavior, have been recorder for a maximum applied field of 30 kV/cm in order to

assess the effects of GS variation. The piezoelectric characteristics have also been explored in the search of a critical GS or range of sizes characterized by enhanced values of functional properties.

Acknowledgements: The financial support of the Romanian UEFISCDI PN-III-P1-1.1-PD-2021-0531 project is acknowledged.

[1] L. Mitoseriu, L.P. Curecheriu, Nanostructured Barium Titanate Ceramics: Intrinsic versus Extrinsic Size Effects, in Nanoscale Ferroelectrics and Multiferroics, (John Wiley & Sons, Ltd, UK) **2016**, 473–511.
[2] Y. Huan *et al.*, J. Am. Ceram. Soc. **2013**, 96, 3369–3371.
[3] L. Padurariu *et al.*, Materials (Basel) **2020**, 13, 4386.

T9-O: Structure and morphology of Sn nanostructured films grown by Supersonic Cluster Beam Deposition

J.E. Martinez Medina[1,2], D. Arl[1], J. Polesel[1], A.M. Philippe[1], P. Grysan[1], J. Guillot[1], C. Vergne[1], E. Barborini[1]

[1]Materials Research and Technology department, Luxembourg Institute of Science and Technology, Belvaux, Luxembourg
[2]Department of Physics and Materials Science, University of Luxembourg, Esch- Sur-Alzette, Luxembourg

Since decades, SnO_2 has been considered for gas sensing applications for its chemoresistive properties. Sensitivity and response dynamics of gas sensors based on SnO2 can be improved by nanostructuring the sensing layers in order to enhance the interaction with the atmosphere [1].
Supersonic Cluster Beam Deposition (SCBD) enables the production of highly porous nanostructured films by soft assembling of atomic clusters, which preserve their individuality during film growth [2].

The characteristics of the cluster-assembled films, such as cluster size distribution, thickness, surface morphology, and porosity, can be controlled through the parameters of the SCBD process. This is of particular interest for applications where functional layers are expected to interact with the environment -as indeed gas sensing- since not only the surface of the functional layer plays an active role, but also the volume fraction.

Here we present a study where Sn atomic clusters are produced in the gas phase and deposited in form of a nanoporous film using SCBD, in high-vacuum conditions, at room-temperature. Transmission Electron Microscopy (TEM) unveils that, after room-temperarure oxidation in air, Sn particles exhibit size-dependent oxidation, where particles with sizes below 14 nm are fully oxidized while above this size, particles show metal-oxide core-shell structures (Fig. 1).

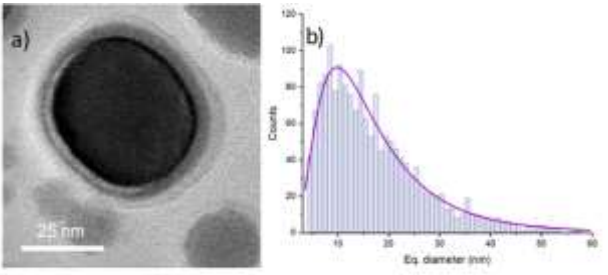

Fig. 1. a) TEM image on Sn nanoparticle after oxidation due to air exposure. b) size distribution of Sn clusters.

Crystalline planes in the Sn metallic core are clearly observed although the deposition process takes place at room-temperature. X-ray Photoelectron Spectroscopy (XPS) shows that both SnO and SnO2 are present in the cluster-assembled films. The combination of these analysis suggests that the

room-temperature oxidation mechanism of the Sn nanoparticles can be described by Cabrera-Mott model [3]. Morphological features of cluster assembled Sn films characterized by AFM will be also reported.

[1] M. S. Chavali and M. P. Nikolova, SN Appl. Sci. **2019**, 1, 607.
[2] F. Borghi, et al., Phys. Rev. Applied **2018**, 9, 044016.
[3] E. Sutter, et al., Part. Part. Syst. Charact. **2014**, 31, 879-885.

T9-O: Study of surface relief patterning based on diffraction methods

A. Meshalkin[1], E. Achimova[1], V. Abaskin[1], C. Losmanschii[1], V. Botnari[1], V. Pakstas[2,3]

[1]*Institute of Applied Physics, Chisinau, Moldova*
[2]*Center for Physical Sciences and Technology, Vilnius, Lithuania*
[3]*JSC Elektronikos perdirbimo technologijos, Vilnius, Lithuania*

In this work we present the surface relief pattering on photosensitive materials based on chalcogenide glasses and azopolymers by holographic recording and it's study by the optical diffraction methods. Chalcogenide nanomultilayer structures based on As_2S_3-Se and carbazole-containing azopolymers were used for direct surface relief grating formation by polarization holographic recording. Analyses of diffraction efficiency kinetics and AFM images of recorded gratings showed that two distinct mechanisms of recording are distinguished depending on the polarization of writing beams: small scalar surface modification induced by photoinduced volume change, and giant vectorial surface patterning induced by lateral mass transport. We consider that the main process during polarization holographic recording in investigated materials is surface relief formation

[1]. This implies that the diffraction efficiency (DE) value depends on the surface relief height and we can investigate the surface relief patterning by means of the measuring in-situ of DE value during holographic recording [2]. It was revealed that surface relief patterning rate is much more for gratings with greater periods, while the modulation depth remains approximately the same for all gratings and consists about 0.22. In order to calculate the surface relief height from the experimental data and compare them with the theoretical prediction, we have derived the expression for the first order diffraction efficiency as a function of surface relief height $\eta = J_1^2\left(\frac{\pi}{\lambda}\cdot\left(h\cdot(n-1)\right)\right)$, where J_1 – is Bessel function; λ – wavelength, used for DE measurement; n – refractive index of grating material; h – surface relief height.

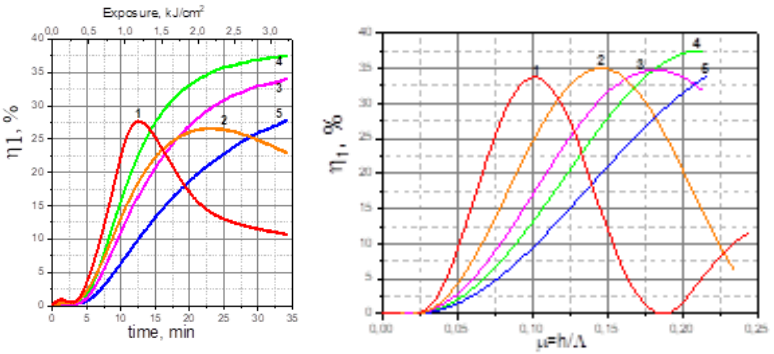

Fig. 1. Experimental and simulated DE kinetics.

Simulated diffraction efficiency kinetics curves showed good agreement with the experimental results. Analyses of diffraction efficiency kinetics and AFM images of recorded SRG showed that grating period increasing led to the SRG depth increasing in linear way. It was revealed that SRG recording

rate was characterized by non-linear behavior, while modulation depth remained approximately the same value for all gratings.

Acknowledgements: This work has received funding from the ANCD projects (20.80009.5007.03 and 21.80013.5007.1M) and partially from European Union's Horizon2020 research and innovation programme under the grant №778357-SMARTELECTRODES.

[1] A. Meshalkin, C. Losmanschii, E. Achimova, V. Abashkin, Adv. Phys. Res. **2019**, 1(2), 86-98.
[2] V. Cazac, A. Meshalkin, E. Achimova, V. Abashkin, Appl. Opt. **2018**, 57(3), 507-513.

T9-O: The dependency of strain hardening on Dislocation Statistics in cold Rolled 1050 Aluminum Alloy

P. Chakravarty[1], J. Gy. Batorfi[1], J. J. Sidor[2]

[1]Faculty of Natural Sciences, Eotvos Lorand University (ELTE)) P.O. Box 32, Budapest, 1518-Hungary
[2]Savaria Institute of Technology, Faculty of Informatics, Eotvos Lorand University, Karolyi Gaspar ter 4, Szombathely, 9700-Hungary

Present contribution describes various physical factors associated with the process of cold rolling in Al1050. One of the most important aspects of cold rolling is impartment of work hardening or strain hardening. However, the phenomenon of hardening is directly dependent on the evolution of dislocation density and controlled by different components of total dislocation density (ρ), namely GND (Geometrically Necessary Dislocation) and SSD (Statistically Stored Dislocation) [1]. The study of work-hardened state of the material was performed with the help of experimental

techniques like microindentation [2] and electron backscattering diffraction (EBSD) [3]. The material under investigation was deformed by means of symmetric, non-lubricated rolling for various reduction levels starting from 5.3% to 76%.

The experimental results indicate an increase in both microhardness and dislocation density with the increase in strain, with lowest strain (*e*) of 0.06 corresponding to $\rho = 4.08 \times 10^{13}$ m^{-2} up to highest strain of 1.69 with $\rho = 2.94 \times 10^{14}$ m^{-2} (Fig.1).

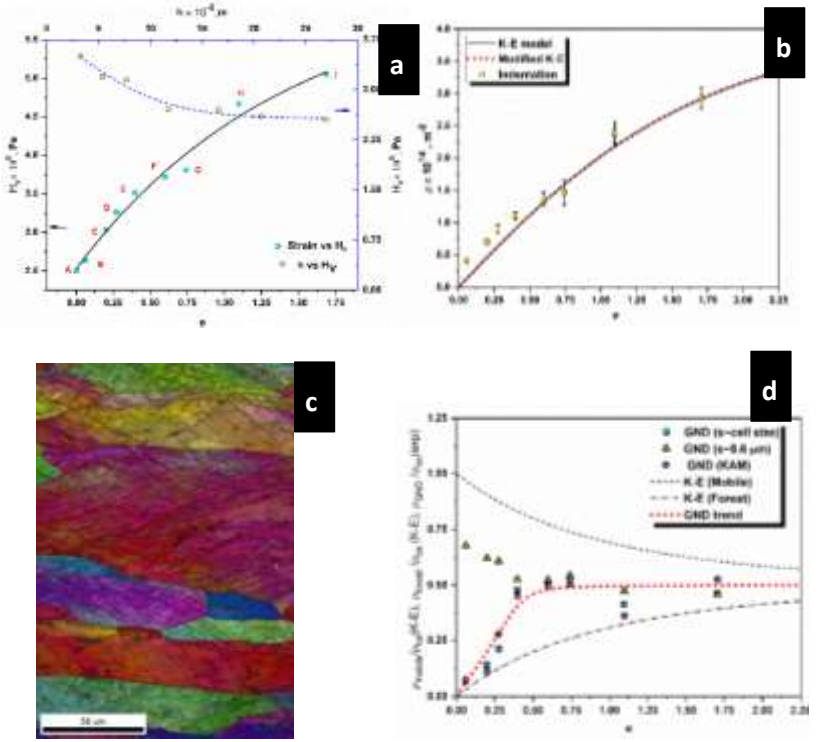

Fig. 1. Al1050 alloy: a) hardness; b) Dislocation density, c) EBSD IQ+IPF map, d) GND map.

On the other hand, further study suggests that, at lower straining levels the generated GNDs are trapped at grain boundaries and have a high contribution towards forest dislocations but with an increase of strain, the GNDs have a tendency to contribute nearly equally to mobile and forest dislocations.

Acknowledgements. Project no. TKP2021-NVA-29 has been implemented with the support provided by the ministry of Innovation and Technology of Hungary from the National Research, development and Innovation Fund, financed under the TKP2021-NVA funding scheme.

[1] F. J. Humphreys, G. S. Rohrer, A. D. Rollett, Recrystallization and related annealing phenomena, Third edition. Amsterdam Oxford Cambridge, MA: Elsevier, 2017.
[2] J. J. Sidor, P. Chakravarty, J. Gy. Batorfi, P. Nagy, Q. Xie, J. Gubicza, Metals, 2021, 11 (10) 1571
[3] T. Berecz, P. Jenei, A. Csore, J. Labar, J. Gubicza, P. J. Szabo, Mater. Charact., **2016**, 113, 117–124.

T2-O: Tailoring oxide phase formation during pulsed laser depositions process by in situ diagnostic of plasma chemistry

S. A. Irimiciuc[1,2], S. Chertopalov[2], M. Novotny[2], J. Lancok[2], V. Craciun[1,4]

[1]INFLPR, 409 Atomistilor street, Magurele, RO-077125, ROMANIA
[2] Institute of Physics of the Czech Academy of Sciences, Na Slovance 2, Prague, Czech Republic
[3] Physics Faculty, University of Bucharest, Bucharest-Magurele, Romania
[4]Extreme Light Infrastructure for Nuclear Physics, Romania

One of the main research directions within the thin film industry remains upscaling plasma-based deposition

techniques via fundamental development. Controlling and tailoring PLD has been the main developmental pillar in its history with a strong focus on external factors (laser fluence, gas pressure, target bias, target-substrate distance, etc.). Recent results have showed that the laser produced plasma is an active medium during the deposition. To develop a more complete picture of the deposition process we employed a dual approach based on in situ plasma analysis and thin film analysis to find common features that would connect the properties of the plasma with the ones of the deposited film.

Oxide phase tailoring for metal oxides, M_xO_y (Cu_xO_y, Mn_xO_y and Ni_xO_y), has been performed by in situ analysis on transient plasmas generated by ns-laser ablation in various background gases (Ar and O_2) using angular and time-resolved Langmuir probe technique and space- and time-resolved Optical Emission Spectroscopy (OES). The work was focused on understanding the complex dynamics of ablation plasma by controlling/adjusting the ionic energy distribution during the deposition process. A distinctive feature of the study is the focus on the floating regime of the probe as time-of-flight measurement tool. These results are discussed in the framework of multiple double layer formation during plasma expansion. Complementary, OES allowed for the spatial and temporal monitoring of visible and UV emission of the plasma. The nature and pressure of each gas influences the emission in a unique manner. M_xO_y molecule formation has specific signature, which was identified for all the deposition conditions with changes in both temporal and angular distributions. Plasma potential, charge density and electron excitation temperature were increasing with the gas pressure while electron temperature and expansion velocities were decreasing. Using a semi-empirical model, estimation of ion acceleration field, neutral temperature and densities were

performed. Space- and time-resolved OES confirmed the plume splitting indicated by LP measurements and provided insight into the plasma multiple structuring scenario. Thin films were fabricated in identical conditions and comparison between the properties of the plasma and those of the deposited films were made. Clear correlations were found between the oxide phase generated in the thin film and specific charges kinetic energies, plasma temperature or plasma potential.

Acknowledjments. This work was supported by Romanian Ministry of Education and Research, under Romanian Nat. Nucleu Program LAPLAS VI –n. 16N/2019, ELI-RO_2020_1, and PED_599_2022. We acknowledge the Operational Program Research, Development and Education financed by European Structural and Investment Funds and the Czech Ministry of Education, Youth and Sports SOLID21 (CZ.02.1.01/0.0/0.0/16_019/0000760).

T2-O: Paper archives can be protected against biodeteriogens with a custom-made cold atmospheric plasma applicator

A. Ciorita[1], C. L. Vacar[2], C. Tudoran[1], D. Podar[2], R. Carpa[2], C. Mircea[2]

[1]National Institute for Research and Development of Isotopic and Molecular Technologies, Cluj-Napoca, Romania
[2]Department of Molecular Biology and Biotechnology, 'Babes-Bolyai' University, Cluj-Napoca, Romania

Preserving patrimony artworks is a timeless pursuit as cultural heritage conservation stands beyond individual interests. Apart from maintaining optimal storage conditions there are few treatment options for important artworks. The main

threats are biodeteriogens consisting mainly of microorganisms. This work brings forward cold plasma as a suited tool for the treatment of paper deteriorated by cellulolytic bacteria. Cold plasma was applied in three different modes on *Bacillus velezensis* isolated from a book in personal collection. The herein designed cold plasma applicator proved efficient against *B. velezensis*, when applied for five minutes at a power of 50 W and current density of 12 mA/cm^2.

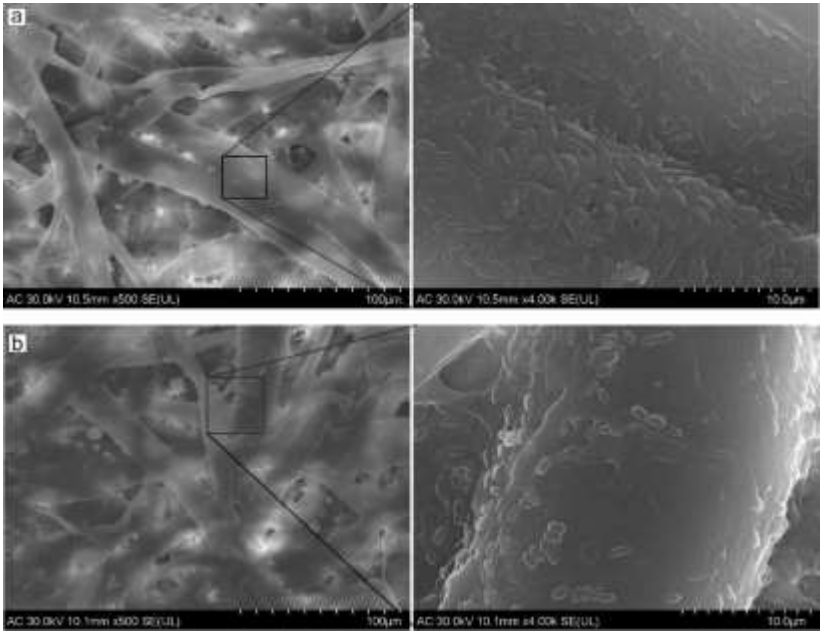

Fig. 1. SEM micrographs of paper fibers inoculated with *Bacillus velezensis*: a – untreated sample, b – sample treated with cold athmospheric plasma.

The same conditions were applied to bacteria grown on membranes and directly on paper, where they sporulated (Fig. 1). This study shows that cold plasma can inhibit the

development of cellulolytic bacteria, without affecting the substrate, which is an important step in preserving patrimony artworks [1].

Acknowledgments: This work was supported by a grant of the Ministry of Research, Innovation and Digitization, CNCS - UEFISCDI, project number PN-III-P1-1.1-TE-2021-0661, within PNCDI III; and by POC A1-A1.2.3-G-2015, UBB-TeMATIC-Art - ID P-40-374 – Partnership for transfer of innovative technologies and advanced materials in visual arts (production, conservation, restoration). Also, this work was supported by

[1] C.L. Vacar, et al., *in press*, **2022**.

T2-I-online: Plasma and electron-beam irradiation approaches for obtaining chitosan - based patches with Ag nanoparticles inclusion for wound healing

B. Mitu[1], M. Demeter[1], A. Ardeleanu[1], A. Scarisoreanu[1], I. Calina[1], V. Satulu[1], A. Bonciu[1], G. Dinescu[1], V. Mitran[2], A. Campean[2], C. M. Saviuc[2], M. Popa[2], C. Chifiriuc[2], E. Matei[3], A. Roseanu[4], L. Sima[4], C. Coman[5], A. Salagean[5]

[1]National Institute for Laser, Plasma and Radiation Physics, 409 Atomistilor, Magurele Ilfov 077125 Romania
[2]University of Bucharest, Faculty of Biology, 60101, Bucharest Romania
National Institute for Material Physics, 405 Atomistilor, Magurele Ilfov 077125 Romania
Institute of Biochemistry of Romanian Academy, Splaiul Independenței 296, Bucharest 060031Romania
National Institute for Medical-Military Research Cantacuzino, Splaiul Independenței 103, Bucharest 050096 Romania

Healthcare is one of the growing fields nowadays, with a special dedication to the skin wound healing because of huge costs in terms of money and human suffering. As such, the

development of new, advanced patches, to minimize the infection risk, reduce the pain and enhance the healing rate is on demand. This work is presenting two approaches based on plasma and electron-beam irradiation for the synthesis of patches based on nanocomposites including chitosan and Ag nanoparticles (30 nm diameter) with concentration in the range 0.05 – 0.2 mg/mL.

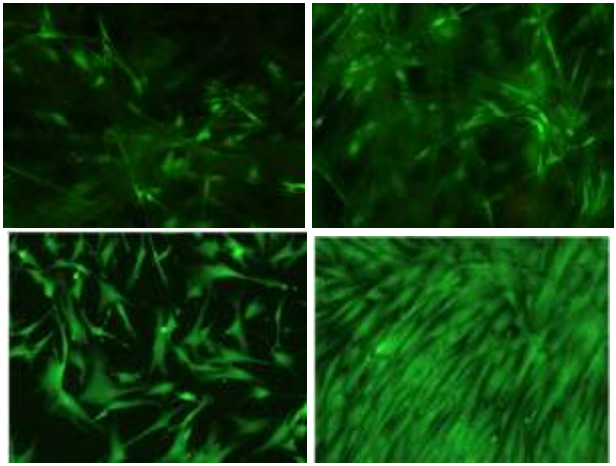

Fig. 1. Fibroblasts cells grown onto the plasma patches (up) and electron-beam patches (down) for 1 and 3 days after staining with LIVE/DEAD Kit (live cells -green fluorescence; dead cells-red fluorescence).

The plasma experiments were perfomed with an atmospheric plasma source operating in argon, at 30 W, using a non-woven polyesther substrate as support which is functionalized in a first step and onto which plasma induced graft polymerization (PIGP) of chitosan/AgNPs process is provisioned in the second step. Different total loading of Ag can be ensured on the volume of the patch, either by tuning the concentration, or the number of immersions in the aqueous solution of chitosan,

AgNPs, acetic acid. The electron beam approach was based on the irradiation of a aqueous solution of chitosan, poly(vinylpyrrolidone) – PVP, poly(ethylene glycol) -PEG, poly(ethylene oxide) - PEO, N'N-methylene-bis(acrylamide) - MBA, and acrylic acid . ALID-7 electron accelerator with energy of 6 MeV was used, and various doses in the field 10 – 30 kGy were tested for the synthesis of hydrogels.The antimicrobial activity was tested against both gram-negative and gram-positive bacteria, showing similar mechanisms regardless the type of patches. The in vitro response of fibroblasts in contact with the plasma-dressings evidenced that under moderate Ag NPs loading biocompatibility is achieved, while for the electron beam-based hydrogels high biocompatibility is shown.

Acknowledgments. This work was supported by the Romanian Ministry of Research, Innovation and Digitalization, CCCDI – UEFISCDI, projects PN-III-P1-1.2-PCCDI-2017-0728, PN-III-P1-1.1-PD-2021-0552 and by Nucleus-Programme, ctr 16N/2019, project nr. 19150101.

Oral and Invited Session (HALL 1)

T7-O: Influence of CNC concentration on the structure and sorption properties of gelatin

M-C. Popescu, D. Timpu, C-M. Popescu

Department of Physical Chemistry of Polymers, Petru Poni Institute of Macromolecular Chemistry, Iasi, Romania,

Biobased composite materials present a great interest in many fields due to their structural properties, as well as due to their biodegradability.

The aim of our study was to reinforce gelatin with cellulose nanocrystals (as nanofiller) in order to obtain nanocomposite systems with improved properties. The effect of nanofiller and its concentration on the structural features of the bio nanocomposite materials was evaluated by Fourier transform infrared spectroscopy and X-ray diffraction. The materials sorption properties were assessed by using water vapour sorption isotherms coupled with NIR spectroscopy. Further, the films morphology was investigated by using scanning electron microscopy.

The presence of interactions was observed taking place between the polymeric matrix and nanofiller, between the C-O, C-OH and N-H groups of the two componetns especially via hydrogen bond interactions. Following this, a more compact structure was obtained and a good compatibility and homogenous distribution of nanofiller into the polymeric matrix was observed. Further the sorption ability of water molecules decreased with the increase of the CNC content into the polymeric matrix.

T7-O: Polydopamine Analogues from Structure to Properties

A. Petran, M. Suciu, T. Radu, J. Liebscher

Physics of Nanostructured Systems, National Institute for Research and Development of Isotopic and Molecular Technologies, Cluj-Napoca, Romania

Polydopamine is one of the most versatile polymers studied in the last 15 years due to its simple polymerization process on almost every surface and a multitude of applications [1]. These applications are in domains such biomedicine, catalysis, sensors, environment or energy and these can be improved

by their synthetic procedures or choosing the right surface [2]. Even the reaction mechanism of this polymer is not really known, there are only suppositions regarding chain length, types of interaction and covalent bonds between the monomeric units in the matrix, this is one of the main reasons why this polydopamine field is still in trend and different perspective towards better understanding of their mechanism and applications are developed [3]. Based on this catechol amine structure the class of polydopamine analogues (PDANAs) is a good candidate for [4]. These PDANAs can be obtained in three different ways: post modification of functional groups of PDA, copolymerization of dopamine with other monomers or polymers and the chemical modification of dopamine molecule and their polymerization. Our work is focused more on chemical modification of the dopamine molecule especially on the alkylic chain [5]. Having these new modified dopamine analogues, we studied their reaction mechanism as self-polymer, as coating and their applications, highlighting the importance of developing these PDANAs in the broad field of polymers.

Acknowledgment. This work was supported by a grant from the Ministry of Research, Innovation and Digitization, CNCS/CCCDI – UEFISCDI, project number PN-III-P1-1.1-TE-2021-0048, TE 131.

[1] (a) H. Lee, S. M. Dellatore, W. M. Miller, P. B. Messersmith, Science **2007**, 318 (5849), 426–30; (b) J. H. Ryu, P. B. Messersmith, H. Lee, ACS Appl. Mater. Interfaces **2018**, 10, 7523−7540.
[2] Y. Liu, Kelong Ai, L. Lu, Chem. Rev. **2014**, 114, 5057−5115
[3] J. Liebscher, Eur. J. Org. Chem. **2019**, 1–20.
[4] R. Mrowczynski, R. Markiewicz and J. Liebscher, Polym. Int. **2016**, 65, 1288–1299.

[5](a) A. Petran, N. D. Hădade, C. Filip, X. Filip, A. Bende, A. Popa, J. Liebscher, Macromol. Chem. Phys. **2018**, 219, 1700564 (1-10); (b) A. Petran, R. Mrowczynski, C. Filip, R. Turcu, J. Liebscher, Polym, Chem. **2015**, 6, 2139-2149; (c) C. Lar, S. Radu, E. Gál, A. Fălămaş, J.-Z. Szücs-Balázs, C. Filip, A. Petran, Anal. Lett. **2022**, https://doi.org/10.1080/00032719.2022.

T14-O: Cyanobacteria facing nanoplastics showed changes in the resonance Raman signal of carotenoids

I. Nesterovschi[1], R. Forfota[2,3], M. Bocaneala[2,4], A. Ciorita[2,3], S. G. Macavei[5], L. Barbu-Tudoran[2,3], S. Cinta Pinzaru[1,6]

[1]Babeș-Bolyai University, Physics Faculty, 7 "Ioan Ursu" Institute, Kogălniceanu 1, 400084 Cluj-Napoca, Romania

[2]Electron Microscopy Centre, Babeș-Bolyai University, Biology and Geology Faculty, Cluj-Napoca, Romania

[3]Integrated Electron Microscopy Laboratory, National Institute for Research and Development of Isotopic and Molecular Technologies, Cluj-Napoca, Romania

[4]Department of Molecular and Biomolecular Physics, National Institute for Research and Development of Isotopic and Molecular Technologies, Cluj-Napoca, Romania

[5]Physics of Nanostructured Systems Department, National Institute for Research and Development of Isotopic and Molecular Technologies, Cluj-Napoca, Romania

[6]RDI Laboratory of Applied Raman Spectroscopy, RDI Institute of Applied Natural Sciences (IRDI-ANS), Babeș-Bolyai University, Cluj-Napoca, Romania

Macroplastics waste from environment is constantly exposed to degradation and fragmentation processes induced by environmental conditions and solar radiation [1]. Micro- and nanoplastics interference in metabolic processes from living organisms are yet challenging to understand and manage [2].

In this Raman spectroscopy study, changes on carotenoids level on Spirulina Arthrospira platensis sp. are evidenced when cyanobacteria were exposed to polyethylene nanoparticles. This interaction has been tracked over a period of 30 days and the measurements have been run at various stages, at every 5 days along the whole period.

Fig.1 A) Image of samples with *Arthrospira platensis* exposed to nanoplastic (left) and unexposed (right) and B) cyanobacteria under microscope Leica with objective of 100X, C) typical resonance Raman spectrum of a cyanobacteria and the result of the deconvolution of the ν_1(C=C) mode at 1511 cm^{-1} from the skeletal structure of carotenoids.

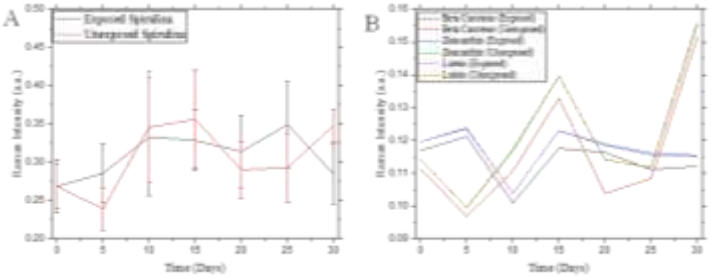

Fig.2 A) Time dependence of the intensity of the 1511 cm^{-1} RR band along the plastic exposure (days) and B) time dependence of the intensity of carotenoids band along 30 days experiment Spirulina exposed to micro- and nano-PE compared to the unexposed case.

A Cobolt DPSS air cooled laser emiting at 532 nm has been used for Raman excitation. This line produces a pre-

resonance effect on carotenoids and the resonance Raman (RR) spectra acquisition has been made at the single cell level, thus, the information about carotenoids is taken from individual cell [3].

The carotenoids known to be present in Spirulina are beta-carotene, asthaxanthin, zeaxanthin, lutein, all having very similar RR spectra. So, their differentiation is made by deconvolution of peaks, especially the one of 1511 cm^{-1} (Fig.1, C). The effects of polyethylene nanoparticles on the cell is seen by the descending tendency of the intensity of the 1511 cm^{-1} band after 25 days, which is opposite to unexposed case (Fig.2 A). Regarding the intensity of each carotenoid component showed in the Fig.2 B, there were not observed any differences in the relative concentration in time and the time dependence plot has similar trend for each component.

[1] I. Marica, M. Aluas, S. C. Pinzaru, Waste Mangm, **2022**, 144, 479-489,
[2] G. Mahadevan, S. Valiyaveettil, **2021**, Sci Rep 11,
[3] I. V. Ermakov, M. Sharifzadeh, M. Ermakova, W. Gellermann, J Biomed. Opt. **2005,** 10(6), 064028.

T14-O: Chemical structure, morphology and bioeconomy of the biogenic material derived from the invasive gastropod *Rapana venosa* shell by multi-laser Raman, XRD and SEM-EDX

D-Al. Dumitru[1], G. Lazar[1,2], F. Nekvapil[1,2], T. Tamas[3], L. Barbu-Tudoran[4], S. Cinta Pinzaru[1,2]

[1]Ioan Ursu Institute, Babeș-Bolyai University, Cluj-Napoca, România
[2]RDI Institute in Applied Natural Sciences, Babeș-Bolyai University, Cluj-Napoca, România
[3]Department of Geology, Babeș-Bolyai University, Cluj-Napoca, România

[4]*Electron Microscopy Center, Department of Experimental Biology, Babeş-Bolyai University, Cluj-Napoca, România*

The gastropod *Rapana venosa* raised high alert due to its invasive and predatory characteristics and the biogenic calcium carbonate shell, considered waste, becomes interesting for the development of new and efficient biomaterials while reducing whelk's negative impact on the Black Sea ecosystem [1]. In this paper we focus on the elucidation of shell's morphology and chemical structure, using three main analytical techniques. Further, the proposal of possible biomedical and pharmaceutical applications is aimed.

Raman spectroscopy was the main analytical tool used for the chemical characterization of *Rapana venosa* wasted biogenic material. Localized structural information on shell's inorganic component, the bands around 157, 206, 704 and 1085 cm^{-1}, indicates the presence of aragonite and calcite, having an alternating dominance from the interior towards the interior sides. The organic component determination, characterized by the bands at around 1014, 1126 and 1515 cm^{-1}, is challenging, due to the complex Raman spectral feature when multiple laser excitation is applied, suggesting multiple pigments which are not consistent with the visual color aspect of different shell parts. For example, different spectral pattern was recorded from light blue, orange-pink and dark blue (black) shell counterparts within the same specimen. Thus, Raman spectra of SERS extracts obtained from orange-pink and blue pigmented fragments indicate the presence of beta-carotene.

The information recorded by XRD diffractograms from pigmented fragments powder complements the inorganic

structure indicated by Raman spectra, of calcite and aragonite in unequal concentrations in different fragments. No diffraction peaks are present from the organic component, which sits bellow the detection limit. SEM-EDX imaging highlights shell's ultrastructure and chemical composition of Ca, C, and O, due to the presence of calcium carbonate polymorphs, with traces of Mg, Si, Al, and Fe. Presence of heavy metals, such as Fe, could turn the gastropod into an important bioindicator of the Black Sea ecosystem's pollution grade [2]. A 90.5% ratio of biogenic calcium carbonate makes the derived biomaterial suitable for use following the concept of blue bioeconomy.

Utilization of *Rapana venosa* shell could bring some advantages from an economic and ecological point of view: in bioeconomy, the reuse of the waste-considered shell for manufacturing of added-value products [3][4].

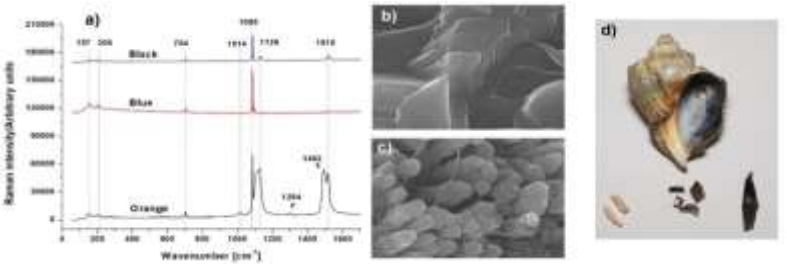

Fig. 1. a) Raman spectra acquired from interior side of orange, blue, and black fragments of the *R. venosa* shell with 532 nm excitation. b) SEM image of shell's margin. c) SEM image of shell's apex. d) Specimen of *R. venosa* with multicolored pigmentation.

[1] V. Zolotarev, Marine Ecology, **1996**, 17, 227-236.
[2] L. Bat, Ö. C. HasanWalailak J. Sci. & Tech. **2016**, 13(9), 715-728.

[3] F. Nekvapil, M. Aluas, L. Barbu-Tudoran, M. Suciu, R. A. Bortnic, B. Glamuzina, S. Cinta Pinzaru, ACS Sustaina. Chem. Eng, **2019**, 7, 16820-16827.
[4] L. Ogresta, F. Nekvapil, T. Tămaș, L. Barbu-Tudoran, M. Suciu, R. Hirian, M. Aluaș, L. Geza, E. Levei, G. Branko, S. Cîntă-Pînzaru, ACS Omega, **2021**, 6(42), 27773-27780.

T14-O: Innovative biofertilizer from two aquatic waste materials and its influence on carotenoid content in lettuce crop

F. Nekvapil[1,2,3], G. Lazar[1,2], R. Hirian[1], M. Aluas[1], M. Suciu[3,4], T. Tamas[5], L. Barbu-Tudoran[3,4], S. Tomsic[6], B. Glamuzina[6], S. Cinta Pinzaru[1,2]

[1]Ioan Ursu Institute, Babeș-Bolyai University, Cluj-Napoca, Romania;
[2]RDI Institute in Applied Natural Sciences, Babeș-Bolyai University, Cluj-Napoca, Romania
[3]National Institute for Research and Development of Molecular and Isotopic Technologies, Cluj-Napoca, Romania
[4]Electron Microscopy Centre, Babeș-Bolyai University, Cluj-Napoca, Romania
[5]Department of Geology, Babeș-Bolyai University, Cluj-Napoca, Romania
[6]Applied Ecology Department University of Dubrovnik, Dubrovnik, Croatia

Seaweed biomass and crustacean shells currently have attached costs related to waste management or beaches cleanup. Shells of blue crabs (*Callinectes sapidus*) and the green crab (*Carcinus aestuarii*) feature a nanoporous structure composed of Mg-calcite enriched also with Na, P, K, S and Cl [1]. On the other hand, the seagrass *Posidonia oceanica* biomass was shown to exhibit biostimulative properties to plants, enhance growth rate, antioxidants content or microbial resistance [2,3].

We report here the physico-chemical characterization of the novel biostimulant, a composite combining the benefits of crustaceans solid residues and seagrass extracts, using Raman spectroscopy techniques in conjunction with XRD and SEM-EDX. Further we evaluated the influence of biostimulant on lettuce crops using an innovative approach relying on the resonance Raman spectroscopy of carotenoids from lettuce leaf. SERS analysis of seaweed extracts (Fig. 1a) revealed the presence of β-carotene in both *P. oceanica* and *C. fragile*, with characteristic bands at 771, 1176, 1306, 1360, 1512, 1570 and 1647 cm^{-1} [4]. Carotenoids were analyzed in leafs of lettuce grown in presence of our biofertilizer, in (1) controlled environment and (2) outdoors, with a micro-Raman system and a portable Raman instrument (Fig. 1b), respectively, with 532 nm excitation. Measurements show increased carotenoid Raman signal relative to control in the leaves of treated specimens (Figl 1c). Our novel biofertilizer allows the development of functional food from ordinary crops using bio-based recycled materials.

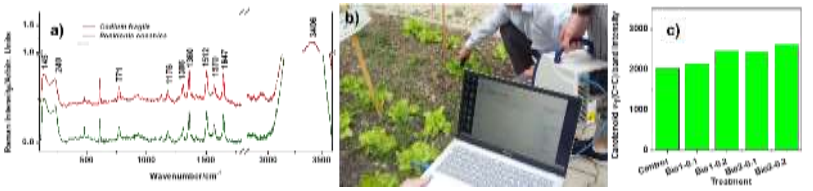

Fig. 1. a) SERS spectra of the seaweed aqueous extracts, b) on-site measurement of carotenoid content in lettuce using a portable Raman system, c) carotenoid Raman signal intensity in lettuce treated with our novel biostimulants, Bio1 - with crustacean powder loaded with *P. oceanica*, Bio2 - with *C. fragile* extract, and 0.1 and 0.2 represent % dw of biostimulant mixed into the growing soil.

Acknowledgement: This work was supported by the grant of the Romanian Ministry of Eudcation and Research, CCCDI-UEFISCDI, project number PN-III-P2-2.1-PED-2019-4777, within PNCDI III and by the grant of the Ministry of Research, Innovation and Digitalization, CNCS-UEFISCDI, project number PN-III-P1-1.1-PD-2021-0477, within PNCDI III.

[1] Nekvapil, F. et al. Sci. Rep.-UK, **2020**, 10, 3019.
[2] Benito-Gonzalez et al. Mar. Drugs **2019**, 17, 409.
[3] Cinta Pinzaru et al. J. Raman Spectrosc. **2015**, 4, :597-604.

T9-I-online: Transparent Niobium-doped titanium Dioxide Thin Films with high Seebeck coefficient for thermoelectric applications

J. M. Ribeiro[1], F. C. Correia[1], F. J. Rodrigues[1], J. S. Reparaz[1], A. R. Goni[2,3], C. J. Tavares[1]

[1]Centre of Physics of the Universities of Minho and Porto, 4804-533 Guimaraes, Portugal
[2]Institute of Materials Science of Barcelona (ICMAB-CSIC), Esfera UAB, 08193, Bellaterra, Spain
ICREA, Passeig Lluis Companys 23, 08010 Barcelona, Spain

The design of a transparent thermoelectric material is a promising technology for touchscreen displays and solar cell applications, rendering a more sustainable powering of the device. In order to enhance the thermoelectric performance, the material must have a high Seebeck coefficient, high electrical conductivity but low thermal conductivity [1]. Modifying the atomic structures of TiO_2 by deliberately introducing defects can enhance its properties to a great extent, while a cationic doping of TiO_2 has been documented to improve its electrical conductivity [2]. This work reports the

production and characterization of optically transparent Nb-doped TiO_2 thin films with enhanced thermoelectric properties deposited on glass and Si by reactive d.c. magnetron sputtering in high vacuum.

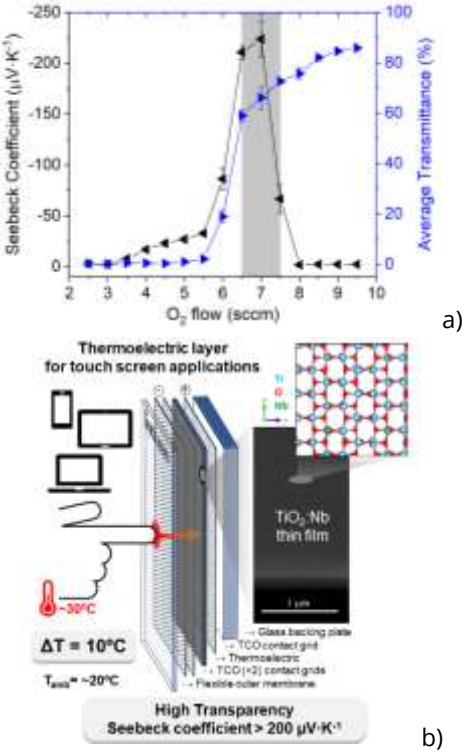

Fig.1. a) Dependence of Seebeck coefficient and average transmittance on oxygen flow; b) thermoelectric layer for touchscreen applications.

The purpose of these films is to harvest thermal energy from the environment and convert it to electrical energy. Several process parameters, such as reactive and working gas flow rate, deposition temperature, target current density and post-annealing conditions, directly affect the morphology and

crystalline structure of the thin films. Fig. 1.a) shows the Seebeck coefficient and average transmittance (400-700 nm) in relation to the oxygen flow rate during deposition. The optimization of these parameters results in thin films with thickness of 120-300 nm, maximum average optical transmittance in the visible range of 73 %, n-type electrical resistivity of 0.05 W·cm, thermal conductivity below 1.7 $W \cdot m^{-1} \cdot K^{-1}$ and a maximum absolute Seebeck coefficient of 223 $mV \cdot K^{-1}$. The resulting maximum thermoelectric power factor is 60 $mW \cdot K^{-2} \cdot m^{-1}$ and the maximum thermoelectric figure of merit is 0.014. Hence, modifying the optical, electric, thermal and thermoelectric properties of the thin films enables their suitability for applications as transparent electrodes in photovoltaic systems and touch displays, amongst other devices (Fig.1. b)).

Acknowledgements. Joana Ribeiro is grateful to the Fundação para a Ciência e Tecnologia (FCT, Portugal) for the Ph.D. grant SFRH/BD/147221/2019. Filipe Correia is grateful to the FCT, Portugal, for the Ph.D. grant SFRH/BD/111720/2015. Funding is also gratefully acknowledged from FCT/PIDDAC through the Strategic Funds project reference UIDB/04650/2020-2023 and from the Spanish Ministerio de Ciencia e Innovación (MICINN) through grants SEV-2015-0496 (FUNMAT) and CEX2019-000917-S (FUNFUTURE) in the framework of the Spanish Severo Ochoa Centre of Excellence program, and grant PID2020-119777GB-I00 (THERM2MAIN).

[1] R. Venkatasubramanian, E. Siivola, T. Colpitts, B.O. Quinn, Nature, **2001**, 413, 597–602.
[2] C.J. Tavares, M. V. Castro, E.S. Marins, A.P. Samantilleke, S. Ferdov, L. Rebouta, M. Benelmekki, M.F. Cerqueira, P. Alpuim,

E. Xuriguera, J.P. Riviere, D. Eyidi, M.F. Beaufort, A. Mendes, Thin Solid Films, **2012**, 520, 2514–2519.

T8-I-online: Application of Lipid Cubic Phases for Drug Delivery of Lipidated Peptides

B. Angelov[1], M. Drechsler[2], A. Angelova[3]

[1]Institute of Physics, ELI Beamlines, Academy of Sciences of the Czech Republic, Na Slovance 2, CZ-18221 Prague, Czech Republic,
[2]Keylab "Electron and Optical Microscopy", Bavarian Polymerinstitute (BPI), University of Bayreuth, D-95440 Bayreuth, Germany,
[3]Université Paris-Saclay, CNRS, Institut Galien Paris-Saclay UMR8612, F-91400 Orsay, France

Lipid cubic phase nanostructures are receiving increasing attention as drug delivery systems. The self-assembly organization and the stability of lipid-peptide conjugates depend both on the properties of the anchored lipid moiety and the hydrophobic-hydrophilic balance of the aminoacid sequence of therapeutic importance. A lipid-peptide conjugate of docosahexaenoic acid (DHA) and pituitary adenylate cyclase-activating polypeptide (PACAP) was synthesized for the purpose of loading and delivery by lipid cubic nanoparticles (cubosomes, Fig.1). PACAP is a neuropeptide, which plays a key role in neurogenesis and neuronal function. DHA exerts neuro-regenerative activities as well. Nanoscale structures were obtained using monoolein-based lipid mixtures. A small-angle X-ray scattering (SAXS) study was performed of the self-assembly behaviour of the lipidated peptide PACAP-DHA in aqueous medium containing monoolein-based nanoassemblies stabilized by the PEGylated amphiphile vitamin E a-tocopheryl polyethylene glycol 1000 succinate

(VPGS-PEG$_{1000}$) [1]. The results confirmed the formation of monoolein-based cubosomes with incorporated PACAP-DHA peptide. The obtained structural information is significant for the development of future nanomedicine-based strategies against neurodegenerative disorders [1,2].

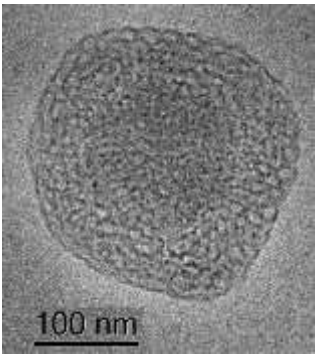

Fig. 1. A small cubosome particle of a PACAP-DHA/MO/DHA/vitamin E/VPGS-PEG1000 composition preserving the inner cubic structure upon dispersion from the bulk liquid crystalline phase

Acknowledgments. The performed research was funded by the projects “Advanced research using high-intensity laser produced photons and particles” (CZ.02.1.01/0.0/0.0/16_019/0000789) and “Structural Dynamics of Biomolecular Systems” (ELIBIO) (CZ.02.1.01/0.0/0.0/15_003/0000447) from the European Regional Development Fund. B.A. obtained a financial support from the collaborative project with JINR, Dubna (3+3 program, No. 204, item 27 from 25.03.2020). AA acknowledges a membership in CNRS GDR2088 BIOMIM network.

[1] A. Angelova, M. Drechsler, V. M. Garamus, B. Angelov, ChemNanoMat. **2019**, 5, 1381-1389.
[2] A. Angelova, B. Angelov, M. Drechsler, T. Bizien, Y. E. Gorshkova, Y. Deng, Front. Cell Dev. Biol. **2021**, 9, 617984.

T2-O-online: Atmospheric pressure plasma jet treatment of polymer filaments: correlation of plasma opto-electrical parameters and physico-chemical surface properties

A. V. Nastuta[1], I. Topala[2], V. Tiron[3]

[1]Physics and Biophysics Education Research Laboratory, Biomedical Science Department, Faculty of Medical Bioengineering, `Grigore T. Popa' University of Medicine and Pharmacy Iasi, Iasi, Romania
[2]Iasi Plasma Advanced Research Center (IPARC), Faculty of Physics, `Alexandru Ioan Cuza' University of Iasi, Iasi, Romania
[3]Research Center on Advanced Materials and Technologies, Science Department, Institute of Interdisciplinary Research, Alexandru Ioan Cuza University of Iasi, Iasi, Romania

An important patway of surface science research focuses on surface modifications of polymers for better surface adhesion, chemistry or wetability, interaction with the human body or body fluids, for biomedical purposes.
Due to its versatility, electrical gas discharges (plasmas) are widely used in biomaterials processing [1-5]. Using a 10W high voltage power supply, a dielectric barrier discharge was ignited in He (2 slm). Basic electrical diagnosis was applied for monitoring the applied vortage and discharge current. Plasma excited species were investigated through optical emission spectroscopy. Several polymeric filaments (1.75 mm diameter) surfaces: acrylonitrile butadiene styrene (ABS), polyethylene terephthalate (PET) and polylactic acid (PLA), were plasma treated in order to prove the plasma source efficency in terms of surface modifications. Atomic force microscopy, ATR-FTIR spectroscopy and static water contact angle (SWCA)

techniques were used in the surface properties modification studies, after plasma exposure. We used atomic force microscopes (Solver Pro-M), an ATR-FTIR spectrometer (Jasco FT/IR 4700) and a home made static contacte angle set-up for surface modifications investigations.

A correlation of plasma parameters, treatment time, morphological and chemical modification of plasma exposed materials was performed. These experimental findings suggest that our plasma source is suitable for modifying polymeric materials for increasing surface adhesion as well as for future biomedical applications.

Acknowledgements. The support of UEFISCDI PN-III-P1-1.1-TE-2021 no. 150 / 09.06.2022 is highly acknowledged.

[1] A.V. Nastuta, G.B. Rusu, I. Topala, A.S. Chiper, G. Popa, JOAM **2008**, 10(8), 2038.
[2] A.V. Nastuta, I. Topala, C. Grigoras, V. Pohoata, G. Popa, J. Phys. D: Appl. Phys. **2011**, 44(10), 105204.
[3] A.V. Nastuta, V. Pohoata, I. Topala, J. Appl. Phys. **2013**, 113(18), 183302.
[4] A.V. Nastuta, I. Topala, V. Pohoata, I. Mihaila, C. Agheorghiesei, N. Dumitrascu, Rom. Rep. Phys. **2017**, 69(1), 407.
[5] A.V. Nastuta, G. Popa, Rom. Rep. Phys. **2019**, 71(4), 413.

T1-O-online: Engineering of V_2O_5 thin films surface properties via the control of the growth parameters

M. P. Suchea[1,2], I. V. Tudose*[2,3], L. Draghiciu[1], C. Romanitan[1], C. Pachiu[1], R. Gavrila[1], O. A. Brincoveanu[1], I. Mihalache[1], F. Comanescu[1], R. Mueller[1], A. Dinescu[1] E. Koudoumas[2]

[1]*National Institute for Research and Development in Microtechnologies (IMT-Bucharest), 126A Erou Iancu Nicolae Street, Voluntari 077190, Romania*
[2]*Center of Materials Technology and Photonics, School of Engineering, Hellenic Mediterranean University, 71410 Heraklion, Crete, Greece*
[3]*Chemistry Department, University of Crete, 70013 Heraklion, Greece*

Since V_2O_5 is one of the best materials for many electronic applications, many efforts have been published related to the improvement of its performance for use as a sensor, an electrode, or for smart windows, supercapacitors, and photovoltaic applications. Analysing the progress that has been done in recent years, in relation to the preparation of the V_2O_5 films, the results show a complex relationship between the synthesis approach and the physical properties, the later making the material suitable for the targeted application.
This presentation concerns recent achievements on thin films surface properties engineering via the control of the growth parameters in a spray pyrolysis deposition process [1- 4]. Thin films of V_2O_5 with different thickness were grown onto different types of substates by air carrier spray pyrolysis, using different precursor quantities and post-deposition annealing. The evolution of the surface properties was studied by SEM and AFM (Fig.1). Additionally, structural XRD and Raman spectroscopy as well as UV-vis optical characterization were performed. It was observed that the V_2O_5 thin films surface

properties can be tailored via the control of the growth parameters as well as the substrate type.

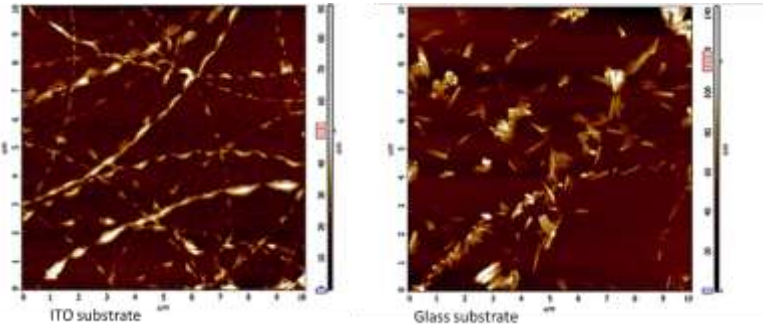

Fig. 1. Examples of AFM images of V_2O_5 thin films grown on two various substrates.

As a result, a completely different growth of the V_2O_5 material can appear, resulting on outstanding structural and morphologic features with important consequences on the V2O5 application.

Acknowledgments. This research was partially financed by "MICRO-NANO-SIS PLUS" core Programme and MicroNEx, Contract nr. 20 PFE din 30.12.2021, financed by the Ministry of Research, Innovation and Digitalization through Program 1—Development of the National R & D System, Subprogram 1.2—Institutional Performance—Projects for Institutional Excellence.

[1] K. Mouratis, V. Tudose, C. Romanitan, C. Pachiu; O. Tutunaru, M. Suchea, S. Couris, D. Vernardou, K. Emmanouel, Materials, **2020,** 13, 3859.
[2] C. Pachiu, M. Carp, K. Mouratis, I.V.Tudose, C. Romanitan, O. Tutunaru, S. Couris, E. Koudoumas, M.P. Suchea, Intern. Semic. Conf. (CAS), **2020**, pp. 191-194.

[3] C. Romanitan, I.V. Tudose, K. Mouratis, M.C. Popescu, C. Pachiu, S. Couris, E. Koudoumas, and M. Suchea, Phys. Status Solidi A, **2022**, 210043.
[4] K. Mouratis, I.V. Tudose, Bouranta, A. C. Pachiu, C. Romanitan, O. Tutunaru, S. Couris, E. Koudoumas, M. Suchea, Nanomaterials, **2020**, 10(12):2397.

T7-P-online: Antimicrobial nanocomposite materials for food packaging applications -fabrication and properties

A. Bouranta[1], I. V. Tudose[1], C. Romanitan[2], C. Pachiu[2], I. Rosca[3], K. Petrotos[4], S. Zaoutsos[5], G. A. Fragkiadakis[6], M. P. Suchea[1,2], E. Koudoumas[1,7]

[1]Center of Materials Technology and Photonics, School of Engineering, Hellenic Mediterranean University, 71410 Heraklion, Crete, Greece
[2]National Institute for Research and Development in Microtechnologies (IMT-Bucharest), Bucharest, 023573, Romania
[3]Petru Poni" Institute of Macromolecular Chemistry, 41A Grigore Ghica Voda Alley, 700487, Iasi, Romania
[4]Department of Agriculture-Agrotechnology, Laboratory of Food and Biosystems Engineering, University of Thessaly, Geopolis of Larissa, 41500, Greece
[5]Department of Energy Systems, School of Technology, University of Thessaly, Larissa, 41500, Greece
[6]Department of Nutrition & Dietetics Sciences, School of Health Sciences, Hellenic Mediterranean University, 72300 Sitia, Crete, Greece
[7]Department of Electrical and Computer Engineering, School of Engineering, Hellenic Mediterranean University, 71410 Heraklion, Crete, Greece

The food industry faces numerous challenges to assure provision of safe tasty food with extended lifetime and showing long-term preservation of high-quality. Research and development of antimicrobial materials for food applications have provided active antibacterial packaging technologies that

are able to meet these challenges. Furthermore, consumers expect and demand sustainable packaging materials that would reduce environmental problems associated with plastic waste.

In that respect, polylactic acid (PLA) is an excellent biodegradable matrix and can be effectively used in fabricating composite food packaging. Generally, polymeric composite materials can be fabricated with various techniques including printing and roll-milling techniques. The present work regards composite materials that were produced by hot roll-mill mixing two kinds of encapsulated natural extracts with polylactic acid (PLA) in a pellet form. The composite materials were characterized using microscopy techniques, XRD and Raman spectroscopy and their antimicrobial activity was evaluated using a modified Kirby-Bauer methodology. Composite materials with good antimicrobial efficiency depending on the type and the concentration of the active material were obtained.

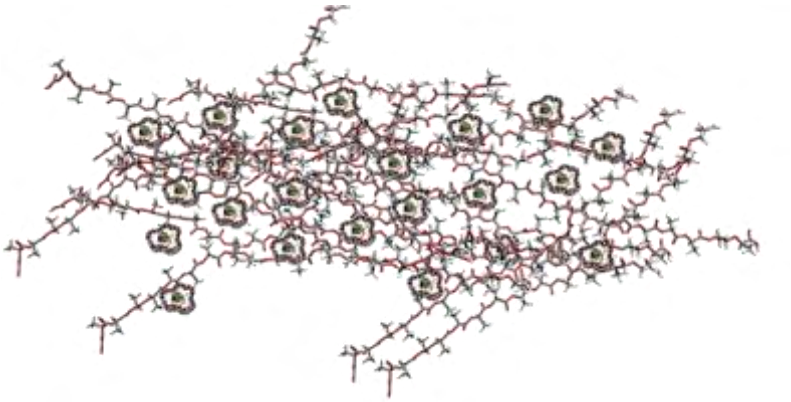

Fig. 1. Schematic representation of encapsulated natural extracts-PLA composite material.

Acknowledgments. This research was funded by the project NanoBioPack which is co-financed by the European Union and Greek national funds through the Operational Program Competitiveness, Entrepreneurship and Innovation, under the call 'Specific Actions, Open Innovation for Industrial Materials' (project code: T6YBП-00307). M.P.S. contribution was partially financed by the Romanian Ministry of Research, Innovation and Digitalisation thorough „MICRO-NANO-SIS PLUS" core Programme and MicroNEx, Contract nr. 20 PFE din 30.12.2021.

T4-P-online: Left-handed properties of the nanocrystaline ferromagnetic microwires for GHz shielding applications

G. Ababei, I. Murgulescu, V. Dobrea, N. Lupu

National Institute of Research and Development for Technical Physics, Iasi, Romania

Recently, the properties of ferromagnetic microwires have been investigated intensively to develop artificial structures - known as metastructures - with left-handed properties, for high frequency shielding applications [1-3].

The aim of this work was to study the left-handed properties of nanocrystaline $Fe_{73.5}Cu_1Nb_3Si_{13.5}B_9$ magnetic microwires arranged in parallel configurations as free-standing systems to develop new metastructures for GHz shielding applications. The diameter, interwires distance and the microstructure influence on the left-handed properties of the new metastructures were investigated, too.

$Fe_{73.5}Cu_1Nb_3Si_{13.5}B_9$ microwires with diameters of 60 μm and 90 μm were obtained by cold-drawing process, by successive reductions of the diameter of an amorphous microwire with the initial diameter of 130 μm, prepared by in-rotating-water

spinning method. The nanocrystalline structure of the microwire was induced by annealing at 500^0C.

The left-handed characteristics of the metastructures were determined by measuring the reflection, S_{11}(dB), and the transmission, S_{21}(dB), coefficients by using a WR90 type X-band microwave guide connected to a PNA L5230 Agilent Vector Network Analyzer after a SOLT (short-open-load-through) calibration of the set-up, in the frequency range 8.2÷12,4 GHz. The magnetic field, H, applied parallel with the long axis of the microwires was ranging from 0 to 32 kA/m [4]. Interwire distances ranging from 1 mm to 3 mm were chosen to achieve a negative dielectric permittivity of the structure [5]. The metastructures properties are dependent on their geometrical parameters and on the intrinsic properties of the microwires, offering flexibility for achieving different engineering requirements.

The absorbtion window of the metastructure with 3 mm interwire distance and 60 μm microwire diameter is obtained from 10.5 GHz to about 11.35 GHz. For the metastructures with the same interwire distance, but 90 μm microwire diameter, the frequency interval of absorbtion window is decreasing with about 1 GHz. By decreasing the interwires distance from 3 mm to 1 mm, for the same diameter of the microwires, the absorbtion window of the metastructures is increasing with about 0.5 GHz.

Acknowledgments. Financial support by the NUCLEU Program (PN 19 28 01 01) and PFE Program (Contract # 5 PFE/2022) is gratefully acknowledged

[1] H. Garcia-Miquel, J. Carbonell, V.E. Boria, J. Sanchez-Dehesa, Appl. Phys. Lett. **2009**, 94, 054103.

[2] M. Vasquez, A.L. Adenot-Engelvin, J. Magn. Magn. Mater. **2009**, 321, 2066–2073.
[3] X. Qin, H.X. Peng, M.H. Phan, L.V. Panina, M. Ipatov, A. Zhukov, Sensors Actuat. A: Phys. **2012**, 178, 118-125.
[4] G. Ababei, C.S. Olariu, N. Lupu, and H. Chiriac, J. Appl. Phys. **2015**, 117, 17A502.
[5] J.B. Pendry, A.J. Holden, W.J. Stewart, and I. Youngs, Phys. Rev. Lett. **1996**, 76, 4773-4776.

T5-P-online: Copper complexes of salen-type ligand containing siloxane segment: synthesis and structural characterization

A. Soroceanu

Inorganic Polymers Department, "Petru Poni" Institute of Macromolecular Chemistry Iasi, Romania

A series of mononuclear copper(II) salen-type complexes containing a disiloxane unit derived from 2-hydroxybenzaldehyde, 3,5-di-bromo-2-hydroxybenzaldehyde and 1,3-bis(3-aminopropyl)tetramethyldisiloxane, prepared *in situ* in the presence of copper(II) salt or by direct reaction between copper(II) salt and a presynthesized Schiff bases.

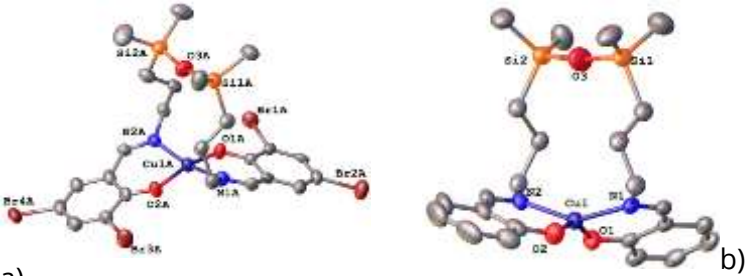

a) b)

Fig.1. Mononuclear copper (II) salen-type complexes:
a) CuL; b) CuL'.

Complexes proved to be soluble in a wide range of organic solvents, from dichloromethane to dimethylformamide.
The compounds were characterized by spectroscopic methods (IR, ^{1}H NMR) and the structures of compounds have been determined by single-crystal X-ray diffraction analyses (Fig. 1 a, b). The coordination polyhedron of the central atom could be characterized as a distorted tetrahedron.

Acknowledgements: This work was supported by a grant of the Ministry of National Education, CNCS – UEFISCDI, project number PN-III-P1-1.1-PD-2021-0687 (Contract 33/2022).

T5-P-online: Preparation, surface morphology and optical properties of $CdGa_2S_4$/native oxide nanostructures

V. Sprincean[1], D. Untila[1,2], V. Gurau[1], L. Leontie[3], S. Gurlui[3], C. Doroftei[4], A. Carlescu[4], F. Iacomi[3], M. Caraman[1]

[1]Moldova State University, A. Mateevici, 60, MD-2009, Chisinau, Republic of Moldova
[2]Technical University of Moldova, Stefan cel Mare si Sfint bd., 168, MD-2004, Chisinau, Republic of Moldova
[3]Faculty of Physics, Alexandru Ioan Cuza University of Iasi, Bulevardul Carol I, Nr. 11, RO-700506 Iasi, Romania
[4]Integrated Center for Studies in Environmental Science for the North-East Region (CERNESIM), Department of Exact Sciences, Institute of Interdisciplinary Research, Alexandru Ioan Cuza University of Iasi, Bulevardul Carol I, Nr. 11, RO-700506 Iasi, Romania

This work investigates the chemical and elemental composition, as well as optical properties in the region of fundamental absorption edge of the composite of micro- and nanocrystallites of Ga_2O_3, CdO and $CdGa_2O_4$ formed on the surface of $CdGa_2S_4$ crystals by heat treatment in normal

atmosphere, at temperatures below the melting point of this compound.

Chemical and elemental composition of the surface layer of $CdGa_2S_4$ crystal was determined from the analysis of XRD patterns and EDXS spectra. The examined layer shows a composite of $CdGa_2O_4$, with a small excess of Ga_2O_3 and CdO. As revealed by SEM analysis, the surface morphology of $CdGa_2S_4$/native oxide structure is characterized by a composition of nanowires, nanolamellas and micro- and nanotowers. The submicrometer-sized components of this layer are able to produce intense scattering the incident light.

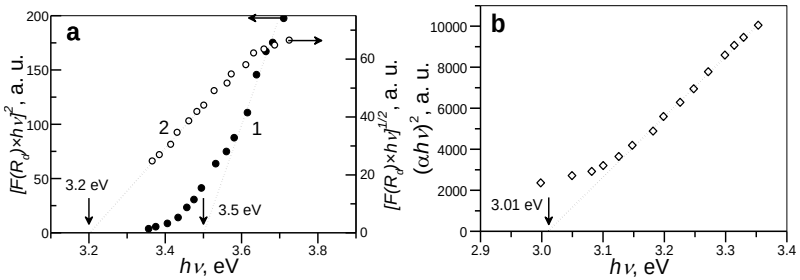

Fig. 1. a) Dependence of $[F(R_d)\times h\nu]^n$ function on photon energy for the native oxide nanocomposite layer on $CdGa_2S_4$ substrate: curve 1 – direct optical transitions (n=2), curve 2 – indirect optical transitions (n=1/2).
b) Optical band gap of $CdGa_2S_4$ crystals.

The absorption edge of $CdGa_2O_4$ was studied by measurements of the spectral dependence of diffuse reflection coefficient, R_d, using the Kubelka-Munk function $[F(R_d)]$ [1] in the spectral range of 330–370 nm, where R_d increases from 0.24 to 0.60. The character of the optical transitions was determined from the analysis of $[F(R_d)\times h\nu]^n$=f($h\nu$) dependence (Fig. 1) [2].

In the energy range of 3.55–3.85 eV, the absorption edge is described by direct optical transitions with the bandgap E_{gd}=3.5 eV, while at lower photon energies, by indirect optical transitions with E_{gi}=3.2 eV (Fig. 1, a). The absorption threshold of $CdGa_2S_4$ crystals is determined by direct optical transitions with a bandgap of ~3.01 eV (Fig. 1, b).

Both the $CdGa_2S_4$ compound and the oxide layer on $CdGa_2S_4$ substrate are photoluminescent materials in the visible range. The PL spectra of this material, both at room temperature and 80 K, fall in the wavelength range of 450–750 nm (Fig. 2).

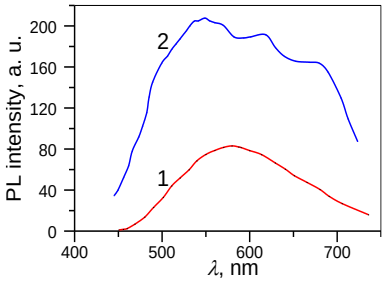

Fig. 2. PL spectra of the oxide layer on $CdGa_2S_4$ substrate at: room temperature (1) and 80 K (2).

At room temperature, the PL maximum is located at 580 nm. At 80 K, 4 particularities are emphasized at 500 nm, 545 nm, 620 nm and 630 nm. Their nature is analyzed from the dependences of PL intensity on the PL excitation intensity and from thermal quenching of photoluminescence.

[1] A. B. Murphy. Sol. Energ. Mat. Sol. C. **2007**, 91 (14), 1326.
[2] S. Kumar, C. Tessarek, S. Christiansen, R. Singh. J Alloy Compd. **2014**, 587, 812.

T5-P-online: Preparation and optical properties of Eu-doped β-Ga_2O_3 neoformations

D. Untila[1,2], I. Evtodiev[1,3], V. Sprincean[1], L. Leontie[4], S. Gurlui[4], N. Spalatu[5], A. Carlescu[6], F. Iacomi[4], M. Caraman[1]

[1]Moldova State University, A. Mateevici, 60, MD-2009, Chisinau, Republic of Moldova
[2]Technical University of Moldova, Stefan cel Mare si Sfint bd., 168, MD-2004, Chisinau, Republic of Moldova
[3]University of European Political and Economic Studies "Constantin Stere", Stefan cel Mare si Sfint bd., 200, MD-2004, Chisinau, Moldova
[4]Faculty of Physics, Alexandru Ioan Cuza University of Iasi, Bulevardul Carol I, Nr. 11, RO-700506 Iasi, Romania
[5]Tallinn University of Technology, Department of Materials Science, Ehitajate tee, 5, EE-19086 Tallinn, Estonia
[6]Integrated Center for Studies in Environmental Science for the North-East Region (CERNESIM), Department of Exact Sciences, Institute of Interdisciplinary Research, Alexandru Ioan Cuza University of Iasi, Bulevardul Carol I, Nr. 11, RO-700506 Iasi, Romania

The β-Ga_2O_3/GaSe:Eu^{3+} structures were obtained by heat treatment in air of single crystalline GaSe:Eu (0.5–3.0 at. %) plates, at temperatures up to 950 °C. Through 6–12 h thermal treatment, both the flat surface of GaSe(0001):Eu plates and their edge are covered with a layer consisting of β-Ga_2O_3 nanoplates and nanowires with lengths in the micrometer range (Fig. 1).

Presence of Eu in GaSe single crystals is manifested by the enhancement of several XRD lines in 2ϑ angular ranges of 28–35 ° and 48–55 °. These reflections are also observed in the XRD patterns of β-Ga_2O_3/GaSe:Eu micro- and nanocomposite structures, in which, at the same time, the characteristic reflections of Ga_2O_3 are also present.
Raman spectra of the layer composed of β-Ga_2O_3 nanowires and nanolamellas, obtained by heat treatment in air of GaSe

plates doped with 1.0 and 3.0 at. % Eu, in the wavelength range of 80–800 cm^{-1}, contain 11 bands characteristic of *β*-Ga_2O_3 phase. As resulted from EDX analysis, Eu concentration in *β*-Ga_2O_3 layers coincides with that in primary material (GaSe:Eu).

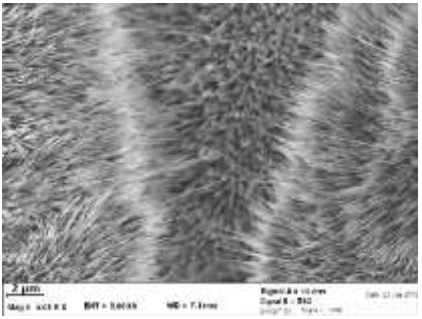

Fig. 1. SEM image of the surface of Ga_2O_3 layer obtained by 12 h thermal treatment in air of GaSe:Eu (3 at. %) plates, at 1100 K.

The absorption edge of *β*-Ga_2O_3 layer (nanowires and nanolamellas) was determined from the analysis of diffuse reflectance spectra, using the spectral dependence of the Kubelka-Munk function. The direct band gap of nanoformations decreases from 4.68 eV for undoped *β*-Ga_2O_3 to 4.54 eV in the case of Ga_2O_3:Eu (3 at. %).

PL spectra of *β*-Ga_2O_3:Eu^{3+} nanoformations cover the wavelength range of 390–750 nm. In the 390–520 nm range, a complex PL band is present, with a maximum located at 450 nm. PL bands of Ga and O vacancies in *β*-Ga_2O_3 are also present in this spectral range. PL emissions in the wavelength range of 520–750 nm can be interpreted as $^5D_{0\text{-}4} \rightarrow {}^7F$ transitions of Eu^{3+} ion. In this domain, a band with a maximum at 614 nm prevails, determined by $^5D_0 \rightarrow {}^7F_2$ transition of Eu^{3+} ion. A similar structure of orange PL emission is also characteristic for the electroluminescence spectrum of *β*-Ga_2O_3:Eu^{3+} layers on GaAs substrate [4].

[1] Z. Chen, K. Saito, T. Tanaka, et. al., J. Crist. Growth **2015**, 430, 28–33.
[2] N. F. Santos, J. Rodrigues, A. J. S. Fernandes, et. al., Appl. Surf. Sci. **2012**, 258 (23), 9157–9161.
[3] J. Zhao, W. Zhang, E. Xie, et. al., Appl. Surf. Sci., **2011**, 257, 11, 4968–4972.
[4] Z. Chen, D. Guo, P. Li, et. al., Appl. Phys. Express, **2019**, 12, 6, 061009.

T6-P-online: Graphene oxide based electronic memory devices

I. Salaoru[1], M. Ignat[2], A. Muhammad[1], F. Iacomi[3], S. Paul[1]

[1] Emerging Technologies Research Centre, De Montfort University, Hawthorn Building, The Gateway, Leicester LE1 9BH, UK
[2]Faculty of Chemistry, Alexandru Ioan Cuza University of Iasi, 11 Carol I Bvd., Iasi, 700506, Romania
[3]Faculty of Physics, Alexandru Ioan Cuza University of Iasi, 11 Carol I Bvd., Iasi, 700506, Romania

In today's world, the electronic memory elements are the essential components of all electronic devices from computers to toys and from heath monitors to space technology. Numerous candidates for emerging electronic memory technologies such as ferroelectric (FeRAM), phase-change random access memory (PCRAM), magneto-resistive (MRAM), resistive random-access memory (ReRAM) and organic memory have been investigated by a number of research groups worldwide [1-5]. Recently, functional graphene-based materials (GBMs), such as: graphene oxide [6], hydrogenated graphene, combinations of graphene oxide with polymers or metal nanoparticles, offer a promising alternative to other classes of materials as the active core for solid state memory devices. In light of this, here, we investigate graphene oxide (GO) as a functional active layer of a two therminal memory

devices. GO based memory devices are fabricated by depositing graphene oxide between two metal electrodes. The primary aim is to produce devices that exhibit two distinct electrical conductance states when a voltage is applied. These two states can be viewed as the realisation of non-volatile memory.

T9-P-online: Tribological behavior, microhardness properties and surface morphology of a hard chromium coating prepared by electrodeposition on 17-7PH stainless steel

S. Djemmah[1,2], M. Voue[2], Y. Madi[1], D. Allou[3], A. Haddad[3]

[1]*University of Science and Technology Houari Boumediene, P.O. Box 32, Algiers (Algeria)*
[2]*University of Mons, Physics of Materials and Optics Unit (LPMO), Research Institute for Materials Science and Engineering, Mons (Belgium)*
[3]*Research Center in Industrial Technologies (CRTI), P.O. Box 64, Cheraga, Algiers (Algeria)*

The aim of this study is to improve some properties of the 17-7PH stainless steel in order to resist better in severe conditions. To that purpose, a hard chromium deposit was performed from trivalent (Cr III) electrolyte solution onto the steel surface. The mechanical, tribological and morphological characterization of the Cr-deposit were performed. More precisely, in this study, the coating experiments were carried out from a trivalent chromium bath (Cr III) at temperature of 30 ± 1 ◦C, current density of 0.3 A/cm2 and a treatment period of 2 hours. Our deposition method yields a 50 µm-thick metallic coating showing a significant adhesion between the

substrate and the Cr layer. Micrographic characterization revealed the apparition of two adherent layers exhibiting micro-hardness values of 745 HV0.01 and 136 HV0.01, respectively. Furthermore, micro-cracks were found to exist in the Cr-deposit.

The EPMA results revealed that the hard chromium deposits accommodate a mixed morphology dispersed around the substrate, containing metallic chromium Cr and oxides like Cr2O3. Moreover, the Cr-deposit showed surface roughness confirmed with statistical studies, in addition to a low friction coefficient. Subsequently, the results of the tribological analysis, micro- hardness experiments and the surface parameters roughness show that a correlation between these parameters exists: a low average roughness of the Cr-deposit (Ra) and a high micro-hardness value correlates with the low friction coefficient, low value of the wear rate and hence an efficient tribological behavior.

T5-P-online: Ge_xSn_{1-x}:H thin film with high spectral response in SWIR range deposited by magnetron sputtering

A. Slav[1], C. Palade[1], I. Stavarache[1], G.A. Lungu[1], M. Braic[2], S. Iftimie[3], V.S. Teodorescu[1], M.L. Ciurea[1], T. Stoica[1]

[1]National Institute of Materials Physics, 405A Atomistilor St., 77125 Magurele, Romania.

[2]National Institute for Optoelectronics, 409 Atomistilor St., 77125 Magurele, Romania.

[3]University of Bucharest, Faculty of Physics, 405 Atomistilor Street, 077125 Magurele, Romania

The crystalline GeSn binary alloys have been extensively investigated for their application in Si-compatible integrated photonic devices due to their advantage in extending Ge's NIR sensitivity and obtaining a transition to direct bandgap IV-group semiconductors with higher optoelectronic properties [1,2]. The increased Sn concentration above 8% in relaxed GeSn results in the transition from the indirect for Ge to direct bandgap GeSn, where the optical transitions occur band-to-band with higher probability, and the photo-detection is increased [3]. However, the structural defects in amorphous or nanocrystalline GeSn induce sharp deterioration of photoelectric properties. By hydrogenation, the GeSn layers are improved by reducing micro-voids and dangling bonds defect density [4]. Thus, the structural defects in Ge_xSn_{1-x}:H with 6-10% Sn are healed by hydrogen bonding, and photosensitivity extends in SWIR spectral range. The crystalline growth of the GeSn layer is difficult due to low solid solubility below 1 at. % of the the large lattice mismatch between α – Sn (6.4700 Å) and Ge (5.6512 Å) and also the strong segregation of Sn. Therefore, obtaining crystalline layers of GeSn requires the non-equilibrium growth processes such as molecular beam epitaxy, chemical vapor deposition, and magnetron sputtering (MS). The deposition Ge_xSn_{1-x}:H is performed by reactive MS using hydrogen diluted in argon as working gas with various partial pressure. Some samples are post-deposition annealed by rapid thermal annealing method at 350 ^oC – 550 ^oC in 20% H_2 diluted in Ar atmosphere to improve the nano-crystalline state of Ge_xSn_{1-x}. Morphology, crystallinity and composition of Ge_xSn_{1-x} films are investigated by X-ray diffraction, X-ray photoelectron spectroscopy, energy-dispersive X-ray spectroscopy, high-

resolution transmission electron microscopy, Raman and FT-Ir spectroscopy. The optical absorption spectra are obtained using the transmission-reflection data measured within the wavelength range of 0.6 – 3 μm. The photoconductive properties are evaluated by measurement of spectral photocurrent and dark current at different temperatures and different bias voltages.

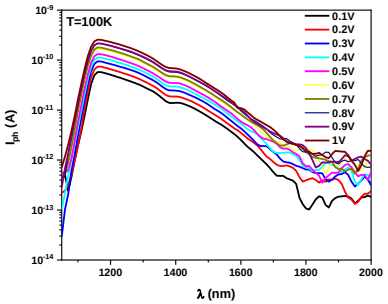

Fig.1. Spectral photocurrent for Ge_xSn_{1-x}:H layers deposited at 200 ^oC in 30%H.

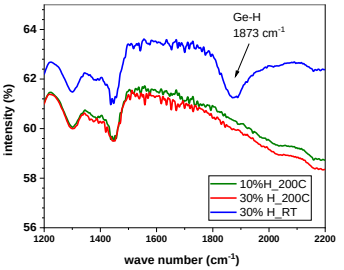

Fig.2. Transmittance FT-IR spectra for Ge_xSn_{1-x}:H layers.

Acknowledgments. This work was supported by a grant of the Romanian Ministry of Education and Research, CCCDI - UEFISCDI, project number PN-III-P2-2.1-PED-2019-4468 and project number PN-III-P1-1.1-PD-2019-1038, within PNCDI III; NIMP Core Project 21N/2019.

[1] K.A. Mader, A. Baldereschi, Solid State Commun., **1989**, 69 (12), 1123-1126.
[2] R. A. Soref, L. Friedman, Superlat. Microstruct., **1993**,14 (2–3), 189-193.
[3] J. Zheng et al., Applied Phys. Letter, **2016**, (108), 033503.
[4] Jaehyun Cho et all, J. Nanosci. Nanotechnol., **2016**, 16, 4870-4874.

T7-I-online: Ordering of polymers: a powerful tool to exploit the structure-property relationship

I. Botiz

Interdisciplinary Research Institute on Bio-Nano-Sciences, Babes-Bolyai University, Cluj-Napoca, Romania

A plethora of technological applications that currently shape the development of our society are based on polymeric materials. Whether we consider industries such as automotive and aeronautics, or insulator and semiconductive materials, or various medical devices and antibacterial applications, polymers have demonstrated their tremendous use. Mostly, this is due to the continuous development of polymer processing methods that allow us to control the structure-property relationship, and thus, the final properties of polymers. Here, we focus on several processing methods utilized to alter the properties of various polymers and blends in films and solutions by establishing control over the chain arrangements and conformation.

Acknowledgments. The author acknowledges the financial support of the Romanian National Authority for Scientific Research and Innovation, CNCS – UEFISCDI, project no. PN-III-P1-1.1-TE-2021-0388.

T7-O-online: Fabrication and properties of GNPs-PDOT:PSS nanocomposite films by air-carrier spray pyrolysis

I.V. Tudose[1], T. Alupului[2], L. Punga[2], G. Bulai[3], M. Dobromir[4], G. G. Rusu[2], S. Teodoroff[2], G. Tifui[2], S. Tascu[5], D. Timpu[5], E-L. Ursu, E. Koudoumas[1,7], M.P. Suchea[1,8,9], F. Iacomi[2]

[1]Center of Materials Technology and Photonics, School of Engineering, Helenic Mediterranean University, Heraklion, Greece
[2]Faculty of Physics, Alexandru Ioan Cuza University of Iasi, Romania
[3]CERNESIM, Alexandru Ioan Cuza University of Iasi, Romania
[4]Department of Research, Faculty of Physics, Alexandru Ioan Cuza University of Iasi, Romania
[5]RAMTECH, Alexandru Ioan Cuza University of Iasi, Romania
[6]Petru Poni Institute of Macromolecular Chemistry, Iasi, Romania
[7]Department of Electrical and Computer Engineering, School of Engineering, Mediterranean University, Heraklion, , Greece
[8]National Institute for Research and Development in Microtechnologies-IMT Bucharest, Romania
[9]Chemistry Department, University of Crete, Heraklion, Greece

Poly(3,4-ethylenethiophene):poly(styrene sulfonate), PEDOT:PSS, due to its high electrical conductivity, high stability and commercial availability is largely used in composite materials fabrication [1,2]. Graphene/PEDOT:PSS composites were obtained by various methods and the performed studies concluded that the important factors in improving composites properties are graphene dimension, orientation, interaction and dispersion [3,4].

We studied the fabrication of graphene/PEDOT:PSS nanocomposite layers by air-carrier spay pyrolysis, using commercially available graphene nanoplatelets (GNPs).

A precursor GNPs solution was prepared by dispersing 0.2g GNPs in 19 ml distilled water and 1ml Tween 20 solution. The

solution was sonicated for 30 min and used for preparation of deposition solutions (0.0 – 0.8 ml solution GNPs in 3ml 1% PEDOT:PSS solution).

By spraying the deposition solutions onto clean glass substrates heated at 150 °C, layers of a thickness of 1µm were obtained. The so obtained layers were structurally and morphologically investigated by using XRD, AFM, SEM and XPS methods. It was evidenced that the process of GNPs intercalation reduces the PSS/PEDOT ratio and that the GNPs exfoliation is more efficient when higher contents of disperdion solution is used.

The investigation of optical and electrical properties established the layer transmittance decreases nonlinearly with the increase in GNPs content and the electrical conductivity increases linearly (Fig.1.a, b).

[1] C. Teng et al. Carbon, **2011**, 49, 5107-5116.
[2] R. Atif, I. Shyha, F. Inam, Polymers, **2016**, 8, 281.
[3] R. K. Layek, A. K. Nandi, Polymer, **2013**, 54, 5087-5103.
[4] S.K. Jebur, A. J. Braihi, A. S. Hassan, Mater. Today:Proc., **2022**, 49, 7, 1733-2740.

Thursday, September 15, 2022

08:00	**Plenary Session** HALL 1-University of Dubrovnik
10:20	**Coffee break**
10:50	**Plenary and Invited Session** Hall 1
13:25	**Closing Ceremony** HALL 1
13:55	**Lunch**

PL-online: Femtosecond laser micro- and nano-structuring of polymers for optical and thermal applications

V. Mizeikis

Research Institute of Electronics, Shizuoka University, Hamamatsu, Japan

Ultrashort femtosecond and picosecond laser pulses are widely used for the fabrication of 2D and 3D structures in various materials using additive or subtractive local photomodification of the initial homogeneous material by a tightly focused laser beam [1]. Ultrafast laser structuring enables realization of maskless 3D lithography with very high spatial resolution, reaching deeply into the sub-micrometric region (Fig. 1(a)). This approach can be especially fruitful in organic photo-polymerizable materials, where new optical and thermal functionalities can be created exclusively via laser structuring, i.e., without the need to tailor these cheap and abundant materials on the atomic or molecular level. Here we report on the fabrication of 3D micro- and nanostructures in hybrid organic-inorganic photoresist SZ2080[2] and organic photoresist SU-8[3]. Using tightly focused femtosecond laser beam, whose focal region is scanned in the bulk of the initial material along the desired trajectory, two-photon polymerization is induced at the focus, and fine 3D exposure patterns are created in the photoresist. Subsequently, they become transformed into 3D micro- and nanostructures using chemical development (Fig. 1(a)). We will describe several classes of polymeric structures exhibiting novel optical and thermal functionalities arising from the laser structuring: 3D

photonic crystals [1] (Fig. 1(b), electromagnetic metasurfaces [6] (Fig. 1(c), and environmental sensors [7] (Fig. 1(d)).

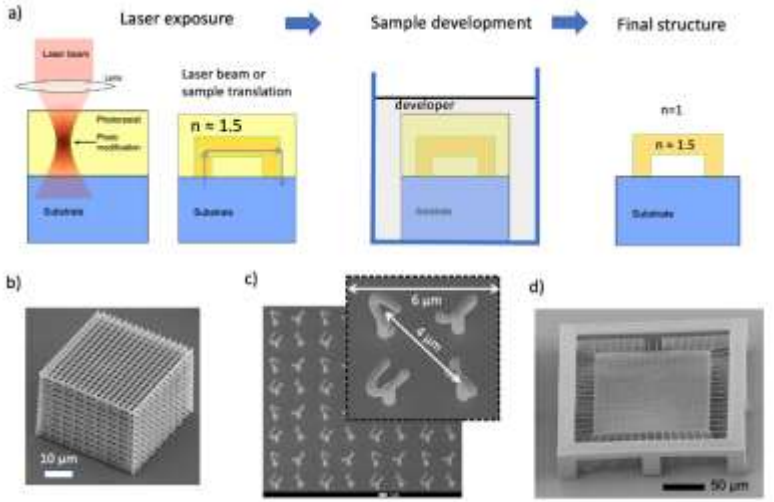

Fig. 1. Laser structuring and its applications: a) principle of laser fabrication based on two-photon polymerization, examples of various structures, b) photonic crystal, c) optical metasurface, d) environmental sensor structure.

[1] M. Malinauskas et al., Light: Sci.&Appl. **5**, e16133 (2016).
[2] A. Ovsianikov et al., Las. Chemistry **2008**, 493059 (2008).
[3] https://kayakuam.com/products/su-8-photoresists/
[5] M. Malinauskas et al., Light: Sci.&Appl. **2016**, 5, e16133.
[6] I. Faniayeu, V. Mizeikis, Opt. Mater. Express, **2017**, 7, 1453-1410 (2017).
[7] S. Rekstyte, D. Paipulas, V. Mizeikis, Opt. Lett., **2019**, 44, 4602-4604.

PL: Growth of metallic nanopatterns and superconducting nanodevices by Focused Ion Beam (FIB)

J. M. De Teresa[1,2], A. Salvador-Porroche[1], A. T. Escalante-Quiceno[1], F. Sigloch[1], L. Herrer[1], P. Orus[1], S. Sangiao[1,2], C. Magen[1,2], P. Cea[1,2], P. Philipp[3]

[1]Instituto de Nanociencia y Materiales de Aragón (INMA, CSIC-Universidad de Zaragoza), Zaragoza, Spain,
[2]Laboratorio de Microscopías Avanzadas (LMA, Universidad de Zaragoza), Zaragoza, Spain,
[3]Advanced Instrumentation for Nano-Analytics (AINA), MRT Department, Luxembourg Institute of Science and Technology (LIST), Belvaux, Luxembourg

Focused Ion Beam (FIB) techniques are very relevant to pattern materials down to the nanoscale, either through the local removal of material or through the change of physical properties produced by the ion beam. Moreover, in combination with precursors, the ion beam gives rise to the growth of nanomaterials, a technique known as Focused Ion Beam Induced Deposition (FIBID). Unfortunately, FIBID is a slow technique, which limits its applicability. In the first part of our contribution, two strategies that improve the throughput of FIBID by a few orders of magnitude will be shown. The first one is based on the condensation of precursors delivered through a gas injection system onto a cooled substrate (Cryo-FIBID) [1, 2]. The second one is based on the ion-induced dissociation of spin-coated metalorganic films, in particular Palladium Acetate films [3], as sketched below (Fig. 1). Both strategies have been applied to produce metallic nanopatterns with high lateral resolution and fast growth rate, and some applications will be shown. In the second part of the talk, our work on the growth of superconducting

nanostructures by FIBID will be presented. In particular, the use of the $W(CO)_6$ precursor has been found to be very convenient to produce FIBID-based nanodevices [4].

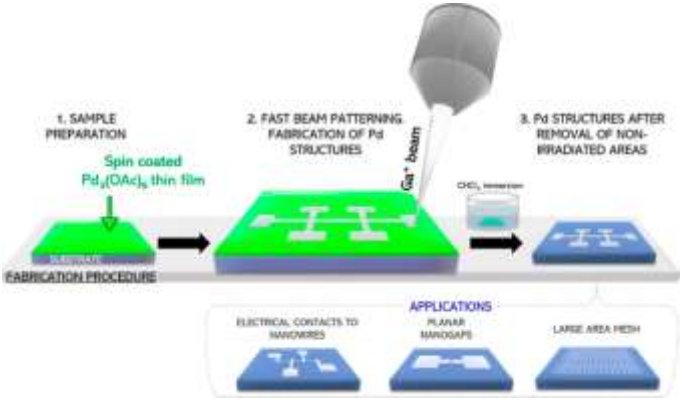

Fig. 1. Method for high-throughput growth of Pd micro- and nanostructures and the applications explored [3].

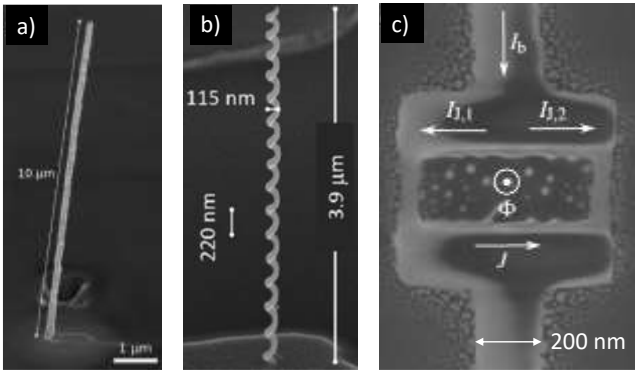

Fig. 2. W-C superconducting nanostructures by Focused Ion Beam Induced Deposition: a) using Ga^+-FIB [5]; b) using He^+-FIB [6]; c) nanoSQUID using Ga^+-FIB. [7].

Our recent efforts to grow out-of-plane superconducting nanostructures [5, 6] and in-plane nanoSQUIDs [7] will be presented and the potential applications will be discussed.

[1] J. M. De Teresa et al., Micromachines **2019**, 10, 799.
[2] A. Salvador-Porroche et al., Nanoscale Advances **2021**, 3, 5656
[3] A. Salvador-Porroche et al., ACS Appl. Mater. & Inter. **2022**, 14, 28211
[4] P. Orús et al., Nanomaterials **2022**, 12, 1367
[5] P. Orús et al., J. Solid State Chem. **2022**, doi : 10.1016/j.jssc.2022.123476
[6] R. Cordoba et al., Nano Letters **2019**, 19, 8597.
[7] F. Sigloch et al., arXiv.: 2203.05278

PL: Silicene: a dream comes true

P. Castrucci

Department of Physics, University of Roma Tor Vergata, Roma, Italy

Among graphene-like two-dimensional materials, silicene has been for a long time a dream for the scientific community for its theoretically predicted unique conductive properties due to its massless fermion carriers [1,2], the possibility to engineer its small energy bandgap by doping, applying electric or magnetic fields and to exploit its abilities in vertical and/or all metal (e.g. graphene/silicene) devices [1,3]. Due to Si inherent sp^3 hybridization giving rise to no Si van der Waals (vdW) exfoliable structure, experimentally the only possibility to obtain silicene is through Si chemical or/and physical deposition methods. In this respect, substrate proved to play a fundamental role in the Si atom absorption process leading, in case of metal substrates, to a mixed phase formation [4-7] and, for vdW chemical inert substrates, to Si atom

intercalation occurring even at room temperature [8-12]. Such an intercalation has been recently associated to the presence of surface defects [11-12]. Lately, hundreds of nanometer area quasi-free standing silicene has been successfully reported to be grown on top an almost ideal epitaxial graphene layer synthesized on 6H-SiC substrate [13]. In the present talk, a review of the most recent studies on silicene formation on inert surfaces will be elucidated, providing an efficient and simple way to produce high quality and large-scale material on an inert and well-ordered surface.

[1] M. Spenser, T. Morishita (Eds) Silicene. Structure, Properties and Applications, Springer, **2016**.
[2] S. Cahangirov, M. Topsakal, E. Akturk, H. Sahin, S. Ciraci, Phys. Rev. Lett. **2009**, 102, 236804.
[3] Y.Y. Wang, Z.Y. Ni, Q.H. Liu, R.G. Quhe, J.X. Zheng, M. Ye, D.P. Yu, J.J. Shi, J.B. Yang, J. Li, J. Lu, Adv. Funct. Mater. **2015**, 25, 68-77.
[4] P. Vogt, P. De Padova, C. Quaresima, J. Avila, E. Frantzeskakis, M.C. Asensio, A. Resta, B. Ealet, G. Le Lay, Phys. Rev. Lett. **2012**, 108,155501.
[5] Lin et al., Phys. Rev. Lett. **2013**, 110, 076801.
[6] L. Meng, Y.L. Wang, L.Z. Zhang, S.X. Du, R.T. Wu, L.F. Li, Y. Zhang, G. Li, H.T. Zhou, W.A. Hofer, H.J. Gao, Nano Lett. **2013**, 13 685-690.
[7] L. Huang, Y.F. Zhang, Y.Y. Zhang, W.Y. Xu, Y.D. Que, E. Li, J.B. Pan, Y.L. Wang, Y.Q. Liu, S.X. Du, S.T. Pantelides, H.J. Gao, Nano Lett. **2017**, 17, 1161-1166.
[8] R. van Bremen, Q.R. Yao, S. Banerjee, D. Cakir, N. Oncel, H.J.W. Zandvliet, Beilstein J. Nanotech. **2017**, 8,1952-1960.
[9] M. De Crescenzi, I. Berbezier, M. Scarselli, P. Castrucci, M. Abbarchi, A. Ronda, F. Jardali, J. Park, H. Vach, ACS Nano, **2016**, 10,11163-11171.

[10] I. Kupchak, F. Fabbri, M. De Crescenzi, M. Scarselli, M. Salvato, T. Delise, I. Berbezier, O. Pulci, P. Castrucci, Nanoscale **2019**, 11, 6145-6152.
[11] F. Ronci, S. Colonna, R. Flammini, M. De Crescenzi, M. Scarselli, M. Salvato, I. Berbezier, F. Jardali, C. Lechner, P. Pochet, H. Vach, P. Castrucci, Carbon **2020**, 158, 631-641.
[12] F. Fabbri, M. Scarselli, N. Shetty, S. Kubatkin, S. Lara-Avila, M. Abel, I. Berbezier, H. Vach, M. Salvato, M. De Crescenzi and P. Castrucci, **2022** submitted to Surfaces and Interfaces
[13] Z. Ben Jabra, M. Abel, F. Fabbri, J.-N. Aqua, M. Koudia, A. Michon, P. Castrucci, A. Ronda, H. Vach, M. De Crescenzi, I. Berbezier, ACS Nano **2022**, 16, 5920–5931.

Plenary and Invited Session (HALL 1)

T4-PL: Growth mechanisms and magnetic properties of ultrathin ferrite films

K. Kuepper, T. Pohlmann, J. Thien, J. Rodewald, K. Ruwisch, J. Wollschlager[1]

University of Osnabrück, Department of Physics, Barbarastraße, 7, 49076 Osnabrück, Germany

Transition metal ferrites with (inverse) spinel structure are in the focus of current research due to a number of intriguing properties, including high Curie temperatures and significant magnetic saturation moments. Here magnetite, Fe_3O_4 is one of the most frequently investigated materials due to its predicted half-metallic behavior with 100% spin polarization.
In the other hand, the magnetic insulator cobalt ferrite, $CoFe_2O_4$, is an interesting candidate due the so-called spin filter effect, which is a result of the exchange splitting of the energy levels in the conduction band that leads to different

tunnel barrier heights for spin-up and spin-down electrons. However, the theoretical promises were never quite met experimentally up to now. These drawbacks are associated to the structural properties of the ultrathin ferrite films at the interface between thin film and substrate such as antiphase boundaries (APBs) or other interface effects. Also the exact cationic distribution (degree of spinel inversion) at the interface and the surface of the thin films are of utmost importance.

Therefore, we performed a series of experimental works to investigate the growth mechanisms and the chemical and magnetic properties in depth. We performed time resolved x-ray diffraction and photoelectron spectroscopy of the growth of Fe_3O_4 and $CoFe_2O_4$ thin films in order to investigate the thickness-dependent evolution of Bragg reflections sensitive to the octahedral and tetrahedral sublattices of the inverse spinel structures [1,2]. The magnetic properties of magnetite thin films at the interface to the substrate and the surface were studies in detail employing a combination of x-ray magnetic circular dichroism and x-ray resonant magnetic reflectivity [3,4]. We also worked out an alternate pathway to form ultrathin $Co_xFe_{3-x}O_4$ films by interdiffusion of Fe_3O_4/CoO [5] and CoO/ Fe_3O_4 [6,7] bilayers instead of Co and Fe co-deposition.

[1] T. Pohlmann et al., Phys. Rev. B **105**, 045412 (2022) .
[2] K. Ruwisch et al., Materials **15**, 2377 (2022).
[3] T. Pohlmann et al., Phys. Rev. B **102**, 220411(R) (2020).
[4] T. Pohlmann et al., Phys. Rev. B **105**, 235436 (2022) .
[5] J. Rodewald et al., Phys. Rev. B **100**, 155418 (2019).
[6] J. Thien et al., J. Phys. Chem. C **124**, 23895 (2020).
[7] J. Thien et al., Materials **15**, 46 (2022).

PL-online: Screen printed flexible thermoelectric generators (TEGs) for large-scale thermal energy harvesting

L. Tzounis[1,2], F. Simopoulos[2,3], P. Mangelis[2,3], E. Kymakis[2,3], E. Koudomas[2,3]

[1]Mechanical Engineering Department, Hellenic Mediterranean University, Estavromenos, 71004 Heraklion, Greece
[2]Center of Materials Technology and Photonics, Hellenic Mediterranean University, 71410 Heraklion, Crete, Greece
[3]Electrical and Computer Engineering Department, Hellenic Mediterranean University, Herakleio 71004, Greece

Waste heat produced globally by the most common end-use sectors including transportation, industrial, commercial & residential as well as electricity generation on a global scale, it is estimated at 72% of the global primary energy consumption. In more detail, 63% of the aforementioned waste energy concerns temperatures below 100°C. Thermoelectric (TE) energy harvesting through the so-called thermoelectric generator (TEG) devices could be an emerging and promising technology of renewables in a wide range of applications

In this talk, highly efficient screen-printed flexible TEGs consisting of single walled carbon nanotubes (SWCNTs) will be discussed in detail regarding i.e. the SWCNT ink formulations, the screen printing parameters, the TEG device characterisation as well as practical applications powered-up by the TEG device [Fig. 1]. Namely, in our previous published articles [1], we have achieved the highest to date thermoelectric properties and eficiency of p- and n-type SWCNTs as well as the resulting TEG device that will be discussed in this presentation; i.e. S >50 μV/K for p-doped and <-40 μV/K for n-doped CNT nanomaterials,

electrical conductivity σ = 104 S/m with power factors PF> 350 μW/mK2 and 300 μW/mK2 for the p-type and n-type films (increased Power Factor by 10 times and ZT: 0.5-1.0 reaching TEG device efficiency of n= 5-10%.).

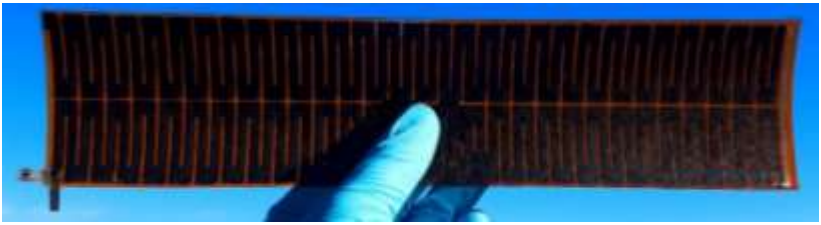

Fig. 1. TEG device (300mm length – 50mmwidth) screen printed onto a Kapton polymeric and flexible substrate, consisting of serially interconnected p- and n-type SWCNTs.

The TEGs presented herein would be highly scalable potentially to be fabricated in a continuous roll-to-roll (R2R) printing process, allowing the large-scale manufacturing/industrial production of highly efficient flexible TEGs and consequently large-scale thermal energy harvesting. In Figure 2, a TEG device is demonstrated, capable of powering-up a commercial step-up converter from body temperature- lost heat up to different thermal gradients, allowing potential practical applications e.g. self-powered IoT devices, wearable sensors, etc. This TEG device shown consists of p-type and n-type SWCNT films beyond 308 μW/mK2 and 258 μW/mK2 power factors, respectively, at ΔT=150K (THOT=175°C) and outstanding stability in air without advanced and expensive encapsulation, while it delivers an open-circuit voltage VOC= 1.05 V and short-circuit current ISC= 1.30 mA at ΔT= 150 K (THOT=175°C) with an internal resistance of RTEG= 806 Ω, generating a maximum power output (Pmax) of 342 μW.

[1] Tzounis et. al. ACS Appl. Mater. Interfaces **2021**, 13, 9, 11151–11165.

PL-online: Emerging 2-Terminal Memory Devices – Creation and Exploitation of Internal Electric Field for Realisation of Memory Deivces

S. Paul

Emerging Technologies Research Centre, De Montfort University, Leicester, UK

Intensive research is currently underway to exploit the highly interesting properties of nano-bits and/or sub-nano bits ("nano-sized particles, atoms and organic molecules") for optical, electronic and other applications. Memory devices play an important role in the electronics arena and inspire advances in the technologies. There is always growing need to look for inexpensive, fast, high density and longer data retention time memory devices. This work describes the use of nano-bits and sub-nano bits in two terminal electronic memory devices. These devices show two electrical conductance states ("high" and "low") when voltage is applied, thus rendering the structures suitable for data retention. These two states can be viewed as the realisation of non-volatile memory. The progress in the use of "nano/sub-nano-bits" in memory devices will be presented and invoke the conundrums that scholars of this field are currently faced with, such as questions about the electrical charging mechanism and stability of devices, proposed theories explaining the experimental data, contradictions in the published work by different groups.

[1] F. Paul, K. Nama Manjunatha, S. Paul, Materials. Advances, **2022**, 3, 5363 - 5374

[2] F. Paul, S. Paul, Small, **2022** 18 (21), 2106442.

[3] Paul, S. 2007, *IEEE Trans. Nanotechnol.,* **2007**, 6 (2) 191-195.

T6-I-online: Polymer based two terminal electronic memory devices

I. Salaoru

Emerging Technologies Research Centre; De Montfort University, The Gateway, Leicester, LE1 9BH, United Kingdom

Currently, the electronic memory elements are the important components of all electronic devices from computers to health monitors and from sensors to space, military and defence technologies. This is why these devices attract a huge interest from both the research and industry communities. Numerous candidates for emerging electronic memory technologies such as ferroelectric (FeRAM), phase-change random access memory (PCRAM), magneto-resistive (MRAM), resistive random-access memory (ReRAM) and organic memory have been proposed and investigated by a number of research groups worldwide [1,2]. On another hand, the current trend in electronics is to replace rigid substrates with flexible ones, supporting the development of flexible, bendable electronics. In this context of re-defining memory technology, organic materials are the best candidates to fulfill the current pathway in memory technologies and applications. It should be highlighted that the organic materials offer a large number of advantages such as: being able to be processed at a low temperature over large area on flexible substrates using wet-processing techniques, have low weight and great mechanical flexibility [3-5].

The organic memory devices can be fabricated either by depositing a polymer blend or a polymer composite (blend of polymer and small organic molecules or nanoparticles) between two metal electrodes.

We obtained organic (polymer blend and admixture of organic polymer, small organic molecules and nanoparticles) based

two terminal non-volatile memories. The physical switching/charging mechanism(s) along with experimental evidence are studied. Along with the electrical experimental results, we have also used the chemical characterization tools to further understand the operating mechanism that is also discussed.

Acknowledgments The author would like to thank the EPSRC (Grant #EP/E047785/1) for supporting this work.

[1] S. Lee, S. Kim, and H. Yoo, Polymers, **2021**, 13(21), 3774.
[2] S. Lombardo, B. de Salvo, C. Gerardi, and T. Baron, Microel. Eng., **2004**, 72, (1–4), 388–394.
[3] C.W. Tang, S.A. Vanslyke, Appl. Phys. Lett. **1997**, 51 (12), 913.
[4] G. Yu, J. Gao, J.C. Hummelen, F. Wudl, A.J. Heeger, Science **1995**, 270, 1789.
[5] F. Garnier, R. Hajlaoui, A. Yassar, P. Srivastava, Science **1994**, 265, 1684.

T5-I-online: III-V nanowires and nanotructures grown by HVPE

Y. Andre[1,2], E. Chereau[1], G. Gabin[1], H. Hijazi[1], M. Zheghouane[1], G. Avit[1], C. Bougerol[3], D. Paget[4], V. Dubrovskii[5], Ph. Shields[6], N. I. Goktas[2], R. R. LaPierre[2], A. Trassoudaine[1], E. Gil[1]

[1]University of Clermont Auvergne, Clermont Auvergne INP, CNRS, Institut Pascal, F-63000 Clermont-Ferrand, France.
[2]Department of Engineering Physics, McMaster University, Hamilton, Ontario, Canada, L8S4L7
[3] University of Grenoble Alpes F-38000 Grenoble, France, CNRS, Institut Neel, F-38042 Grenoble
[4]Physique de la matiere condensee, Ecole Polytechnique, CNRS, Universite Paris-Saclay, 91128 Palaiseau, France
[5]Saint-Petersburg State University, Russia
[6]Department of Electronic & Electrical Engineering, University of Bath, Claverton Down, Bath BA2 7AY, UK

III-V semiconductor materials enable a wide range of novel optic and spintronic devices. Nanometer-scale nitride semiconductor structures are often at the hearth of such applications. The performances of such devices are strongly dependent on the crystallographic, electronic and optical properties of the semiconductor material and thus on the growth processes used to synthesize the crystal structures.
Hydride Vapor Phase Epitaxy (HVPE) process exhibits unexpected properties when growing III-V and III-Nitride semiconductor micro- and nanostructures. With respect to the classical well-known methods such as Metal Organic Phase Epitaxy (MOVPE) and Molecular Beam Epitaxy (MBE), this near-equilibrium process is based on hot wall reactor technology, and the aim of this presentation is to investigate the potential of the versatile HVPE process implementing III- chloride

precursors, and describe why it has been developed in the recent and last decades to grow III-Nitride and III-V semiconductor nanostructures and nanowires.

This presentation will address the growth through several regimes: selective area growth (SAG), vapor liquid solid growth (VLS) and self-catalyzed growth in the HVPE environment. In SAG, the chloride precursors are so volatile that they provide the most suitable environment for implementing selective and localized growth without any adsorption on the dielectric surface. The HVPE growth process is ruled by surface kinetics that is, by the intrinsic growth anisotropy of crystals. The facet growth rate can be set by varying the experimental parameters of temperature and vapor phase composition. In VLS-HVPE, under high mass input, the synthesis and doping are demonstrated for nanowires with a constant cylinder shape over unusual length and free of crystal defects with great optical, quantum, spin and charge transport properties [1,2,3,4].

[1] D. Paget, et al., Phys. Rev. B, **2021,** 103, 195314
[2] G. Gabin, et al., CrystEngComm, **2021** 23 (2), 378-384
[3] H. Hijazi, et al., Nano Lett. **2019**, 7, 4498-4504
[4] G. Avit et al., Nano Lett. **2014**, 14, 2, 559–562.

Author index

A

Ababei, G., 184, 341
Abaskin, V., 310
Abel, M., 147
Achimova, E., 310
Adiguzel, 26
Aldrigo, M., 162
Aliev, F. G., 140
Allou, D., 350
Al-Matarneh, C. M., 225
Aluas, M., 51, 328
Alupului, T., 355
Amara, K., 258
Amato, M., 299
Anadon, A., 49
Anastasoaie, V., 282
Andre, Y., 371
Andrei, F., 267
Angelov, B., 333
Angelova, A., 333
Angyus, S. B., 89
Antohe, V. A., 113
Aoki, T., 111
Aqua, J-N., 147
Ardeleanu, A., 318
Arl, D., 308
Asandulesa, M., 213
Astilean, S., 16, 58, 92, 231
Atanasov, R., 190
Avit, G., 371
Avramescu, V., 262

B

Badea, L., 158
Badreeva, D., 76
Baia, L., 264
Baia, M., 129, 264
Bajama, I., 51, 84, 291
Balasz, I., 188
Banciu, M., 58
Banici, A-M., 267
Barborini, E., 127, 308
Barbu, L., 190, 197, 203, 204, 206, 247, 303
Barbu-Todoran, L., 84
Barbu-Tudoran, 290
Barbu-Tudoran, L., 51, 106, 239, 284, 323, 325, 328
Bardeanu, H. M., 91
Barsukov, V., 119, 176, 216
Barutiak, M., 79
Batorfi, J. Gy., 312
Bauckhage, Y., 269
Bedjaoui, W., 258
Belik, A. A., 23
Belkessa, B, 246
Belkessa, B., 243, 248, 251, 258
Ben Jabra, Z., 147
Benova, E., 79
Benvenuti, G., 127
Berbezier, I., 147
Bhatnagar, A., 23
Birjega, R., 267
Blanita, G., 207
Bleotu, G., 295

Bobanova, Zh., 254
Bocaneala, M, 284
Bocaneala, M., 290, 323
Boerasu, I., 173
Bonciu, A., 53, 318
Bortnic, R., 106, 188, 190, 303
Borza, F., 178
Bostiog, A-I., 56
Botiz, I., 354
Botnari, V., 310
Bougerol, C., 371
Bouranta, A., 339
Bousseksou, A., 44
Bozin, E. S,, 145
Brajnicov, S., 267
Bratos Cetinic, A., 84
Brezeanu, M., 262
Brezestean, I., 247
Brezestean, I. A., 249
Brincoveanu, O., 232, 282
Brincoveanu, O. A,, 160
Brincoveanu, O. A., 337
Brinza, E., 190
Budei, D., 234
Buerger, J., 109, 121
Buiu, O., 262
Bulai, G., 355
Bumbac, M., 262
Burzo, E., 106
Butenko, O., 119, 216
Butnaru, I., 35, 213

C

Cadis, A., 195
Calina, I., 318
Calkovska, A., 77
Campean, A., 318
Campu, A., 58
Capel Berdiell, I., 145
Caraman, M., 344, 347
Carlescu, A., 344, 347
Carpa, R., 316
Caruntu, G., 168
Caruntu, V., 165
Caso, D., 140
Castrucci, P., 362
Cea, P., 360
Cernica, I., 256
Cesiulis, H., 82, 135, 180
Chakravarty, P., 312
Cheniti, B., 243, 246, 248, 251, 258
Chereau, E., 371
Chernysh, O., 119, 216
Chertopalov, S., 314
Chicinas, 40
Chifiriuc, C., 318
Chioncel, L., 296
Chiriac, A. P., 35, 211, 213
Chiriac, H., 182
Cimpan, R., 44
Cimpean, A., 53
Cimpoesu, A. G., 143
Cinta Pinzaru, S., 51, 84, 89, 193, 239, 284, 286, 288, 290, 291, 323, 325, 328
Ciobanu, V., 44
Ciorita, A., 89, 284, 290, 316, 323
Ciurea, M. L., 351
Cojocaru, C., 18, 86
Colis, S., 152, 193, 301

Colnita, A., 247, 249
Coman, C., 318
Comanescu, B., 279
Comanescu, F., 337
Constantin, C. P., 32, 133, 218, 220
Correa, C. A., 154
Correia, F. C., 330
Cosmulescu, F., 86, 88
Cosmulescu, S. F., 18
Cotet, L. C., 264
Cotojman, L., 40
Craciun, D., 28, 158, 172, 227, 234, 240, 295
Craciun, G., 227
Craciun, M., 231
Craciun, V., 28, 158, 164, 172, 227, 234, 240, 295, 314
Creanga, D-E., 60
Cristea, D., 227, 279, 282
Curecheriu, L. P., 94, 307

D

Dahiya, R., 123
Damaceanu, 32
Damaceanu, M. D., 35, 133, 211, 213, 218
Dan, M., 37
Dare, D. K., 157, 164
De Teresa, J. M., 360
Deac, I. G., 42, 190
Deltsidis, A., 145
Demeter, M., 318
Di Bartolomeo, A., 71
Diaconu, A., 44, 165, 168
Dikusar, A., 254
Dimofte, M-G., 225
Dina, N. A., 249
Dina, N. E., 199
Dinca, V., 53
Dinescu, A., 15, 256, 282, 337
Dinescu, G., 318
Dinia, A., 152
Dinu, L. A., 162
Dippong, T., 42
Djama, M., 246
Djemmah, S., 350
Dobrea, V., 341
Dobromir, M., 355
Dorcioman, G., 158, 227, 234
Doroftei, C., 344
Doutre,F., 96
Drabavicius, A., 180
Draghiciu, L., 337
Dragoman, D., 15
Dragoman, M., 15
Dragos-Pinzaru, O-G., 178
Drechsler, F., 23
Drechsler, M., 333
Droghetti, A., 296
Dubrovskii, V., 371
Dudric, 106
Dudric, R., 106
Dumbravescu, N., 262
Dumitrescu, L. N., 267
Dumitrescu, N., 53
Dumitru, A., 295
Dumitru, D. A., 51
Dumitru, D-Al., 325
Dupeyrat, C., 101, 104, 277
Dupont, S., 84

Dushanov, E>, 76

E

Enache, A. C., 18
Epurescu, G., 267
Ermakova, E., 76
Escalante-Quiceno, A. T., 360
Evtodiev, I., 347

F

Fabian, J., 140
Faella, E, 71
Falamas, A., 197, 304
Farcasanu, I., 236
Farcau, C., 304
Fekete, L., 154
Filip, T. A., 266
Filip, X., 37
Fitl, P, 20
Fitl, P., 154
Fix, T., 150
Floare, C. G., 224
Fochuk, P., 168
Focsan, M., 92, 231
Fodchuk, I., 168
Forfota, R., 284, 323
Fort, C. I., 264
Fragkiadakis, G. A., 339
Franckevicius, M., 180
Fuentes-Garcia, J. A., 138

G

Gabin, G., 371
Garlisi, C., 127
Garoi, P., 28, 158, 172, 234, 240, 295
Gavrila, R., 162, 337
Geanta, V., 227
Ghiarasim, R., 55, 225
Gil, E., 371
Girardeau, T., 101, 104, 277
Giroire, B., 101, 104, 277
Giubileo, F., 71
Glamuzina, B., 51, 239, 328
Glamuzina, L., 84
Goktas, N, I., 371
Goni, A. R., 330
Gonzalez-Ruano, C., 140
Goya, G. F., 138
Grad, O., 207
Gradisteanu, N., 53
Grase, L., 117
Graur, A., 165
Grdan, S., 84
Grigoras, M., 184
Groll, M., 109
Grosan, C., 293
Grysan, P., 308
Guillot, J., 127, 308
Gurau, V., 344
Gurlui, S., 344, 347
Gutoiu, S., 207
Gyulavari, T., 129

H

Hada, A-M., 231
Haddad, A., 350
Haisch, C., 199
Hakem, M., 243, 246, 248

Halder, A., 296
Harabagiu, V., 18, 86, 88
Hehn, M., 140
Heinrich, A., 269
Henning, X., 152
Hijazi, H., 371
Himcinschi, C., 23
Hirian, R., 51, 89, 106, 188, 190, 239, 303, 328
Hodges, P., 271
Hrostea, L., 96, 99, 137
Hrubovcak, P., 79
Hruska, M., 154
Hruska, P., 154
Hubcik, L., 77

I

Iacomi, F., 209, 344, 347, 349, 355
Ibanescu, S-A., 55
Ibarra, M. R., 138
Iftimie, S., 351
Ignat, M., 86, 209, 349
Inkielewicz-Stepniak, I., 229
Intonti, K, 71
Ionescu, O. N., 91, 119
Ionita, E-R., 267
Ionita, M-D, 267
Irimiciuc, 28
Irimiciuc, S. A., 172
Irimiciuc, S. A., 295, 314
Isnard, O, 40
Ivankov, O, 76
Iwata, F., 111

J

Johnsen, L. G., 140
Jones, V., 186
Juodkazis, S., 68

K

Kacso, I., 224, 290
Kampf, A. P., 298
Kholmurodov, Kh., 76
Khomenko, V., 119, 176, 216
Kiraly, N., 131
Kondrotas, R., 180
Kool, D., 273
Kopidakis, G., 145
Kortus, J., 23
Kosuth, J., 79
Koudia, M., 147
Koudomas, E., 366
Koudoumas, E., 119, 160, 216, 337, 339, 355
Kralovic, N., 77
Kucerca, N., 76
Kucerka, N., 77
Kuepper, K., 364
Kuklin, A., 76
Kumar, A., 71
Kumar, D., 74, 157, 164, 186
Kunnathully, V. S., 121, 170
Kurakin, S., 76
Kuryptia, Ya., 119, 216
Kusovaca, T., 89
Kymakis, E., 366

L

Lancok, J., 20, 154, 314
Langer, T., 170
LaPierre, R. R., 371
Lappas, A., 145
Laszlo, E. A., 227
Lazar, G., 51, 89, 239, 291, 325, 328
Lazar, L., 84
Lazea-Stoyanova, A., 267
Lefevre, C., 49
Leontie, L., 137, 344, 347
Leostean, C., 191, 193, 195, 197, 203, 204, 206, 207, 301
Les, A., 60
Levinas, R, 135
Liebscher, J., 321
Linder, J., 140
Lindner, J. K. N., 14, 109, 121, 170, 269, 271, 273, 275
Linnik, I., 250
Losmanschii, C., 310
Lostun, M., 182, 184
Lu, X., 157
Lukacs, V. A., 94
Lukacs, V. K., 307
Lunca Popa, P., 127
Lungu, G. A., 351
Lupu, N., 178, 182, 184, 341

M

Maamache, B, 251
Maamache, B., 243, 248
Macavei, S., 191, 193, 195, 197, 207, 301
Macavei, S. G., 284, 290, 323
Madi, Y., 350
Magen, C., 360
Magyari, K., 129
Maksimovic, J., 68
Manea, E., 256
Mangelis, P., 366
Marconi, D., 247, 249
Marica, I, 304
Marica, I., 288, 290
Marinas, I. C., 232
Marinca, T., 200
Marinca, T. F., 40
Marinescu, M-R., 262
Marquina, C., 138
Marsal, C., 101, 104, 277
Martinez Medina, J. E., 308
Marza-Rosca, J., 234
Matei, A., 267
Matei, E., 318
Mathieu, S., 246
Maudez, W., 127
Megiel, E., 229
Menguelti, K., 127
Mesaros, A., 200
Meshalkin, A., 180, 310
Mic, M., 224
Mican, S., 143
Michel, M., 127
Miclaus, M., 224
Mihai, M. D., 158
Mihalache, I., 337
Mihet, M., 89
Mimura, H., 111
Min, G., 123
Mirza-Rosca, J. C., 227

Mitoseriu, L., 94, 307
Mitran, V., 318
Mitu, B., 318
Mizeikis, V., 358
Mogildea, G., 240
Mogildea, M., 240
Moldovan, C. S., 290
Molnar, Cs., 224, 286
Molnar, G., 44
Moon, J., 111
Moraru, D., 69, 111
More-Chevalier, J., 154
Mueller, A, 15
Mueller, R., 337
Muhammad, A., 349
Mulvihill, D. M., 123
Muratis, K., 119
Murgulescu, I., 341
Murugova, T., 76
Mykhailovych, M., 168
Mykhailovych, V., 165, 168

N

Nagy, L., 79
Nan, 37
Nastase, F., 162
Nastuta, A. V., 335
Năsui, M., 200
Naujokaitis, A., 180
Neamtu, B. V., 40
Negrescu, A. M., 53
Nekvapil, F., 51, 84, 89, 239, 303, 304, 325, 328
Nemec, P., 22
Neo, Y., 111
Nesterovschi, I., 288, 323
Ng, S-H., 68
Nicolescu, C., 262
Novotny, M., 20, 154, 314

O

Odusanya, A., 164
Olar, G. C., 264
Olariu, M. A., 266
One, R., 143
Onufrijevs, P., 115
Orus, P., 360
Ouali, 251
Ouali, N., 243, 246, 248, 258
Ozden, A., 23

P

Pachiu, C., 160, 262, 337, 339
Padeletti, G., 81
Padurariu, L., 94, 307
Paget, D., 371
Pakstas, V., 180, 310
Palade, C., 351
Palage, M., 224
Pana, O, 204
Pana, O., 191, 193, 195, 197, 200, 203, 206, 207, 293, 301
Panaitescu, A. M., 113
Panchout, E., 101, 104, 277
Parvulescu, C., 256, 279, 282
Pascariu, P., 125
Patlun, D., 176
Paul, S., 349, 368
Paumier, F., 101, 104, 277
Pelella, A., 71

Pelteacu, M., 279
Pena Corredor, A., 49
Perhaita, I., 195
Petit-Watelot, S., 49
Petran, A., 206, 221, 321
Petrenko, V., 254
Petrotos, K., 339
Pfeifer, M. A., 164
Philipp, P., 360
Philippe, A. M., 308
Pillai, S. C., 75
Pinteala, M., 55, 56
Pirnau, A., 224
Pistillo, B. R., 127
Podar, D., 316
Pohlmann, T., 364
Pokorny, P., 154
Polesel, J., 308
Pop, V., 188
Popa, A,, 195
Popa, A., 191, 193, 197, 203, 204, 206, 293, 301, 304
Popa, F., 40, 188
Popa, M., 318
Popescu, A., 30
Popescu, C-M., 320
Popescu, M-C., 320
Porcescu, M., 182, 184
Potara, M., 231, 290
Poupon, M., 154
Precanica, M., 89
Predeanu, G., 18, 86, 88
Prevot, G., 147
Preziosi, D., 49
Prokop, D., 154
Proschwitz, J. L., 23
Punga, L., 355
Purica, M., 256

R

Radonjic, M. M., 296
Radu, R. D., 133
Radu, T, 321
Radu, T., 37, 221
Rambu, A. P., 96, 99
Rastei, M. V., 152
Rehspringer, L., 150
Reparaz, S., 330
Reuter, D., 170
Ribeiro, J. M., 330
Riedl, T., 121, 170
Risca, I-M., 165
Rodewald, J., 364
Rodrigues, F. J., 330
Roge, V., 127
Rojas-Sanchez, C, 49
Romanitan, C., 160, 162, 232, 337, 339
Rosca, I., 339
Roseanu, A., 318
Rostas, A., 290
Rostas, A. M., 236
Rotaru, A., 44, 165, 168
Roy, M., 157, 164
Rungger, I., 296
Rusen, L., 53
Rusu, G. G., 355
Rusu, R. D., 220
Ruwisch, K., 364

S

Sacarescu, L., 86
Salagean, A., 318
Salagean, C., 264
Salaoru, I., 209, 349, 369
Salmon, L., 44
Salvador-Porroche, A., 360
Samoila, P., 18, 86, 88
Sanchez, F., 13
Sandu, M. R., 96, 99
Sangiao, S., 360
Sarkar, K., 157, 164, 186
Saszet, K., 129
Satulu, V., 318
Savencu, S. A., 234
Saviuc, C. M., 318
Scarisoreanu, A., 318
Seguy, I., 44
Selagea, M. N., 234
Senyk, I., 119, 216
Serban, A. B., 162
Serban, B-C., 262
Shields, Ph., 371
Sidor, J. J., 312
Sigloch, F., 360
Silipas, D., 203, 206
Silipas, T. D., 204
Sima, L., 318
Simionescu, N., 55, 56
Simonelli, L., 145
Simopoulos, F., 366
Singh, R. S., 111
Slaoui, A., 150
Slav, A., 351
Smith, B., 157
Smith, D., 68
Som, J., 157, 164
Soran, M-L., 89
Soroceanu, 39
Soroceanu, A., 343
Souca, G., 106, 188
Spalatu, N., 347
Sprincean, V., 344, 347
Stăncioiu, L., 199
Stanciulescu, A., 222
Stavarache, I., 351
Stefan, M., 191, 193, 195, 197, 203, 204, 206, 293, 301, 304
Stirbu, R. S., 94
Stiufiuc, 290
Stiufiuc, R., 106
Stiufiuc, R. I., 290
Stoeffler, D., 150
Stoian, G,, 178
Stoian, G., 182, 184
Stoica, T., 351
Stroescu (Nistorescu), S., 53
Stroici, E., 295
Suarasan, S., 58, 231
Suchea, M., 119
Suchea, M. P., 91, 160, 216, 337, 339, 355
Suciu, M, 51
Suciu, M., 84, 207, 247, 249, 290, 321
Suciu, R-C., 293
Sulinova, Z., 79
Surdu, V. A., 173
Susu, L., 92
Szatmari, A, 106
Szatmari, A., 303

Szekely, I., 129
Szucsova, J., 79

T

Takagi, K., 111
Tamas, T., 51, 84, 239, 291, 325, 328
Tarta, A., 290
Tascu, S., 96, 99, 355
Tavares, C. J., 330
Teodorescu, C. M., 191, 301
Teodorescu, C. T., 46
Teodorescu, V. S., 351
Teodoroff, S., 355
Tetean, R., 42, 106, 303
Thien, T., 364
Tifui, G., 355
Tihauan, B. M., 224
Timpu, D., 88, 320, 355
Tiron, A., 225
Tiron, C. E., 225
Tiron, V., 96, 335
Tiusan, C., 140, 143
Toloman, D., 191, 193, 195, 197, 203, 204, 206, 236, 293, 301
Toma, V., 106
Tomescu, R., 279, 282
Tomsic, S., 51, 328
Topala, I., 335
Toth, Zs-R., 129
Trapp, A., 170
Trassoudaine, A., 371
Trusca, R. D., 173, 222
Tsuchiya, T., 66
Tsyntsaru, N., 25, 135
Tucureanu, V., 232
Tudoran, C., 316
Tudose, I. V., 119, 160, 337, 339, 355
Tuero, P., 140
Turcan, L., 266
Turcu, E., 86
Tverdokhleb, V., 119
Tverdokhlib, V., 216
Tzounis, L., 366

U

Udrea, R., 28, 158, 172, 234, 295
Uhrikova, D., 77
Untila, D., 344, 347
Ursescu, D., 295
Ursu, E-L., 355

V

Vacar, C. L., 316
Vailakis, G., 145
Varganici, C-D., 55
Vasile, B. S., 173, 200, 222
Vasile, E., 222
Vasile, O. R,, 173
Vasile, O. R., 222
Venugopal, H., 273
Vergne, C., 127, 308
Viart, N., 49
Vilcek, S., 79
Viscardi, L., 71
Vizman, D., 30
Vodnar, D. C., 293
Voiculescu, I., 227
Volfova, L., 20, 154

Vollondat, R., 150
Vorokhta, M., 20
Voue, M., 350
Vrnata, M., 20
Vulpe, S., 162
Vulpoi, A., 58

W

Wagner, E., 127
Walch, D. S., 23
Wang, K., 147
Weiss, J. S. C., 271
Wendling, L., 152
Wessel, C. L., 275
Wieland, K., 199
Wolff, A., 269
Wollschlager, J., 364

X

Xu, Y., 123

Y

Yamamoto, T, 64
Yilmaz, F., 298
Yip, S. K., 298

Z

Zahn, D. R. T., 149
Zakhozhai, Z., 216
Zaoutsos, S., 339
Zelenak, V., 79, 131
Zelenakova, A., 79
Zgura, S. I., 240
Zheghouane, M., 371
Zietlow, C., 275
Zutic, I., 140


ICPAMS
interactions,
complex phenomena and
advanced materials
society